Gas sensors using organic thin films at room temperature

Agbor, N.E.

GAS SENSORS USING ORGANIC THIN FILMS AT ROOM TEMPERATURE

BY

N.E. AGBOR BSc. MSc.

Graduate Society

A Thesis submitted in partial fulfilment of the requirements for the degree of PhD.

School of Engineering and Computer Sciences
University of Durham
June 1993.

DECLARATION

I hereby declare that the work carried out in this thesis has not been previously submitted for any degree and is not currently being submitted in candidature for any other degree.

The work in this thesis was carried out by the candidate.

Signed.....

Director of Studies

DEDICATION

This thesis is dedicated to my late father Mr. AGBOR TARH.

ACKNOWLEDGEMENTS

It would have been impossible to complete this work without the help of certain individuals who could not all be mentioned but to whom I am grateful for the part they each played during my stay in Durham. First I would like to thank my supervisors: at Durham University, Dr. Mike Petty and Dr. Andy Monkman; and at British Gas Plc: Dr. Marry Harris, Dr. Stanley Peacock, Mr. David Jones and Dr. Lindsay Houseman. I would like to thank the highly dedicated Mr. Peter Friend whom with his skilfully professional team of Mr. Ian Hutchinson, Mr. Colin Dart and Mr. Mike Wilson, constructed the electronic components of this project. Furthermore, I would like to thank Mr. Friend for the interview by his son on radio Newcastle. I would also like to thank Mr. Norman Thompson and Mr. Chris Pearson, first for their friendship and secondly for the maintenance of the LB troughs, microscopes and evaporator systems. The dedication of Mr. Brian Blackburn with his team of Mr Roger Little, Harry and Brian is acknowledged. I would like to thank Mr. Frank Spence who was our departmental superintendent until his retirement in June 1991; he was a good and professionally efficient man. His replacement Mr. Terry Brown is also acknowledged for his professionalism. The drawing and photographic services of Mrs Kay Seaton, Mrs July Morgan and Mrs Pauline Russell, Mr. Mike Lee and Vicky Greener are acknowledged. The tea ladies Katy and Olive are acknowledged for their friendship. The secretaries Ann, Silvia, Sharon and Julie; my friends in the five-a-side football team [Davy, Steve, Ian, Ian, Mike, and Tony] with whom three medals were won for my three years in Durham, are all acknowledged.

Outside the department, I would like to thank Dr. Robert Judd of British Gas Plc for teaching me how to operate the infrared spectrophotometer; Dr. Yipping for some FTIR work; the scientists at P.N. Lebedev Research Institute Moscow for the supply of lutetium bisphthalocyanine; and Mr. Alex Milton for the supply of polyaniline. I would like to thank Dr. Haider Al-alhlak whose reading and constructive criticism was particularly helpful.

On a personal front, I would like to thank my mother Mrs Elizabeth Ndip, Ms Hilda Nakakuwa, Miss Besong Margaret Eyere, My wife Mrs Enompang Eneke Agbor, Mrs Agbor Ketchen, and Mrs Pankeu Magdalene, for all their help and support.

The ultimate acknowledgement goes to British Gas and the Cameroon Government, whom both sponsored the project.

ABSTRACT

The thesis describes work on the thin film deposition, characterization and gas sensing of three groups of organic materials: polyaniline, lutetium bisphthalocyanine and metallotetraphenylporphyrins. These materials were deposited by evaporation, spinning and using the Langmuir-Blodgett technique. Film characterization by dc conductivity, scanning electron microscopy, surface plasmon resonance, ultraviolet/visible and infrared spectroscopy is described. Gas-induced changes in devices coated with the thin organic films were monitored at the molecular level using Fourier transform infrared spectroscopy and at the macroscopic level using a chemiresistor and surface plasmon resonance. The gases used have included NO_x, H_2S, SO_2, CO and CH_4 at room temperature and pressure. Devices made with the thin organic films were reversibly sensitive to some of the gases at low concentrations (<10ppm), but the reactions were irreversible at high concentrations (>100ppm).

Polyaniline is shown to exhibit a different chemical structure, reflecting the conditions of its deposition. Spun films were found to be in the emeraldine base form, the evaporated films were physically and chemically similar to leucoemeraldine base while the Langmuir-Blodgett films were closer to pernigraniline, the completely oxidized form of polyaniline. All the types of polyaniline films were sensitive to H_2S and NO_x at concentrations down to 4ppm. Only spun and evaporated films were responsive to SO_2. The spun layers were most sensitive to SO_2 and least sensitive to NO_x. In contrast, the evaporated layers were most sensitive to NO_x. The changes recorded in these measurements occurred after a delay time of few seconds, but were completely irreversible for exposure to high gas concentrations. However, no response was observed when exposed to CO or CH_4 even at very high concentrations. Infrared spectroscopy studies indicated the irreversible changes, for example when exposed to NO_x, are due to oxidation of benzoid rings into quinoid structures.

Lutetium bisphthalocyanine has been deposited by the Langmuir-Blodgett technique. Using changes in conductivity, LB layers of lutetium bisphthalocyanine showed responses to NO_x, H_2S and SO_2 at concentrations below 100ppm. However, using surface plasmon resonance, only the NO_x

induced changes could be measured at concentrations below 100ppm. These responses occurred after a delay time of a few seconds and were partially reversible.

Cobalt (II) methoxyltetraphenyl porphyrin has been deposited mainly by the Langmuir-Blodgett technique. Gas induced changes in the film were monitored using changes in dc conductivity and surface plasmon resonance. In all cases, NO_x was reversibly detected, but at a much higher concentration (>100ppm) than for the other materials in this thesis.

CONTENTS

CHAPTER ONE

INTRODUCTION

There is an increasing need for low power, sensitive, selective and reliable gas sensors. This is partly a result of increased levels of pollution, especially from environmentally dangerous gases such as SO_2, NO_x, CO, CO_2 and H_2S. Traditional gas sensing materials are generally based on inorganic semiconductor oxides, such as SnO_2 and ZnO. Devices manufactured from these compounds are now commercially available but suffer from a number of disadvantages. The main problems concern the lack of sensitivity to toxic gases at low concentrations, a high sensitivity to ambient moisture and an inherent lack of selectivity. Furthermore, such devices normally operate at elevated temperatures, which could preclude battery operation. It is therefore not surprising that recently there has been considerable interest in the development of new gas sensing materials. One group of such compounds that is being investigated is organic semiconductors.

In this thesis, we have undertaken an extensive study of solid state gas sensing devices based on novel organic materials. The chemical structure of these compounds can be easily changed (by attachment of side-groups) to obtain a degree of selectivity presently lacking in inorganic semiconductor devices. The materials include macrocyclic compounds such as metalloporphyrins, characterized by a ring network of π-electrons. Other materials, such as polyaniline, are characterized by a chain of π-electrons. Because the gas/material interaction is usually a surface dominated effect, these materials are deposited into very thin films to increase their sensitivity.

The results from this research are presented in nine chapters in this thesis. Chapter two is a review of existing gas sensing materials and techniques. In the first part, the various materials used for gas sensing are described. The compounds used during this work are also introduced. These include lutetium bisphthalocyanine, cobalt (II) methoxyltetraphenyl porphyrin and polyaniline. This is followed by a brief discussion of the various techniques used for gas

sensing. These are broadly classified as electrochemical, optical, thermal and mass sensing methods.

Chapter three contains a detailed description of the experimental methods used in depositing and characterizing the thin films before and after exposure to a gaseous ambient. The three main methods of film deposition used are evaporation; spin-coating; and the Langmuir-Blodgett technique. Film characterization techniques include temperature dependent dc conductivity, scanning electron microscopy, reflection-absorption Fourier transform infrared spectroscopy, ultraviolet/visible spectroscopy, surface plasmon resonance and thickness measurements using a surface profiling Talystep. Gas/material interactions were sometimes monitored at room temperature using changes in dc conductivity, surface plasmon resonance conditions (which includes: resonance depth, resonance position and half width at half maximum) and infrared spectra. The gases used in this work were SO_2, NO_x, H_2S, CO and CH_4.

Chapter four gives the results of studies of thin films of 'undoped' polyaniline that were deposited by spin-coating. A similar series of measurements were undertaken for evaporated polyaniline, presented in chapter five and for polyaniline Langmuir-Blodgett films in chapter six.

Chapter seven is concerned with the deposition, characterization and gas sensing effects for thin films of lutetium bisphthalocyanine, processed by the Langmuir-Blodgett technique. Previous reports of phthalocyanine gas sensors have been based mainly on the mono- rather than the bis-derivatives.

Chapter eight presents the results of a new selective gas sensor for NO_x. The device used cobalt (II) methoxyltetraphenyl porphyrin as the sensing element. Porphyrins are chemically similar to haemoglobin, a compound that is well known for oxygen and carbon dioxide binding. The closing chapter includes the conclusions and suggestions for future work.

CHAPTER TWO

GAS SENSING REVIEW: MATERIALS AND TECHNIQUES

2.1 PREFACE

A detailed review of gas sensing technology is presented in this chapter. This begins in section 2.2 with the different materials reported in the literature for gas sensing. These can be divided into two main groups: namely, the widely exploited inorganic elements or compounds (e.g. Pd or ZnO) and the more recent and novel organic materials (e.g. phthalocyanines or conductive polymers). Presented in section 2.3 is a description of the common methods used for preparing the thin films. Finally, in section 2.4, an overview of the methods of gas sensing is given.

2.2 GAS SENSING MATERIALS

Inorganic materials have been used successfully in gas sensors for many years. Semiconductor oxides and transition metals have mainly been used.

Semiconductor oxide compounds used for gas sensing include SnO_2 [Coles et al, 1991, Gardner et al, 1991, Geloven et al, 1991, Wlodek et al, 1991 and Xu et al, 1991], ZnO [Jones et al, 1984, Raju et al, 1991], TiO_2 [Schierbaum et al, 1991] and strontium titanate ($SrTiO_3$) [Gerblinger et al, 1991]. They are generally porous crystalline materials, with grain sizes (in the case of SnO_2) between 3.0-25.0nm, depending on the processing conditions [Lalauze et al, 1991]. The application of these compounds to gas sensing is usually confined to elevated temperatures, e.g. >400°C.

Amongst the metallic elements employed for gas sensing are palladium, platinum, gold and nickel. In many instances, these have been used as gates on metal/oxide/semiconductor field effect transistors [Ackelid et al, 1991, Janata et

al, 1985 and Poteat et al, 1982]. These devices utilise a change in the metal work function which, in turn, alters the threshold voltage of the transistor. Metals have been used as resistive elements for gas sensing. For example, gold in thin film form has been used for mercury detection [Janata, 1989]. They have also been used as catalytic layers, sometimes in a mixture with a non-transition metal [Gentry et al, 1984]. Generally, the out of balance voltage across a half Wheastone bridge is used as a measure of gas/material interaction.

Sensors based on inorganic materials suffer from a number of disadvantages. Amongst these is the high temperature (>400°C) normally required for their operation. This limits the range of applications and may also result in the possible breakdown of the material/metal ohmic contact [Tanaka et al, 1991]. Such devices may also suffer from water vapour poisoning [Geloven et al, 1991], as well as poisoning from combustion products [Tanaka et al, 1991]. The result can be both short and long term drifts, reducing the reliability. Further problems concern the lack of selectivity and insensitivity to gases at low concentrations.

In order to circumvent some of the above difficulties, workers have developed other compounds, such as BiO_3 [Coles et al, 1991]. Alternatively, a technique of temperature pulsing has been used [Wlodek et al, 1991]. The latter exploits the temperature dependence of the catalytic reaction occurring at the surface of the metal.

Organic compounds may be suitable alternatives as gas sensing elements. These materials offer a number of advantages, such as room temperature operation, low power consumption (no warm-up required), high sensitivity and, above all, the ease of modification of the chemical and/or physical structure to enhance the sensitivity and/or selectivity. Other benefits include processibility and compatibility with the well established silicon technology [Wohltjen et al, 1989]. A wide range of organic materials has been reported for gas sensing purposes. The most prominent classes of compounds are metallophthalocyanines [Archer et al, 1989, Baker et al, 1985, Van Ewyk et al, 1980, Wohljen et al, 1989, Wright, 1987 and Zhu et al, 1990],

metalloporphyrins [Tredgold et al, 1985] and conductive polymers [Miasik et al, 1986].

Metallophthalocyanines (MPcs) are the most widely investigated of the above materials. They are generally p-type semiconductors [Hassan et al, 1989], the conductivity varying in the presence of adsorbed oxidising or reducing gases. Gas sensing using MPcs has been reported for non-crystalline, unpolymerised derivatives, either grown into thick films by sublimation [Sadaoka et al, 1989] or deposited by the Langmuir-Blodgett technique [Wohltjen et al, 1989]. Amongst the various MPcs studied are lead (PbPc) and copper (CuPc) compounds. These both exhibit a high degree of sensitivity but incomplete recovery after exposure to the electrophilic gas NO_x at room temperature. Reports show PbPc to combine the highest conductivity, sensitivity and complete recovery to NO_x at 170°C [Miasik et al, 1986]. A structural investigation of PbPc has demonstrated that its sensitivity is dependent not only on its mode of deposition but also on the nature of the underlying substrate. The as-grown material is amorphous, but forms crystallites when heated to 300°C [Sadaoka et al, 1989]. There is also a small phase transition during this heating, making the device more liable to long term drift.

Although metallophthalocyanines exhibit a number of advantages over SnO_2 devices, their commercial development has been hindered by their low conductivity, typically of the order $10^{-11}Scm^{-1}$ [Wohltjen et al, 1989] and slow speed of response and recovery at room temperature. Unfortunately, the use of elevated temperatures (170°C) may result in material volatility as well as long term drifts in the contacts. Gases detected using these compounds include inorganic pollutants such as NO_x, H_2S, NH_3, SO_2, Cl_2, F_2 and BF_3 [Miasik et al, 1986]. MPcs are generally insensitive to combustion products such as CO and CO_2.

In this work, a new MPc material was studied which possesses a different chemical structure from that discussed above. The material used is lutetium bisphthalocyanine ($LuPc_2$) and its chemical structure is given in figure 2.1.

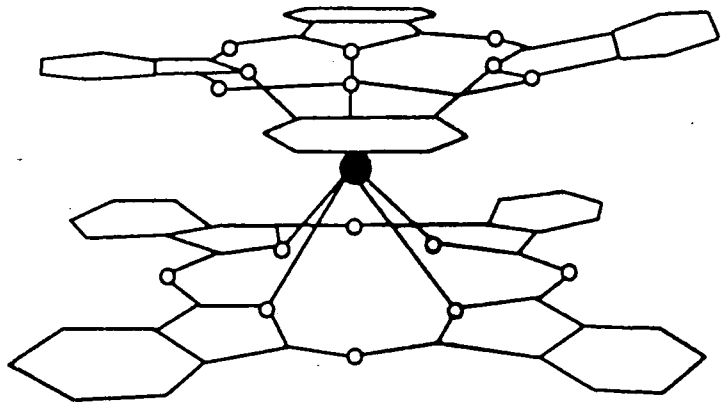

● Lutetium
○ Nitrogen

Figure 2.1: Molecular structure of lutetium bisphthalocyanine.

Metalloporphyrins (MPs) have not been as widely investigated as the metallophthalocyanines, partly because of their even lower conductivity and lower melting points of ~ 200°C [Tredgold et al, 1985]. Studies undertaken on these compounds have shown their interaction with gas molecules to be largely dependent on the electronegativity of the central metal ion [Catalano et al, 1984]. The metal also influences the binding site and rate. It has also been shown that the utilisation of porphyrins as gas sensors is dependent on factors such as the film thickness [Li et al, 1990] and peripheral substituents on the molecular ring [Tredgold et al, 1985]. Most reports have been based on the sensing of NO_x and generally this reaction was found to be partially reversible at room temperature. However, CO has been detected in a frozen solution of piperidine [Wayland et al, 1971]. In other work, porphyrins have been used in an alternating layer structure consisting of a molecular activator and the porphyrin itself [Lecomte et al, 1985]. The molecular activator induces the metal in the porphyrin core to form a bond with a gas molecule.

A list of the metalloporphyrins used in this project is given in figure 2.2. Because of its closeness to haemoglobin, cobalt (II) 5,10,15,20-tetrakis (4-methoxyl)21H,23H-porphine (CMTPP-compound 5 in figure 2.2) was studied in some depth.

MATERIAL	STRUCTURE
① NiTPP 5,10,15,20 - Tetraphenyl - 21H, 23H - Porphine Nickel II.	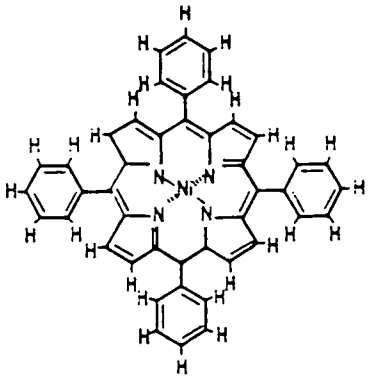
② CuTPP 5,10,15,20 - Tetraphenyl - 21H, 23H - Porphine Copper II.	Same structure as above except replacing Ni by Copper.
③ ZnTPP 5,10,15,20 - Tetraphenyl - 21H, 23H - Porphine Zinc II.	Same structure as NiTPP except Zn replacing Ni.
④ VTPP 5,10,15,20 - Tetraphenyl - 21H, 23H - Porphine Vanadium IV oxide.	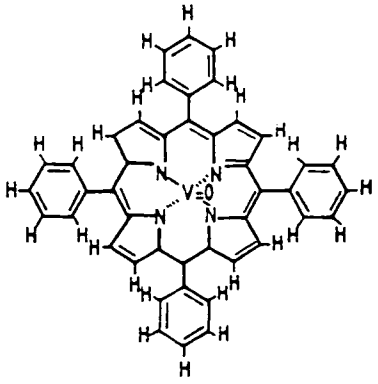
⑤ CMTPP 5,10,15,20 - Tetrakis (4 - methoxyphenyl) 21H, 23H - Porphine Cobalt II.	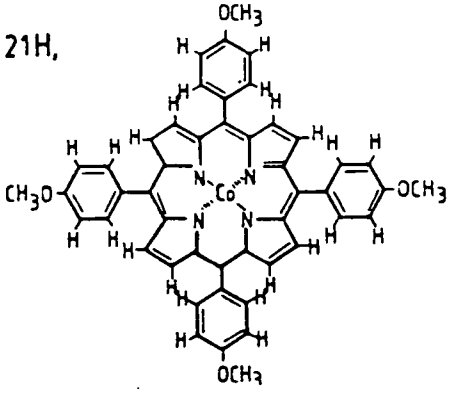

(6) FeMTPP
5,10,15,20-Tetrakis (4-methoxyphenyl)-
21H, 23H Porphine Iron III Chloride.

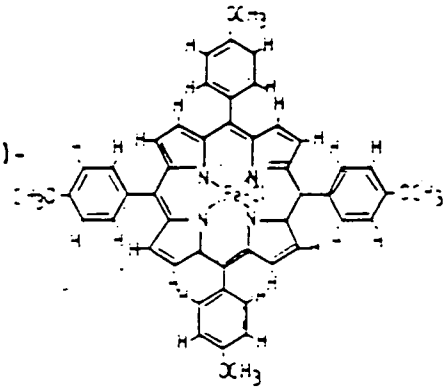

(7) FeTFPP
5,10,15,20-Tetrakis (pentafluorophenyl)-
21H, 23H Porphine Iron III Chloride.

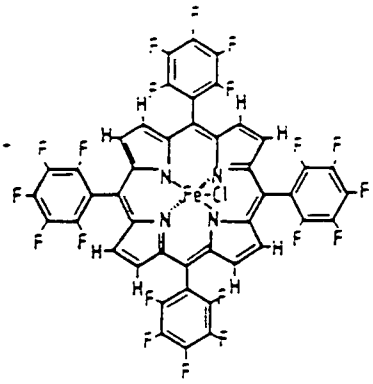

(8) MEDE
Mesoporphyrin IX dimethyl ester.

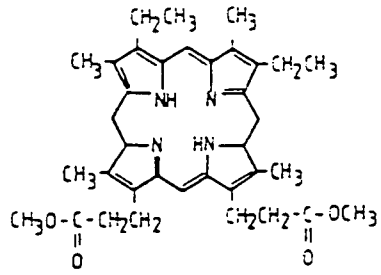

(9) HEMIN
(chloroprotoporphyrin IX iron III).

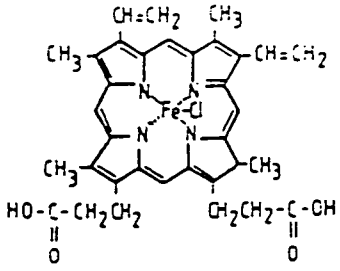

(10) HEMATIN

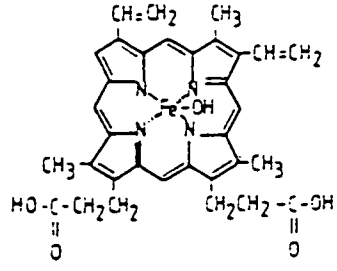

Figure 2.2: Structures of metalloporphyrins used in this project.

Conducting polymers are a new class of organic materials now being studied for gas sensing. This is partly a result of an ability to increase or decrease the conductivity by chemical 'doping' [Monkman, 1989]. Although values as high as $10^5 Scm^{-1}$ for polyacetylene [Kivelson et al, 1988 and Naarmann et al, 1987] and $350 Scm^{-1}$ for free standing polyaniline [Monkman et al, 1991] have been reported, the conductivity of many of these 'doped' compounds is not stable enough for gas sensing purposes over a prolonged period of time. Nevertheless, fast reversible changes in conductivity may be observed when exposed to vapours at room temperature [Barlett et al, 1989].

Unfortunately, most conductive polymers are intractable, which has limited their large scale exploitation. In order to circumvent this problem, some polymers have been synthesised directly over the measurement electrodes, for example polypyrrole [Ando et al, 1989], while others have been chemically modified so that they can be dissolved in an organic solvent. Examples of the latter materials include polythiophene [Punka et al, 1991] and polypyrrole [Ando et al, 1989], which have both been deposited over interdigitated electrodes by the Langmuir-Blodgett method. Amongst the various polymers known to date, the polyaniline family is special in that it can be cast from a solution of N-methylpyrrolidinone (NMP) to form thin films and can also be compressed into disk from powder [Monkman et al, 1991]. A list of some common conductive polymers is shown in figure 2.3. Polyaniline (PANi) was used in this work.

2.3 THIN FILM DEPOSITION TECHNIQUES.

There are numerous ways of depositing thin films on devices. In this work, three methods were adopted: Langmuir-Blodgett deposition; evaporation; and spin-coating. A qualitative description of each method is given below.

2.3.1 Langmuir-Blodgett Films

Langmuir-Blodgett (LB) films are ultrathin, highly ordered monolayers or multilayers of organic compounds on a solid substrate. The classic LB materials

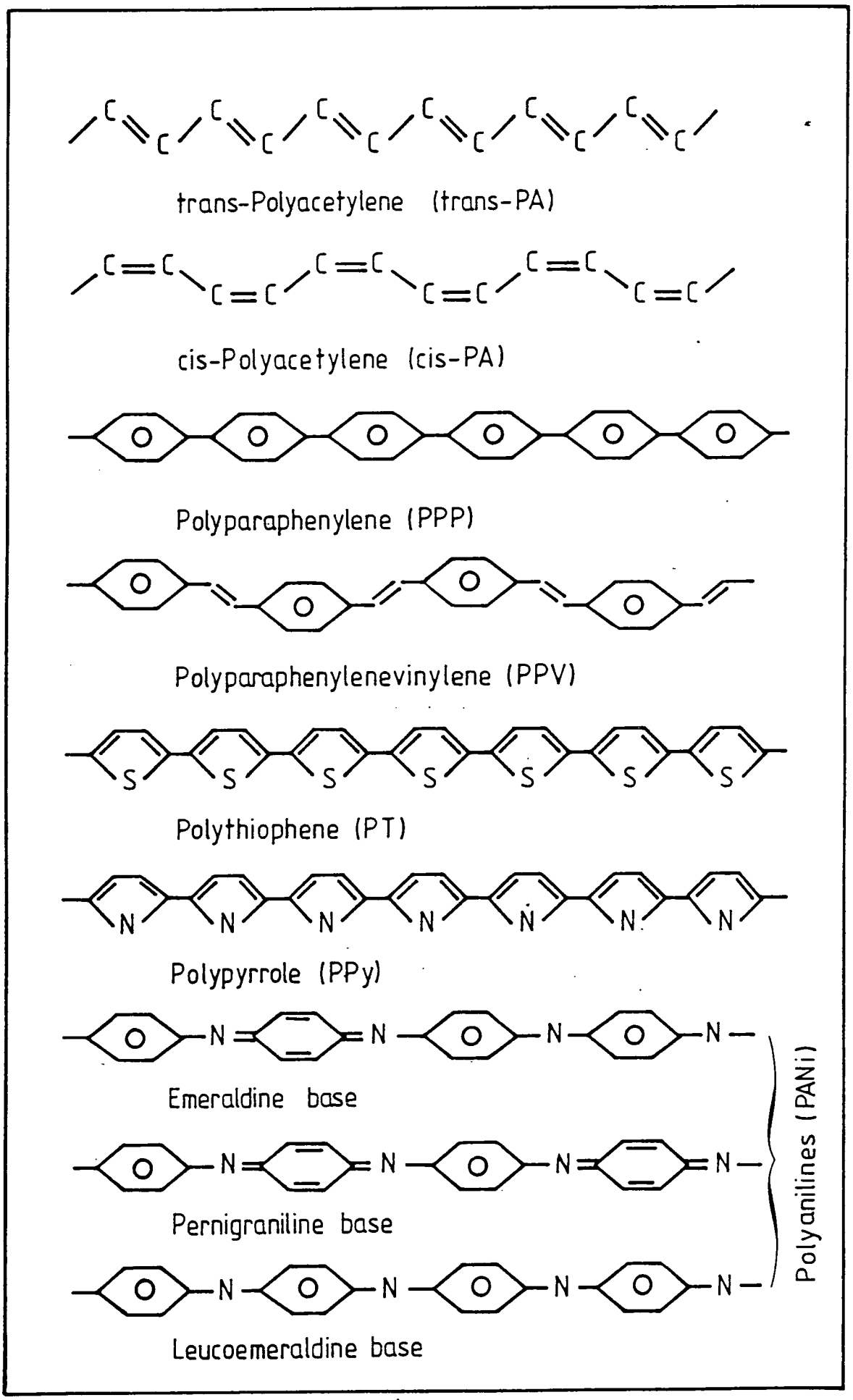

Figure 2.3: A list of some common conducting polymers.

are fatty acids and fatty acid salts, which possess both hydrophilic and hydrophobic chemical groups; these molecules are generally referred to as amphiphiles. LB films are produced by first taking a small quantity of the material, dissolved in a suitable solvent (such as chloroform), and applying it to a clean water surface. The solvent is allowed to evaporate leaving an expanded monolayer on the subphase surface. By slowly compressing the film, a close-packed two-dimensional analogue of a pure solid results. Simple materials, such as fatty acids, can exhibit a multiplicity of phases, similar to the mesophases of liquid crystals. The compressed monolayer can then be transferred to a solid substrate by moving the latter through the air-water interface. By this procedure, films can be built-up with controlled symmetry, thickness and molecular orientation.

The different phases exhibited on the water surface by stearic acid at 20±2°C are shown in the pressure versus area isotherm in figure 2.4 [Petty et al, 1987]. During compression, these phases can also be viewed by fluorescence microscopy [Weisenburg et al, 1991]. Although the compressed film is in a close-packed state, it must remain sufficiently fluid so as to facilitate its transfer from the subphase to the substrate. From the isotherm plot, the area per molecule can be calculated by extrapolation from the condensed phase to the line of zero pressure, provided the concentration, volume and the molecular weight of the material are known. By comparing this value with that obtained from space filling models, it is possible to speculate on the orientation of the molecules on the water subphase. However, problems can arise due to factors such as the dissolution of the material into the subphase, evaporation, film buckling or collapse [Gaines, 1966].

Monolayers for LB film deposition may be left under compression to investigate their stability. Fatty acids have been shown to be relatively unstable (continuous decrease in surface area under compression) but this effect can be reduced by the introduction of Cd^{2+} (or other divalent cations) ions into the subphase [Gaines, 1966]. Film deposition usually takes place at a fixed surface pressure which can be measured using a Wilhelmy plate suspended from a microbalance, as shown in figure 3.1 of the experimental section. When dipping is underway, this surface pressure is maintained by means of a feedback circuit. The quality of the deposited film is dependent on a large number of

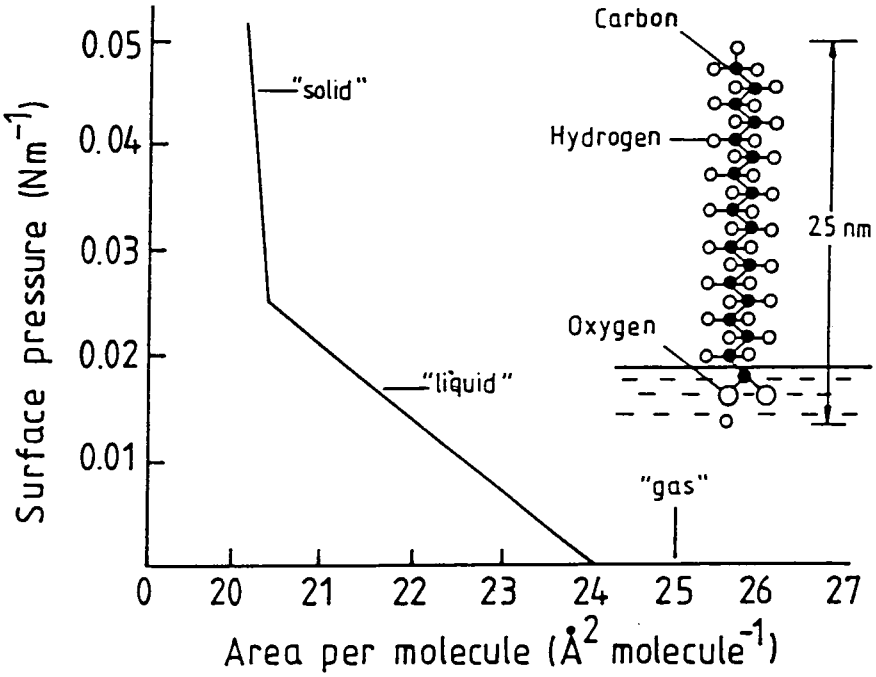

Figure 2.4: Surface pressure versus area isotherm of stearic acid at 20±2°C showing the different phases under different surface pressure. Inset shows the alignment of one molecule on the water subphase surface [Petty et al, 1987].

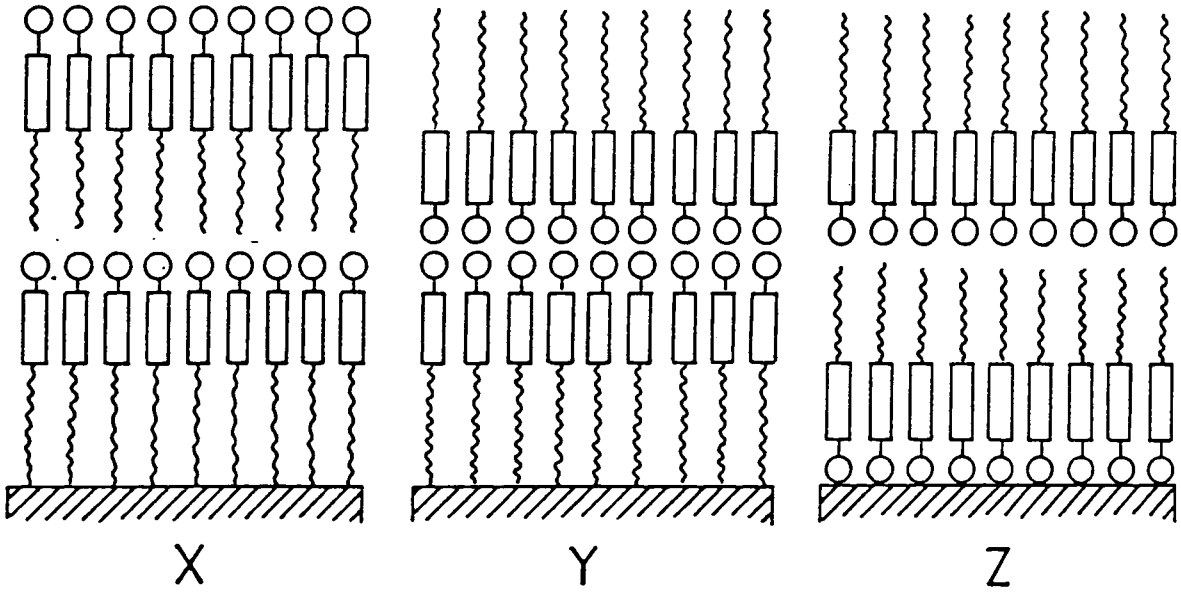

Figure 2.5: Common modes of LB film deposition on a substrate [Kalita 1991].

factors such as the cleanliness, temperature and pH of the subphase and the surface nature of the substrate. Lack of control of these variables can result in the films possessing a very high density of defects such as pinholes, microcollapses and grain boundaries [Lesieur et al, 1987].

The deposition of floating monolayers onto substrates can take three different forms: Y-, X- and Z-type deposition. These were first described by Blodgett [Blodgett, 1935] and are illustrated in figure 2.5. Y-type deposition refers to the situation in which a substrate picks up material from the subphase on every downstroke and upstroke. X-type deposition describes the pick up of material on downstroke only while Z-type deposition refers to the situation where the substrate picks up material only on the upstroke. Detailed discussions on the LB process, materials that can be used and possible applications of these ultrathin layers may be found in the books by Gaines, [1966] and Roberts, [1990].

2.3.2 Thermal Evaporation.

The deposition of thin films by thermal evaporation usually takes place at reduced pressure, typically below 10^{-1}mbar [Kaldis, 1975]. This is a non-equilibrium process, involving a series of steps: evaporation; transfer to substrate; condensation; nucleation and growth.

The conversion of the solid to a vapour phase may take place at temperatures below the melting point (sublimation). In the vapour phase, the molecules travel at high velocities making frequent collisions with others in the system. The statistical average distance these travel between collisions is called the mean free path, λ, which for one molecule is given by:

$$\lambda = \frac{kT}{2\pi\sigma^2 p} \qquad (2.1)$$

where σ is the molecular diameter and p the vapour pressure of the evaporant [Glaser et al, 1987]. From the above equation, it is evident that the mean free

path increases with a decrease in pressure in the system. For example, oxygen has a mean free path of 5.3cm at a pressure of 10^{-3}mbar which rises to 5300cm as the pressure is decreased to 10^{-6}mbar [Glaser et al, 1987].

As more material is evaporated, the vapour pressure of the evaporant above the source increases. When this pressure becomes greater than the equilibrium vapour pressure of the evaporant at the substrate temperature (supersaturation), condensation, the first step of crystal growth, results.

The condensed molecules are continuously adsorbed and coalesce to form stable two-dimensional nucleation sites that act as centres for growth of the film. The monolayer then grows into a film covering the entire substrate. A continuous film may not be formed until the film is many monolayers thick (e.g. several 10's of nm for metals). This contrasts with LB film deposition in which a complete coverage can be achieved at the nm level.

2.3.3 Spinning

One of the simplest and quickest means of depositing thin films is by spinning. Like the other deposition techniques discussed above, this process also involves a series of steps: dissolution of the material into a suitable solvent; filtration to remove particulate matter; finally, spreading and spinning at a predetermined speed and time. This process has been used widely in the electronics industry for the deposition of photoresist for silicon device processing. Materials deposited by this method do not require to be amphiphilic, as for Langmuir-Blodgett films. Moreover, for organic materials, there are reduced possibilities of material decomposition than for thermal evaporation. The quality of film deposited can be controlled by adjusting the substrate temperature during spinning, the spinning speed and time. Example of materials deposited by this method for sensing include some phthalocyanines [Crichley et al, 1992].

2.3.4 Other Deposition Techniques.

Electrochemical deposition has been used to deposit intractable materials such as conductive polymers directly onto interdigitated electrodes. This process, unlike evaporation, does not require vacuum and takes place at room temperature in solvent resistant cells, usually made of glass. Polymers which have been deposited by this method include polyaniline [Barlett et al, 1989 and Monkman, 1989], polythiophene [Hanawa et al, 1989] and polypyrrole [Takakubo, 1987]. Other thin film deposition methods include screen printing and casting, used for SnO_2 sensors [Geloven et al, 1991].

2.4 GAS SENSING TECHNIQUES.

There are four main methods for monitoring gas/material interactions. These can be broadly classified as electrochemical, optical, thermal and mass sensing techniques. The principles involved in each method will be outlined below with examples.

2.4.1 Electrochemical Sensors

There are three types of electrochemical sensors depending on the physical parameter being measured. These include potentiometric sensors for the measurement of a gas-induced potential difference generated at the device terminals, amperometric devices for current measurement over a potential range and conductimetric structures for conductivity measurement at a fixed potential. A typical electrochemical sensor is shown in figure 2.6. Depending on the biasing conditions, this device can be used as an amperometric, conductimetric or potentiometric sensor. It is often mounted in a cell with three electrodes, namely the sensing electrode that measures current flow, the reference electrode used to maintain stability and the counter electrode used as a reserved reference electrode. Such systems have been used mainly in the detection of species in solution, such as enzymes in biosensors [Miyahara et al, 1991]. Generally, these devices all function by the transfer of charge from the

electrode through the bulk of the sample into another phase which can be a solid or liquid [Janata, 1989]. As in the case of gas sensors, changes in potential or current resulting from the process of charge/mass transport through the sample are measured at the electrode.

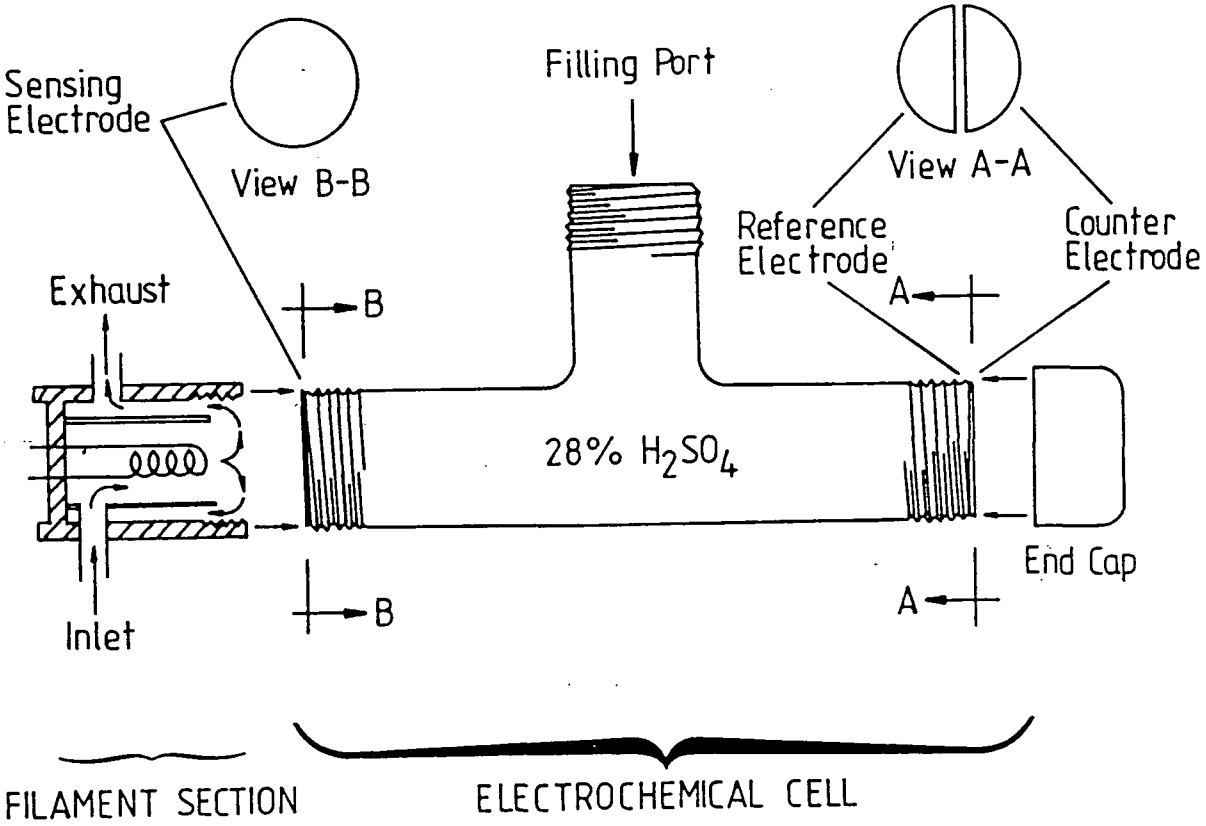

Figure 2.6: A typical electrochemical sensor showing the sensing, counter and reference electrodes [Stetter et al, 1984].

Potentiometric gas sensing devices are based on the fact that when a gas is introduced into the system, it dissolves into the electrolyte, via the porous metal electrode, where it is hydrolysed. This process induces a variation in the local ion-activity. This in turn produces a change in the measured potential between the sensing and reference electrodes which is used as the basis for gas sensing. The reaction involved has a typical time constant of 10-20 seconds [Janata, 1989].

The selectivity in such systems can be achieved by coating the electrode with a semi-permeable membrane and the sensitivity improved by making sure the

measured response is due entirely to one and only one reagent in the electrolyte, e.g. an H^+ ion. An example of such a system has been described for CO_2 [Janata, 1989] whereby, upon dissolution into water (used as the electrolyte), HCO_3^- and H^+ ions are produced. With a pH meter, the effect due to H^+ ion can be measured while changes in HCO_3^- ions are negligible because of a higher background concentration provided by $NaHCO_3$ added to the cell solution. Gas sensing in such systems can be described in terms of changes of the ionic concentration produced by the gas molecules.

Devices such as the suspended-gate field-effect transistor (SGFET) and the insulator-gate field-effect transistor (IGFET) can also be used as potentiometric gas sensors. These devices function on the same principles as the simple field effect transistor, described in detail in many text books, for example [Sze, 1981]. The gas is initially absorbed by the gate (porous metal or polymer), is ionised and then diffuses to the gate/insulator interface. This effectively produces a change in the work function of the metal which can be related to the concentration of the gas. Gases detected in this way include CO_2, NH_3, NO_x, SO_2, H_2S, HCN, Cl_2 and HF [Janata, 1989].

Amperometric gas sensors operate with the sensing electrode being either the cathode or the anode depending on whether electrons are being added or withdrawn from the sample. The cross-sectional view of a typical sensor is shown in figure 2.7. These have been used mainly as biosensors for the sensing of glucose level in the body [Fortier et al, 1990]. As with gas sensors, such devices have been used in conjunction with semi-permeable membranes through which a gas diffuses into an electrolyte. The gas is then either oxidized or reduced resulting in a change in steady-state current through the device within a scanned range of potential. The most widespread use for this type of sensor has been in the field of medicine for in-vivo oxygen sensing. Response times below 1.0 second may be achieved [Hurrell et al, 1988]. Other gases detected include benzene, acetic acid, chloroform, ethylacrylate, pyridine and nitro-benzene [Stetter et al, 1984].

Figure 2.8 shows a typical conductimetric gas sensor, generally referred to as a chemiresistor. A simple chemiresistor is made up of two electrodes for measurement of signal input/output and a gas sensitive layer on the surface of

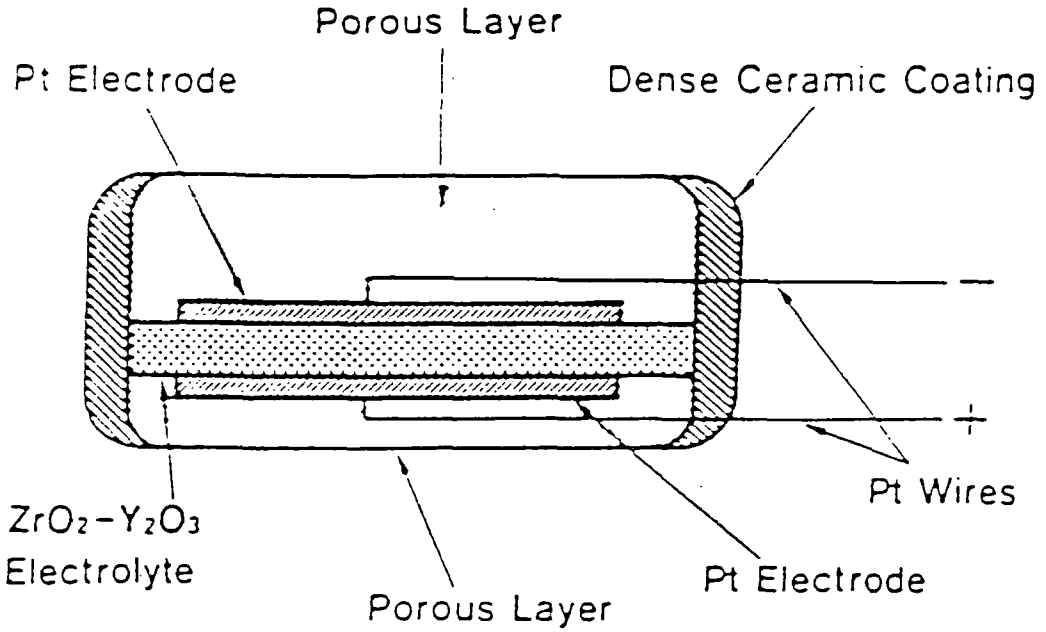

Figure 2.7: The cross section of an amperometric sensor [Göpel et al, 1991].

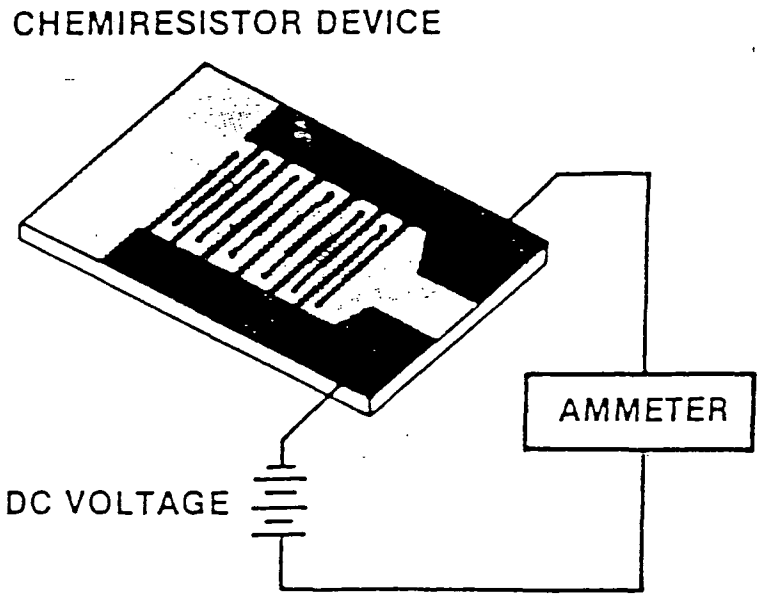

Figure 2.8: A schematic diagram of chemiresistor device.

the electrodes. For such devices, the most important parameters are the geometry of the electrode, the chemistry of the selective layer and the establishment of good ohmic contact. The electrodes are usually made of gold, nickel, platinum, palladium or aluminium with dimensions of the order of microns.

The conductance of the device [metal-electrode (1) / selective-layer /metal-electrode (2)] is measured either in a bridge arrangement or as a current. This is dependent on the mobility and concentration of charge carriers. When a gas molecule interacts with the selective layer, either of these parameters may change thus altering the conductivity. Such changes may be surface and/or bulk dominated and can be reversible. The conductivity of the selective layer can be given as:

$$\sigma = q\mu_p[p] + q\,\mu_n[n] \qquad (2.2)$$

where q is the electronic charge, [p] the hole concentration, [n] the electron concentration, and $\mu_{p,n}$ the hole,electron mobilities.

2.4.2 Optical Sensors.

Optical sensors are a result of the interaction of electromagnetic waves with matter. These can be based on infrared absorption or (ultraviolet/visible absorption), surface plasmon resonance, evanescent waves, chemiluminescence and interferometry.

Infrared sensors are based on the fact that every compound (gas, liquid or solid) with a covalent bond and a net dipole moment interacts with infrared radiation at a characteristic frequency. When a gas molecule interacts with a chemically sensitive layer, the result may be the formation of new, and/or suppression of old, absorption bands. The difference observed in the spectrum can be related to the site of interaction and the nature of the reaction. Sensitivity in this system is high and selectivity may be enhanced through restriction of the wavelength region, using narrow band optical filters, sources and detectors.

Gases detected include CO, CH_4, CO_2 and NO_x [Hanawa et al, 1989 and Li et al, 1990].

Surface plasmon resonance (SPR) has only recently been used for gas sensing, although other work reported has been in the field of medicine for the detection of antigen-antibody interactions [Flanagan et al, 1984, Fontana et al, 1990 and Liedburg et al, 1983]. Gas sensing using this technique is based on the interaction of the gas molecule with a selective layer on a metal surface. This interaction will produce changes in the refractive index and/or thickness of the overlayer. This in turn changes the coupling efficiency of an incident light beam to surface plasmons, which results in a change in reflectivity. Gases detected include halothanes [Nylander et al, 1982/83] and NO_x [Lloyd et al, 1988 and Zhu et al, 1990], both at room temperature.

Evanescent wave gas sensors are based on the fact that when light travels through a waveguide, e.g. an optical fibre, part of the radiation travels as an evanescent wave in the medium outside the guide. If this medium contains absorbing species at the wavelength of the travelling light, then there will be a reduction in the transmitted light arriving at the detector. From this measurement, the concentration of the absorbing species can be inferred from the local energy loss. Gases detected include methane and combustion products [Janata, 1989].

Chemiluminescence is a fairly new optical technique for gas sensing, used mainly in medicines for in-vivo blood analysis [Wolfbeis et al, 1988]. The method involves coating the tip of an optical fibre with, for example, an immobilised fluorescent pH indicator. The fibre is put into a buffer solution which is trapped in a gas permeable polymer matrix. The fibre guides a light beam to the sensing tip and returns the emitted wavelength to an optical detector. When a gas dissolves in the buffer solution, species are produced which change the intensity of fluorescent light. The changes recorded by the detector can be used to characterize the gas. Gases that have been detected by this method include CO_2 and O_2 [Wolfbeis et al, 1988].

2.4.3 Thermal Sensors

Devices used as thermal gas sensors are based on measuring the heat evolved during the interaction of the gas molecule with a chemically selective layer. These include pyroelectric and catalytic devices which are designed by depositing the selective layer on a thermal probe. In this assembly, the heat evolved in its interaction with the gas can be measured, either as a change in temperature of the sensing element or as a change in the heat flux through it. Enzymatic reactions represent the ideal application, because they combine a high degree of specificity with amplification. Gases detected include mainly combustion products [Janata, 1989].

2.4.4 Mass Sensors

The most common mass gas sensors are piezoelectric or surface acoustic wave devices (SAWs). The heart of the piezoelectric device is a quartz crystal oscillator processed into a so-called 'AT' cut [Janata et al, 1985]. The resonance frequency of the crystal oscillator is sensitive to changes in the crystal mass. By coating the crystal with a gas sensitive layer, the adsorption and desorption of gas molecules can be monitored as changes in its resonant frequency. These changes can then be related to the mass of the gas, although the process is rather complex. Hence these devices are sometimes referred to as gravimetric sensors. The first reported gas sensors were by King et al, in 1968. Since that time progress in this field has been growing. Gases detected include: SO_2, NH_3, H_2S, HCl, and H_2O [Hlavay et al, 1980].

The response of SAW gas sensors can be monitored in the same way as for the piezoelectric sensors, in terms of changes in the resonant frequency. The physics of this device has been described in detail [Wohltjen, 1984] and will not be repeated here. SAW structures have been used for chemical sensing because of their small size, low cost, ruggedness, sensitivity and adaptability to a wide range of vapours. They can be introduced as part of a delay line or interfaced with other devices for the detection of gases such as NO_x [Snow et al, 1989].

2.5 SUMMARY

A review of gas sensing materials and their modes of deposition have been presented. The materials discussed have ranged from inorganics to organics. The potential advantages of using organic materials for gas sensing have been discussed. Amongst the reviewed methods of thin film deposition, the LB technique is the most promising in terms of the control of film architecture, while spinning and thermal evaporation techniques are more widely used. Electrochemical sensors have been shown to represent the largest class of potential gas sensors. The operation of these devices could be significantly improved by the availability of new materials and by better signal processing techniques.

REFERENCES

Ackelid, U. and Petersson, L.G. : Sensors and Actuators B, **3** (1991) 139-146

Ando, M., Watanabe, Y., Iyoda, T., Honda, K. and Shimidzu, T. : Thin Solid Films, **179** (1989) 225-231

Archer, P.B.M., Chadwick, A.V., Miasik, J.J., Tamizi, M. and Wright, J.D. : Sensor and Actuators, **16** (1989) 379-392

Baker,S. : PhD thesis, Durham University,1985

Baker, S., Roberts, G.G. and Petty, M.C. : IEE Proceedings, **130** (1983) 260-263

Barlett, P.N. and Ling-chung, S.K. : Sensors and Actuators, **20** (1989) 287-292

Blodgett, K.B. : J. Am. Chem. Soc., **57** (1935) 1007

Catalano M.M., Crossley, M.J., Harding, M.M. and King, L.G. : J. Chem. Soc., Chem. Commun. (1984) 1535-1536

Coles, G.S. and Williams, G. : Sensors and Actuators B, **3** (1991) 7-14

Crichley, S.M., Willis, M.R., Maruyama, Y. and Bandow, S. : Abstracts of the 6th International Conference on Electrical and Related Properties of Organic Solids, Italy, May (1992) 107

Flanagan M.T. and Pantell, R.H. : Electr. Letters, **20** (1984) 968-969

Fontana, E., Pantell, R.H. and Strober, S. : Applied Optics, **29** (1990) 4694-4704

Fortier, G., Brassard, E. and Bélanger D. : Biosensors and Bioelectronics, **5** (1990) 473-490

Gadner, J.W., Shurmer H.V. and Corcoran, P. : Sensors and Actuators B, **4** (1991) 117-125

Gaines Jr., G.L. : 'Insoluble Monolayers at Liqiud-Gas Interface', Interscience, New York, 1966

Geloven, P.V., Honore, M., Roggen, J., Leppavuori, S. and Rantala, T. : Sensors and Actuators B, **4** (1991) 185-188

Gentry, S.J. and Walsh, P.T. : Sensors and Actuators, **5** (1984) 229-238

Gentry, S.J. and Walsh, P.T. : Sensors and Actuators, **5** (1984) 239-251

Gerblinger, J. and Meixner, H. : Sensors and Actuators B, **4** (1991) 99-102

Glaser A.B; and Sharp, S. : 'Integrated Circuit Engineering', John Wiley and Sons, New York, 1987

Göpel, W., Hesse, J. and Zemel, J.N. (eds), Sensors 'A Comprehensive Survey', VCH, Weinheim, Germany, 1991

Hanawa, T., Kuwabata, S., Hashimoto, H. and Yoneyama, H. : Synthetic Metals, **30** (1989) 173-181

Hlavay, J. and Guilbault, G.G. : Analytical Chem., **49** (1980) 1890-1898

Hurrell, H.C. and Abruna, H.D. : Analytical Chem., **60** (1988) 254-258

Janata, J. : 'Principles of Chemical Sensors', Plenum Press, New York and London, 1989

Janata, J. and Huber, R.J. : 'Solid State Chemical Sensors', Acedemic Press Inc., New York, 1981

Jones, A., Jones, T.A., Mann, B. and Firth, J.G. : Sensors and Actuators, **5** (1984) 75-88

Kaldis, E. : 'Liquid Layers on Vapour Grown Crystals', in 'Crystal Growth and Characterisation'., Ueda R. and Mullin J.J. North (eds), Holland Publish., Company (1975) 225-242

King Jr., W., Camilli, C.T. and Findeis, A.F. : Analytical Chem., **40** (1968) 1330-1335

Kivelson, S. and Heeger, A. : Synthetic Metals, **22** (1988) 371-384

Lalauze, R., Breuil, P. and Pijolat, C. : Sensors and Actuators B, **3** (1991) 175-182

Lecomte, C., Baudin, C., Berleur, F., Ruaudel-Teixier, A., Momenteau, M. and Barraud, A. : Thin Solid Films, **133** (1985) 103-112

Lesieur, P., Barraud, A. and Vandevyver, M. : Thin Solid Films, **152** (1987) 155-164

Li, J.P., Tredgold R.H. and Jones, R. : Thin Solid Films, **186** (1990) 167-176

Liedberg, B., Nylander, C. and Lunström, I. : Sensors and Actuators, **4** (1983) 299-304

Lloyd, J.P., Pearson, C. and Petty, M.C. : Thin Solid Films, **160** (1988) 431-443

Miasik, J.J., Hooper, A. and Tofield, B.C. : J. Chem. Soc., Faraday Trans., **82** (1986) 1117-1126

Miyahara, Y., Tsukada, K. and Miyagi, H. : Sensors and Actuators B, **3** (1991) 287-293

Monkman, A.P. : PhD thesis, London University,1989

Monkman, A.P. and Adams, P. : Synthetic Metals, **40** (1990) 87-96

Naarmann, H. and Theophilou, N. : Synthetic Metals, **22** (1987) 1-8

Nylander, C., Liedberg, B. and Lind, T. : Sensors and Actuators, **3** (1982/83) 79-88

Petty, M.C. : in 'Polymer Surfaces and Interfaces', Feast, J. and Munro, H. (eds), John Wiley & Sons Ltd (1987) 163-187

Petty, M.C. and Roberts, G.G. : in 'Encyclopedia of Material Science and Engineering', Bever, M.B. (ed), Pergamon Press, Oxford (1987) 2494-2496

Poteat, T.L. and Lalevic, B. : IEE Trans. on Electr. Devices, **ED-29** (1982) 123-129

Punka, E., Rubner, M., Hettinger, J.D., Brooks, J.S. and Hannahs, S.T. : Physical Review, B, **43** (1991) 9076-9086

Raju, A.R. and Rao, C.N.R. : Sensors and Actuators B, **3** (1991) 305-310

Sadaoka, Y., Jones, A. and Gopel, W. : J. Mat. Sc. Letters, **8** (1989) 1095-1097

Schierbaum, K.D., Kirner, U.K., Geiger, J.F. and Gopel, W. : Sensors and Actuators B, **4** (1991) 87-94

Snow, A.S. and Barger, W.R. : 'Phthalocyanine Films in Chemical Sensors', in Phthalocyanines: Properties and Applications', Leznoff, C.C. and Lever, A.B.P. (eds) (1989) 345-392

Stetter, J.R., Zaromb, S. and Findlay, Jr., M.W. : Sensors and Actuators, **6** (1984) 269-288

Sze, S.M; 'Physics of Semiconductors' Wiley-interscience Publ., New York, 1981

Takakubo, M. : Synthetic Metals, **18** (1987) 53-58

Tanaka, K., Morimoto, S., Sonoda, S., Matsuura, S., Moiya, K. and Egashira, M. : Sensors and Actuators B, **3** (1991) 247-253

Tredgold, R.H., Young, M.C., Hodge, P. and Hoofar, A. : IEE Proceedings, **132** (1985) 151-156

Van Ewyk, R.L.V., Chadwick, A.V. and Wright, A.D. : J. Chem., Society, Faraday Trans, **76** (1980) 2194-2205

Wayland B.B. and Mohajer, D. : J. Amer. Chem. Soc., **93** (1971)5295

Weber, W.H. : Physical Review Letters, **39** (1977) 153-156

Wlodek, S., Colbow, K. and Consadori, F. : Sensors and Actuators B, **3** (1991)123-128

Wolfbeis, W.S., Leiner, M.J.P., Weis L.J. and Ziegler, W.E. : Analytical Chem., **60** (1988) 2028-2030

Wolhltjen, H., Barger W.R., Snow, A.W. and Jarvis, N.L. : IEEE Trans., on Electr., Devices, **ED-32** (1985) 1170-1174

Wright, J.D. : Material Science, **13** (1987) 295-298

Xu, C., Tamaki, T., Miura, N. and Yamazoe, N. : Sensors and Actuators B, **3** (1991) 147-156

CHAPTER THREE

EXPERIMENTAL TECHNIQUES

3.1 PREFACE

This chapter explains the various methods employed to deposit and characterize the thin organic films. In section 3.2, the deposition methods are described with more emphasis on novelty than a repeat of the standard procedures. This is followed in section 3.3 by an analysis of the techniques used to characterize the layers under different gaseous environments. These include ultraviolet/visible spectroscopy, reflection-absorption Fourier transform infrared spectroscopy (RAIRS), surface plasmon resonance (SPR) and dc conductivity. Film morphology was also studied in vacuum using scanning electron microscopy (SEM).

3.2 FILM DEPOSITION TECHNIQUES

The thin films used in this work have been produced by three main techniques: LB deposition, thermal evaporation and spinning. The experimental procedures are described in the following sections.

3.2.1 Langmuir-Blodgett Films

The deposition of LB films was undertaken using troughs designed and built in Durham and housed in a microelectronics clean room. The design of a typical trough used in this work is given in figure 3.1. This shows the glass fibre coated PTFE barrier, driven by a low gear electric motor, and a Wilhelmy plate that is linked to a microbalance for surface pressure monitoring. The steps involved in LB film deposition are described below.

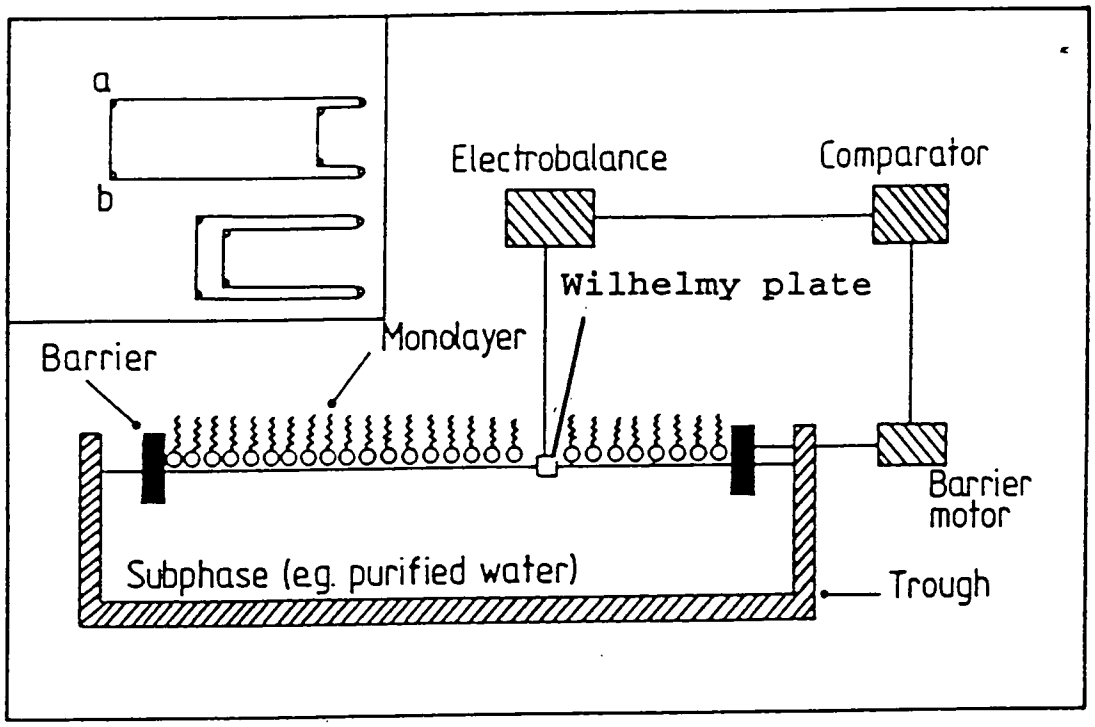

Figure 3.1: A schematic diagram of a Langmuir-Blodgett film trough. Inset shows a plan view of barriers (a) fully opened (b) fully closed.

a. Materials

Materials studied for LB film formation included lutetium bisphthalocyanine, cobalt (II) 5,10,15,20-tetrakis (4-methoxylphenyl) 21H, 23H-porphine (CMTPP) and polyaniline; the chemical structures of these compounds are shown in figures 2.1, 2.2 and 2.3. CMTPP was obtained from Aldrich Chemicals and used without further purification. Lutetium bisphthalocyanine ($LuPc_2$) was obtained from the P.N.Lebedev Institute, Moscow and was also used without further treatment. Polyaniline was synthesised in-house at Durham.

b. Sample Preparation

Organic solvents used included Aristar chloroform, Aristar trichloroethane, acetic acid from BDH and N-methylpyrrolidinone (NMP) from Aldrich

Chemicals. These solvents all had purity standards of more than 99.99%, as quoted by the manufacturers.

A solution of CMTPP was prepared by dissolving 10mg of the material into 10ml of Aristar chloroform. The solute dissolved completely without ultrasonic agitation being used.

The lutetium bisphthalocyanine was provided already dissolved in chloroform. At a concentration of $0.38gl^{-1}$, its solution appeared green in reflection.

A solution of PANi for LB film deposition was prepared as follows. A small quantity of acetic acid was first mixed with 'undoped' polyaniline in a (acid : polyaniline) weight ratio of 1:10. The acid was completely absorbed leaving the polymer without any visible colour change. The solvent used was a mixture of chloroform:NMP in a 1:5 weight ratio. 0.1-1mg of the solid mixture was dissolved in 10ml of this solvent and given an ultrasonic agitation for 30 minutes to aid its dissolution. Rigidity in polyaniline is due mainly to H-bonding between chains. The purpose of the acetic acid was to weaken the degree of H-bonding between chains and so facilitate dissolution and spreading. The solution was blue in reflection and formed suspensions for samples with more than 20% by weight of acetic acid. When left in air for two days, the solution changed colour in reflection, first from the characteristic blue to purple, then to colourless after about 2 weeks. An alternative approach to prepare a solution of PANi for LB films, used just once, involved mixing polyaniline, dissolved in NMP, with tricosanoic acid dissolved in chloroform. The polymer formed a suspension in this mixture that appeared green in reflection, indicating some protonation of PANi had occurred.

c. Substrate Preparation

LB films were deposited onto a wide range of substrates including glass microscope slides, metallized glass slides (gold or nickel on silver) and printed circuit board (PCB) material. The glass substrates were cleaned using Decon 90 and deionised water, sometimes with the aid of ultrasonic agitation [Baker, 1985 and Tredgold et al, 1983]. Metal-coated glass slides were prepared by evaporating a predetermined thickness of the metal using an Edwards 306

evaporation system. This took place under high vacuum ($\approx 10^{-6}$mbar), obtained after about 3 hours pumping. When the high vacuum had been achieved, the metal was heated resistively with the substrate shutter closed. This procedure was used to drive off contaminants from the metal surface. The shutter was then opened and a fixed amount of the metal was deposited on the glass slides, with a typical deposition rate of about 0.5nms^{-1}. The thickness of the deposited metal was measured insitu by a crystal oscillator linked to a thickness monitor. Approximately 50nm of silver and 20nm of gold were used for surface plasmon resonance and infrared measurements. Thicker layers were used as electrodes (40nm).

The PCB substrate was prepared as follows. Using PCB design software (EasyPc), a mask of interdigitated electrodes (33 or 14 electrode pairs) was designed on a substrate of length 75mm, with 15mm electrode overlap length and a finger spacing of 0.38mm, as shown in figure 3.2. The dimensions were chosen to facilitate the measurement of low conducting materials as well as increasing the sensitivity of the chemiresistor. The circuit was printed on A4 paper and then photocopied onto a transparent sheet that served as the mask. The pattern of the mask was developed onto a positive photoresist-covered copper plate by exposure to ultraviolet light for 20 minutes. The exposed plate was put into a solution containing $FeCl_3$ for copper etching. After 4 minutes, it was rinsed twice in deionised water and allowed to dry. After drying, the photoresist was removed using acetone and the PCB further rinsed in deionised water. The copper electrodes were gold-plated by electrolysis, using a solution of gold mixed with potassium cyanide as the electrolyte. This was followed by rinsing and then final drying. All electrical measurements were undertaken using this electrode structure with 14 and/or 33 pair of electrodes depending on the physical dimensions of the substrate holder.

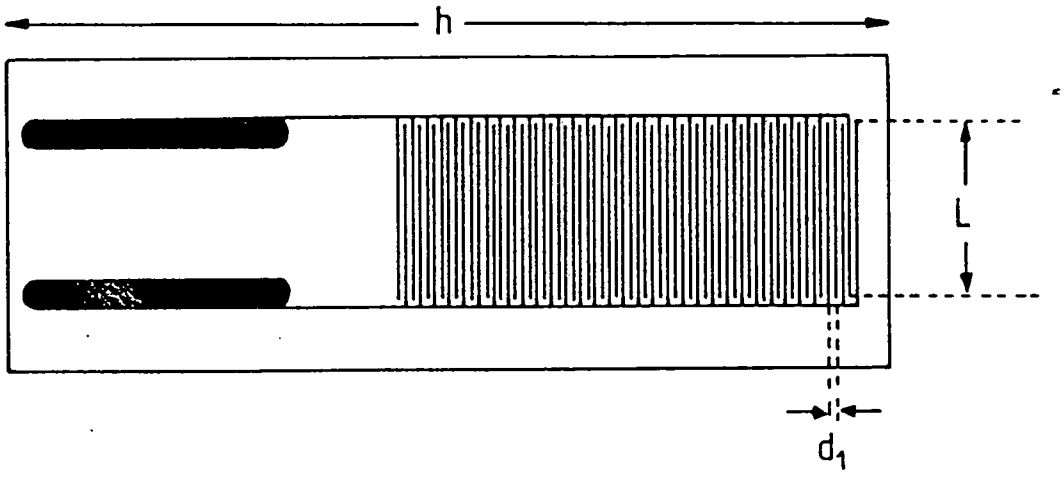

Figure 3.2: A schematic diagram of the interdigitated electrode structure used for dc conductivity and gas sensing measurements, d_1=0.38mm, L=15mm and h=75mm.

d. Subphase Preparation

The subphase used for this work was ultra pure deionised water, obtained using an Elgastat purification system. This operated by recycling water through a reverse osmosis unit, two deionising cartridges, a carbon filter and an UV steriliser to give water of resistivity ≈ 18MΩcm and total organic content (TOC) in the 10's parts per billion (ppb) range. A clean glass trough was filled with the deionised water and the cleanliness of the subphase surface investigated by compressing and expanding the working area between the PTFE barrier and recording any change in the surface pressure. For a large change of surface pressure, the barrier and water surface were cleaned using a suction pipe. This process was repeated until the change in surface pressure was minimised. Usually, with a change in surface pressure of less than 0.5mNm^{-1} between compression and expansion, the subphase would be considered 'clean'.

e. Film Spreading and Deposition

Following the cleaning procedure, a known quantity of the prepared solution (typically 100μl) was spread onto the subphase in the working area defined by the barrier. A built-in fan was switched on for 5 minutes to allow for solvent evaporation.

After spreading, the film was slowly compressed and expanded at a typical rate of $2.0cm^2s^{-1}$ and the variation of the surface pressure with the area of the trough occupied by the molecules was recorded (isotherm). Most of the materials exhibited a hysteresis type plot upon compression and expansion. From the isotherm, a suitable surface pressure was chosen to investigate the stability of the floating film over a period of time. A suction test was also used to investigate its rigidity [Kalita, 1991]. This was undertaken by removing a small quantity of the material from the subphase surface.

The floating film was transferred to the substrate by the LB vertical dipping method. The substrate was attached to the dipping head and the film deposition undertaken at speeds of between $0.03\text{-}0.1mms^{-1}$. For successful film transfer, it was sometimes necessary to use a high speed as well as to allow time (about 10 minutes) for drying between dip cycles (especially for the first cycle). Evidence for deposition was provided by monitoring the changes in surface area of the monolayer as the substrate was raised and lowered. From the plot of surface area (at a fixed surface pressure) versus time, the transfer ratio T_{ratio} was calculated using the formula:

$$T_{ratio} = \frac{A_s}{A_f} \tag{3.1}$$

where A_f is the coated area of the solid substrate and A_s is the decrease in the area occupied by the monolayer on the water surface.

3.2.2 Thermal Evaporation

The equipment used for evaporation is sketched in figure 3.3. This was an Edwards 6E4 system possessing an evaporation chamber of diameter 30cm, employing a water cooled diffusion pump and having a base vacuum level of 10^{-3}mbar. The system was dedicated to polyaniline so as to minimise cross contamination. A series of holes cut into the substrate holder directly above the evaporation crucible, served as the mask. The crucible used was a special glass cuvette from Multilab having a port at its base for a thermocouple. On top of the crucible was a shutter which could be used to control the evaporation. The source temperature was maintained by means of a Radio Spares temperature controller. The system was vented to air circulating in a fume cupboard.

Substrates used were the same as those described above for the LB deposition. Before any evaporation, the system was baked out for about 2 hours at a temperature of 350°C in order to burn off any surface contamination.

A powder of the emeraldine base form of polyaniline was the only material used (see table 3.1). This was chemically synthesised in-house with high reproducibility, molecular weight and purity [Monkman et al, 1991]. 40mg of the material was weighed into the boat then placed into the system and pumped down. When the pressure in the chamber was $\approx 10^{-3}$mbar and stable, the temperature of the boat was raised to 400°C by increasing the current flow through the heating coils. Once equilibrium had been achieved (constant pressure), the shutter was opened and film deposition carried out for a fixed length of time. After evaporation, the system was allowed to cool down to room temperature (~5 hours). It was then opened to air and the substrates were removed.

The films initially appeared colourless on glass microscope slides, indicating the film was in the leucoemeraldine state [Chevalier et al, 1989]. However upon prolonged exposure to air (at least 2 weeks), the film changed colour to purple and eventually became blue, similar to the emeraldine base form of polyaniline. This effect was almost certainly due to the oxidation of the film in the atmosphere.

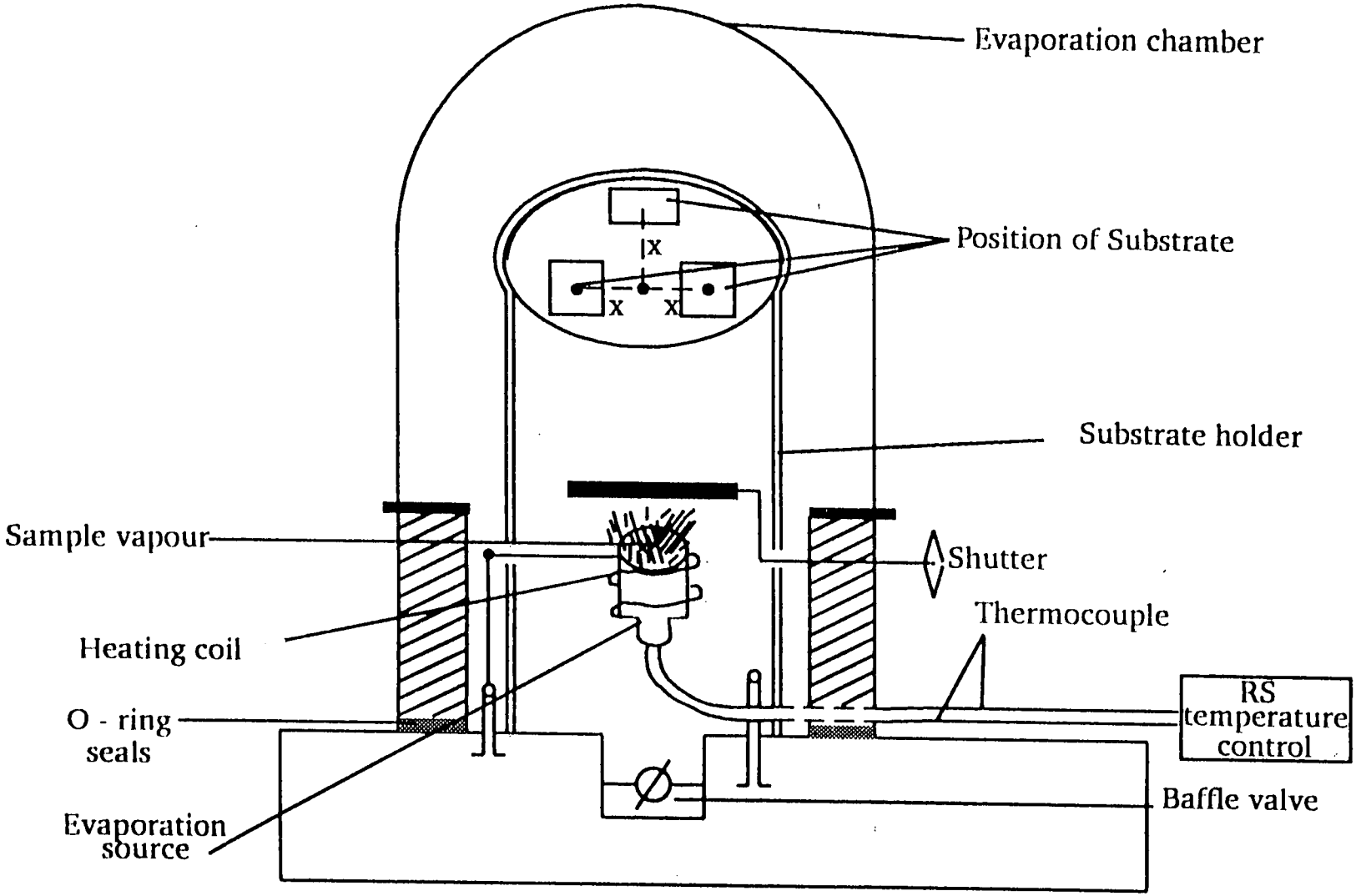

Figure 3.3: Vacuum evaporator for organic thin films.

3.2.3 Spinning

Spinning is one of the most widely used methods for the deposition of organic materials (e.g., photoresists for silicon device processing). In this project, spinning has been undertaken using a Dynapert PRS 14E model spinner to deposit polyaniline films onto glass, metallized glass and PCBs. A vacuum line was used to keep the substrate fixed at spinning speeds of up to 10,000rpm.

Solutions of polyaniline, in concentrations of 0.1%, 1% and 10% by weight of the polymer:NMP, were prepared and placed in an ultrasonic bath for 30 minutes. All three solutions appeared blue in reflected light. These were each spun onto glass, initially at an arbitrarily chosen speed of 3,000rpm for 30 seconds. The spinning time was pre-set automatically on the instrument.

Spun films of polyaniline on glass were then transferred to a vacuum oven at 10^{-2}mbar to evaporate any remaining solvent. The samples were left in the oven at a temperature of 120°C for 10 minutes. After this time, most of the NMP (solvent) had evaporated.

An initial assessment of the films was carried out using optical microscopy in order to check for uniformity, pinholes and lumps of undissolved polymer. Ultraviolet/visible spectroscopy was also used to look for any evidence of material degradation (due to the elevated temperature of the vacuum oven). These initial experiments were then used to select the best concentration of the starting solution for film deposition. For glass substrates, the 1% solution gave the best results in terms of film uniformity and absence of pin holes.

For consistency, a fresh 1% polyaniline solution was prepared for each experiment. Deposition on interdigitated electrodes was accomplished by masking off the electrode contacts using adhesive tape fastened to the back of the substrate. Spinning onto gold and silver produced very patchy films which were too thick for surface plasmon resonance measurements. However, similar samples on gold were used for reflection-absorption infrared spectroscopy.

A summary of the various thin film deposition techniques used in this work is shown in table 3.1 below:

Materials	Thin Film Deposition Methods		
	LB	Thermal Evaporation	Spinning
PANi	yes	yes	yes
$LuPc_2$	yes	no	no
CMTPP	yes	no	no

Table 3.1: A summary of the thin film deposition techniques.

3.3 FILM CHARACTERIZATION METHODS

There are many techniques for the characterization of thin films. In this work, some methods relevant to gas sensing were selected and used to determine the characteristics of the film before and after exposure to a gas.

3.3.1 Ultraviolet/Visible Spectroscopy

The optical absorption spectra were measured on a Perkin-Elmer Lambda 19 ultraviolet/visible/near-infrared spectrophotometer. The ultraviolet/visible spectra were recorded for thin films of the materials, deposited by the methods

outlined above, on glass and fused quartz slides. An uncoated slide placed in the reference beam was used for background correction. Initially, for any sample obeying the Beer-Lambert equation in solution, the absorbance A is given by

$$A = \varepsilon_i cd \tag{3.2}$$

where ε_i is the extinction coefficient, c the concentration of the solution, and d the path length. For an LB film,

$$cd = N\psi \tag{3.3}$$

where N is the number of layers and ψ the surface density of the molecules. From the above equations it can be seen that the absorbance is linearly dependent on the number of layers in the LB film. Hence by measuring the absorbance at a fixed wavelength, the reproducibility of the film deposition process could be ascertained.

3.3.2 Surface Plasmon Resonance

a. Theoretical Background

Detailed theoretical accounts of surface plasmon oscillations have been reported previously [Agranovich et al, 1982, Boardman, 1982; Fiebelman et al, 1989 and Wallis et al, 1986]. A brief review is given below.

When an electromagnetic wave passes through a polarizable medium (e.g. dielectric), it becomes coupled to the medium through the polarization it induces. This coupling mode of excitation is called a polariton. In the case where such a medium is an electron plasma, it is called a plasmon-polariton. It can be bulk or surface dominated. Bulk plasmon-polaritons are purely plasmon in content while surface plasmon-polaritons possess a plasmon and a photon component.

In this work, our interest is mainly in surface plasmon-polaritons (SPPs), which, will later on be used for gas sensing. SPPs have been described as plane surface waves of electron plasma at the interface between two media of different permittivities. Associated with the SPPs are electromagnetic fields which may be described using Maxwell's equations. These fields are sometimes called surface electromagnetic waves (SEW) and travel parallel to the interface between the two media, and decay exponentially normal to the interface over a distance of a few nanometers (see figure 3.4). Such fields exist only in the interface of two media with dielectric functions ε_1 and ε_2 of opposite signs.

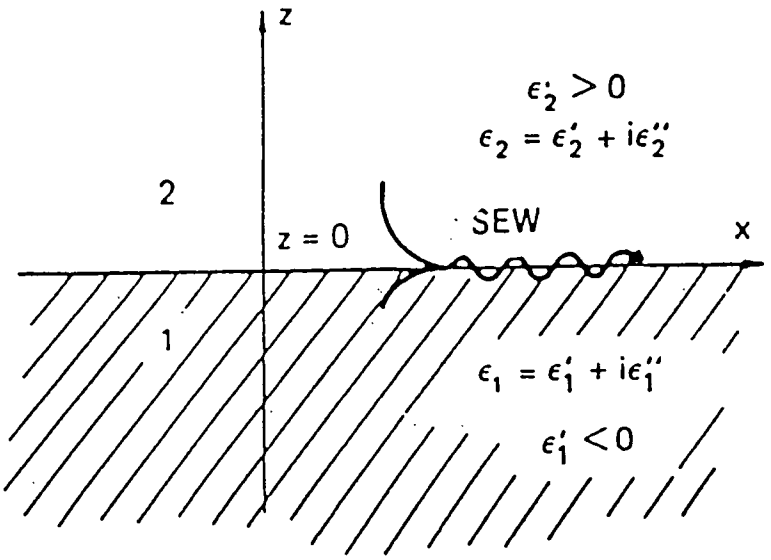

Figure 3.4: A two-dimensional illustration of the electromagnetic fields at the interface of two media with dielectric functions ε_1 and ε_2.

Surface plasmons-polaritons, henceforth called surface plasmons, can be described in terms of a guided electromagnetic wave [Nylander et al, 1982]. They cannot normally be excited with photons incident on the metal-dielectric interface because energy and momentum conservation cannot be obtained simultaneously (the dispersion relation for surface plasmons and incident light do not intersect).

Application of the electric and magnetic boundary conditions to Maxwell's equations shows that surface plasmons are transverse magnetic waves. As a

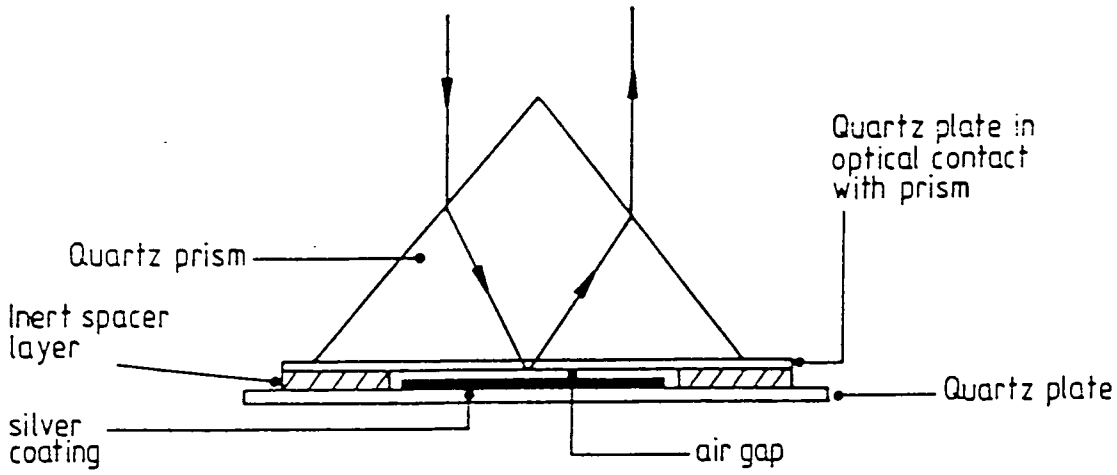

Figure 3.5a: Otto system configuration for excitation of surface plasmon resonance interactions

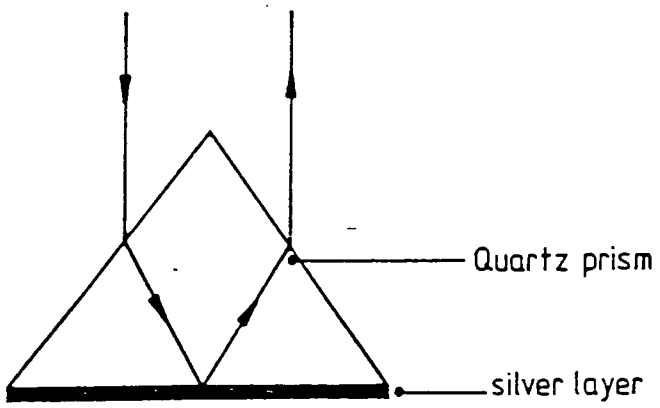

Figure 3.5b: Kretschmann configuration for the excitation of surface plasmon resonance.

result, excitation is only possible using p-polarized waves since a component of the electric field lies in the plane incidence.

Using the arrangements demonstrated by Otto, in figure 3.5.a, and by Kretschmann, figure 3.5.b, frequencies can be selected to excite these waves from the front or back surface of a metal of the correct thickness; ≈50nm in the case for silver [Fontana et al, 1990]. In the Otto configuration, incidence of p-polarized light produces an evanescent field at the quartz prism/air interface which becomes coupled to the surface plasmons through a dielectric (usually air) interface. In the Kretschmann arrangement, used in this work, the evanescent field is produced at the interface between the metal and the glass prism. This field penetrates through the thin metal film, coupling to the surface plasmons.

Theoretically, the thickness of the metal determines the fraction of p-polarized incident light which is coupled to the surface plasmons; maximum coupling is observed as a sharp drop in the intensity of the reflected light to zero as shown in figure 3.6.

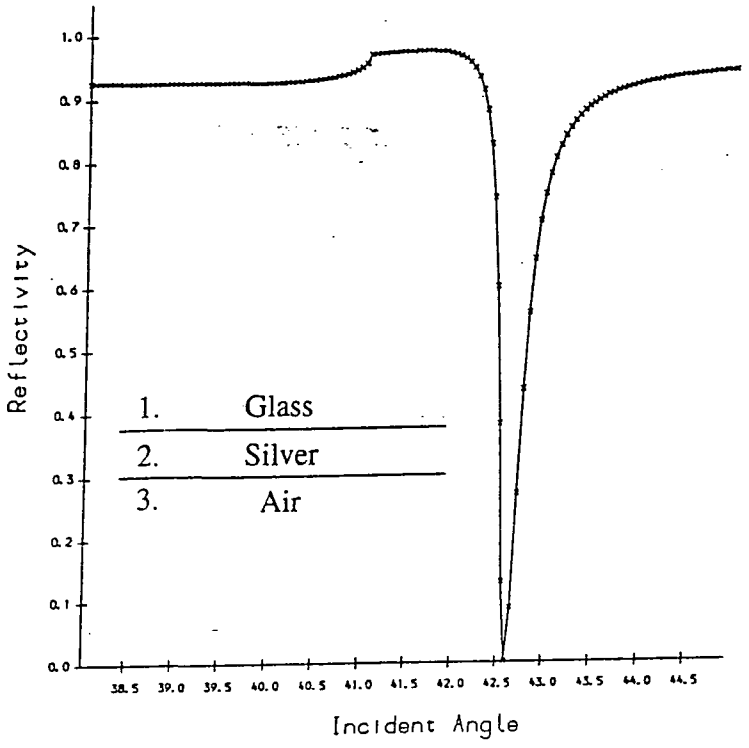

Figure 3.6: A theoretical SPR curve of silver on glass.

Quantitatively, surface plasmon waves can be represented by a propagation wave vector k_{sp} given as:

$$k_{sp} = \frac{\omega}{c}\left[\frac{1}{\varepsilon} + \frac{1}{\varepsilon_m}\right]^{1/2} \tag{3.4}$$

where ε is the complex permittivity of the dielectric medium and ε_m that of the metal (ε for most materials is complex). The matching of this wave vector k_{sp} to that of a p-polarized incident light k_x gives the condition referred to as surface plasmon resonance (SPR). The wave vector of the incident light beam is given as:

$$k_x = \frac{\omega}{c}\sqrt{\varepsilon}\sin\theta \tag{3.5}$$

where θ is the internal angle of incidence which is related to the external angle α at the prism entrance (see figure 3.7) by the relation:

$$n_1 \sin(\theta - \gamma) = n_0 \sin(\alpha - \gamma) \tag{3.6}$$

where γ is the prism angle to the sample and n_0 the refractive index of air [Weber, 1977] (see figure 3.7).

From equations (3.4) and (3.5), it can be seen that the matching of these two wave vectors can be achieved through angular or wavelength scans. This results in two methods for coupling.

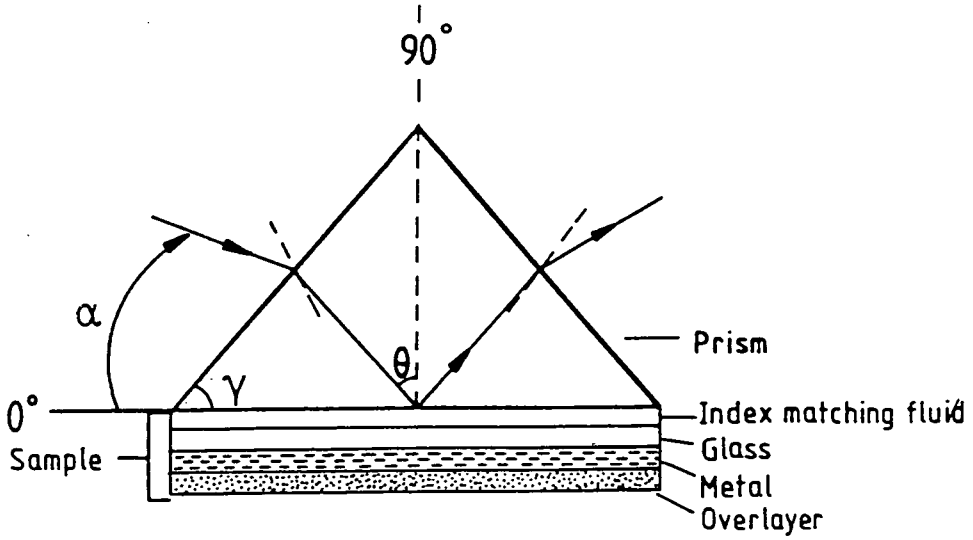

Figure 3.7: SPR system showing the various prism and beam angles as well as all components of the system.

The high surface sensitivity of this system, coupled to its simplicity, has led to many potential application studies which include the study of surface roughness [Raether, 1982], antigen-antibody interactions [Flanagan et al, 1984 and Fontana et al, 1990], monolayer assemblies on metal surface [Pockrand et al, 1977,1978,1982 and Wahling et al, 1979], and gas sensing [Liedberg et al, 1983, Lloyd et al, 1988, Nylander et al, 1982, Vukusic et al, 1992 and Zhu et al, 1989].

b. Review of Overlayer and Gas Effects

Figure 3.8 shows the effect of a non-absorbing overlayer film (LB layers of a fatty acid salt) on the surface plasmon resonance curves for silver. The overlayer produces a simple shift in the resonance angle to higher angles. The shift is due to increase in the finite thickness of the overlayer.

Figure 3.9 shows the effect of a film absorbing in the same energy region as the surface plasmon of a metal. The overlayer (LB layers of a copper pthalocyanine) also produces a shift of the resonant position to higher angles but, in addition, a decrease in the resonance depth. The decrease in resonance depth is due to absorption of the field associated with surface plasmons by the overlayer. This

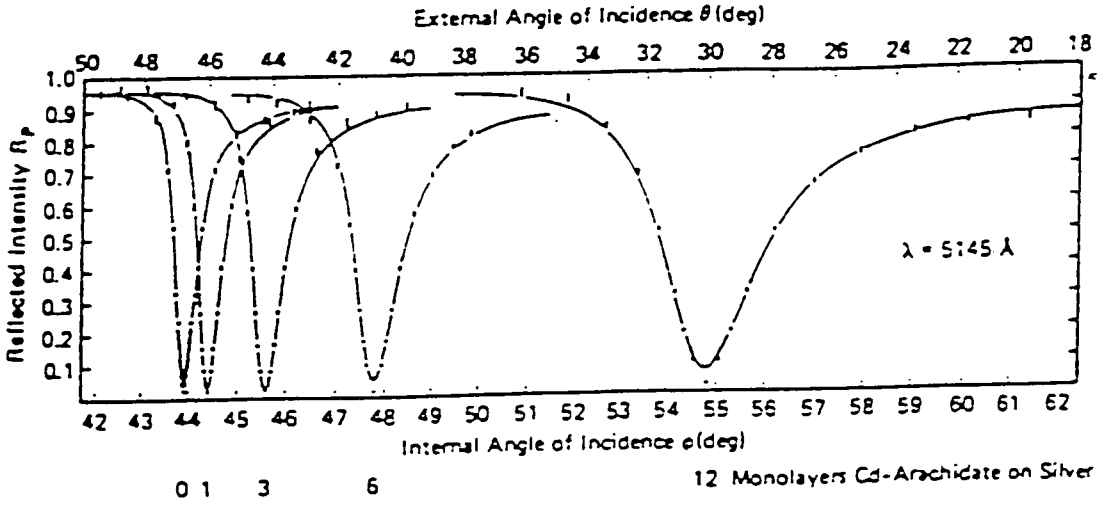

Figure 3.8: The effect of a non-absorbing film at the measuring wavelength on the surface plasmon resonance condition of silver [Pockrand et al, 1977].

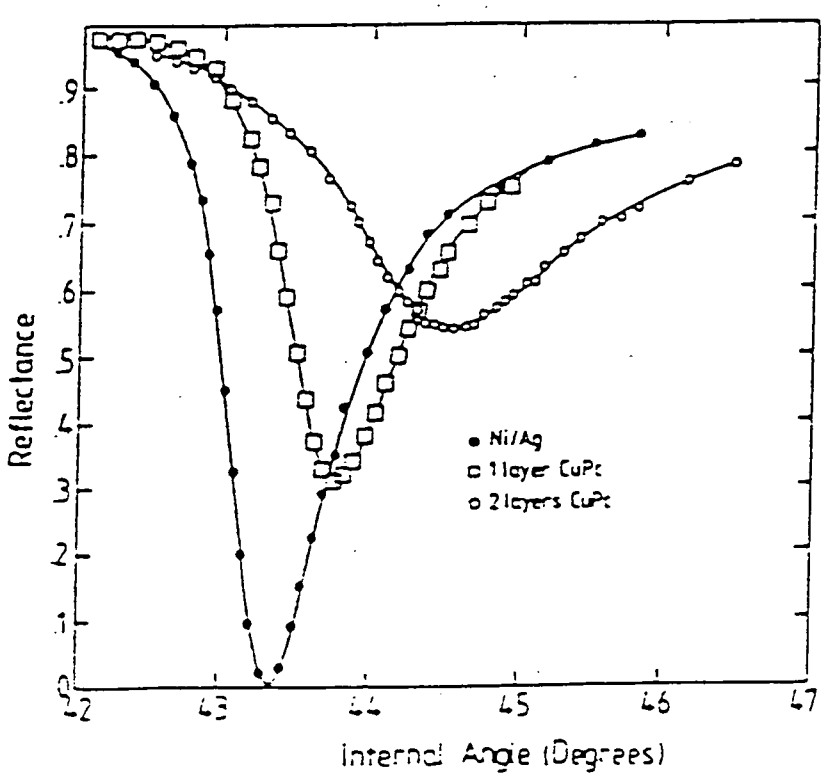

Figure 3.9: The effect of an absorbing film at the measuring wavelength on the surface plasmon resonance condition of nickel/silver [Zhu et al, 1990].

effect increases with the film thickness, as shown in figure 3.9, until the interaction between the surface plasmon and excitons of the overlayer is 'washed-out'. This effect is otherwise classified as damping. Contributory effects to curve broadening include increased surface roughness [Raether, 1982 and Flanagan et al, 1984] and beam scattering [Pockrand et al, 1978]. All the above effects may also be caused by the interaction of a gas on the metal/overlayer combination.

c. System Design and Calibration.

Surface plasmon resonance measurements carried out in this project were conducted with a system based on the Kretschmann configuration. The equipment, shown in figure 3.10, was custom-built with the light source pointing-up from underneath rather than from the top. This was done so that the system could also be used with a liquid on the silver surface. Furthermore, the light beam could be visibly focused onto the sample.

The system used a 1mW p-polarized He-Ne laser source, a neutral density filter to cut down the power of the beam (reducing localised heating effects in the sample and avoiding saturating the photodiodes), a 50-50% beam splitter and two large area photodiodes. At the geometric and optical centre of the system was a 90^{o} glass prism, supporting on its base a purposely made PTFE gas cell with inlet/outlet pipes; this was sealed with o-rings at the top and bottom. Light reflected from the prism base was measured using a large area silicon photodiode. The output from this diode was fed into a custom-built circuit where it was normalised with respect to a reference diode.

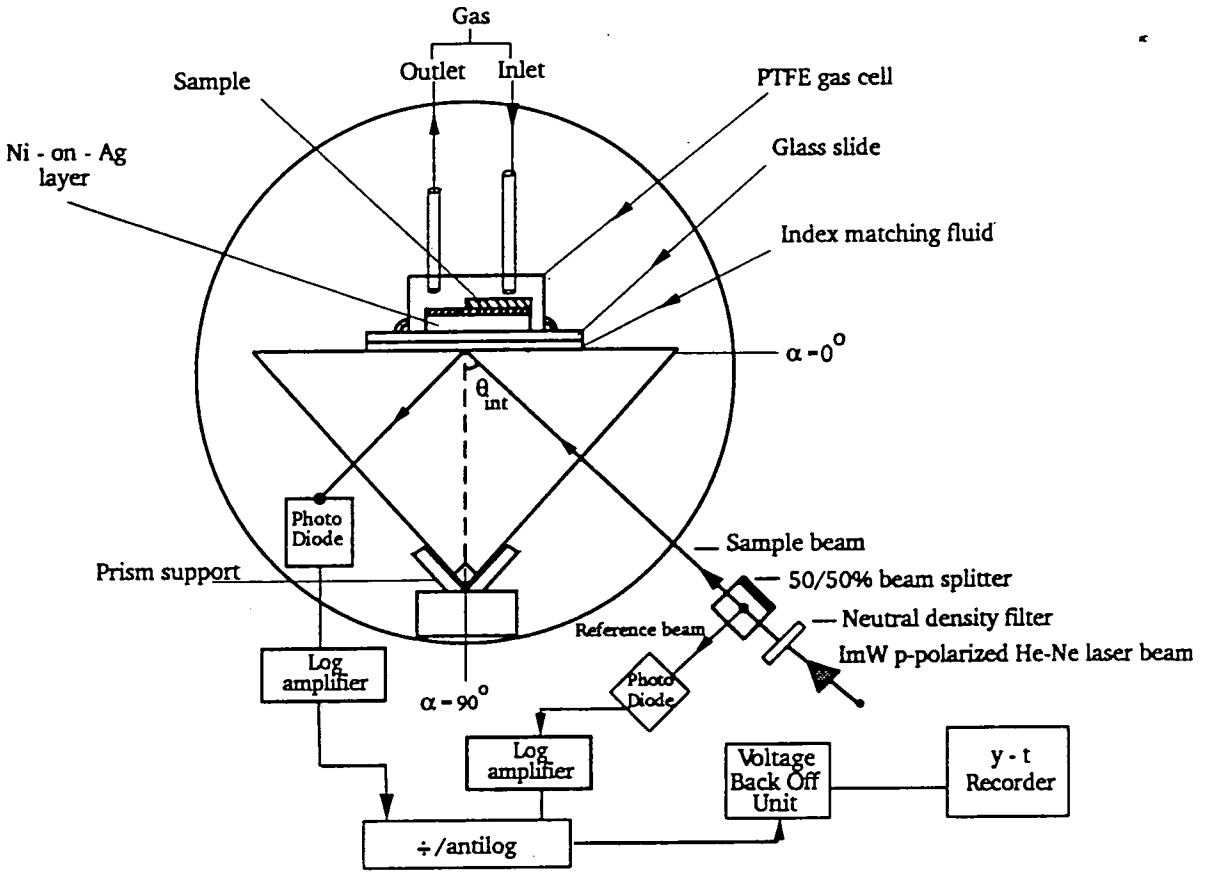

Figure 3.10: SPR system used in this work.

The system was calibrated by measuring the reflectivity of silver and gold and comparing the results to published data in terms of the angle of minimum reflectivity and the half width at half maximum (HWHM). Figure 3.11 shows the SPR curve for 50nm of silver obtained by measuring the intensity of the reflected light as the external angle of incidence at fixed wavelength is varied. At resonance, the reflected intensity is minimised, corresponding to maximum coupling. Compared with the theoretical curve in figure 3.6, it can be seen that the resonance position as well as the resonance depth are slightly different. This is probably due to differences in the thickness of the Ag and some beam scattering from this metal layer.

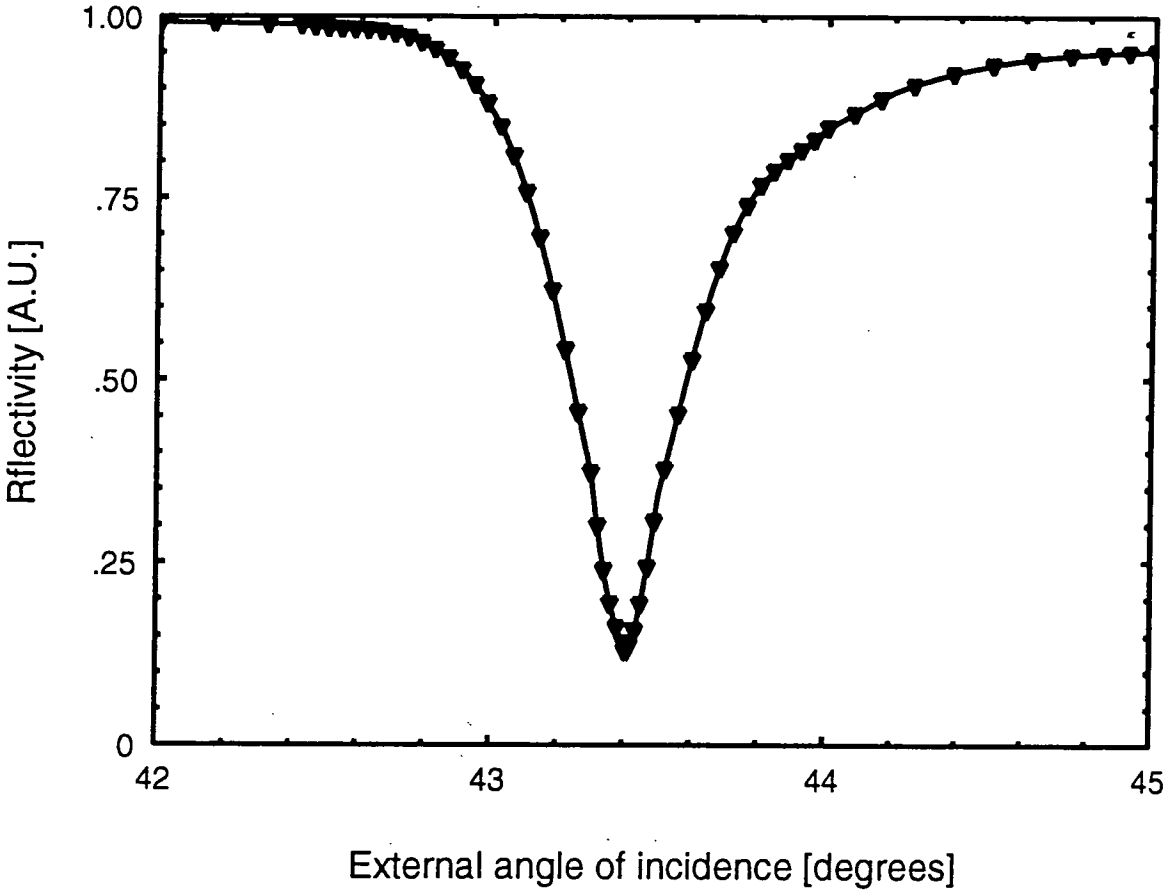

Figure 3.11: Surface plasmon resonance curve for 50nm of silver on glass.

The stability of the system (using a 50nm thick silver film on glass) was also investigated over a period of several hours (figure 3.12). The results show the outputs of the sample, the reference and the sample divided by the reference beams. It can be seen that both the sample and reference beams fluctuate randomly. However, the ratio gives a much more stable output.

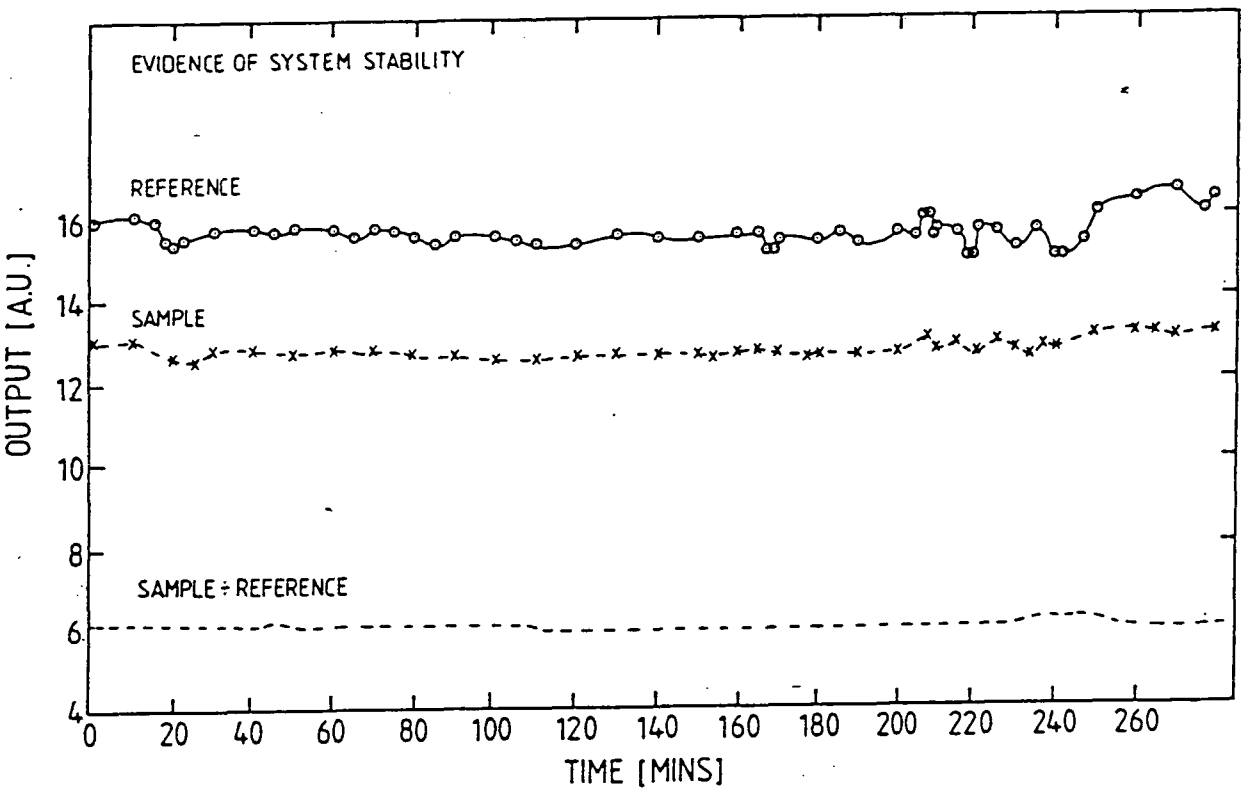

Figure 3.12: The variation of the reference, sample and ratio of the two beams of the experimental system.

d. Sample Preparation and Measurement

Samples used were prepared by the LB method described above in section 3.2.1. Spin-coated samples were very patchy at the film thickness required for SPR and were not investigated. Deposition was always onto gold or onto a thin layer of nickel (0.1nm) deposited on silver (Ni/Ag). Thin films of nickel were used because most of the gases used reacted with silver giving a shift in the SPR curve (see figure 3.13 for H_2S). The reaction with H_2S, can be represented as:

$$Ag + H_2S \rightarrow AgS + H_2 \qquad (3.10)$$

However, when coated with nickel, this reaction is substantially reduced as shown in figure 3.14. A similar screening of the effects of NO_x on the surface

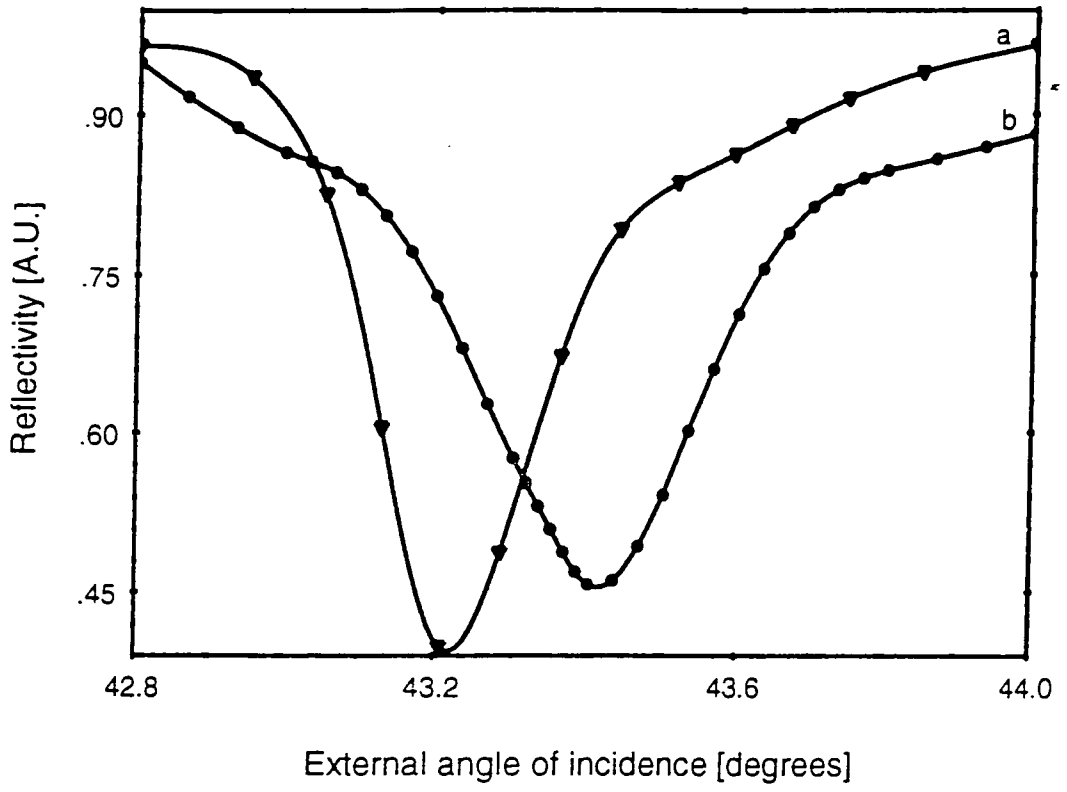

Figure 3.13: SPR curve of Ag (curve a); Ag exposed to 100ppm H_2S for 30 minutes (curve b).

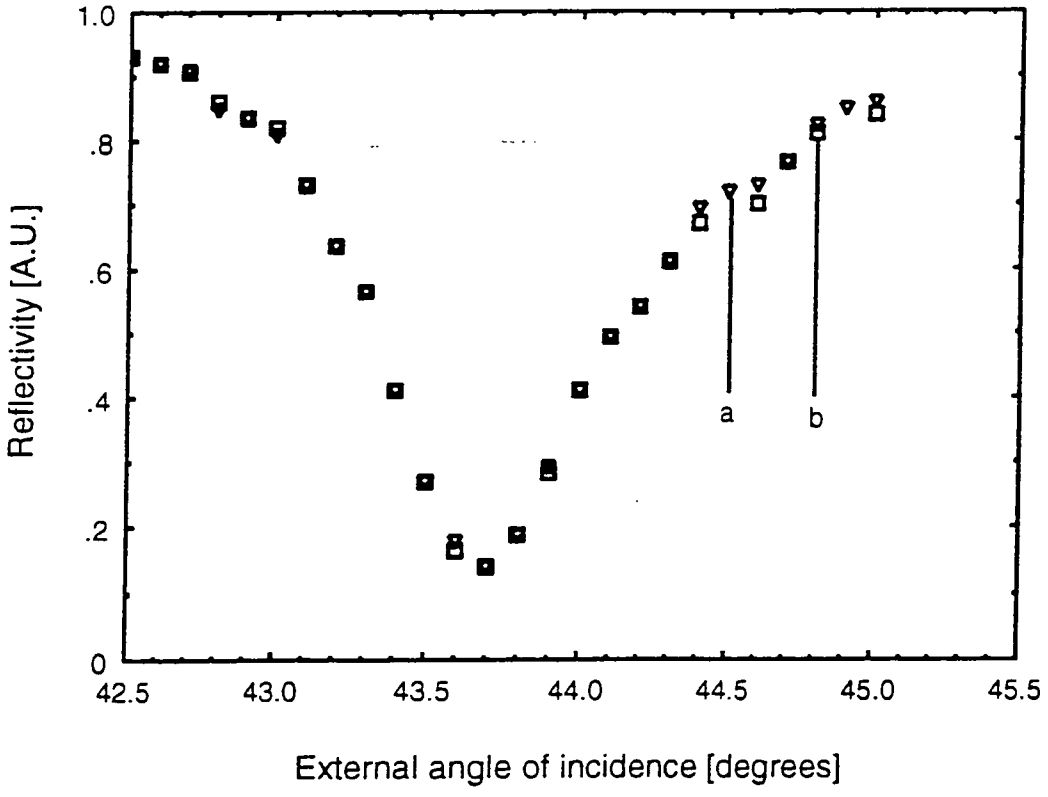

Figure 3.14: SPR curve of Ni/Ag (curve a); Ni/Ag exposed to 100ppm H_2S for 30 minutes (curve b).

plasmon resonance conditions of Ag has been reported using Ni [Zhu et al, 1990].

Gas sensing experiments were undertaken by fixing the beam at an angle of incidence close to resonance, on the steep part of the reflectance curve, and monitoring the changes in reflectivity with time. Measurements were made first for uncoated gold or Ni/Ag substrates and then for the same substrate covered with a film. The output voltage ratio was fed into a voltage 'back-off' unit and then to a chart recorder. When stability was achieved (constant output voltage ratio), dry N_2 gas was allowed into the system. This initially produced a decrease in the output voltage ratio (equivalent to a decrease in reflectivity) which could be attributed to film relaxation as water vapour trapped in the film matrix was removed. This change often lasted for about 1 hour after which stability was again obtained; this formed the baseline for gas sensing. The gases (NO_x, H_2S, CO, CH_4 or SO_2 all diluted in nitrogen) were then fed into the system for times ranging from 6 minutes to 1 hour and changes in the output voltage ratio recorded. Alternatively, if the effect of the gas on the sample was large and reversible, the entire SPR curve would be measured for each gas concentration. Different gas concentrations were provided by a Signal Instruments 850 series gas blender with stainless steel valves. In this work, three types of LB film materials were investigated: polyaniline; lutetium bisphthalocyanine; and CMTPP.

3.3.3 Fourier Transform Infrared Spectroscopy

a. Background.

Infrared (IR) spectroscopy was undertaken using the reflection-absorption Fourier transform infrared technique (RAIRS) at room temperature. An infrared spectrum results from the interaction of infrared radiation with molecules possessing a non-zero transition dipole moment; hence excluded are homonuclear diatomic molecules which have a symmetrical charge distribution about their centre of mass. IR sensitive molecules must possess a component of their transition dipole moment parallel to the incident electric field vector of

the IR beam. Consequently, when the energy associated with a vibrational mode of the molecule is the same as that of the incident photons, it will be absorbed, producing a characteristic band in the spectrum at that particular frequency. IR molecular vibrations can take the form of bending, stretching, wagging or scissoring. There are three main regions of an IR spectrum, namely the near-, mid- and far-IR regions. Measurements in this work have been carried out in the mid IR (4000 to 400 cm^{-1}) region as it represents the range in which most of the vibration bands of interest were found.

b. Experimental

The equipment used was a Nicolet FTIR spectrophotometer. It was used in conjunction with an insitu-diffuse reflection FTIR (DRIFT) accessory (which is credited for its high energy throughput, high collection efficiency and high signal-to-noise ratio) and a catalytic chamber through which gases could be passed. Both extra components were obtained from Spectra-Tech.

The spectrophotometer possessed a silicon carbide source, producing both a single and a double beam, and a liquid nitrogen cooled mercury cadmium telluride (MCT) detector. The optics of the system are based on the Michelson interferometer, shown in figure 3.15. The scan rate was relatively fast and many interferograms could be recorded and then averaged to give the spectrum of the sample. The DRIFT accessory was made of mirrors which were positioned to aid focusing the beam onto the sample, as shown in figure 3.16. Three modes of reflection were possible: purely diffuse; purely specula; and a total reflectance mode. In this project, the system used was the total reflectance mode because of the non-particulate nature of our samples. Consequently, most of the beam was specularly reflected with a weak diffused component [Graf et al, 1987]. The catalytic chamber was screwed to the DRIFT accessory such that no leaks could be detected. This chamber was capable of being used at temperatures up to 900°C and under different environments. On the sides of the chamber were two ZnSe windows, chosen because of their low absorption. Inside the chamber was a stage with a cup structure to accommodate the samples. The samples were positioned at the optical centre of the chamber and, using the mirrors in the DRIFT accessory, red light from the source was focused on to the sample. The gas inlet was underneath the sample stage and outlet at

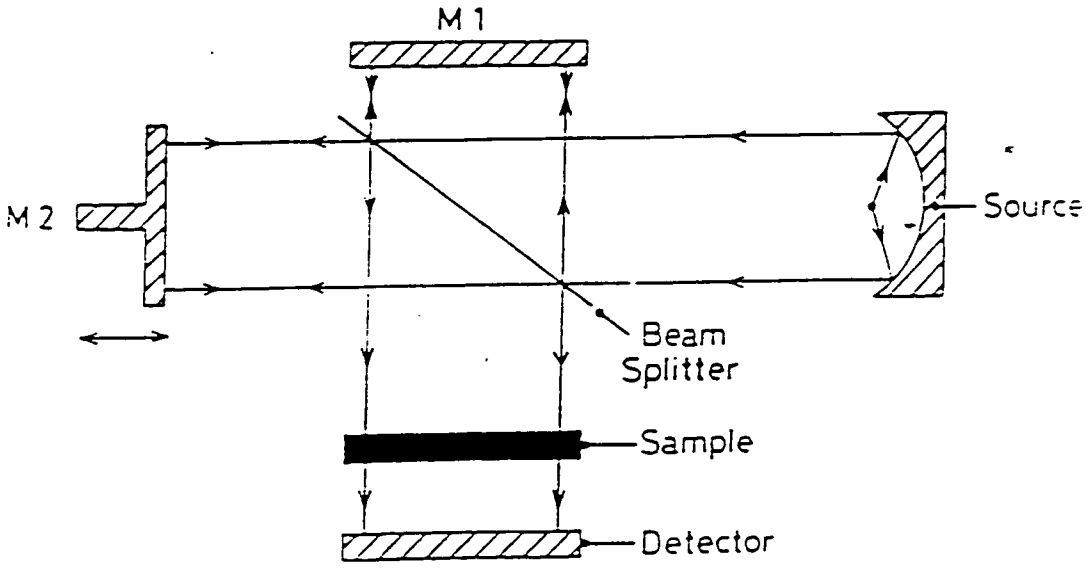

Figure 3.15: The basic optical design of an interferometric spectrometer.

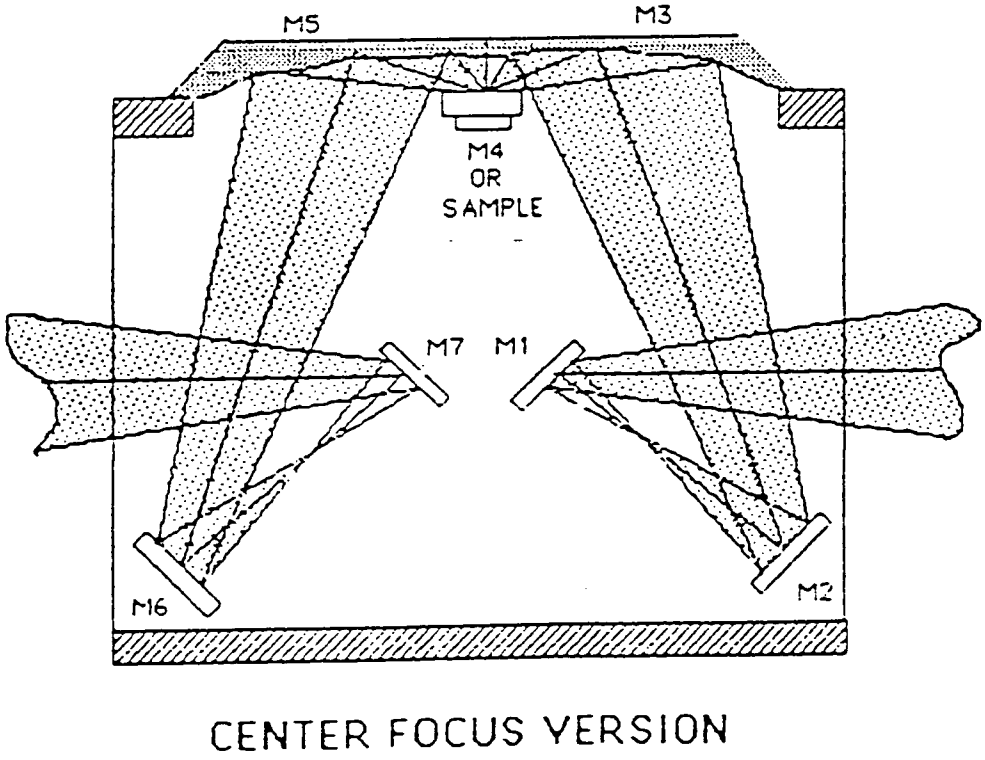

Figure 3.16: Drift accessory used to aid focusing of the beam onto the sample.

the side of the chamber. This arrangement ensured that the sample remained stationary during scanning, as well as maintaining an even distribution of temperature in the system.

The versatility of this closed assembly made it possible for the spectrum to be recorded insitu. The IR spectrum of a sample is known to depend on factors such as the beam entry and exit geometry, the physical state of the sample as well as its chemical composition. Consequently, a new sample was used for each gas so as to avoid any possibility of a secondary induced effect caused by products from any previous gas/material interaction [Li et al, 1990].

All the samples were deposited onto gold because silver would react with some of the gases used. The gold was evaporated onto carefully prepared 2mm square microscope glass slides which made sample handling an important consideration. A sample was placed on the stage and the beam focused onto it by opening the source momentarily and adjusting the position of the DRIFT mirrors. The opening of the system to air resulted in an increased carbon dioxide and water vapour content in the spectrum. The system was then closed and about a litre of liquid nitrogen introduced to cool the detector. The measurement parameters were then set before recording the spectrum. These included the average number of scans, set at 1024, a resolution of $4cm^{-1}$, and the gain of the detector (set at 4). The number of scans was chosen to optimise the signal-to-noise ratio while the gain was chosen so that the energy at the detector would not overload the analogue-to-digital converter. Thus the response of the system would remain linear.

Immediately after these adjustments, the background spectrum of the bare gold sample was recorded. This process lasted 20 minutes and was then followed by 2 hours of purging the system with dry argon gas. Purging was undertaken to reduce the amount of CO_2 and water vapour. There was always some residual water vapour present in the spectrum and complete elimination could take 18 hours or more. In order to improve the quality of the spectrum, a genuine water vapour spectrum was also recorded for comparison. The gases were also introduced to see their effect on the substrate; however, no differences in the spectrum before or after exposure were observed.

The gold substrate was then replaced by a sample and a similar measurement performed. When changes due to water vapour and CO_2 had been minimised, a series of spectra were recorded for each sample over a 20 minute period and the data were stored. Then the gases, NO_x, SO_2, or H_2S, at a concentration of 150ppm, were introduced into the chamber for times ranging from 30 minutes to 6 hours. During this time, the spectrum of the sample was again recorded at fixed intervals of 30 or 60 minutes. This procedure was repeated following the rule 'one sample-exposed to-one gas' (see table 3.2) for reasons noted previously. After some time, the gas was turned off and the reaction monitored for any signs of reversibility. This process was stopped when no differences (0.0001 absorbance units) were observed between consecutive spectra.

Sample	NO_x	H_2S	SO_2
LB PANi	yes	no	yes
LB CMTPP	yes	yes	no
LB $LuPc_2$	yes	yes	yes
Evaporated PANi	yes	yes	yes
Spin-coated PANi	yes	yes	yes

Table 3.2. A summary of RAIRS experiments undertaken using 150ppm of the above gases on thin films deposited onto 20nm gold-coated glass slides. All samples were purged with argon before exposure to any of the above gases.

3.3.4 Scanning Electron Microscopy

In order to study the morphology of the films, scanning electron micrographs were taken using a Cambridge Stereoscan 600 system. This was used in secondary mode with the electron beam accelerated through 25kV. The system offered a wide range of magnification, extending from ×20 to ×100,000. The samples were fixed onto aluminium stubs before being mounted in the microscope. Those prepared on glass substrates were pasted onto the stubs using conducting silver paint which helped earth and stabilise the sample during study. However, highly insulating samples, charged under the electron

beam, producing unstable images. Such samples were coated with a 1nm thick layer of gold, produced by glow discharge on a Polaron Instrument SEM coating unit, to obtain a conducting surface.

3.3.5. Electrical Measurements

Electrical investigations included current versus voltage measurements under various ambients and temperature dependent dc conductivity.

Figure 3.17 shows the system used to measure the current versus voltage characteristics of all devices. It is made up of a Time Electronics dc voltage calibrator and Keithley 410A picoammeter connected to a sealed chamber. On the side of the chamber are two taps used for gas inlet and outlet. Inside the chamber is a sample boat, beneath which is a thermocouple linked to a temperature controller. Two probes on the sample boat were used for electrical contacts. For different supply voltages V, the current I through a sample of thickness t was measured using the picoammeter. These measurements were undertaken for different film thicknesses to determine the nature of the contact between the sample and the electrode.

The system shown in figure 3.17, was also used for gas sensing measurements. Gas sensing was undertaken by measuring changes in current at a fixed supply voltage for different gas concentrations at room temperature and pressure. In the first instance, dry nitrogen was used to replace air trapped in the chamber. This change in ambient over the sample resulted in a decrease in its conductivity, which in some cases lasted up to 1 hour. The nitrogen was used as the background ambient since gases such as NO_x, SO_2, H_2S, CH_4 and CO were also diluted in nitrogen. Each time one of the above gases was introduced, a characteristic time lapse τ followed by a change in current was noted. This time lapse is henceforth called the delay time τ_D as illustrated in figure 3.18. This delay time varied from one ambient to another for the same device. In some cases, it was too short for it to be measured. Figure 3.18 also shows the recovery time τ_R defined in this report as the time it takes for 90% of the original current value to be recovered when the gas is turned off.

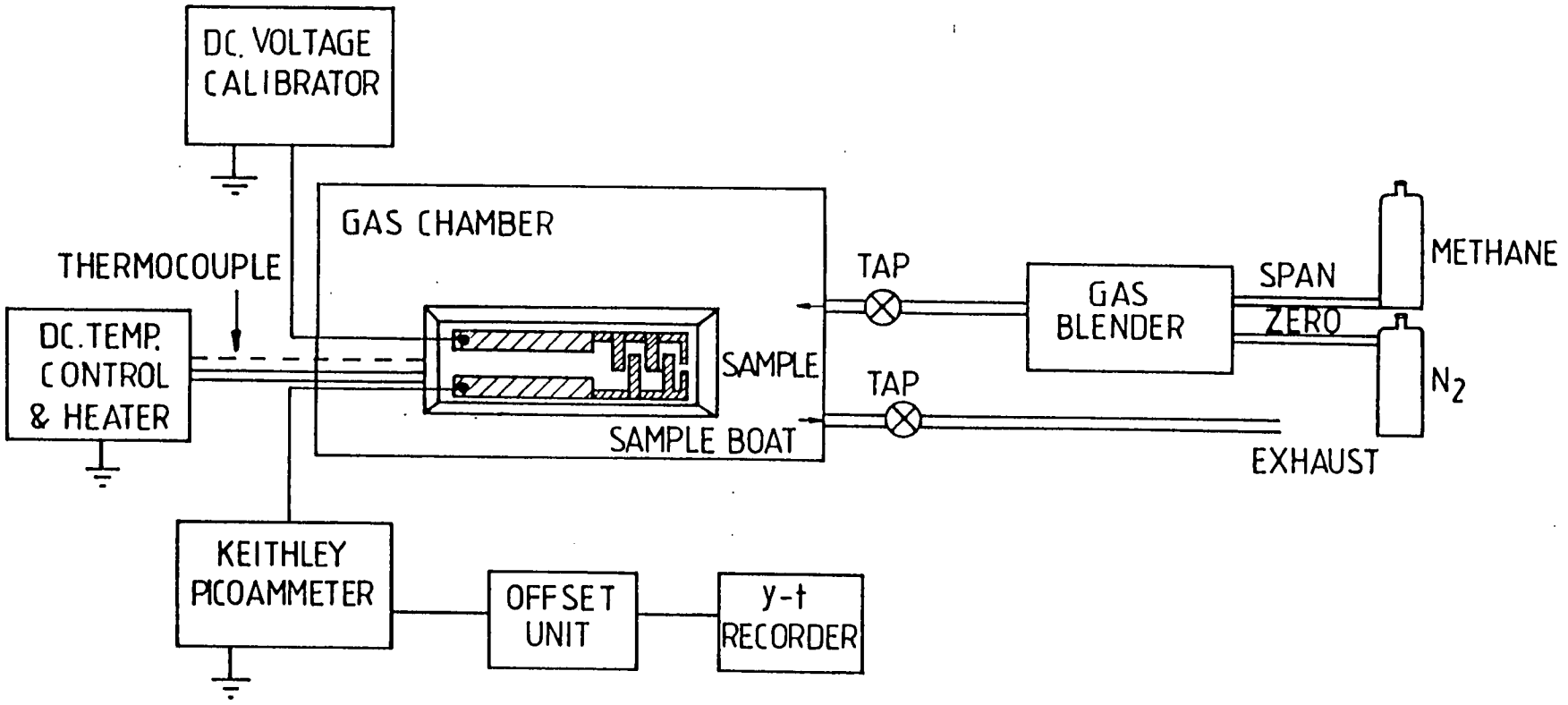

Figure 3.17: The electrical measurement system used for current versus voltage and gas sensing measurement at room temperature.

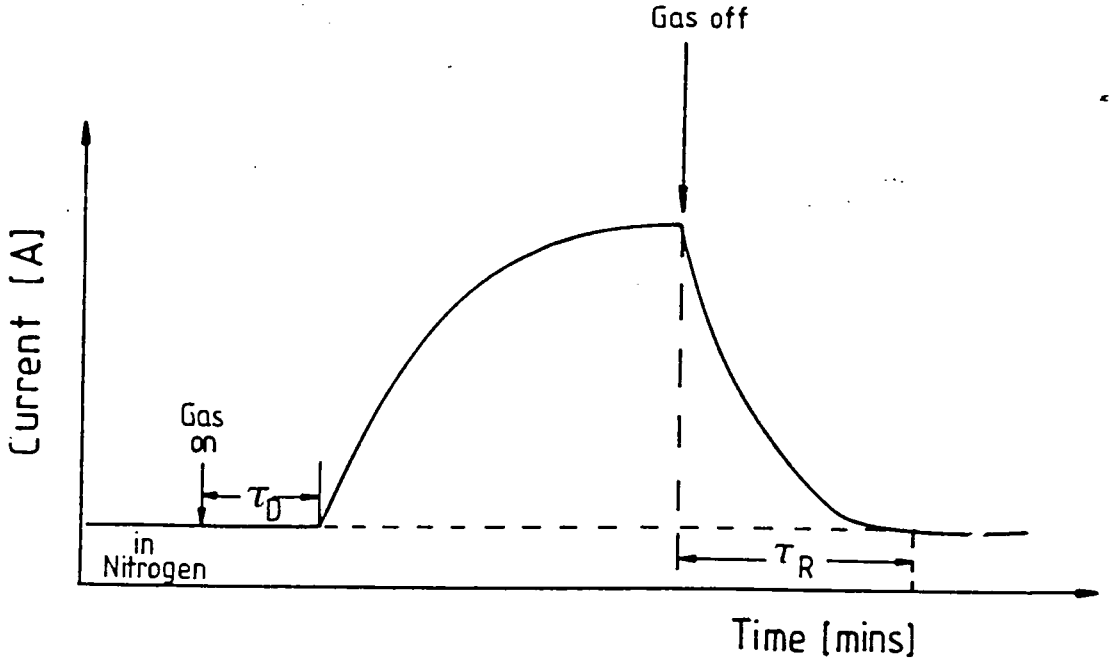

Figure 3.18: The effect of a gas on a chemiresistor showing the delay time τ_D and recovery time τ_R.

Figure 3.19 shows the system used to undertake temperature dependent dc conductivity measurements (290-345K). The system based on a copper block on which samples were mounted. The sample temperature was recorded by means of a platinum resistance thermometer mounted over the sample. A temperature linearizer was also included to control the rate of heating and cooling. The samples were deposited onto interdigitated structures with 14 pairs of electrodes. These measurements were undertaken principally to investigate the conduction mechanisms in the thin films. From the measurements of the dimensions of the electrode and film, the conductivity σ of the sample can be calculated using the formula [Snow et al, 1989]:

$$\sigma = \frac{I}{V}\frac{2d_1}{[2n-2]Lt} \tag{3.11}$$

where I is the current measured, V the voltage, d_1 the spacing between the electrodes, n the number of electrodes, L the overlap length of the electrodes and t the thickness of the sample (see figure 3.2).

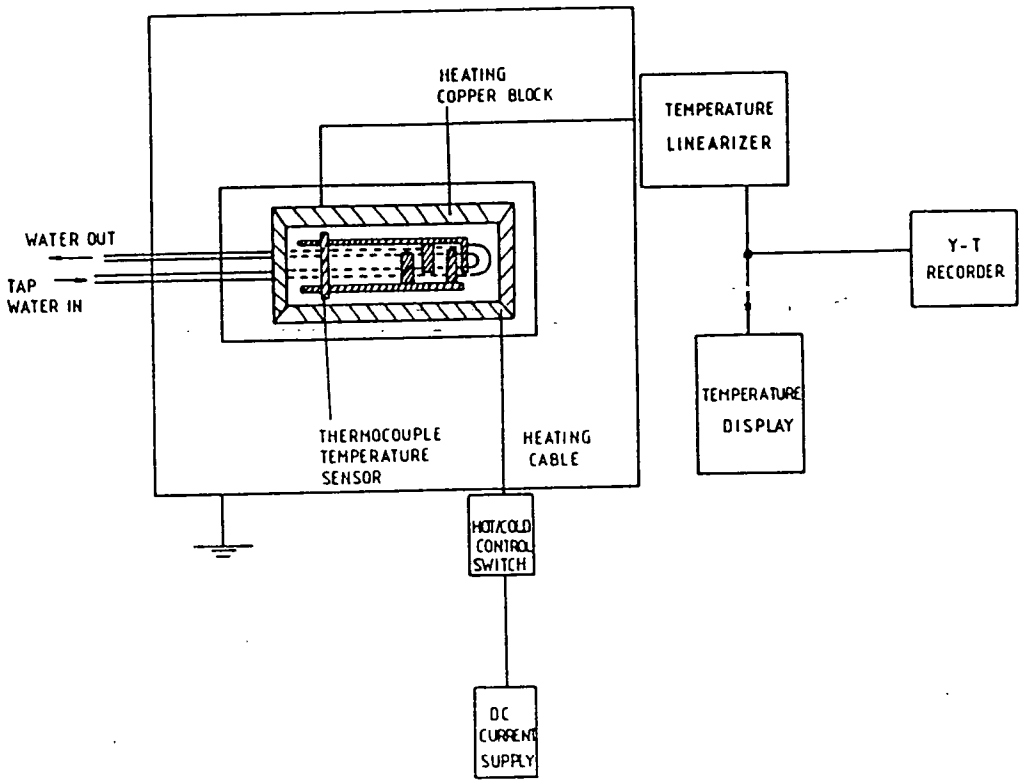

Figure 3.19: The system used for temperature dependent dc conductivity measurements.

3.4 SUMMARY

The methods and equipment used to deposit thin films of organic material have been described. The resulting films have been characterized by optical and electrical techniques in different, well-controlled environments.

REFERENCES.

Agranovich, V.M. and Mills, D.L. (eds). : 'Surface Polaritons', North Holland., New York (1982)

Baker, S. : PhD thesis, Durham University, 1985

Pockrand, I., Swalen, J.D., Santo, R. and Philpott, M.R. : J. Chem. Phys, **69** (1978) 4001-4011

Pockrand, I., Swalen, J.D., Gordon, J.G. and Philpott, M.R. : J. Chem. Phys., **70** (1979) 3401-3408

Raether, H. : Physics of Thin Films, **9** (1977) 145-261

Raether, H. : 'Surface Plasmon Oscillations and their Applications' in 'Surface Polaritons' Agranovich, V.M. and Mills, D.L., (eds)., North Holland Publsh. Comp., New York (1982) 145-255

Snow, A.W. and Barger, W.R. : in 'Phthalocyanine Properties and Applications' Leznoff, C.C and Lever, A.B.P (eds)., VCH Publis., New York (1989) 345-392

Tredgold, R.H. and Smith, G.W. : Thin Solid Films, **99** (1983) 215-220

Vukusic, P.S., Bryan-Brown, G.P. and Sambles, J.R. : Sensors and Actuators B, **8** (1992) 155-160

Wahling, G. and Raether, H. : Thin Solid Films, **58** (1979) 391-395

Wallis, R.F. and Stegeman, G.I., (eds). : 'Electromagnetic Surface Excitations'., Springler-Verlag, New York (1986)

Weber, W.H. : Physical Review Letters, **39** (1977) 153-156

Zhu, D.G., Petty, M.C. and Harris, M. : Sensors and Actuators B, **2** (1990) 265-269

CHAPTER FOUR

SPIN-COATED POLYANILINE FILMS: RESULTS AND DISCUSSION

4.1 PREFACE

The data presented in this chapter result from studies carried out on spin-coated polyaniline films at room temperature. The initial results are presented in section 4.2 and include a series of characterization experiments undertaken to provide an insight into the chemistry, optical properties, conduction mechanism (within the temperature range in which the device would be operational) and morphology of the polymer. Section 4.3 presents the data for conductivity and optical absorbance under different gaseous environments. The gases used were NO_x, H_2S, SO_2, CO, N_2 and CH_4. Mainly 'undoped' films were used for these measurements because, in contrast to 'doped' films, these were more stable, more sensitive and reversible.

4.2 FILM DEPOSITION AND CHARACTERIZATION

4.2.1 Film Structure and Deposition

Polyaniline is known to possess 3 reversible oxidation states, each with a distinct backbone structure composed of different proportions of quinoid and benzoid rings. The quinoid ring forms the oxidized portion of the polymer while the benzoid ring forms the reduced part. For example, emeraldine base polyaniline shown structurally in figure 4.1, possesses one quinoid ring for every three benzoid rings. Other states include leucoemeraldine base polyaniline, where theoretically there are no quinoid (oxidised) units, and pernigraniline where there are equal numbers of quinoid and benzoid rings (see figure 4.1). Based on the description of these different structures, a general formula for polyaniline is shown in figure 4.1. In this work, the sample used was emeraldine base polyaniline. This was chosen because it exhibited the highest electrical conductivity when 'doped' with HCl.

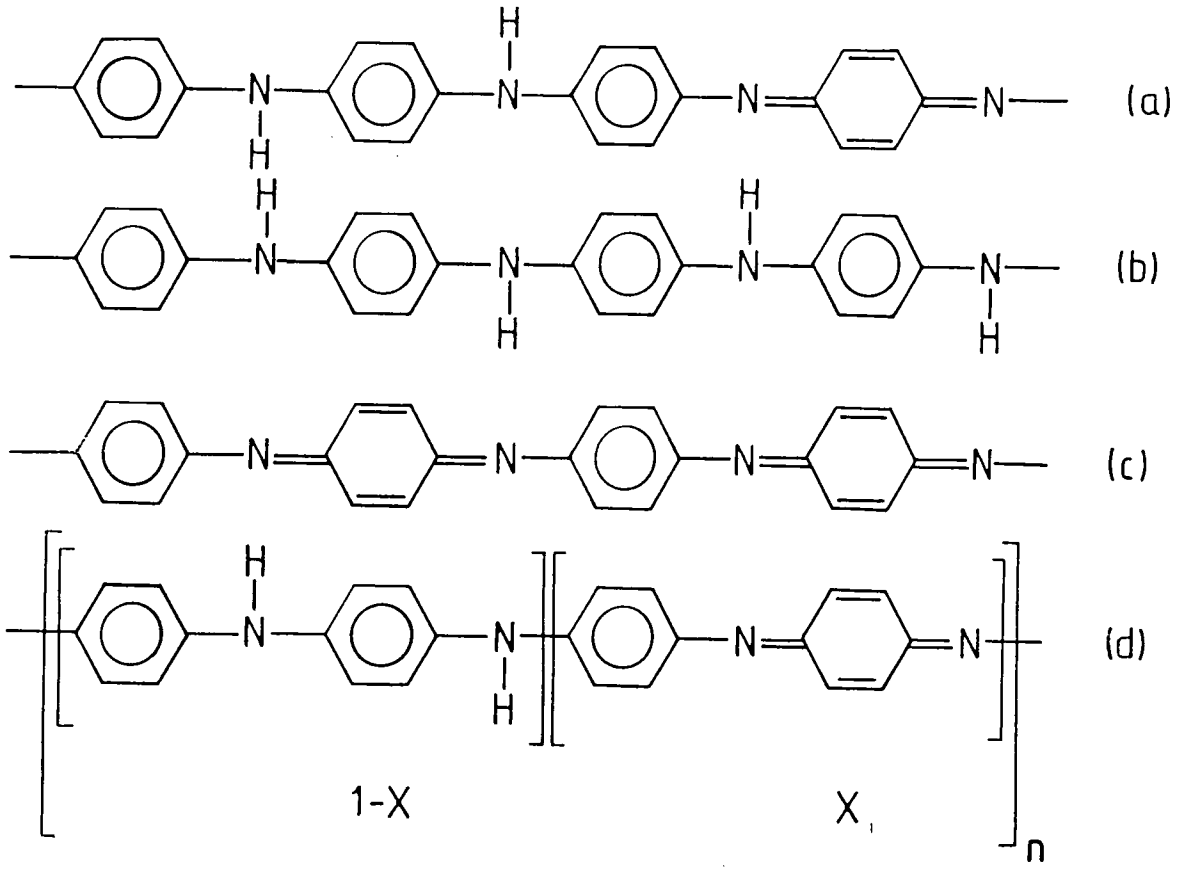

Figure 4.1: The chemical structures of polyaniline (a) emeraldine base (b) leucoemeraldine base (c) pernigraniline base (d) a generic formula for polyaniline where n is a positive integer : x=1/2 for emeraldine base, x=0 for leucoemeraldine and x=1 for pernigraniline.

As noted in section 3.2.3, the 1% solution of PANi in NMP was used as standard for device fabrication. The films deposited were blue in colour by reflection and free from lumps under an optical microscope. The substrates were gold, silver, glass and fused quartz. Films on glass and gold were relatively uniform although the intrinsic spreading behaviour of the material was poor. On silver, deposition was poor. Furthermore, the film completely shrunk during the process of solvent evaporation (in the oven). These effects could be associated with the low sticking coefficient of the polymer on the silver layer. The thickness of the as-deposited films were measured using a Tencor Alpha Surface profiling Talystep and found to be of the order of 1±0.1μm for a 1% solution film deposited at 3,000 rpm for 30 seconds.

4.2.2 Ultraviolet/Visible Spectroscopy

The Ultraviolet/visible spectrum of the as-deposited material is shown in figure 4.2, curve a and confirms it to be the emeraldine base form of polyaniline. This spectrum consists of two main absorption bands, centred on 320nm and 620nm. The peak around 320nm can be ascribed to the π-π^* transition of the benzoid ring along the polymeric backbone while the band at 620nm is attributed to a transition from a benzoid ring to a quinoid ring. This latter transition corresponds to the formation of a localized electron. The quinoid moiety effectively selftraps (localizes) the exciton electron [Duke et al, 1987 and Roe et al, 1989]. The presence of the nitrogen heteroatom along the polymer backbone induces trapping of the excitonic electron on the quinoid ring; hence its broadness. The shape of this spectrum indicates that no thermal degradation of the polymer has occurred during the heating process and that the structure of the film is indeed that of the emeraldine base polyaniline shown in figure 4.1.

When 'doped', the material changes colour from blue to green in reflection. Optically, as shown in figure 4.2, curve b, the quinoid absorption band disappears completely while the intensity of the benzoid band decreases. The disappearance is due to protonation of the imine nitrogen(s) on the polymer backbone [Epstein et al, 1987]. This protonation produces semiquinone cation radicals which have a mixed benzoid/quinoid nature, hence increased π-overlap between adjacent phenyl rings and subsequent charge delocalization [Macdiarmid et al, 1987]. Also visible is a new broad band between 380-500nm which can be associated with charged benzenoid rings. The disappearance of the quinoid band is followed by strong low-energy optical absorption which extends into the infrared, consistent with the spectrum of a metal. This strong absorption peaks around 900nm.

4.2.3 Reflection-Absorption Fourier Transform Infrared Spectroscopy

The reflection-absorption Fourier transform infrared spectrum (RAIRS) of as-deposited polyaniline is shown in figure 4.3. This measurement was taken to elucidate the structure of the material, its degree of protonation and its oxidation state before and after exposure to a gaseous ambient. Overall, the spectrum obtained agrees with published data [Cao et al, 1986, Furukawa et al,

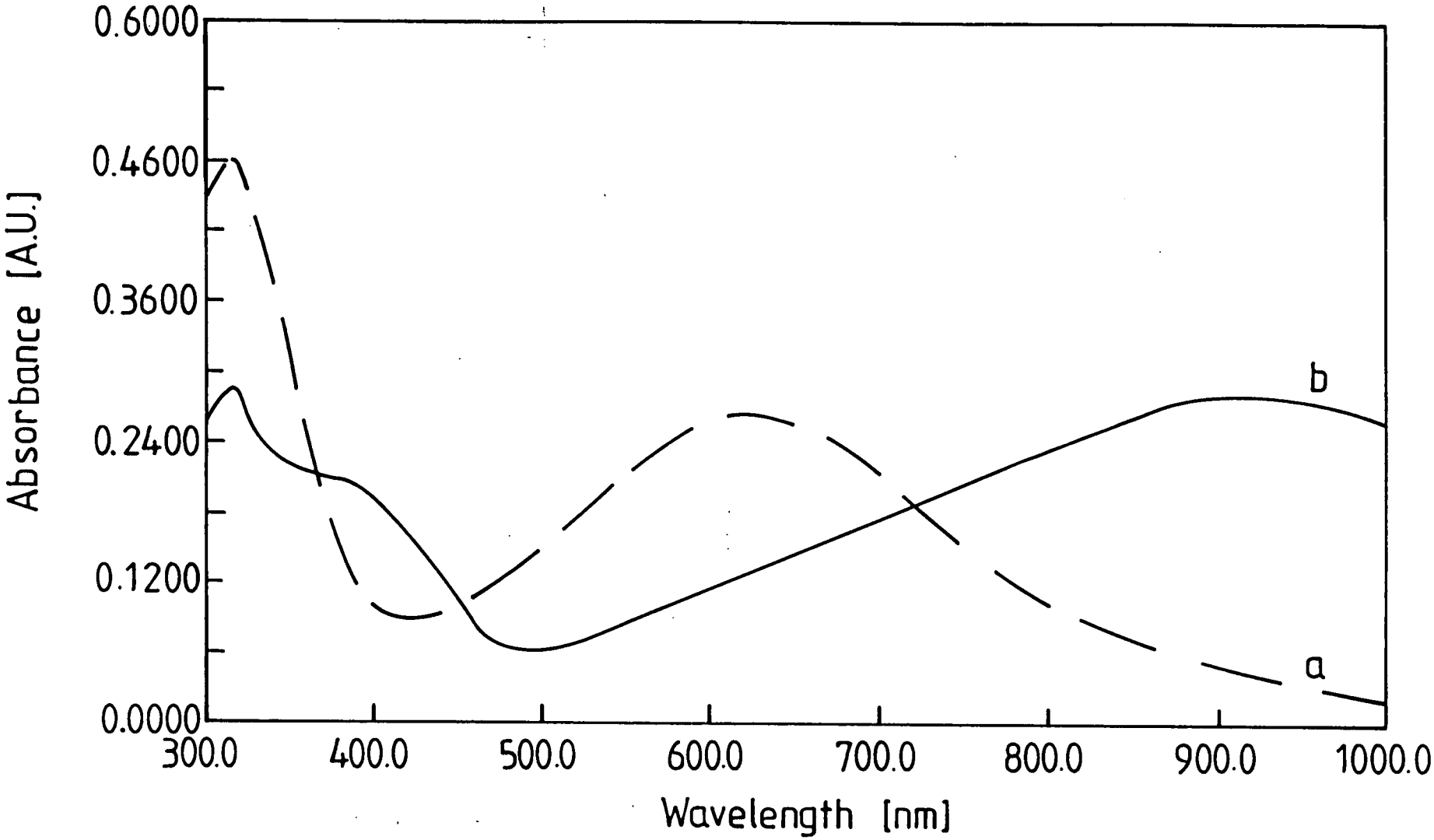

Figure 4.2: Ultraviolet/visible spectrum of as-deposited spun polyaniline on glass (curve a) and after protonation with HCl for 30 minutes (curve b).

1986, Monkman et al, 1991 and Tang et al, 1988]. Band positions are labelled with an error of $\pm 4.0 cm^{-1}$ and were assigned by comparing the relative band positions with published data. A summary is given in table 4.1.

Polyaniline has many infrared active groups and as a result possesses a complex RAIRS spectrum. For simplicity, this spectrum can be divided into five wavenumber regions.

The first region is $3400\text{-}3100 cm^{-1}$. In this region, the absorption bands are broad. The main bands can be seen at $3389 cm^{-1}$ and $3274 cm^{-1}$. The band at $3389 cm^{-1}$ is ascribed to symmetric NH_2 and NH stretches [Tang et al, 1988]. The broadness of this band is because there is more than one infrared sensitive group contributing to the band (NH and NH_2 as well as water effects).

The second region of interest lies between $3100 cm^{-1}$ and $2800 cm^{-1}$. This is the C-H stretching region and absorbances are seen at $3043 cm^{-1}$, $3023 cm^{-1}$, $2921 cm^{-1}$ and $2854 cm^{-1}$. Independent measurements by Tang et al, using varying concentrations of HCl vapour, have shown the relative intensity of the band at $3043 cm^{-1}$ to decrease with increasing HCl concentration. This was associated with ring chlorination hence reducing the number of hydrogens on the ring. As a result, this vibration can be used to determine any change in the number of hydrogens bonded to benzoid rings in the polymer.

The vibration at $2338 cm^{-1}$ is due to asymmetric CO_2 stretch in the background sample. The small vibration at $1721 cm^{-1}$ can be attributed to traces of free CO gas.

A third and very important region is the aromatic ring stretching region centred between $1600\text{-}1450 cm^{-1}$. In this region, two vibrations are evident, one at $1593 cm^{-1}$ and the other at $1504 cm^{-1}$. The latter is attributed to benzoid ring stretch (N-B-N) while the former is attributed to the quinoid ring stretch (N=Q=N). Both are very sensitive to the physical and chemical structure of the film.

A fourth region lies between $1400\text{-}1233 cm^{-1}$. This is the aromatic amine stretching region. Vibrations are observed at $1386 cm^{-1}$, $1300 cm^{-1}$ and $1233 cm^{-1}$. The band at $1386 cm^{-1}$ is attributed the quinoid-trans benzoid-

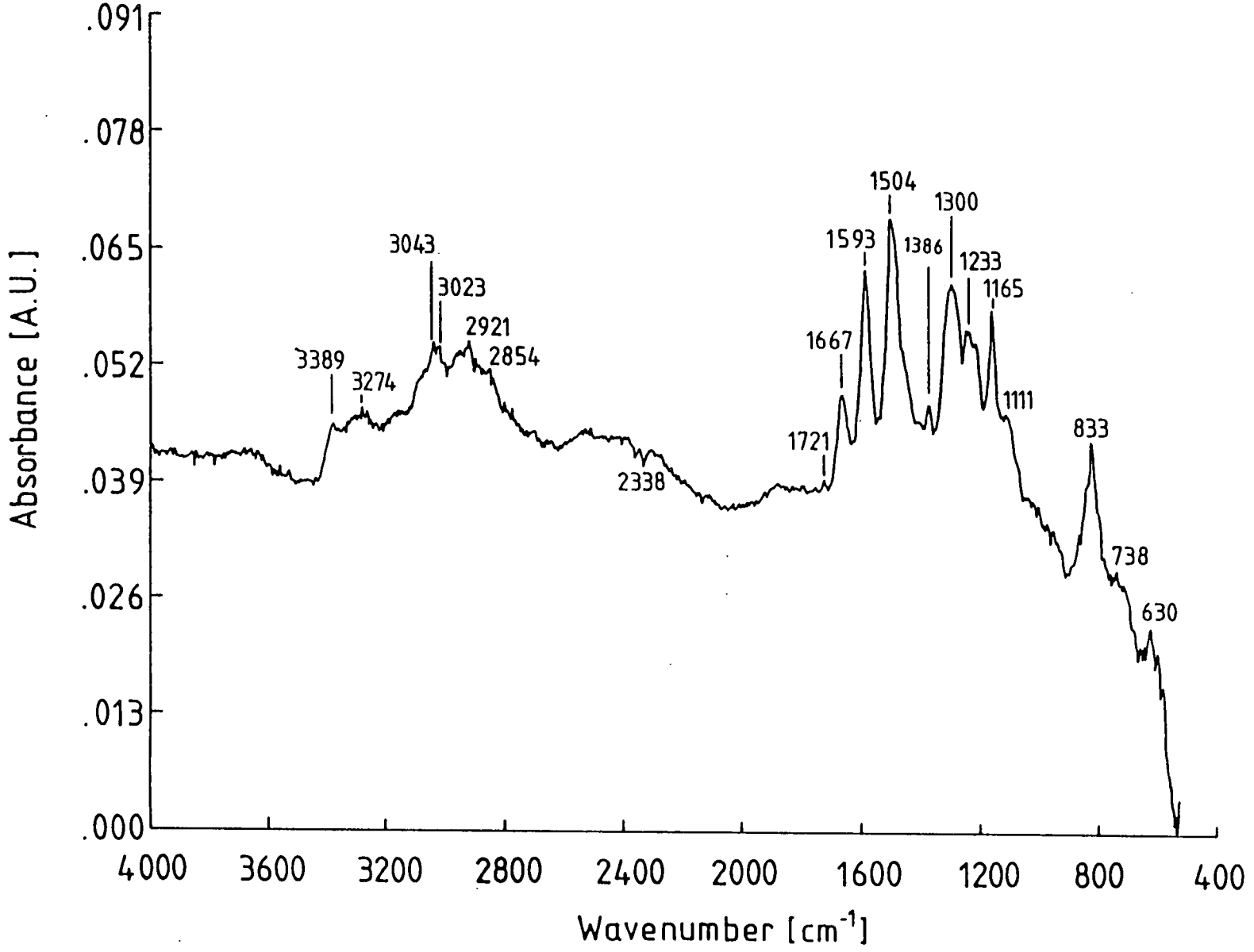

Figure 4.3: Reflection-absorption Fourier transform infrared spectrum of as-deposited spun polyaniline material on gold substrate.

Band Position [cm^{-1}]	Assignment	Comments	References
3389	N-H stretch in neutral B-NH_2 group, NH_2 symmetric stretch	secondary amine	Cao et al, 1986
3274	H_2O	residual water	Monkman et al, 1991
3043	C-H stretch	H atoms bonded to benzene ring	Tang et al, 1988
3023			
2921	symmetric CH_2 stretch	impurities	Traore et al, 1991
2854	asymmetric CH_2 stretch	impurities	Traore et al,1991
2338	asymmtric CO_2 stretch	atmospheric CO_2	
1721	free CO	atmospheric CO	
1667			
1593	quinoid ring [N=Q=N] stretch		Cao et al, 1986
1504	aromatic C-C stretch	benzoid ring stretch	Cao et al, 1986
1386	C-N stretch in Q- B_t-Q		
1300	C-N stretch	secondary aryl amine	Monkman et al, 1991
1233	C-N stretch in B-B-B		
1165	in-plane C-H bending	a mode of N=Q=N	Furukawa et al, 1986
1111	C-H bending on 1,4 ring	in-plane bending	Tang et al, 1988
833	C-H bending on 1,4 ring	out-of-plane bending	Tang et al, 1988
738	C-H bending	out-of-plane bending	"
630	aromatic ring deformation		"

Table 4.1: Band assignments of deprotonated spun polyaniline on a gold substrate. Q=quinoid, B= benzoid, B_t=trans-benzoid rings.

quinoid structure (Q-trans B- Q). During protonation, this remains unchanged but grows during oxidation with iodine vapour to the same intensity as the quinoid rings [Tang et al, 1988]. The slightly broad band at 1300cm^{-1} indicates that more than one vibration is present. It is associated with three possible structures: Q-cis B-Q; Q-B-B; and B-Q-Q. Finally the band at 1233cm^{-1} is attributed to B-B-B.

The last region of interest in the spectrum in figure 4.3 is between 1200-500cm^{-1} and is due to the C-H bending modes. The main absorption bands are located at 1165cm^{-1} and 833cm^{-1} with some weak peaks at 1111cm^{-1}, 738cm^{-1} and 630cm^{-1}. Two independent measurements have confirmed the band at 1165cm^{-1} to shift to lower frequencies on protonation [Hagiwara et al, 1988] or hydrogen substitution [Furukawa et al, 1986]. It is also reported to change in the same proportion as the quinoid band at 1593cm^{-1} [Tang et al, 1988]. As a result, we assume its relative intensity is proportional to the degree of protonation of the polymer (which enhances the delocalization of π-electrons along the polymeric chain). Many other vibrations of polyaniline have not been assigned. However, the ones discussed above will be used to describe, as far as possible, the interaction of the polymer with different gases.

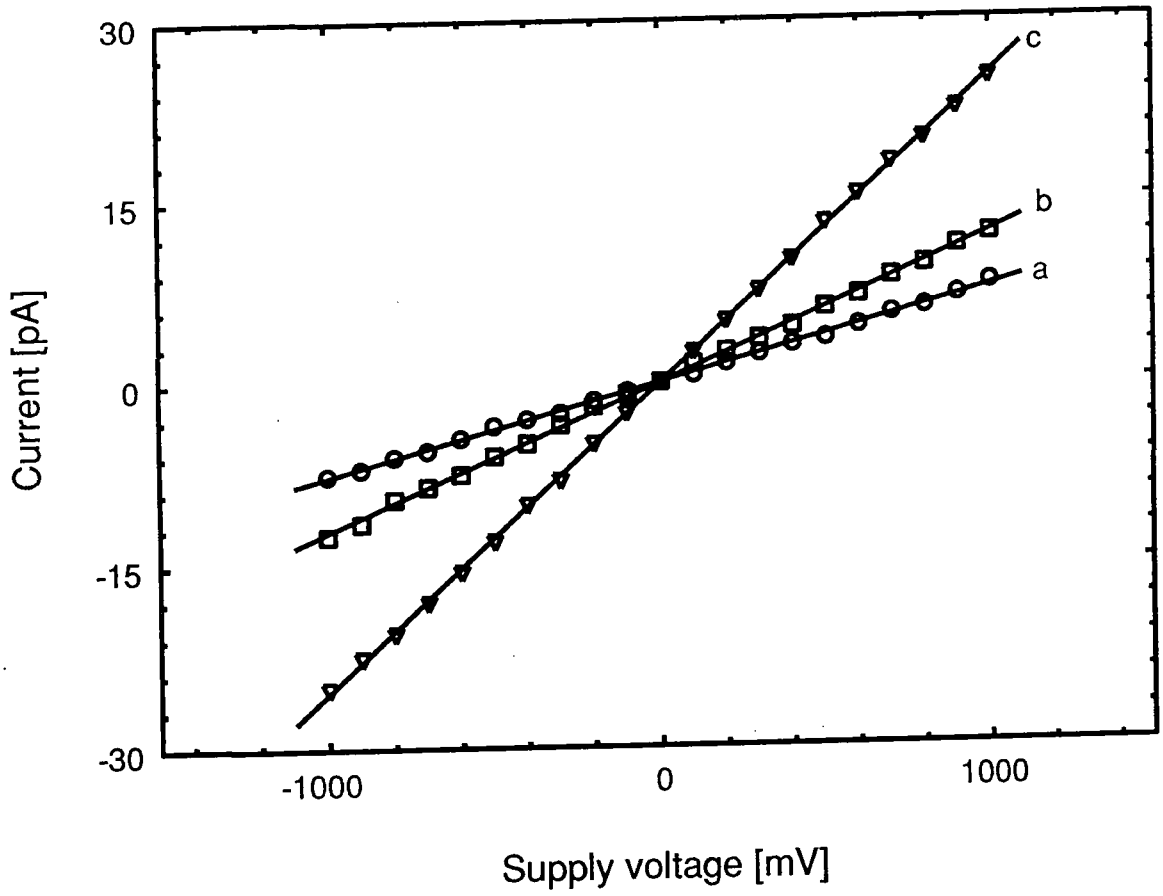

Figure 4.4: The current versus voltage characteristics of spun emeraldine base polyaniline on gold-plated interdigitated copper electrodes for different polymer film thicknesses: curve a=1μm; curve b=2μm; curve c= 4μm .(Temperature 20°C).

4.2.4 Electrical Measurements

The current versus voltage characteristics of spin-coated emeraldine base polyaniline henceforth called 'undoped' polyaniline, on interdigitated electrodes are shown in figure 4.4. The measurements were undertaken in an atmosphere of nitrogen and at room temperature. Data for the uncoated electrode confirmed that the current was flowing through the polyaniline film rather than through the substrate. The change in resistance for different film thicknesses, indicate that ohmic contacts have been established between the gold electrode and the polymer. Using the thickness values from the surface profiler, the average room temperature dc conductivity was calculated to be $4.4\times10^{-11}Scm^{-1}$ which is

comparable with that reported from the literature of $1\times10^{-11}Scm^{-1}$ [Macdiarmid et al, 1987].

The temperature dependent dc conductivity of 'undoped' polyaniline in vacuum is shown in figure 4.5. This was measured using the 14 finger interdigitated electrode in the purpose built rig shown figure 3.19.

Figure 4.5 shows that when the temperature is raised, the conductivity increases. This increase was observed to be reversible. To a first approximation, this increase in conductivity can be described as thermally activated. As the temperature increases, it is possible that localised charges acquire energy enabling them to hop between traps (i.e. thermal detrapping). Furthermore, such hopping may also involve the absorption and/or emission of acoustic phonons in such disordered solids [Emin, 1974]. The increase may also be associated with the generation of new conductive pathways.

Generally, such thermally activated variation of the dc conductivity is, to a first approximation, given as:

$$\sigma = \sigma_0 \exp - \left[\frac{\Delta E_A}{kT}\right] \qquad (4.1)$$

where ΔE_A is the activation energy. A plot of $\ln\{\sigma\}$ versus T^{-1} will give a straight line, as shown in figure 4.5. The activation energy ΔE_A is calculated to be 0.24±0.01eV.

Conduction in 'undoped' polyaniline is mediated by electrons trapped at the quinoidal site [Kivelson et al, 1988]. Other defects contributing to the intrinsic conductivity include the discontinuity in chain length and reduced bond length from oxidised portions of the polymer. These defects form deep site traps, as evidenced for the trapped exciton by the broad absorption band of the quinoid ring (see figure 4.2a) [Emin, 1986]. The deep site is located between adjacent phenyl rings, hence forming small-polarons (because the double bond at the end of one nitrogen forces its p_z orbital to remain parallel to the π-orbital of the quinoid ring hence there will be no overlap with the π-systems of adjacent

phenyl rings, rather a π-σ mixing occurs [Stafström et al, 1986]). This is manifested by a large torsional angle between adjacent quinoid and benzoid rings (typically 90°).

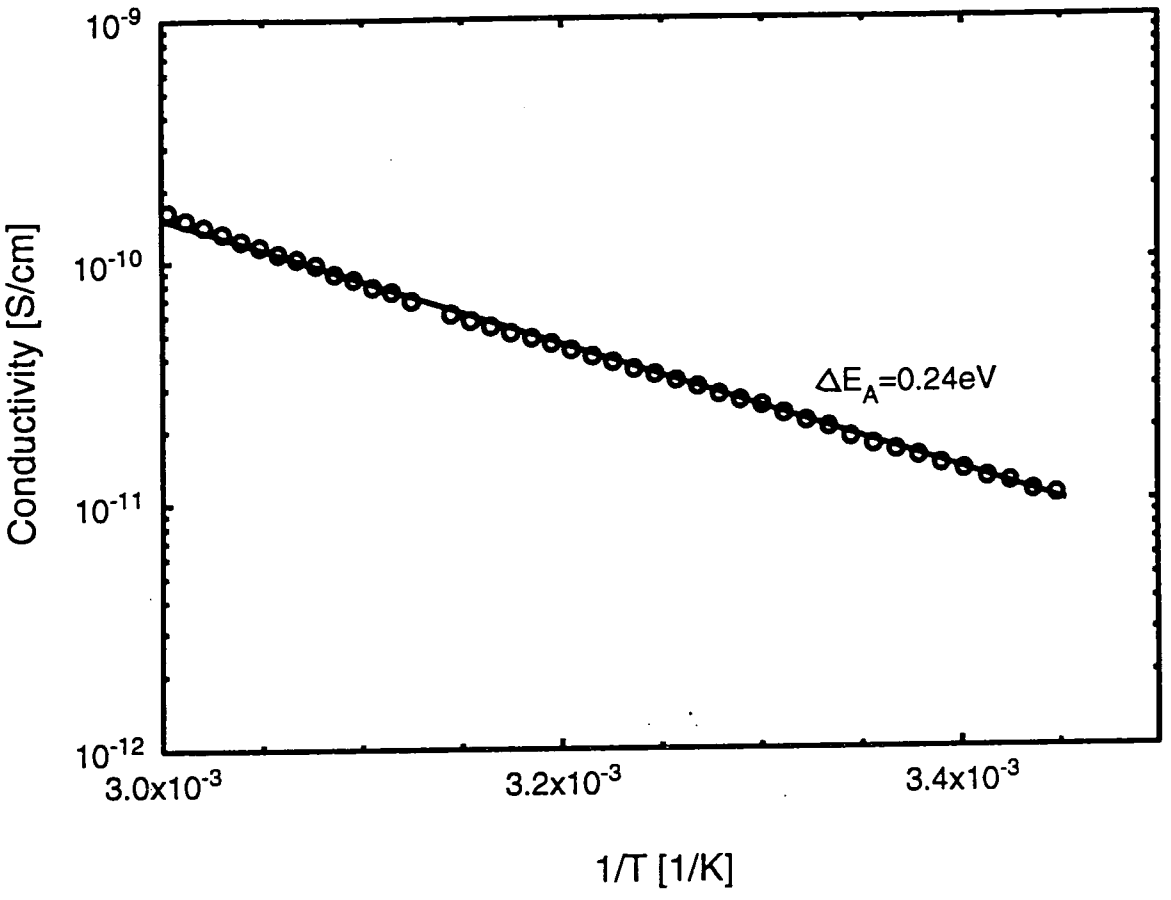

Figure 4.5: The temperature dependent dc conductivity of 'undoped' polyaniline on interdigitated electrode with 14 fingers (3V supply and 10^{-3}mbar vacuum).

Electrical measurements were also taken for 'doped' polyaniline. 'Doping' was achieved by exposing the 'undoped' polyaniline film to HCl vapour in a closed chamber at room temperature for about 30 minutes. 'Doping' is sometimes called protonation. This produced an increase in conductivity due to the formation of conjugated semiquinoid radicals (polaron/bipolaron charges) on the polymer chain [Chiang et al, 1986]. The formation of semiquinoid radicals is equivalent to the formation of holes in the valence band into which the

trapped excitons could hop with concomitant increase in dc conductivity [Laks et al, 1992].

The current versus voltage characteristic of 'doped' polyaniline is shown in figure 4.6. From the dimensions of the electrodes and the film, the room temperature dc conductivity was calculated to be $3Scm^{-1}$, which is comparable with the value obtained for electrochemically polymerised polyaniline [Wessling et al, 1986].

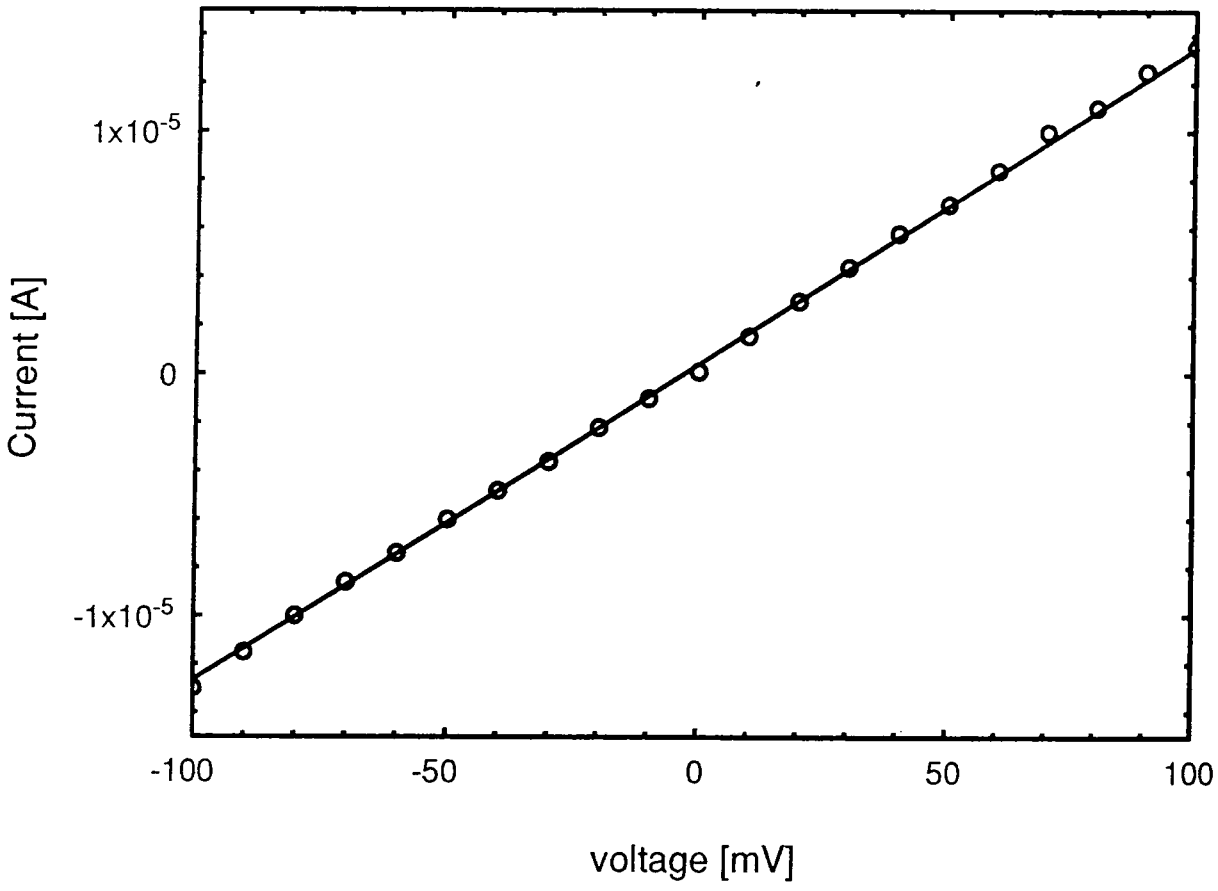

Figure 4.6: The current versus voltage characteristics of 'doped' polyaniline in 10^{-3}mbar vacuum (film thickness 0.1μm).

The temperature dependent dc conductivity, measured in air (curve a) and in 10^{-3}mbar vacuum (curve b), is shown in figure 4.7. In air, the conductivity decreases as the temperature rises. This pseudo-metallic behaviour is due to a combination of factors: the loss of the Cl^- counter ion as the temperature is

increased, loss of water vapour trapped in the polymer matrix and/or an interaction of the protonic charge (H^+) on the polymer chain with the Cl^- counter ions so producing HCl vapour which leaves the material (dedoping). These factors lead to a reduction in the level of protonation with concomitant decrease in dc conductivity. As the temperature was decreased, the change in conductivity was observed to be irreversible.

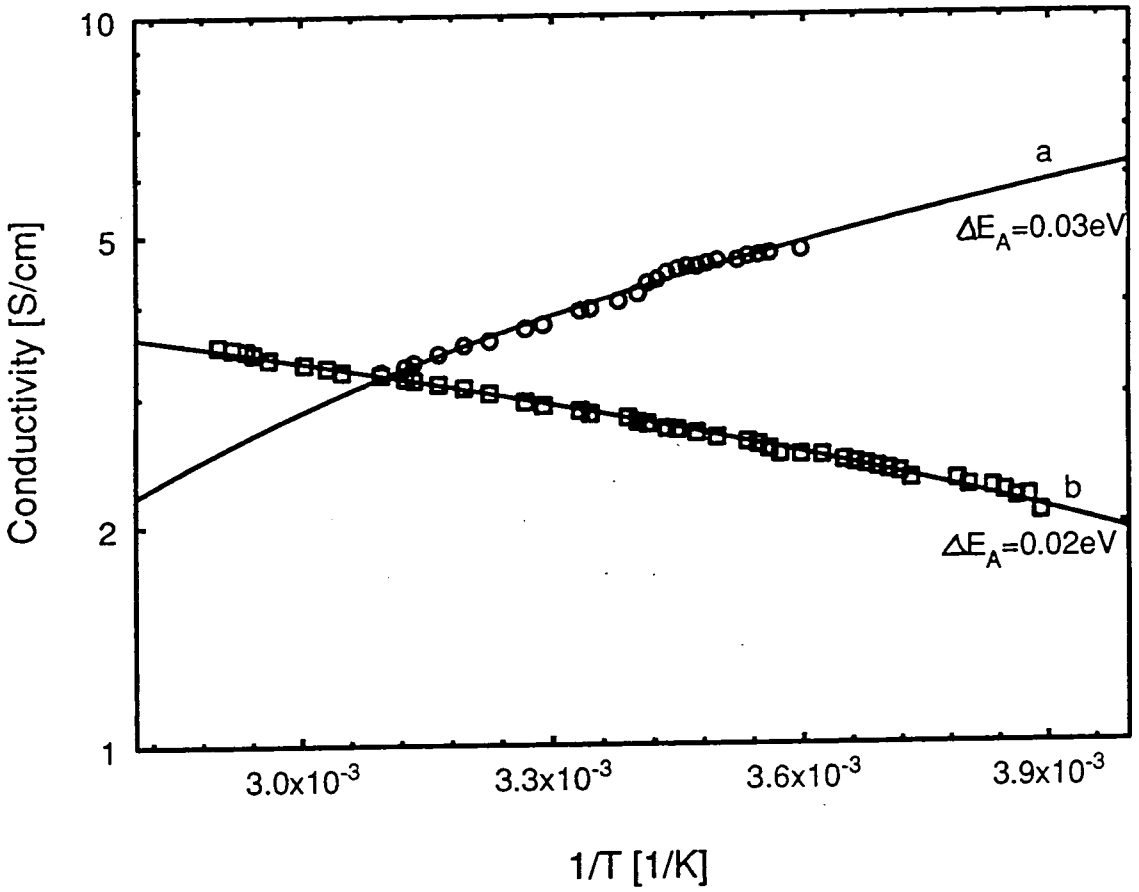

Figure 4.7: The temperature dependent dc conductivity of 'doped' polyaniline on an interdigitated electrode in air (curve a) and in vacuum of $\approx 10^{-3}$mbar (curve b) (film thickness 0.1μm and 10mV supply).

The temperature dependent dc conductivity of protonated PANi in vacuum is shown in figure 4.7, curve b. The result also shows a thermally activated behaviour which was observed to be irreversible when the temperature was reduced. This indicates the loss of a component of the system: probably the

dopant. Conduction in 'doped' polyaniline is mediated by polarons/bipolarons located on quinoid rings. The increase in conductivity with temperature may be associated with the ineffective scattering of the polaron/bipolaron (by bulk phonons) in hopping from a protonated to an unprotonated site. This is likely to be the case because protonation is rarely 100%. Alternatively, this behaviour has been associated with capacitive coupling between conducting islands separated insulating barriers [Javadi et al, 1987]. Capacitive coupling is because the film does not always become fully protonated. Applying equation 4.2, the activation energy of such a barrier was calculated to be 0.02eV±0.001.

4.2.5 Scanning Electron Microscopy

As a result of its highly insulating nature, the scanning electron micrographs of as-deposited 'undoped' polyaniline could not be recorded. Hence it was coated by glow discharge with a gold layer of a thickness of about 1.0nm. A micrograph of the as-deposited 'undoped' polyaniline is shown in figure 4.8. At low magnification (figure 4.8, plate a), the film appears patchy. However, as the magnification is increased, (see figure 4.8, plate b) the film structure is further revealed to be highly fibrous with a large density of pores separating the fibres. This film morphology is an illustration of electroaggregation and has been observed with 'doped' electrochemically deposited polyaniline [Michaelson et al, 1990]. The fibres are arranged in a mesh network and are about the same size in cross section. Such a structure is due to the relatively high degree of polymerization of the aniline monomer [Monkman, 1989]. The merging of these fibres into bundles suggests that there is some degree of cross-linking and that the ends of the fibres could be preferential nucleation sites [Monkman, 1989]. This makes the fibres to look endless and intertwining. This has also been observed by Michaelson et al, 1992.

As far gas sensing is concerned, it is likely that the fibrous mesh network will increase the surface area of interaction (sensitivity) by providing the sample with a geometrically high density of interaction sites. Furthermore, a large number of pores are visible in the mesh network which could provide a higher rate of gas diffusion into the bulk of the film (if the gas possessed a cross section which is much smaller than the pore size).

A micrograph of the 'doped' polyaniline is shown in figure 4.9. At low magnification (figure 4.9, plate a), the only visible features are ridges and spots on the surface. At high magnification, however, (see figure 4.9, plate b) a radically new structure is revealed. In this new structure, the fibres have a preferred orientation. This is in contrast to the randomly arranged fibres seen in 'undoped' polyaniline at high magnification. This 'dopant-induced' fibre realignment is possibly due to a reduction in the degree of H-bonding between chains of the polymer.

With regard to gas sensing, the 'dopant-induced' fibre realignment structure reduces the surface area of interaction as well as limiting the number of diffusion channels into the bulk of the sample. A possible implication is a lower sensitivity.

From the results presented so far, we decided that the 'undoped' materials would make better (more reproducible) gas sensors than 'doped' ones.

4.3 GAS SENSING

The results of the interaction of different gases with 'undoped' spin-coated polyaniline (SPANi) are presented in this section. These include gas-induced change in conductivity and also changes in the RAIRS spectrum of the material.

4.3.1 Insitu-Conductivity Gas Response

The room temperature gas sensing behaviour of 'undoped' polyaniline to the gases N_2, NO_x, SO_2, H_2S, CO, and CH_4 has been studied. The concentration of gases used was varied from 1 to 50,000ppm. These measurements were undertaken by applying a fixed bias to the device and monitoring the current over a period of time. In the following discussion, current changes are interpreted as changes in the conductivity of the material. The conductivity of the sample was monitored as described in chapter three.

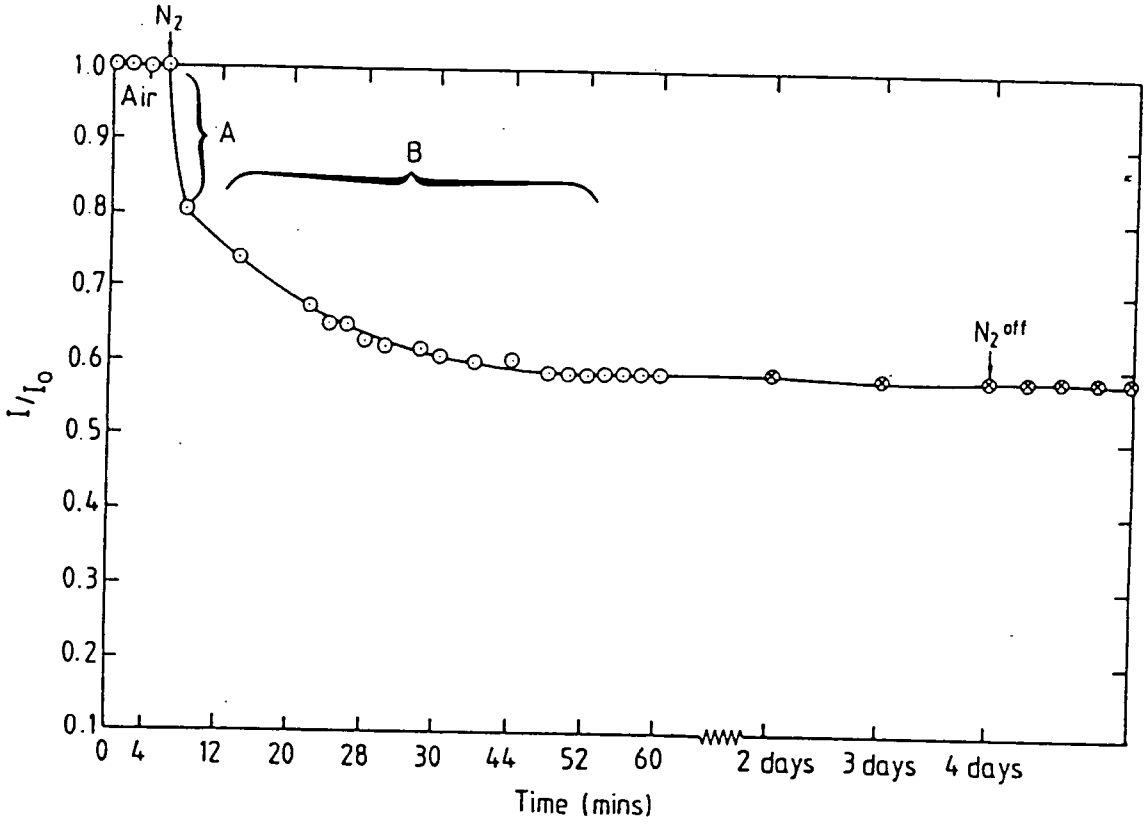

Figure 4.10: The effect of dry nitrogen on the dc conductivity of an 'undoped' spin-coated polyaniline chemiresistor at room temperature.

Figure 4.10 shows the effect of dry N_2 on the dc conductivity of an 'undoped' polyaniline chemiresistor. The conductivity decreased rapidly upon the introduction of N_2 after about 20 seconds. This decrease is two fold: an initially rapid phase (A) followed by a more gradual reduction process (B) until stability is attained after a period of about 1 hour. Stability was obtained only for 'undoped' films and formed a baseline for gas sensing experiments. Furthermore, it lasted for periods ranging up to days. The first phase of the decrease can be associated with two events: a change in gas flow rate over the sample and/or the removal of surface bound water molecules. The second gradual phase is possibly related to the removal of water vapour molecules trapped in the bulk of the film.

Errors in these measurements were calculated for the full range of concentration pre-sets to be about 2.5% of any observable change in

conductivity. This was calculated from changes in device conductivity caused by using a second supply of nitrogen as the active gas.

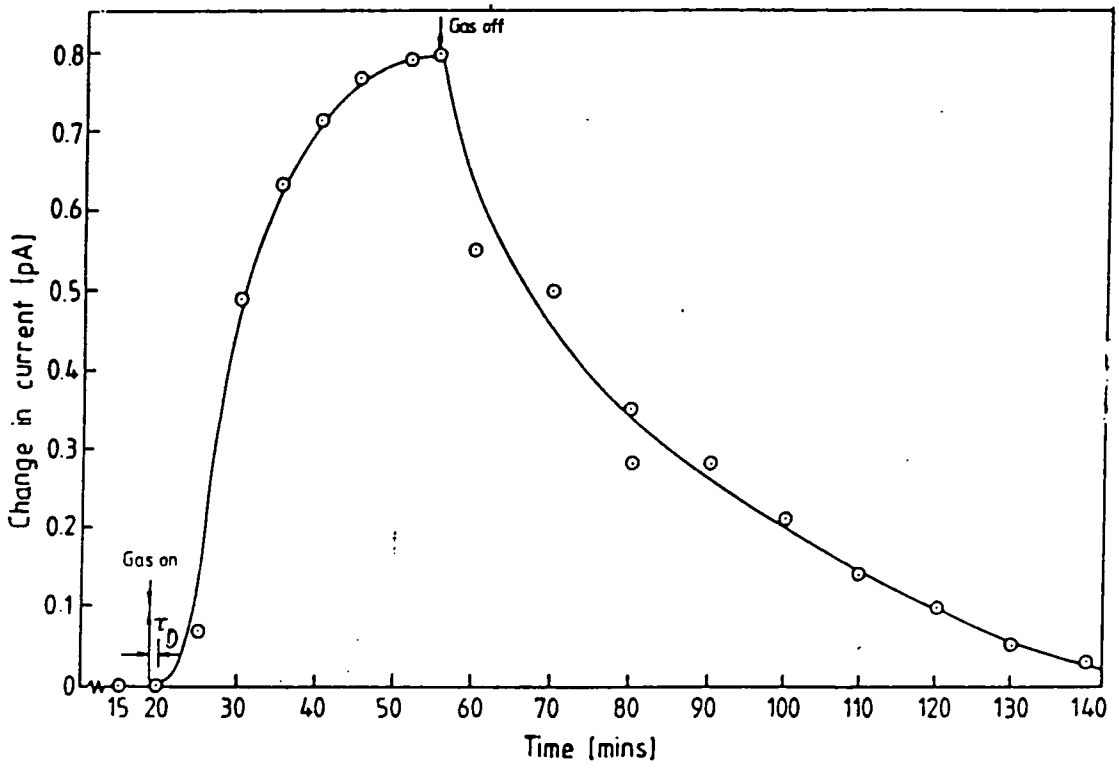

Figure 4.11a: The effect of 10ppm NO_x on an 'undoped' polyaniline chemiresistor at room temperature (200mV supply and film thickness 0.1μm).

Figure 4.11a shows the effect of 10ppm NO_x on 'undoped' spin-coated polyaniline. It can be seen that this gas produced an increase in conductivity of the device. This increase is measurable after a delay time τ_D defined in chapter three. The delay time for this interaction was about 48 seconds for 10ppm of the gas. The exposure was undertaken for a period lasting up to 36 minutes after which the gas was turned off. The reaction then reversed exponentially until the original conductivity was restored. For 10ppm NO_x, the exponential decrease lasted up to about 100 minutes.

A similar measurement using 150ppm NO_x also produced an increase in conductivity. However, as shown in figure 4.11b, this response was not reversible at room temperature: indicating a different reaction mechanism.

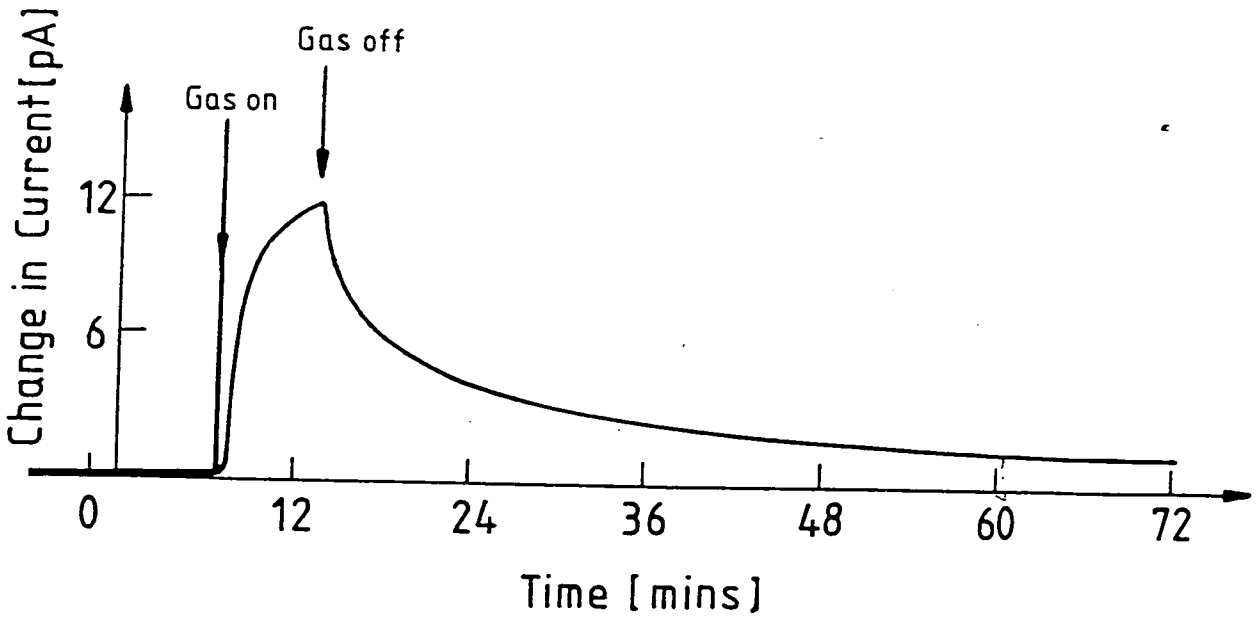

Figure 4.11b: The effect of 150ppm NO_x on an 'undoped' polyaniline chemiresistor at room temperature (200mV supply and film thickness 0.1μm).

A calibration of the device response was carried out by measuring the change in conductivity for different gas concentrations. The result in figure 4.11c, shows a gradual increase in conductivity with gas concentration, with a measured threshold of 4ppm.

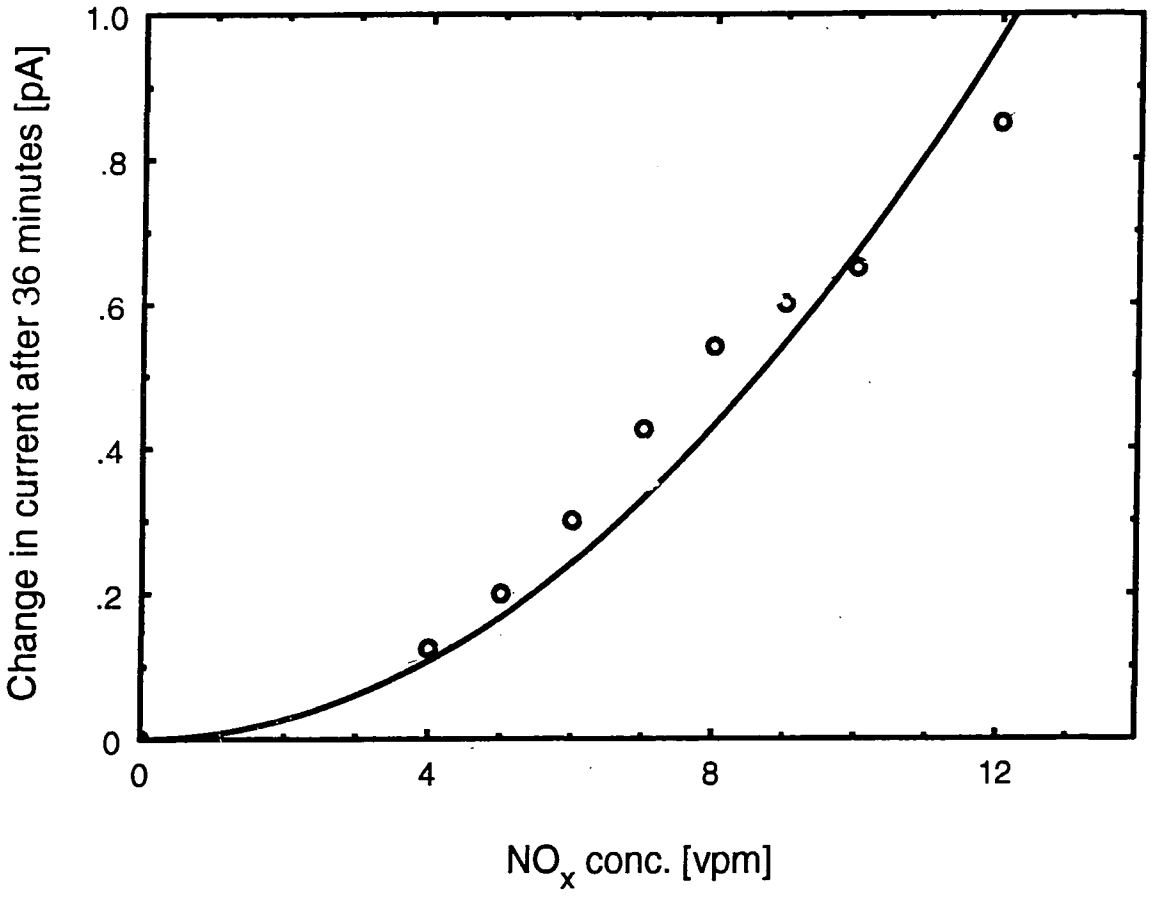

Figure 4.11c: The response of an 'undoped' polyaniline chemiresistor to different concentrations of NO_X.

The interaction between NO_X and 'undoped' polyaniline can be explained as follows: NO_X is a well known oxidising gas, which on contact with the π-electron network of polyaniline (or any other system with electron lone pairs) is likely to result in the transfer of an electron from the polymer to the gas. When this occurs, the polymer becomes positively charged. The positive charge created will subsequently be delocalised along the polymer chain, producing an increase in conductivity. We therefore suggest that NO_X is interacting with the imine nitrogen lone pair electrons in a similar way to protons. And as the gas concentration increases (equivalent to a decrease in pH), new sites e.g. amine nitrogens and/or polymeric benzoid rings, are oxidised. These sites may be characterized by a lower π-electron density. Such a redox reaction can be represented thus:

$$PANi + NO_X \Leftrightarrow [PANi^{m+}NO_X^{n-}] \qquad (4.2)$$

where m and n are constants. In this interaction, the equilibrium is shifted to the right during exposure and to the left during recovery. This mechanism may be compared to the proposed manner of interaction between water and 'undoped' polyaniline. Here it is suggested that proton exchange through hydrogen bonding takes place between imine nitrogens and water molecules [Nechtschein et al, 1986, Lubentsov et al, 1991].

Figure 4.12a shows the effect of 8ppm of H_2S on the chemiresistor at room temperature. This measurement was undertaken using the same device as for NO_X because of the difficulties of reproducing exactly the same device characteristics (e.g., thickness). H_2S also produced an increase in the conductivity of the material. This increase takes place after a delay time of about 36 seconds. Complete recovery was achieved after a period of about 56 minutes.

A calibration of the change in conductivity with different H_2S gas concentrations is shown in figure 4.12b. A continuous increase in conductivity can be seen extending from 4 to 10ppm.

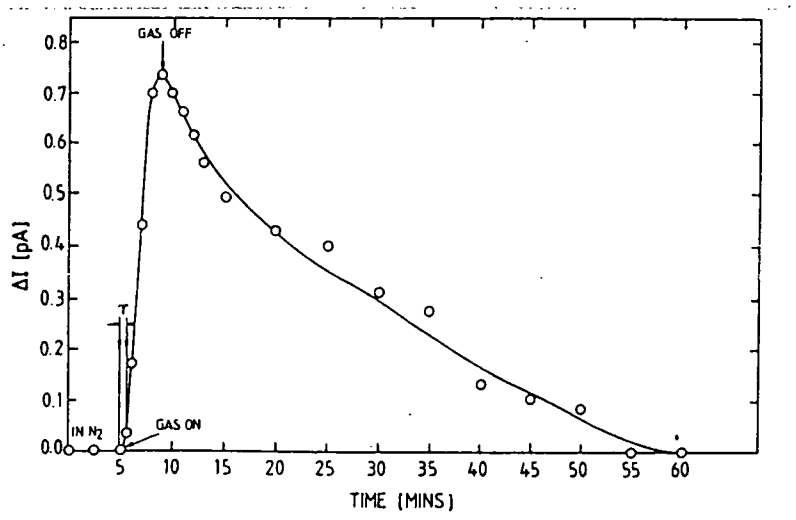

Figure 4.12a: The effect of 8ppm H_2S on an 'undoped' polyaniline chemiresistor at room temperature (200mV supply and film thickness 0.1μm).

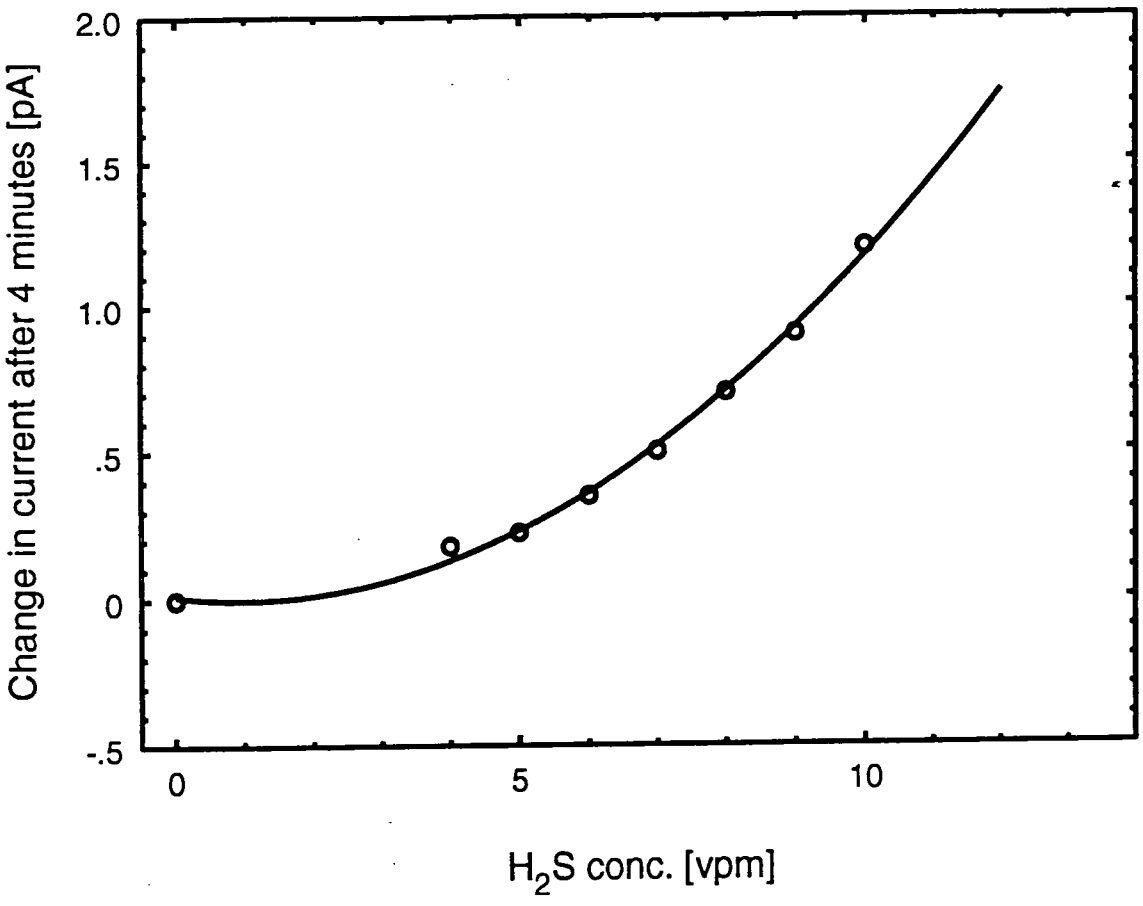

Figure 4.12b: The response of an 'undoped' polyaniline chemiresistor to different concentrations of H_2S.

H_2S is a known reducing gas. Thus, from the discussions above, we would expect to observe a decrease in the conductivity of the polyaniline film. The observed increase in conductivity with H_2S gas indicates that more than one type of reaction site is available and/or a number of different reactions is possible.

At room temperature and pressure, H_2S dissociates in water into H^+ and HS^- [Babero et al, 1982, Carrol et al, 1989, Clark et al, 1972 and Gerrard et al, 1972] as illustrated in figure 4.13.

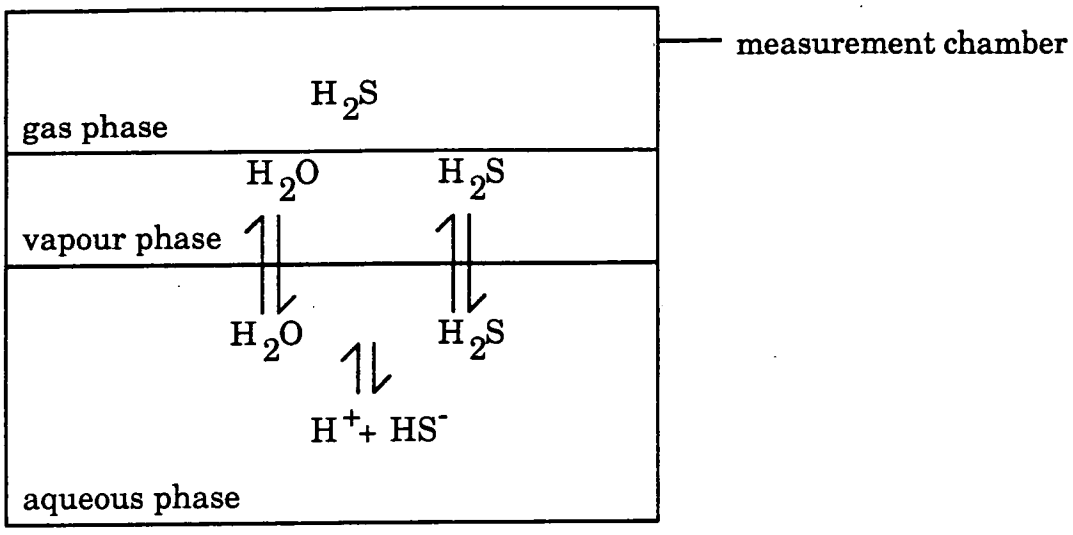

Figure 4.13: An illustration of the state of H_2S in different environments [Clarke et al, 1971]. In this work, the vapour phase is equivalent to H_2S/surface bound water molecules and the aqueous phase is equivalent to H_2S/water molecules trapped in the bulk of the film.

The dissociation of H_2S is subsequently followed by H^+ protonating the polymer:

$$[PANi] + [H^+] \Leftrightarrow [PANiH^+] \qquad (4.3)$$

where the equilibrium is shifted to the right during exposure and to the left after exposure.

As noted in section 4.2.4, this protonation reaction produces semiquinone radicals which are conjugated and consequently results in an increase in the dc conductivity. This explains how H_2S could produce an increase rather than a decrease in the dc conductivity of the 'undoped' polyaniline chemiresistor. Such a reaction can be considered as a bulk dominated process because of the substantially higher concentration of water vapour trapped in the bulk of the film.

The response of the same device to 10ppm of SO_2 is shown in figure 4.14a. This clearly shows an increase in conductivity as well as complete reversibility at

room temperature. The delay time recorded for this interaction was 12 seconds and complete recovery attained after about 100minutes.

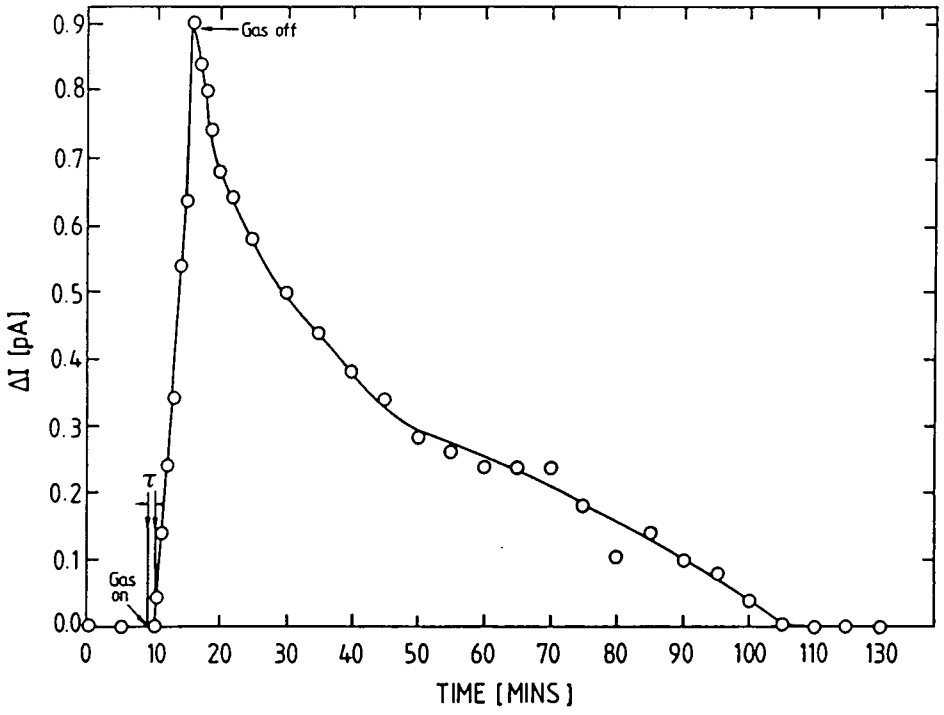

Figure 4.14a: The effect of 10ppm SO_2 on an 'undoped' polyaniline chemiresistor at room temperature (200mV supply and film thickness 0.1μm).

A calibration study of the device sensitivity to different SO_2 gas concentrations is shown in figure 4.14b. Again, the results show a smooth curve for the gas concentrations investigated. Furthermore, it shows that the device is capable of measuring changes down to 2ppm.

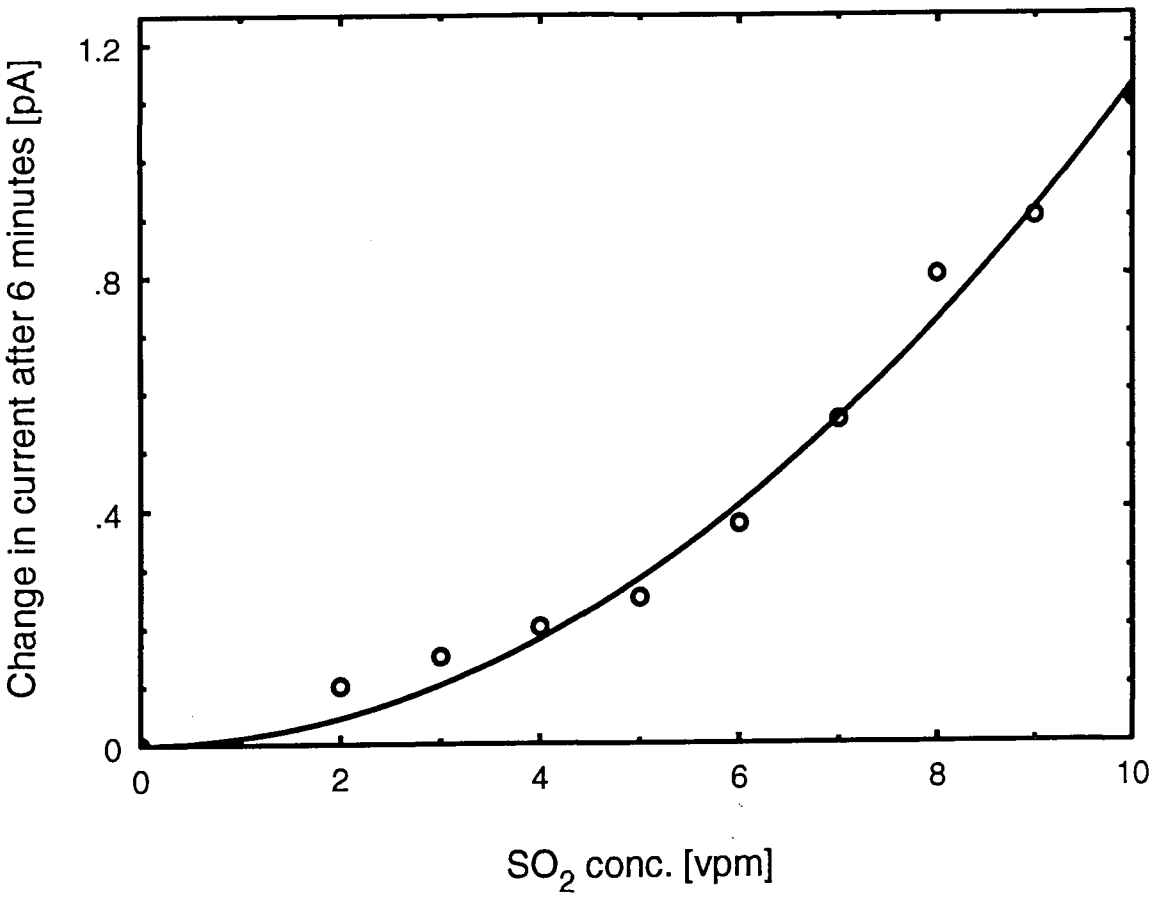

Figure 4.14b: The response of an 'undoped' polyaniline chemiresistor to different concentrations of SO_2.

Gas sensing using very high concentrations of CO (10,000ppm) and CH_4 (50,000ppm) produced no measurable effects even after prolonged periods of exposure.

A summary of the reversible gas sensing studies with 'undoped' polyaniline is shown in table 4.2. The negative sign of change indicates a decrease in device resistance. It is evident that the device is most sensitive to SO_2 and least to NO_X, despite the more oxidising characteristics of NO_X. Exposure of the device to NO_X gas concentrations ≥100ppm produced irreversible changes in conductivity.

Gas	Conc. in N_2 [ppm]	Delay Time τ_D [s]	Exposure Time [mins]	Recovery Time τ_R [mins]	Minimum Detection Level [ppm]	Normalised Change per ppm $\frac{\Delta R}{R} \div$ gas conc in ppm
NO_x	10	48	36	100	4	-0.026 (at 10ppm)
H_2S	10	36	4	56	3	-0.033 (at 10ppm)
SO_2	10	12	6	100	2	-0.036 (at 10ppm)
CO	10000	No observed effect	25	N/A	N/A	N/A
CH_4	50000	No observed effect	25	N/A	N/A	N/A

Table 4.2: Summary of the effect of different gases on a spin-coated polyaniline chemiresistor at room temperature.

4.3.2 Insitu-Reflection Infrared Spectroscopy

Figure 4.15 shows the RAIRS spectrum of 'undoped' polyaniline before exposure (curve a) and after 6 hours of exposure to 150ppm NO_X (curve b) at room temperature.

From figure 4.15, curve b, a general decrease in the baseline absorbance can be seen extending over the whole mid-infrared frequency region (400-4000cm^{-1}). We associate this with the removal of some tightly bound solvents e.g. NMP and/or water vapour .

At first glance, both spectra in figure 4.15 are almost identical. Therefore a difference spectrum, as shown in figure 4.16 was calculated. This is simply the difference between a spectrum before exposure and a spectrum after exposure. Because the changes observed were very small, a systematic investigation of the reaction was also carried out by recording the spectrum under a NO_X environment for times ranging from 1 to 6 hours.

The most significant changes observed in the difference spectra occur in the aromatic stretch region between 1593cm^{-1} and 1400cm^{-1}. From these, it is clear that the relative intensity of the benzoid ring stretch at 1504cm^{-1} decreases while that of the quinoid ring stretch at 1593cm^{-1} increases with increasing exposure time. We attribute the growth of the quinoid peak at 1593cm^{-1} to benzoid ring oxidation into quinoid ring structures. Thus we conclude that the changes observed are real and not due to artefacts.

After six hours exposure to NO_X, the gas was turned off. The spectrum was again recorded after 4 hours in argon but the results showed no signs of reversibility. Hence, the changes discussed above can be related only to the irreversible changes in conductivity observed when the chemiresistor was exposed to higher NO_X gas concentrations. Unfortunately, the infrared technique was not sensitive enough to monitor the reversible changes observed at low gas concentrations.

From both results presented so far we have suggested that at high concentrations, the interaction of NO_X with 'undoped' polyaniline is a complex redox reaction involving the oxidation of benzoid rings to quinoid ones with the

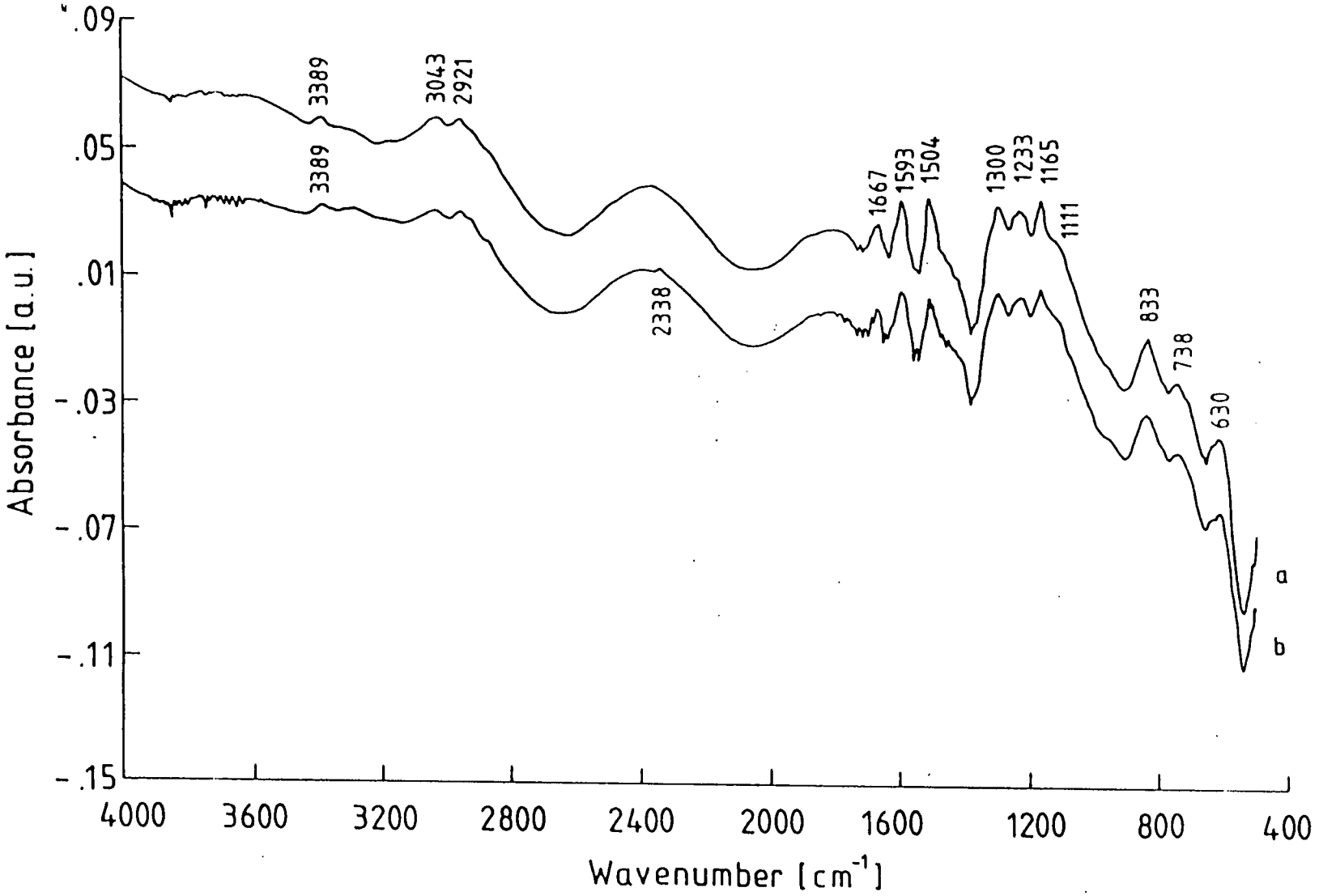

Figure 4.15: Reflection-absorption Fourier transform infrared spectra of 'undoped' spin-coated polyaniline in an argon atmosphere (a) and (b) after 6 hours of exposure to 150ppm NO_x.

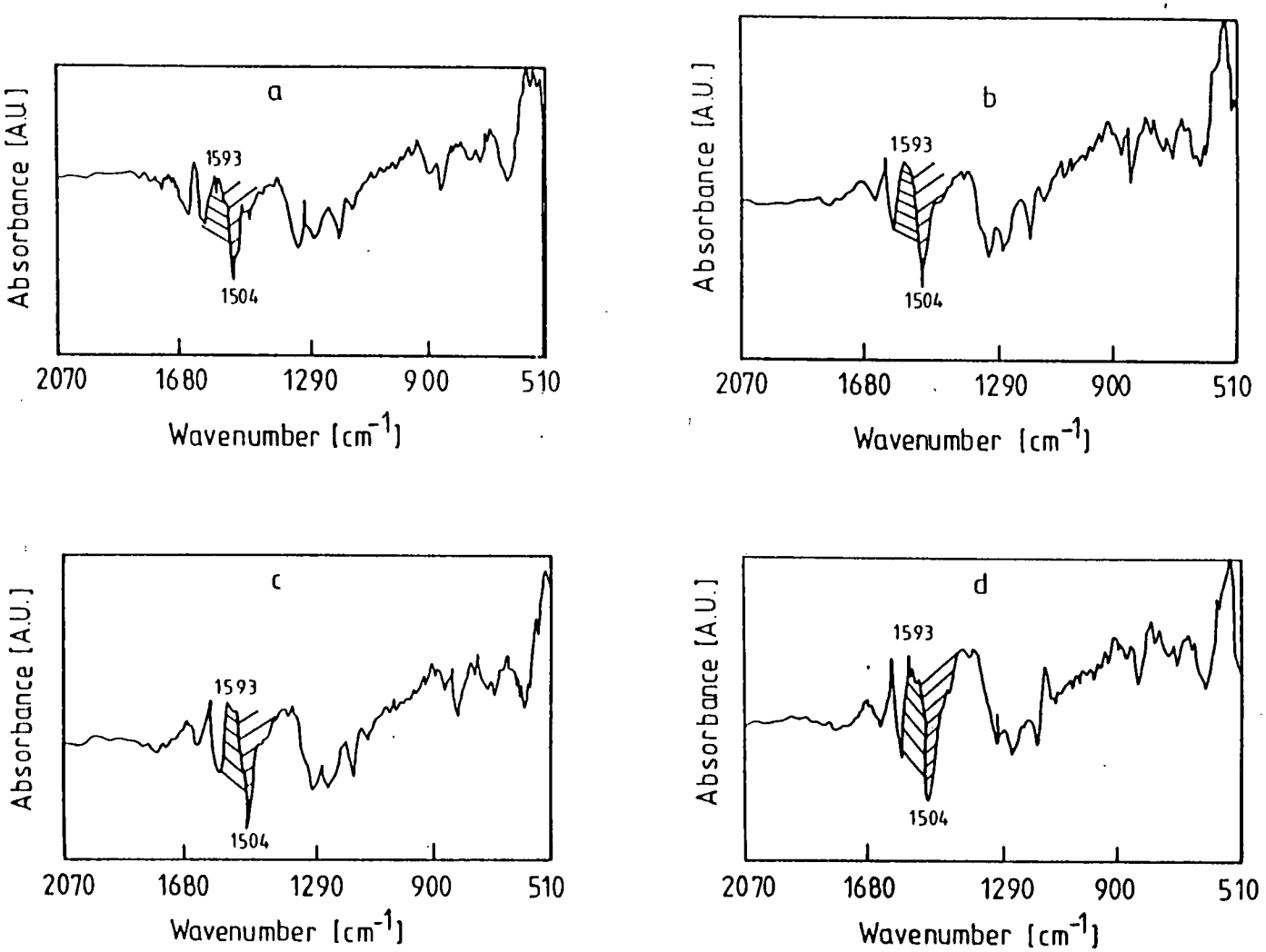

Figure 4.16: Difference spectra of 'undoped' spin-coated polyaniline after exposure to 150ppm NO_x for (a) 1 hour (b) 3 hours (c) 4 hours and (d) 6 hours.

subsequent transfer of electrons from the polymer to the electrophilic gas. And at low concentrations, it is possibly due to formation of a charged transfer complex between the material and the vapour at the imine nitrogen position. Other changes are not excluded, especially as the reaction was undertaken with a relatively high concentration of gas and at large angles of incidence, (limiting the sensitivity of the IR instrumentation).

Figure 4.17 shows the infrared difference spectra of 'undoped' polyaniline after exposure to 150ppm H_2S. The baseline is relatively flat extending from 490cm^{-1} to 4000cm^{-1}. The main changes shown in the difference spectrum occur in the CH_2 stretching region in which a peak can be seen extending from 2800-2900 cm^{-1}. The broadness of this band suggests that more than one vibration is contributing to it. We suggest this might be the result of impurities in the material. The peak at 2338cm^{-1} is due to tightly bound CO_2 in the polymer while the sharp band at 1700cm^{-1} (see figure 4.17, curve b) is a carbonyl vibration which may result from leaks in the system. A weak shoulder can be seen emerging around 3045cm^{-1} in figure 4.17, curve b. The growth of the shoulder at 3045cm^{-1} can be associated with an increase in the number of hydrogens on quinoid rings which may be as a result of film protonation (see section 4.2.3). A broad band can also be seen emerging at 1088cm^{-1}. We are unable to resolve this spectrum into individual vibrations, hence as with NO_x, its interpretation is limited. However, the small increases observed at 3045cm^{-1} and 1088cm^{-1} bands are signatures of the formation of semiquinone radicals.

After two hours exposure, the gas was turned off. And as with NO_x, there were no signs of reversibility.

Figure 4.18 shows the absorption spectrum of 'undoped' polyaniline before and after exposure to 150ppm SO_2 for 4 hours. Prominent amongst the changes observed is an increase in the intensity of the quinoid peak at 1593cm^{-1} with respect to the benzoid one at 1504cm^{-1}. The most probable cause of this change is due to conversion by oxidation of the benzoid rings to quinoid rings, hence the growth of the latter.

The largest feature visible in this figure is a gradual increase in absorption from 2000-4000cm^{-1}. This is equivalent to the creation of a charge transfer band and is likely due to a protonation reaction. We have already noted in

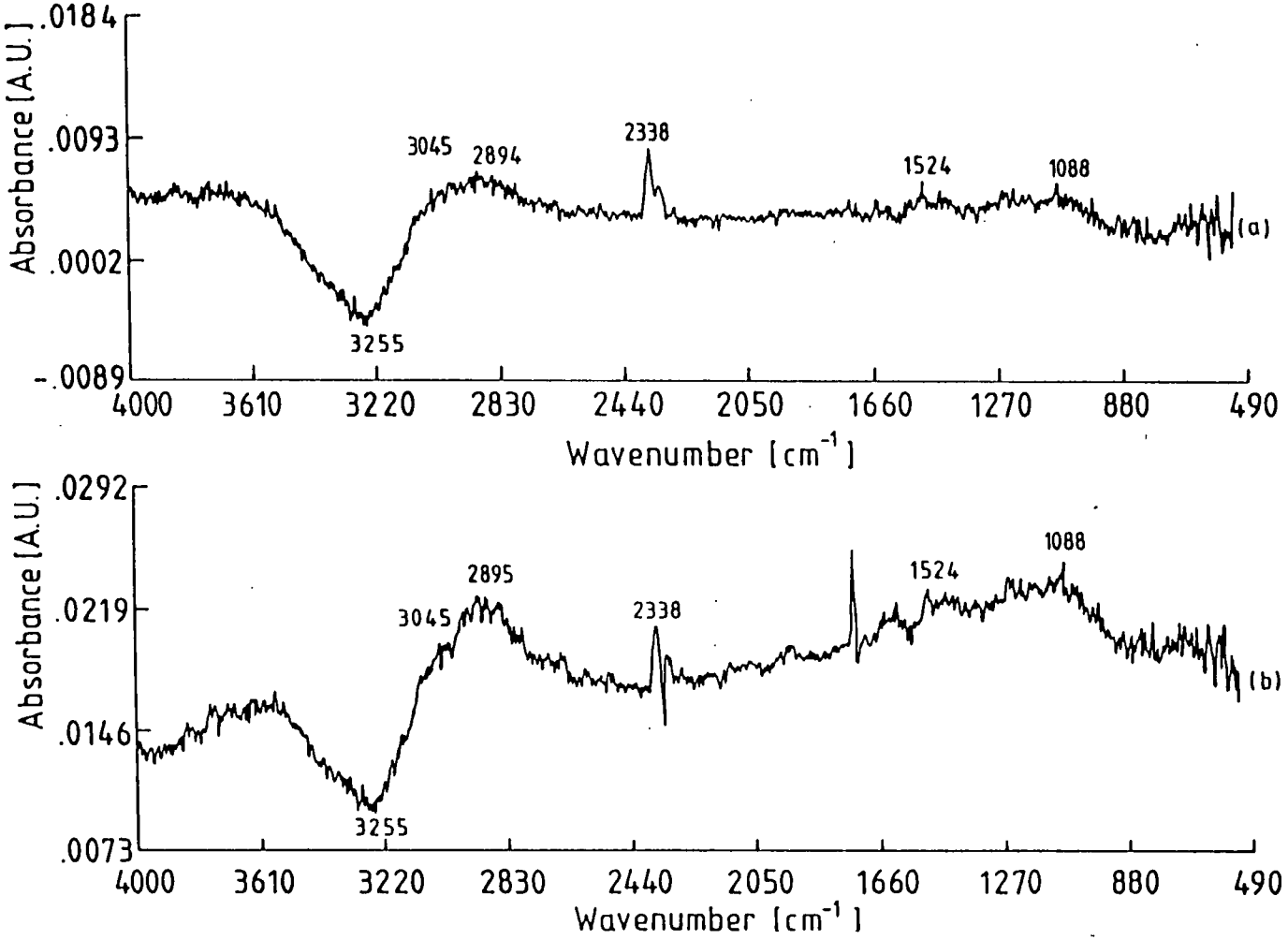

Figure 4.17: Difference spectra of 'undoped' spin-coated polyaniline after exposure to 150ppm H_2S for (a) 1 hour and (b) 2 hours of exposure.

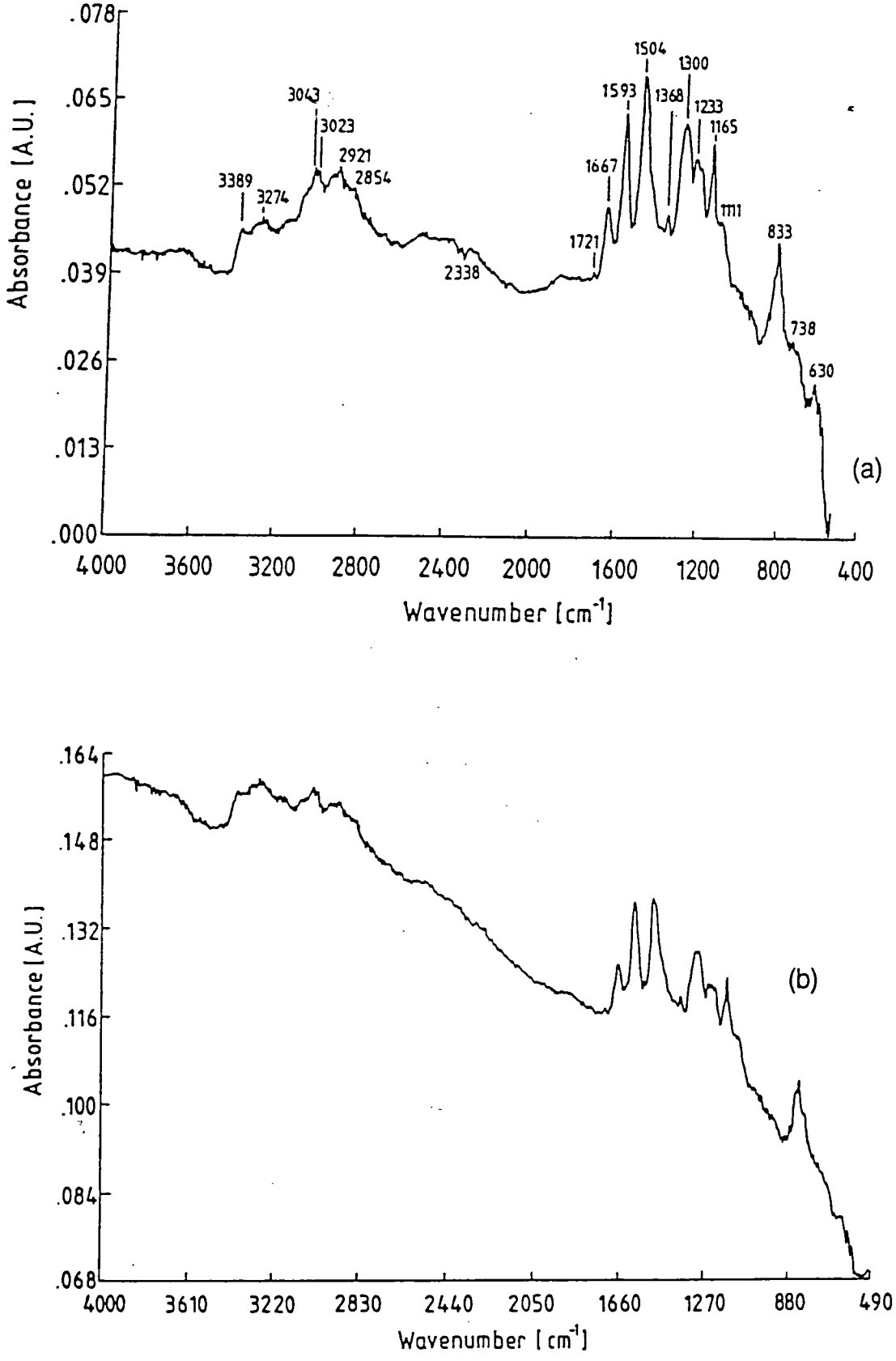

Figure 4.18: Reflection-absorption Fourier transform infrared spectra of 'undoped' spin-coated polyaniline in an argon atmosphere (curve a) and after 4 hours of exposure to 150ppm SO_2(curve b).

section 3.3.3 that there is usually some water trapped in the film. Furthermore, it is widely known that SO_2 forms sulphuric acid when in contact with water [Gerrard et al, 1972]. But sulphuric acid is not a Brönstead acid (existing in equilibrium with $2H^+$ and SO_4^{2-}). Hence, when in contact with the polyaniline polymer, it protonates as well as oxidizes it. Both reactions (protonation and oxidation) result in an increase in dc conductivity. This may explain why the 'undoped' polyaniline chemiresistor was more sensitive to SO_2 rather than NO_x, which is more electrophilic.

Figure 4.19 shows a difference spectrum, obtained insitu by subtracting a spectrum before exposure from the same one after exposure to SO_2. There are virtually no new bands in the difference spectrum after 1 hour exposure. The peak at $2338cm^{-1}$ due to CO_2 and $1350cm^{-1}$ due to SO_2. However, when exposed for 20 hours to 150ppm SO_2, large non-reversible changes can be seen in the difference spectrum. These include the growth of the benzoid band at $1507cm^{-1}$ (due to the formation of semiquinoid radicals) and the growth of the C-H deformation band extending from $1171cm^{-1}$ to $619cm^{-1}$. Changes in these bands are closely linked to protonation and oxidation in which the number of H per ring increases [Furukawa et al, 1986].

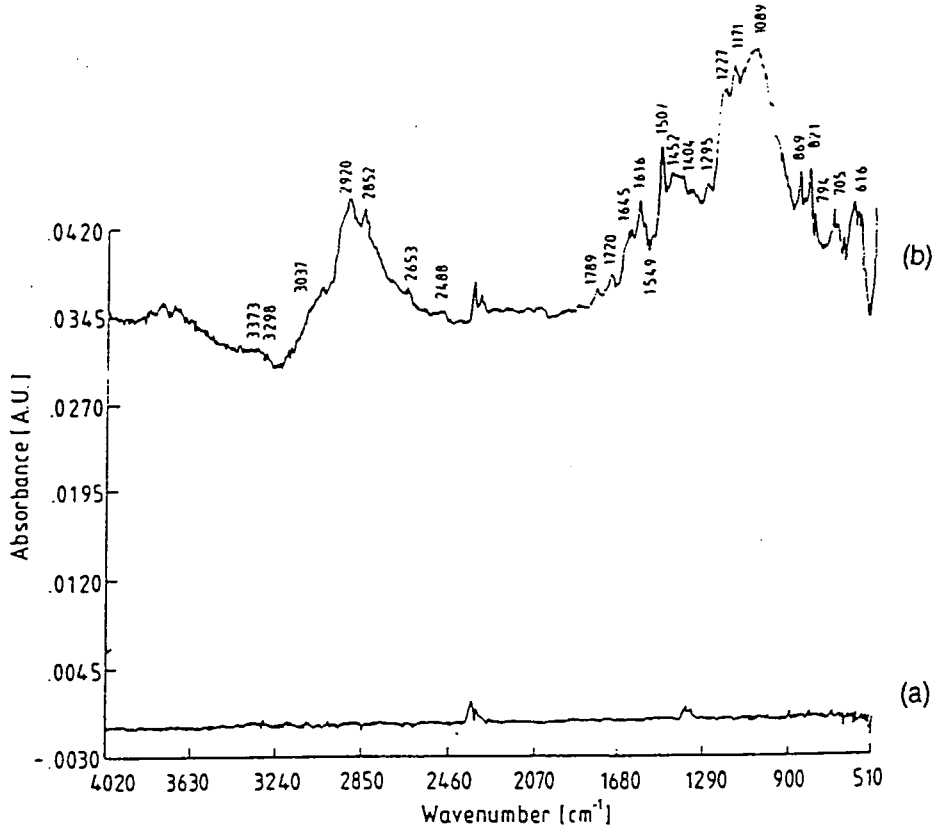

Figure 4.19: Difference spectrum of 'undoped' spin-coated polyaniline after exposure to 150ppm SO_2 for 1 hour (curve a) and 20 hours (curve b).

From the above discussion, we suggest the following reactions may occur:

$$PANi + SO_2 \Leftrightarrow PANi^+SO_2^- \quad (4.4)$$

$$[2H_2O + SO_2 \Rightarrow H_2SO_4 + H_2$$

$$PANi + [2H^+ + SO_4^{2-}] \Rightarrow [PANiH]^{+2}SO_4^{2-}] \quad (4.5)$$

Equation 4.4 refers to the reversible reaction that dominates low gas concentration, while equation 4.5 possibly refers to an irreversible reaction that may occur when the device is exposed to higher gas concentrations.

4.4 SUMMARY

Thin films of 'undoped' polyaniline have been deposited by spinning and characterized using electrical, optical and structural techniques. The deposited films have been shown to be sufficiently conducting with an activation energy of about 10kT and are stable at room temperature for gas sensing applications. The physical structure of the material has been determined to be composed of numerous intertwining fibres with a large surface area for gaseous interaction. We have also shown that the as-deposited material is sensitive to the gases NO_x, SO_2 and H_2S but unresponsive to combustion products such as CO and CH_4 at room temperature. The device response occurs after a delay time of a few seconds and then for low concentrations, recovers completely when gas flow stops. All three gases detected produced an increase in conductivity. Such an effect is unusual for H_2S which is known to be a reducing gas.

By insitu-RAIRS, we have attempted to explain the observed effects for each gas at high concentrations. For NO_x, it is an equilibrium phenyl ring and imine nitrogen oxidation reaction; for H_2S the interaction is an equilibrium quinoid ring protonation and for SO_2 it is an equilibrium phenyl ring oxidation at low concentration for short exposure times and a non-equilibrium quinoid ring protonation reaction at high concentration and/or prolonged exposure. These reactions have been shown to be irreversible for high gas concentrations.

REFERENCES

Barbero, J.A., Mccurdy, K.G. and Tremaine, P.R. : Canadian J. Chem., **60** (1982) 1873-1880

Cao, Y., Li, S., Xue, Z. and Guo, D. : Synthetic Metals, **16** (1986) 305-315

Carroll, J.J. and Mather, A.E. : Geochimica et Cosmochimica, **53** (1989) 1163-1170

Chiang, J. and Macdiarmid, A.G. : Synthetic Metals, **13** (1986) 193-205

Clarke, E.C.W. and Glew, D.N. : Canadian J. Chem., **49** (1971) 691-698

Duke, C.B., Conwell, E.M. and Paton, A. : Chem. Phys. Letters., **131** (1986) 82-86

Emin, D. : Physical Review Letters, **32** (1974) 303-307

Emin, D. : Physical Review B, **4** (1971) 3639-3651

Emin, D. : 'Handbook of Conducting Polymers', Skotheim, T.A., (ed)., Marcel Dekker, New York (1986) 915- 936

Emin, D. : Physical Review B, 4 (1971) 1321-1337

Epstein, A.J., Ginder, J.M., Zuo, F., Bigelow, R.W., Woo, H.S., Tanner, D.B., Richter, A.F., Huang, W.S. and Macdiarmid, A.G. : Synthetic Metals, **18** (1987) 303-309

Furukawa, Y., Hara, T., Hyodo, Y. and Harada, I. : Synthetic Metals, **16** (1986) 189-198

Gerrard, W. : J. Appl. Chem. Biotechnol., **22** (1972) 623-650

Hagiwara, T., Yamaura, M. and Iwata, K. : Synthetic Metals, **25** (1988) 243-252

Javadi, H.H.S., Angelopoulos, M., Macdiarmid, A.G. and Epstein, A.J. : Synthetic Metals, **26** (1988) 1-8

Kivelson, S. and Heeger, A.J. : Synthetic Metals, **22** (1988) 371-384

Laks, B., Dos Santos, D.A. and Galvâo, D.S. : Preprints International Conference on Synthetic Metals, Gorteburg, Sweden (1992)

Lubentsov, B.Z., Timofeeva, O.N. and Khidekel, M.L. : Synthetic Metals, **45** (1991) 236-240

Macdiarmid, A.G., Chiang, J.C., Richter, A.F. and Epstein, A.J. : Synthetic Metals, **18** (1987) 28 5-290

Michaelson, J.C., McEvoy, A.J. and Kuramoto, N. : J. Electroanal. Chem., **287** (1990) 191-198

Michaelson, J.C., McEvoy, A.J. and Kuramoto, N. : Reactive Polymers, **17** (1992) 197-206

Monkman, A.P. : PhD thesis, London University, 1989

Monkman, A.P. and Adams, P. : Synthetic Metals, **40** (1991) 87-96

Nechtschein, M., Santer, C., Travers, J.P., Chroboczek, J., Alix, A. and Ripert, M. : Synthetic Metals, **18** (1987) 311-316

Ohira, N., Sakai, T., Takeuchi, M., Kobayashi, Y. and Tsuji, M. : Synthetic Metals, **18** (1987) 347-352

Roe, M.G., Ginder, J.M., Gustafson, T.L., Angelopoulos, M., Macdiarmid, A.G and Epstein, A.J. : Physical Review B, **40** (1989) 4187-4190

Stafström, S. : Synthetic Metals, **18** (1987) 387-392

Stafström, S. and Brédas, J.L. : Synthetic Metals, **14** (1986) 297-308

Tang, J., Jing, X., Wang, B. and Wang, F. : Synthetic Metals, **24** (1988) 231-238

Wessling, B. and Volk, H. : Synthetic Metals, **16** (1986) 127-131

CHAPTER FIVE

EVAPORATED POLYANILINE THIN FILMS:

RESULTS AND DISCUSSION

5.1 PREFACE

The chapter presents the results of studies of polyaniline thin films produced by thermal evaporation (EPANi). In the first sections, the structure and quality of the films are studied using optical absorption, Fourier transform infrared spectroscopy, electrical conductivity and scanning electron microscopy. This is then followed by an account of gas sensing investigations at room temperature.

5.2 FILM SURFACE PROFILE AND THICKNESS CALIBRATION

The deposition of polyaniline films onto various substrates was undertaken in a vacuum of 10^{-3}mbar. During deposition, the source temperature was kept constant at 400^{o}C. The films deposited onto glass were colourless but, on exposure to air, changed colour initially to purple and then to the blue that is characteristic of emeraldine base polyaniline over a period of several months. The colourless nature of the as-deposited films is consistent with the findings of Chevalier et al, 1989 and Ohira et al, 1987 for the completely reduced form of polyaniline.

A thickness profile of the films on glass revealed an uneven surface as shown in figure 5.1. This may result from the so-called 'slope shadowing' which occurs when a substrate is not placed directly above the source [Glaser et al, 1987]. However, the deposited films appeared uniform and free from pinholes when viewed under the optical microscope.

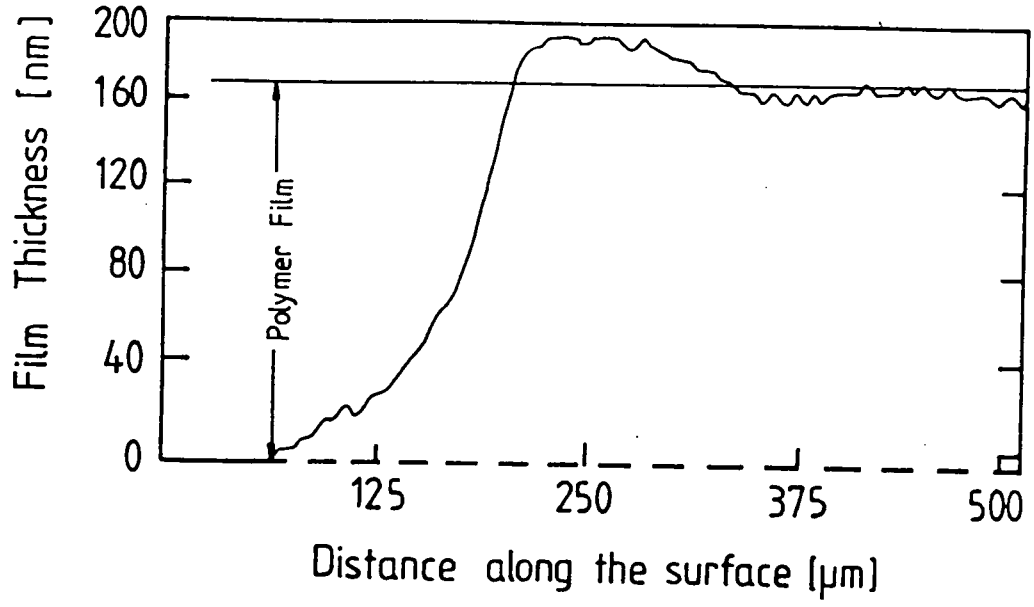

Figure 5.1: A surface profile of evaporated polyaniline on glass.

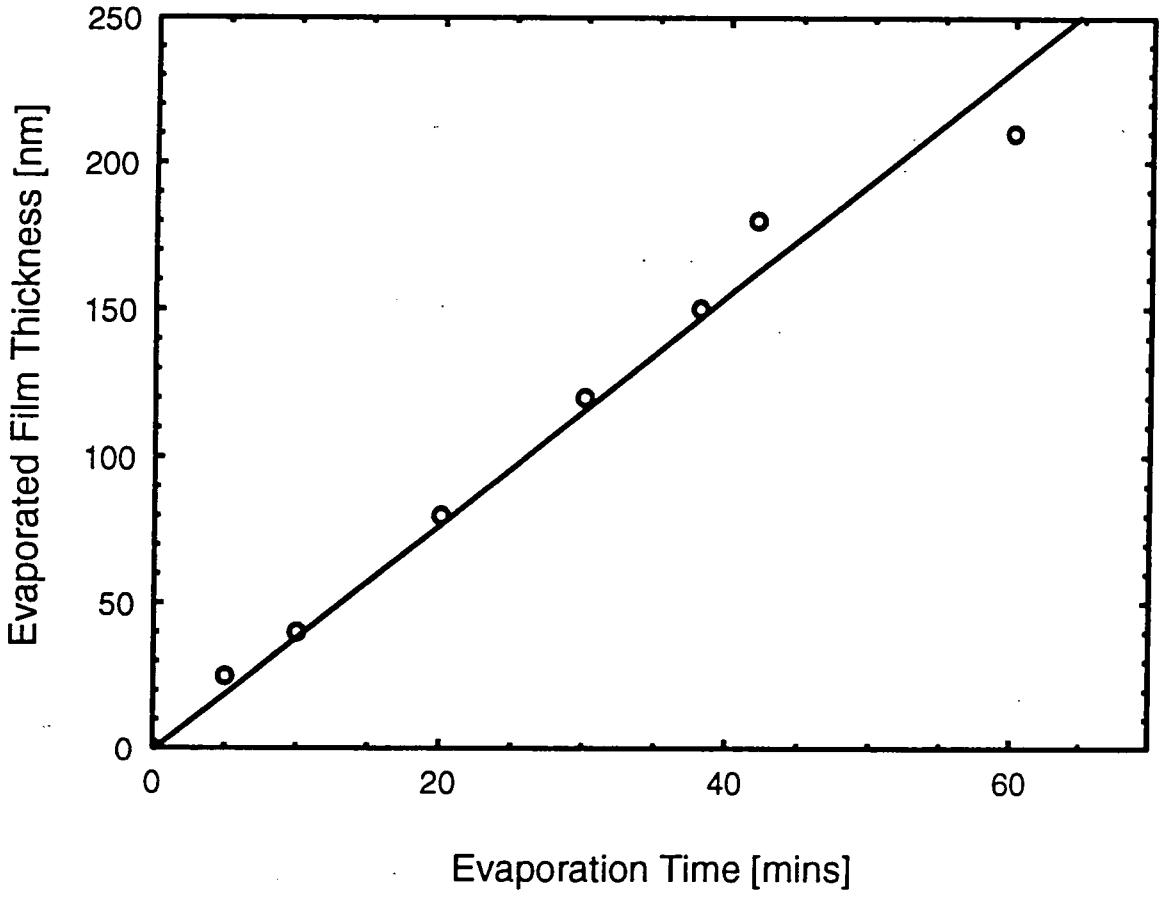

Figure 5.2: Evaporated film thickness versus evaporation time for 40mg of emeraldine base polyaniline (vacuum 10^{-3}mbar).

Figure 5.2 shows the thickness calibration for deposition times ranging from 0 to 60 minutes. This thickness was measured using the surface profiling Talystep from three different directions and then averaged. This was done to account for the orientation of the substrate with respect to the crucible source. Deposition times longer than 60 minutes gave deviations from linearity in terms of the measured thickness. This was probably due to the decreasing amount of material in the crucible source. The slope of this graph gives a molecular evaporation rate of 3.7nm min^{-1} at 10^{-3}mbar pressure.

5.3 EVAPORATED FILM CHARACTERIZATION

Thin films of evaporated polyaniline were characterized using a variety of techniques in order to compare these layers with spun films.

5.3.1 Ultraviolet/Visible Spectroscopy.

Figure 5.3 shows the ultraviolet/visible spectrum of a freshly evaporated polyaniline thin film. This spectrum is significantly different to that obtained for emeraldine base polyaniline (see figure 4.2a). However, some similarities do occur in the high energy region of the spectrum, i.e. at 320nm due to the π-π^* electron transitions of benzoid rings along the polymeric backbone. Also visible in figure 5.3 is the emergence of a broad shoulder around 600nm after 1 hour in air. This is due to the formation of quinoid structures and is probably the result of atmospheric oxidation of the phenyl rings to quinoid ones. We can therefore conclude that benzoid rings are less stable in air than the quinoid ones.

This hypothesis was further tested by exposing the film to oxidizing and reducing vapours at room temperature. The gases used were I_2, HCl and NH_3. The purpose of the I_2 was for oxidation. HCl was used to provide an acid environment which favours the oxidation of the film in air [Dannetun et al, 1989] while NH_3 was administered for deprotonation. Film exposure to I_2 initially produced no change physically or on the spectrum shown in figure 5.3.

Exposure to I_2/HCl produced green films. Subsequent exposure to NH_3 changed the colour from green to a blue coloured film.

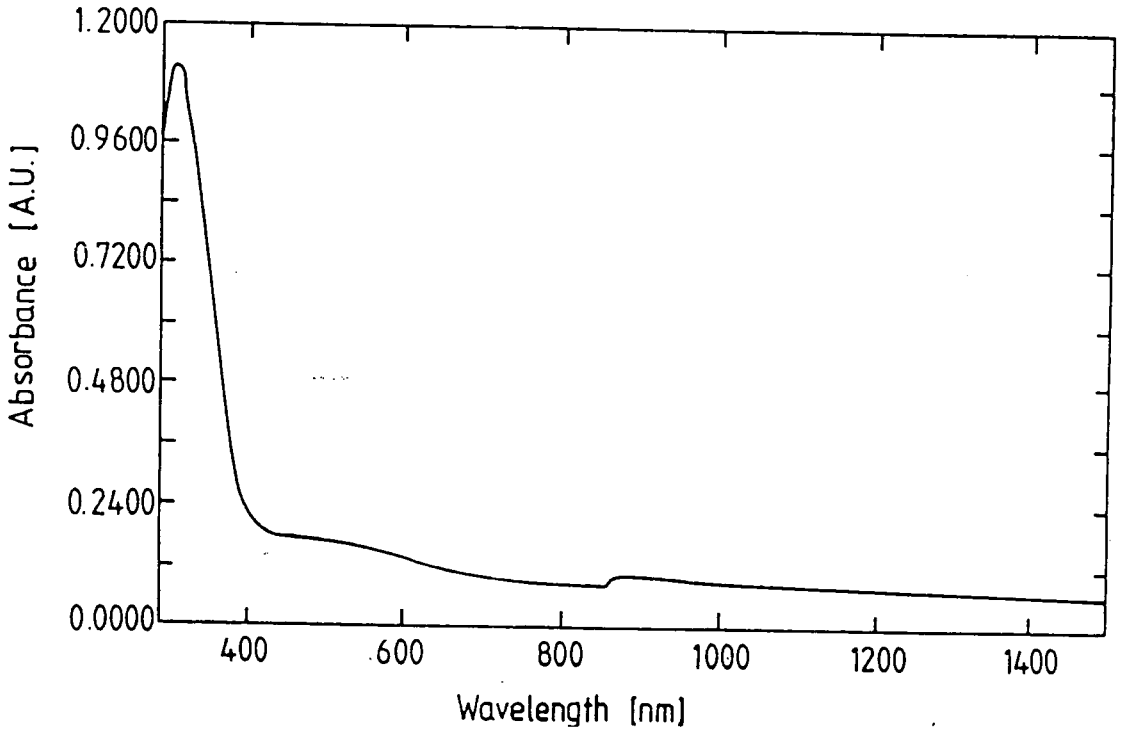

Figure 5.3: The ultraviolet/visible spectrum of evaporated polyaniline film on glass.

Figure 5.4a shows the spectrum after exposure to I_2/HCl vapour. Here we can see that the absorption of the benzoid ring at 320nm decreases while that associated with a quinoid ring at 600nm increases. Also visible in figure 5.4a is the emergence of a shoulder between 400-500nm. This can be associated with polarons resulting from protonation.

Figure 5.4b shows the spectrum for the same sample after exposure to NH_3 (following the I_2/HCl treatment). Here the absorption of the benzoid ring increases while the band between 400-500nm associated with polarons is eliminated. A slightly more intense quinoid band can be seen at about 600nm, as observed for deprotonated emeraldine [Monkman et al, 1991]. These results demonstrate that thin films of evaporated polyaniline are susceptible to oxidising vapours and hence can be converted to the emeraldine base form of polyaniline.

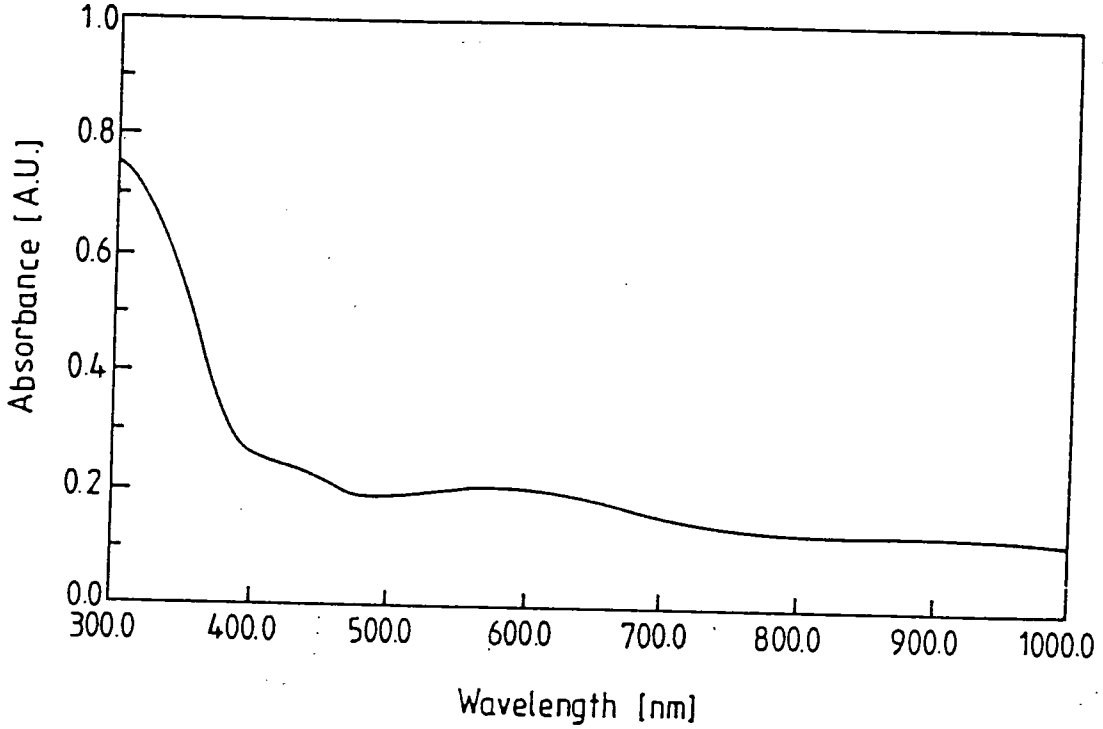

Figure 5.4a: The effect of exposing the evaporated film to I_2+HCl (oxidizing vapour) at room temperature.

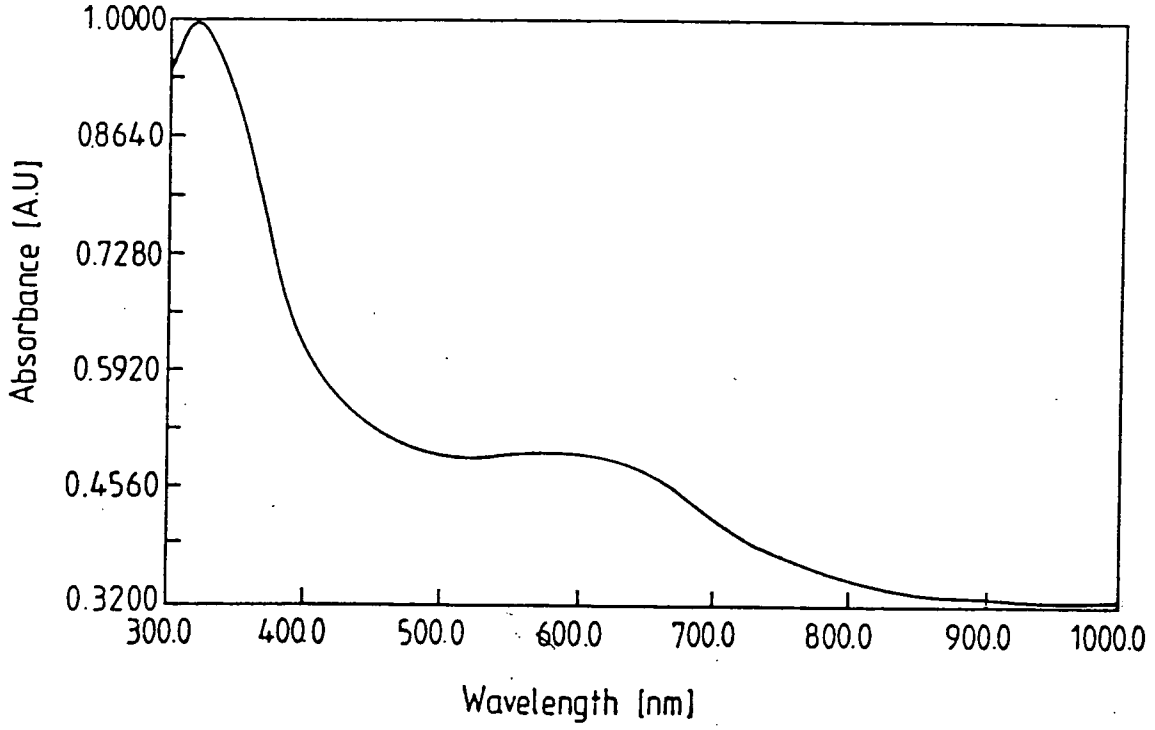

Figure 5.4b: The effect of exposing the evaporated film to NH_3 (reducing vapour) after exposure to I_2+HCl at room temperature.

From the above, we suggest that the evaporated material is in the form of leucoemeraldine; the completely reduced form of polyaniline, as shown in figure 4.1. This structure is composed mainly of phenyl rings. After exposure to I_2/HCl, these rings are oxidised and protonated and material is changed into emeraldine salt. Subsequent exposure NH_3 changes the salt to the emeraldine base form of polyaniline. These structures, as stated in section 4.2, are reversible.

Figure 5.5 shows the variation of the optical absorbance at 320nm for the as-deposited polymer with film thickness. The linearity of the graphs is further evidence that the deposition of polyaniline by evaporation was reproducible. This control of the deposition process made it possible to produce sufficiently thin films for surface plasmon resonance measurements.

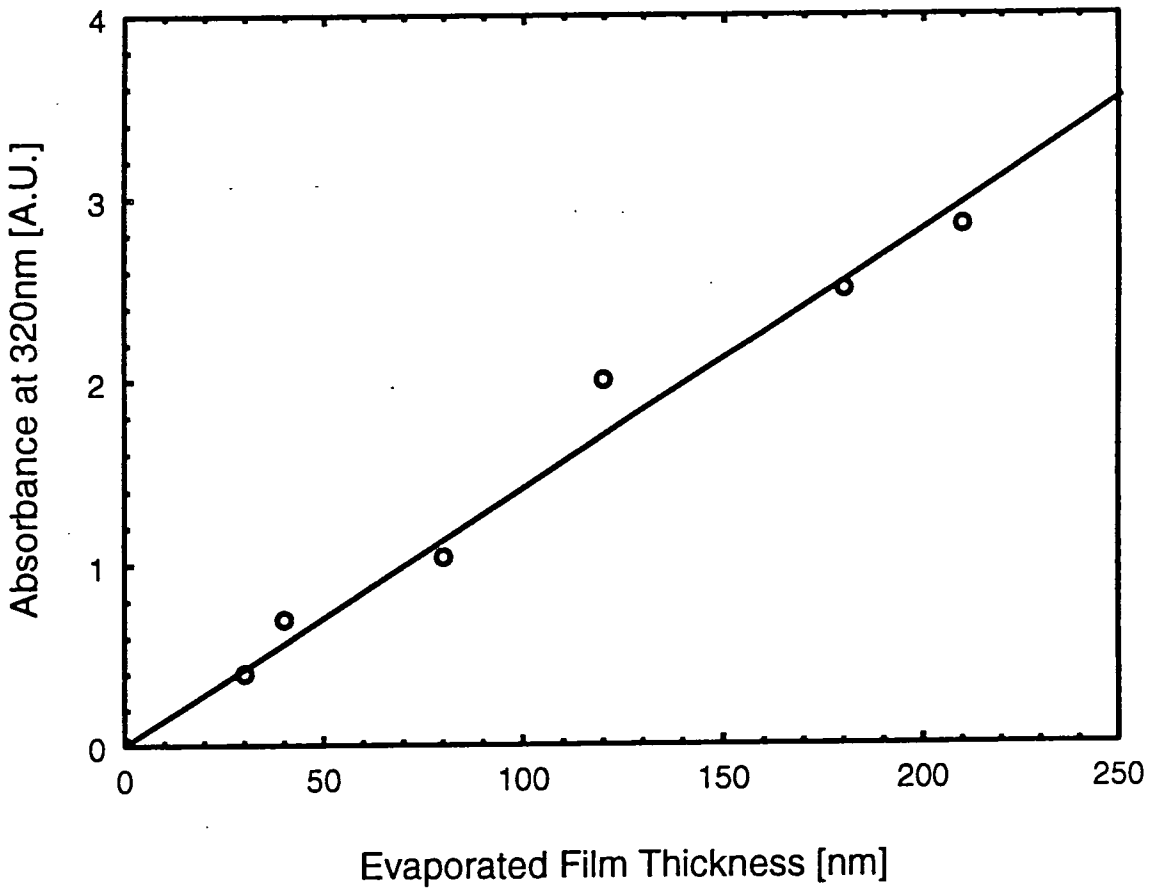

Figure 5.5: The variation of the peak absorbance at 320nm versus evaporated film thickness.

5.3.2 Reflection-Absorption Fourier Transform Infrared Spectroscopy

Figure 5.6 shows the infrared spectrum of the evaporated material. This spectrum must be contrasted to that of spin-coated polyaniline shown in figure 4.3. A number of changes are evident. For example, in the aromatic ring breathing region of figure 5.6, the vibration at $1597cm^{-1}$ (associated with the quinoid ring stretch) can be seen to be weak while the vibration at $1506cm^{-1}$ (associated with benzoid ring stretch) is relatively intense. This produces a change in the ratio of the absorption of the quinoid:benzoid ring stretch from 1:1.5 for the spin-coated to 1:4 in the case of the evaporated film. A summary of the observed vibrations and their assignment are given in table 5.1.

An intense NH stretch band can be seen at $3389cm^{-1}$. This band is due to amine nitrogens (NH). Also visible is a vibration at $3030cm^{-1}$ due to aromatic CH stretch. Its intensity increases with the number of hydrogens on the phenyl ring. In the proposed film structure of leucoemeraldine there are no quinoid rings, thus the number of hydrogens on the rings increases.

The vibration at $1175cm^{-1}$ is due to in-plane CH bending.

Prolonged exposure of the evaporated films to air has already been noted to result in their oxidation. This can be seen from the spectrum in figure 5.7, which shows the intensity of the quinoid vibration at $1597cm^{-1}$ has grown significantly with respect to the benzoid band at $1506cm^{-1}$ after 2 weeks exposure to air.

We suggest that the starting material (emeraldine base) undergoes a thermally-induced decomposition of the molecular chain followed by the conversion (ie. by reduction) of the quinoid rings into phenyl rings in the crucible source. Subsequently, polymerization of the phenyl evaporants occurs in the vapour phase and/or on the substrate through a variety of coupling mechanisms e.g. para-para coupling. Other decomposition products with covalently bonded oxygen are not excluded. As shown in figure 4.1, the overall chemical structure of the leucoemeraldine film is composed of amine units (-NH) which implies the emeraldine chain breaks down mainly at the imine sites (=N-). One obvious reason for this preference is the higher reactivity of the N=C

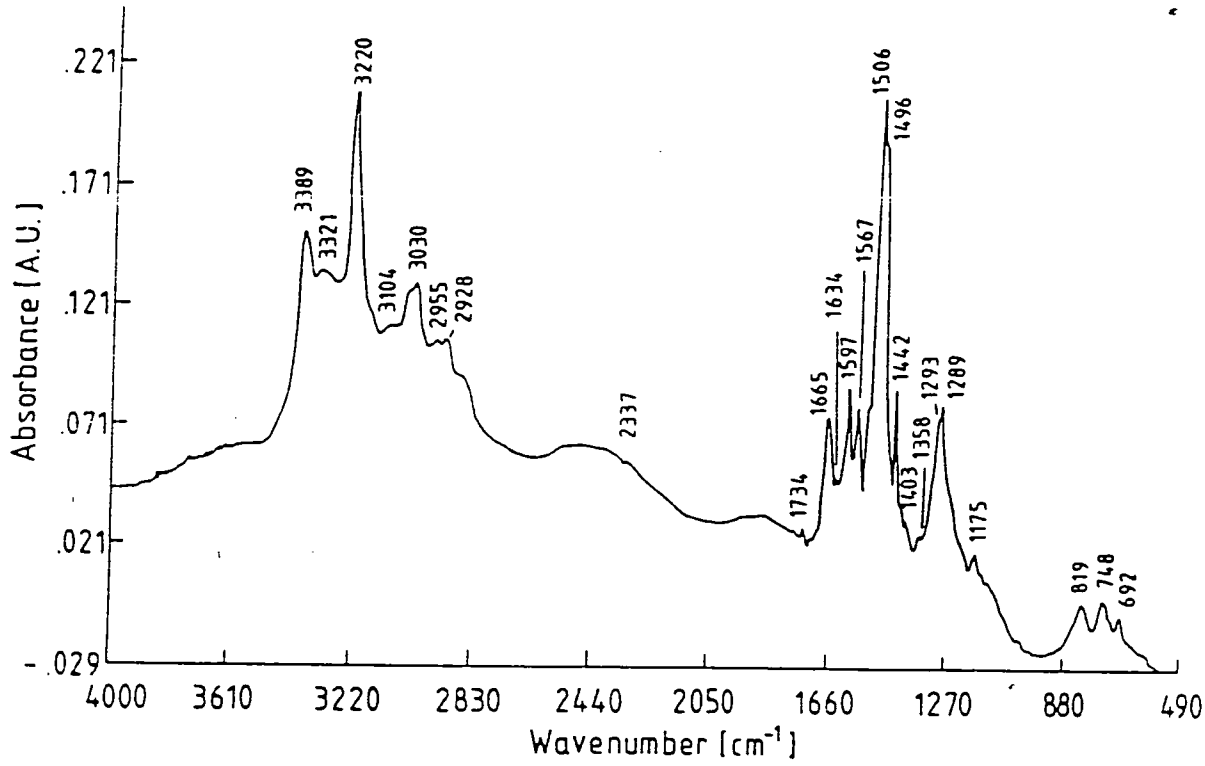

Figure 5.6: Reflection-absorption Fourier transform infrared spectrum of freshly evaporated polyaniline on a thin layer of gold.

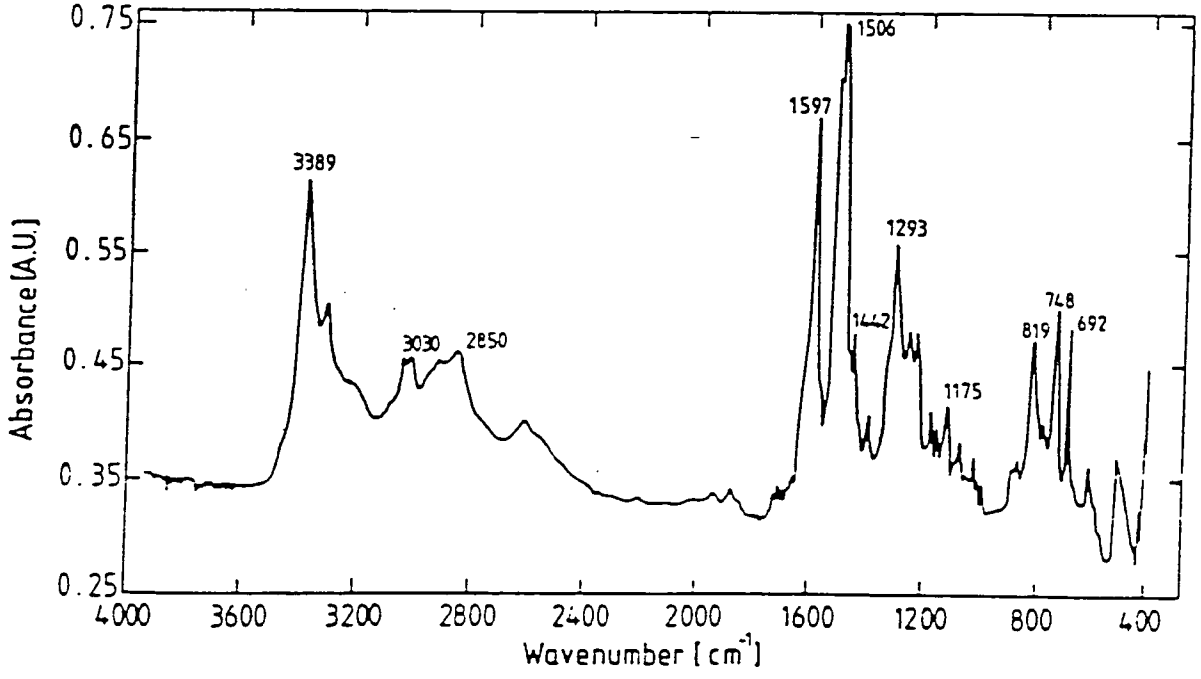

Figure 5.7: Reflection-absorption Fourier transform infrared spectrum of evaporated polyaniline showing the effect of air exposure for 2 weeks.

bond with respect to the N-C bond [Dannetun et al, 1987 and Vachon et al, 1987].

Band Position [cm^{-1}]	Assignment	References
3389	NH stretch	Monkman et al, 1991
3030	aromatic CH stretch	Tang et al, 1988
2995-2928		
1597-1567	quinoid ring stretch	Cao et al, 1986
1506-1496	benzoid ring stretch	Dannetun et al, 1987
1293-1289	CN stretch in aromatic ring	Hagiwara et al, 1988
1175	in-plane CH bending	Monkman et al, 1991
819-692	out-of-plane CH bending,wagging and scissoring vibrations	

Table 5.1: A summary of the infrared absorption bands of freshly evaporated polyaniline on a gold substrate.

5.3.3 Scanning Electron Microscopy

Figure 5.8 shows a micrograph of evaporated polyaniline on a gold substrate. As with the spin-coated film, the micrograph was taken only after the organic layer was coated with a thin layer of gold produced by glow discharge. Figure 5.8, plate a, reveals that the film structure is globular with some featureless regions. These globules are varying in sizes ranging from about 0.1-0.5μm in cross-section and arranged in no distinct fashion. A similar structure has been obtained by quasi-thermoplastic processing of polyaniline [Wessling et al, 1986]. This film structure reduces the surface area of the evaporated film compared with the spin-coated film for gas diffusion and interaction with the material.

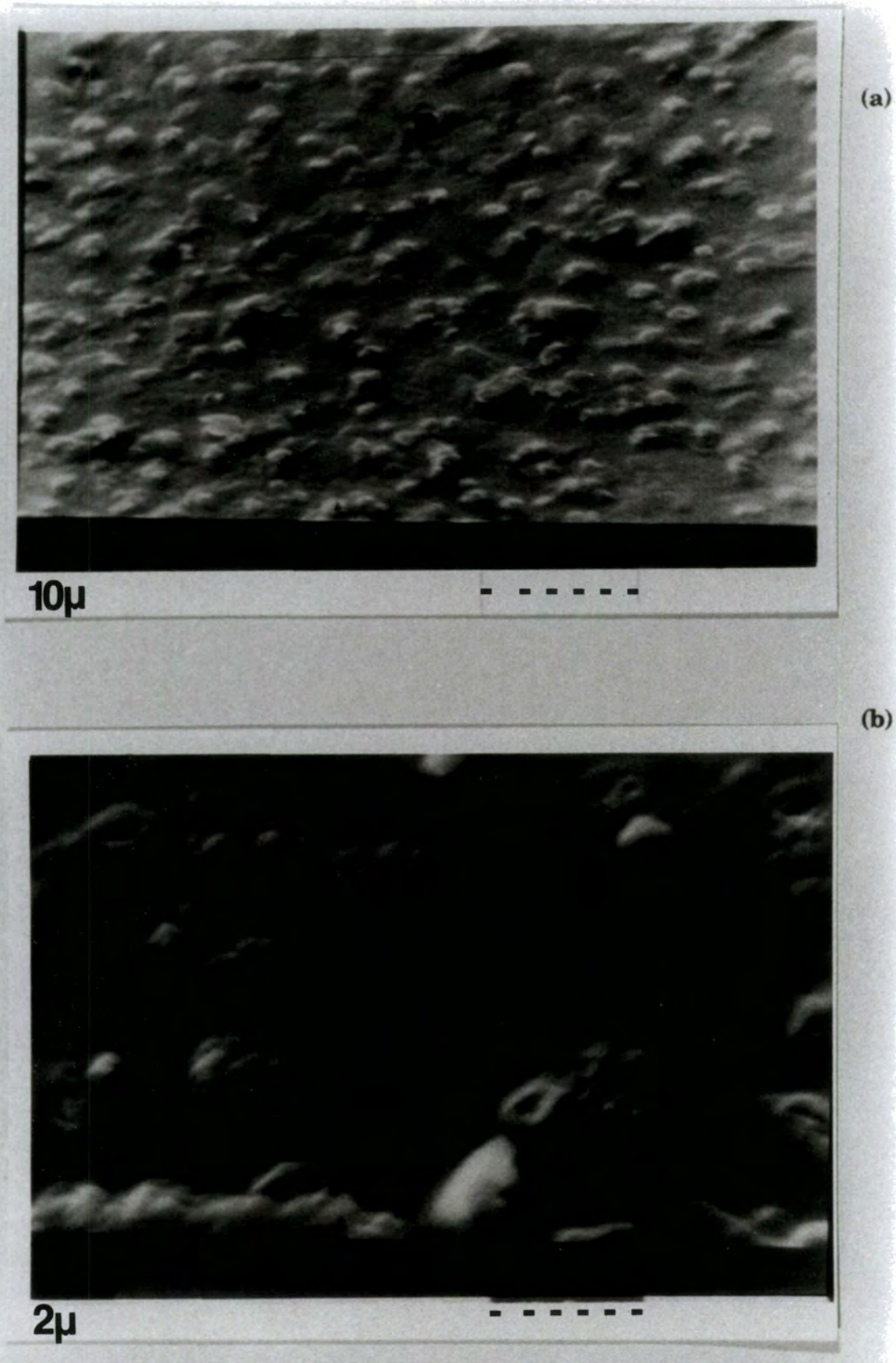

Figure 5.8: Scanning electron micrograph of an 'undoped' evaporated polyaniline on aluminium stubs.

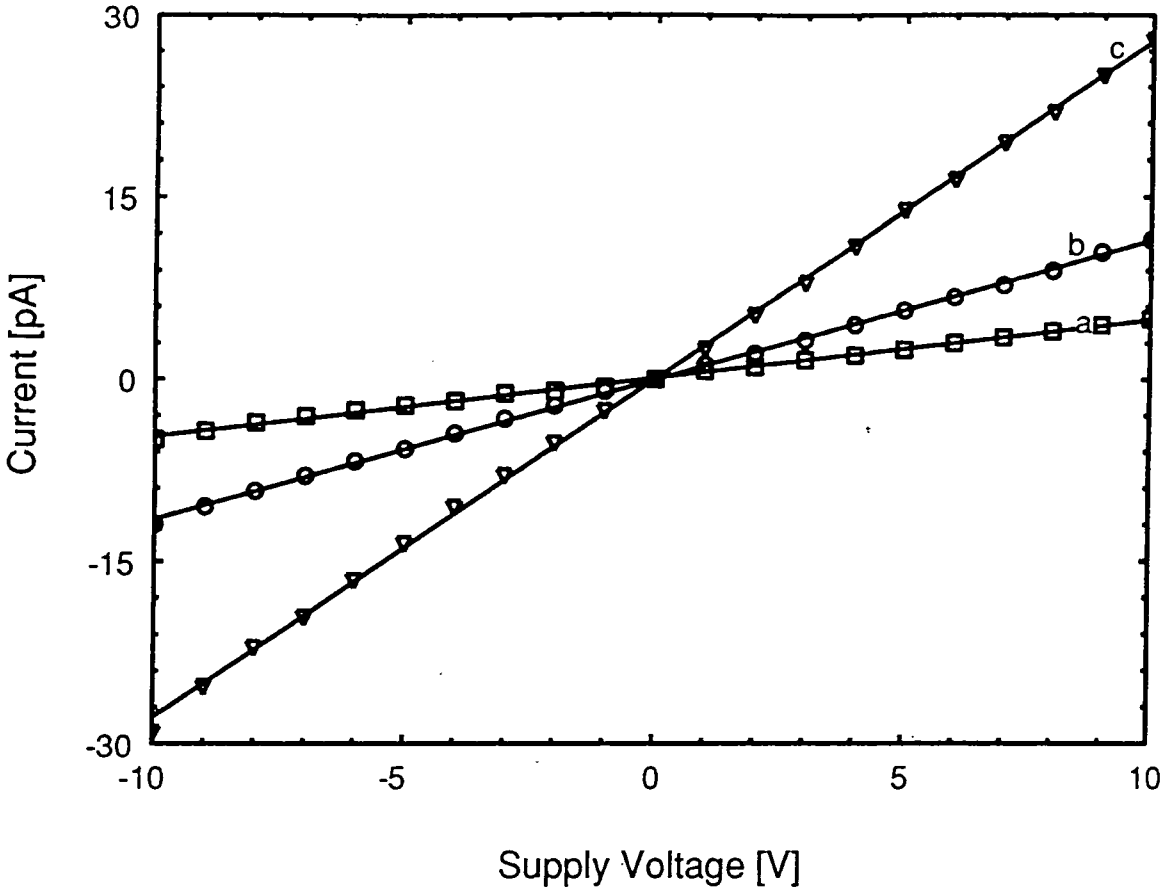

Figure 5.9: The current versus voltage characteristics of evaporated polyaniline measured in 10^{-3}mbar vacuum for film thicknesses of 40nm (curve a), 120nm (curve b) and 210nm (curve c). Temperature 20±2°C.

5.3.4 Electrical Measurements

Electrical studies were undertaken using an electrode structure similar to that shown in figure 3.2, except that this consisted of 14 fingers. Figure 5.9 shows the current versus voltage plot for three separate films (film thicknesses of 40nm, 120nm and 210nm) measured in vacuum of 10^{-3}mbar. Similar measurements on uncovered electrodes indicated that conduction was through the film rather than the substrate. The change in resistance with film thickness indicated that ohmic contacts had been established between the evaporated polymer and the electrodes.

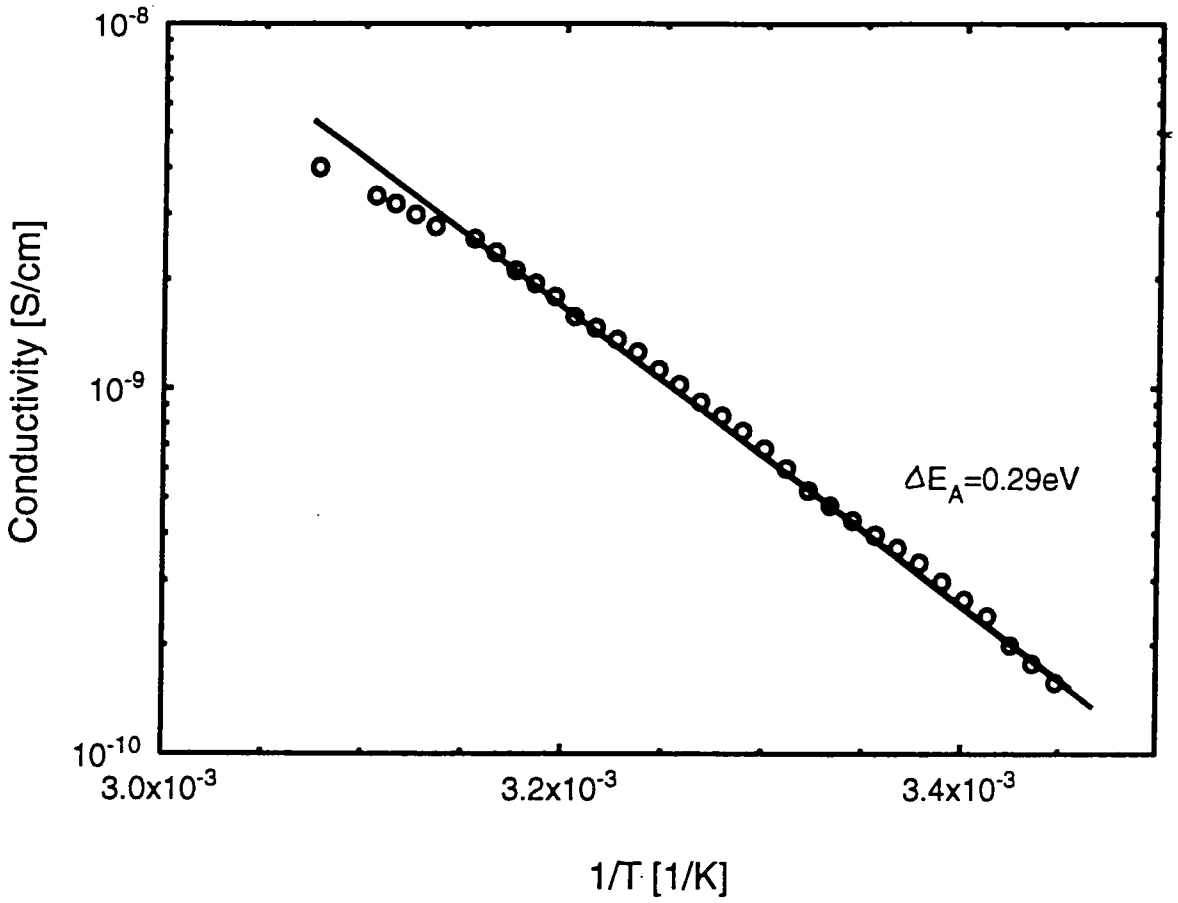

Figure 5.10: Temperature dependent dc conductivity of freshly evaporated polyaniline film measured in 10^{-3}mbar vacuum (film thickness 120nm, 3V supply).

The average room temperature dc conductivity of freshly evaporated polyaniline film, in vacuum, was calculated to be 10^{-10}Scm^{-1}. A wide range of conductivity values are reported in the literature. For example 10^{-10}Scm^{-1} as reported by Chiang et al, 1986 and 2.0×10^{-8}Scm^{-1} as reported by Aktar et al, 1988. The calculated value of conductivity is slightly higher than that for the spin-coated film (1.5×10^{-11}Scm^{-1}). This can be explained by the increased π-π mixing between adjacent benzoid rings in the polymer chain [Stafström et al, 1986].

In air, the conductivity value decreased irreversibly to a value close to that of the spin-coated film. This is due to the oxidation of the benzoid rings. The formation of quinoid rings disrupts the π-π mixing between adjacent benzoid rings resulting in a π-σ mixing, and a lower electrical conductivity.

The temperature dependent dc conductivity of freshly evaporated polyaniline film is shown in figure 5.10, for temperatures ranging from 285K to 333K. The results show the dc conductivity to be a thermally activated process with an calculated activation energy, from equation 4.1, of 0.29±0.01eV. This value is somewhat higher than that for spin-coated films, possibly because of the reduced chain length and/or large torsional angle between adjacent phenyl ring units.

The temperature dependent dc conductivity of 'doped' evaporated polyaniline is shown in figure 5.11. 'Doping' was undertaken by exposure to HCl for 30 minutes. The linearity of the data indicates that this is a thermally activated process. Applying equation 4.1, we estimate the activation energy to be 0.14± 0.01eV which is smaller than that of the freshly evaporated film. The room temperature dc conductivity of the 'doped' evaporated film was calculated to be $1\times10^{-5}Scm^{-1}$ which is much smaller than the value obtained for emeraldine salt in chapter 4. This is likely a result of the very few number of quinoid rings in the leucoemeraldine base.

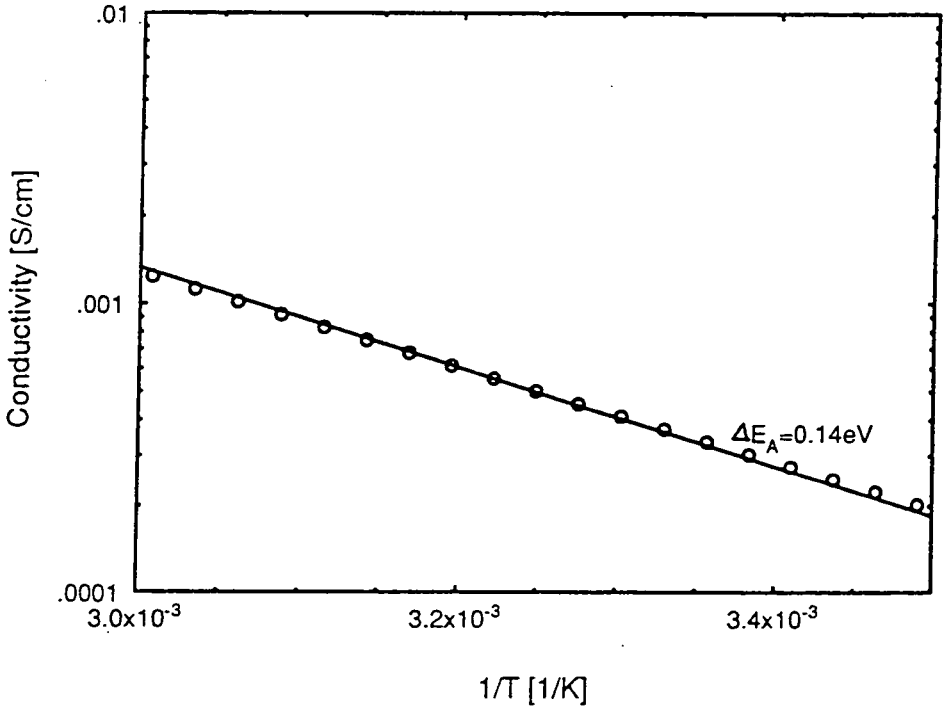

Figure 5.11: Temperature dependent dc conductivity of 'doped' evaporated polyaniline measured in 10^{-3}mbar vacuum (film thickness 120nm, 3V supply).

5.3.5 Surface Plasmon Resonance

Thin films of polyaniline could be evaporated onto metals for surface plasmon resonance studies. Figure 5.12 shows the effect of depositing a thin layer of polyaniline onto Ni/Ag. This film was evaporated over a period of about 30 seconds, resulting in an overlayer thickness of approximately 2nm. The effect of the overlayer on the resonance conditions includes a shift in the resonance angle of approximately 2°, a slight broadening of the curve and a marked decrease in the depth of resonance. The last two effects have been discussed in section 3.4 and result from the finite absorption of the evaporated film at 620nm (see figure 5.4b). The shift in the resonance angle is due to the finite thickness of the polyaniline. Film deposition for these measurements was found to be more difficult to control, as much thinner layers were required than for the electrical experiments. Gas sensing using this device did not show any measureable effect. This is probably due to its poor resolution, exhibited by the broad nature of the resonance curve. This problem could be circumvented using an evaporation system with a much higher vacuum level for film deposition.

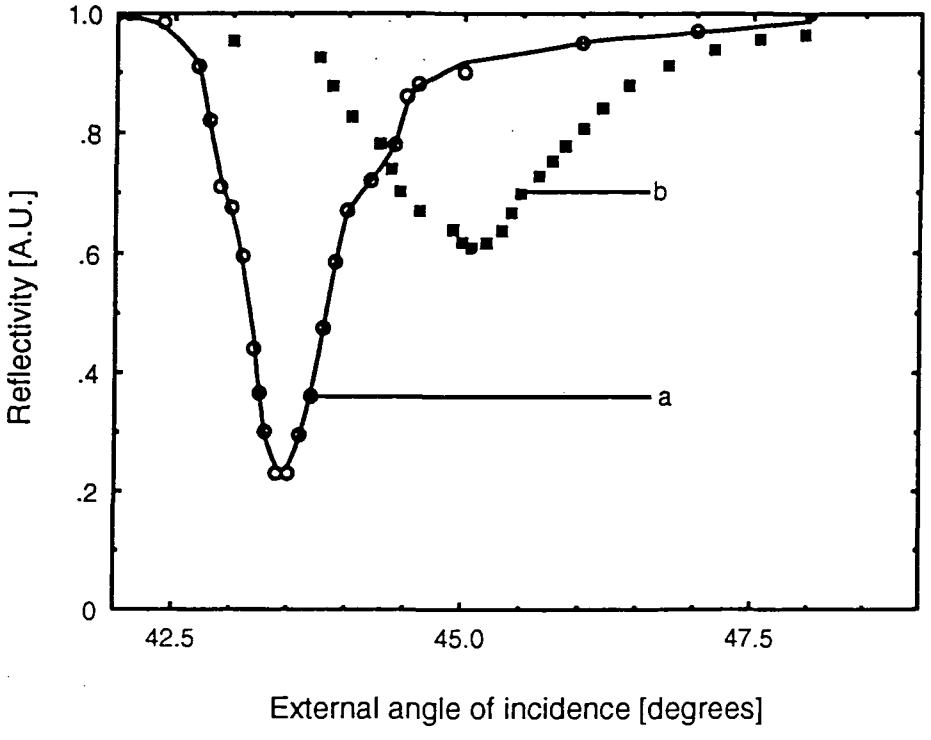

Figure 5.12: SPR curve of Ni/Ag (curve a) and Ni/Ag covered with a thin layer of evaporated polyaniline (curve b).

5.4 GAS SENSING

Gas sensing studies were carried out using conductivity and insitu infrared spectroscopy. These methods were chosen to establish a comparison with spin-coated films. The gases used were the same as for spin-coated films and all measurements were undertaken at room temperature and pressure.

5.4.1 Insitu-Conductivity Gas Response

Gas sensing was initiated using dry nitrogen which served as the background gas. Figure 5.13 shows the effect of dry nitrogen on the dc conductivity of evaporated polyaniline chemiresistor. The gas produced a decrease in conductivity which became stable after only 12 minutes, compared with 1 hour for the spin-coated polyaniline. Furthermore, the percentage decrease in conductivity after 1 hour was 5% compared with 40% for spin-coated films. These differences may be due to the low level of water vapour diffused into the bulk of the evaporated film. Low diffusion of water vapour in air is probably due to the globular structures on the film surface (shown in figure 5.8) that may act as exclusion zones for vapour sorption [Grate et al, 1990].

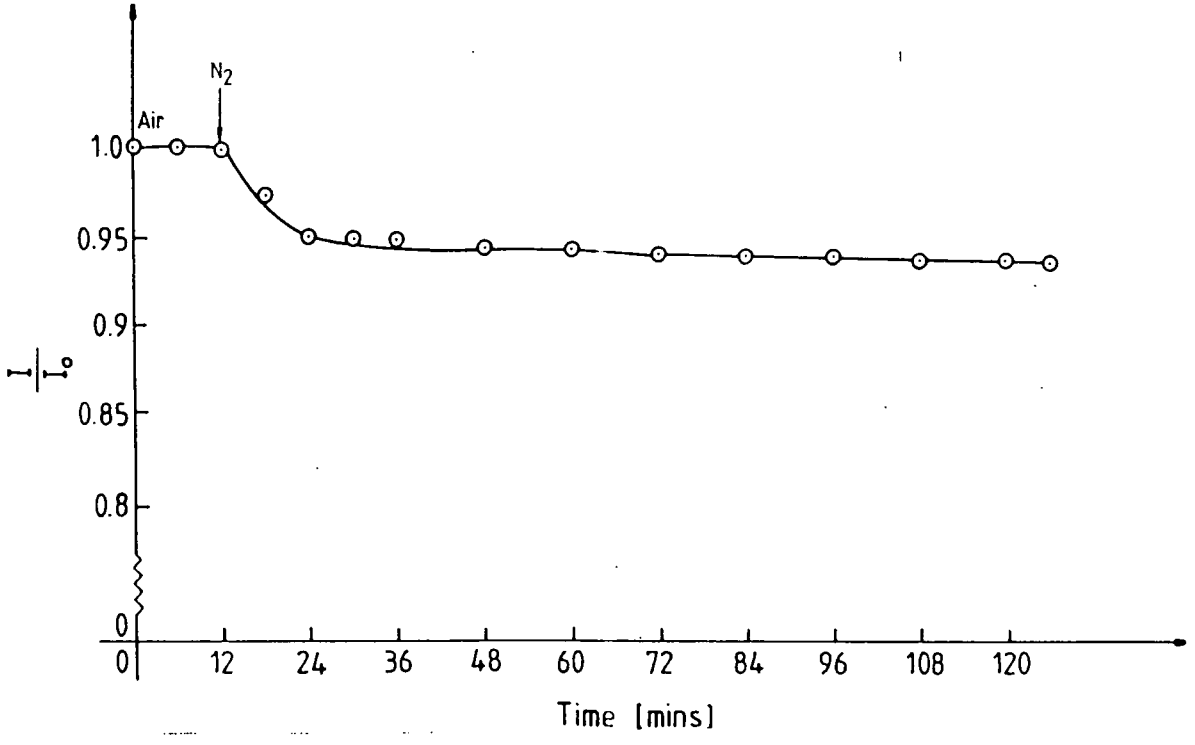

Figure 5.13: The effect of dry nitrogen on an evaporated polyaniline chemiresistor at room temperature (film thickness 210nm, 2V supply).

The effect of NO_x on EPANi in a N_2 atmosphere at room temperature is shown in figure 5.14a and figure 5.14b. This study was undertaken for a range of gas concentrations. For all concentrations, the gas produced an increase in conductivity of the sample. This increase occurred after a delay time of less than 10 seconds for concentrations greater than 40ppm. At low concentrations (<10ppm), the reaction is reversible (see figure 5.14a) while at higher ones (>40ppm), the response is only partially reversible (see figure 5.14b). With prolonged exposure at higher gas concentration, diffusion into the bulk of the film is enhanced. Such 'deeply-diffused' molecules may also be contributing to the non-recovery as does chemically bonded molecules.

The effect of different NO_x gas concentrations on the response of the evaporated polyaniline chemiresistor is shown in figure 5.15; figure 5.15a shows the response for low gas concentrations while figure 5.15b shows the response for high gas concentrations. The change in current flow through the device can be seen to be approximately proportional to $[NO_x]$ for concentrations greater than 20ppm. However, for lower concentrations, the change can be seen to be non-linear. This suggests, at least 2 different interaction mechanisms.

The effect of NO_x on evaporated polyaniline chemiresistor can be explained as an oxidation reaction involving the π-electrons of the benzoid rings on the polymer backbone. At low concentrations, it is likely that a charge transfer complex is formed and as the gas concentration increases, the reaction is driven closer to completion where phenyl rings are oxidised to produce quinoid rings. This increased interaction may change the film structure to that of emeraldine base polyaniline. However, other interactions are possible, especially as all gas sensitive properties of evaporated polyaniline material have not been completely elucidated. Therefore reversibility could be due to physisorption and non-reversibility are due to chemisorption.

Figure 5.16a shows the effect of 10ppm H_2S on EPANi. This shows a non-reversible decrease in conductivity at room temperature. The delay time for this interaction was about 144 seconds, compared to 48 seconds for spin-coated films measured under identical conditions. This difference is likely be due to the difference in the chemical structure and thickness of the spun (0.1μm) and evaporated (210nm) films.

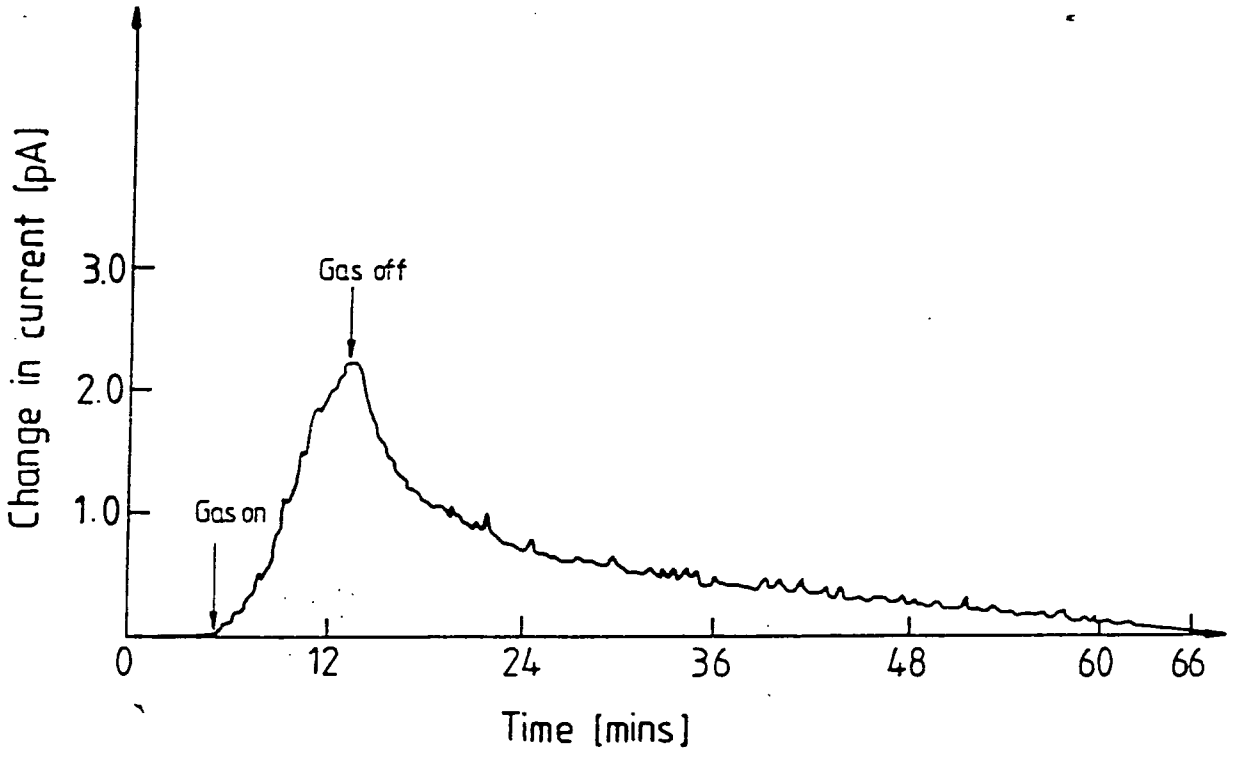

Figure 5.14a: The effect of 8ppm NO_x on an evaporated polyaniline chemiresistor at room temperature (film thickness 210nm, 2V supply).

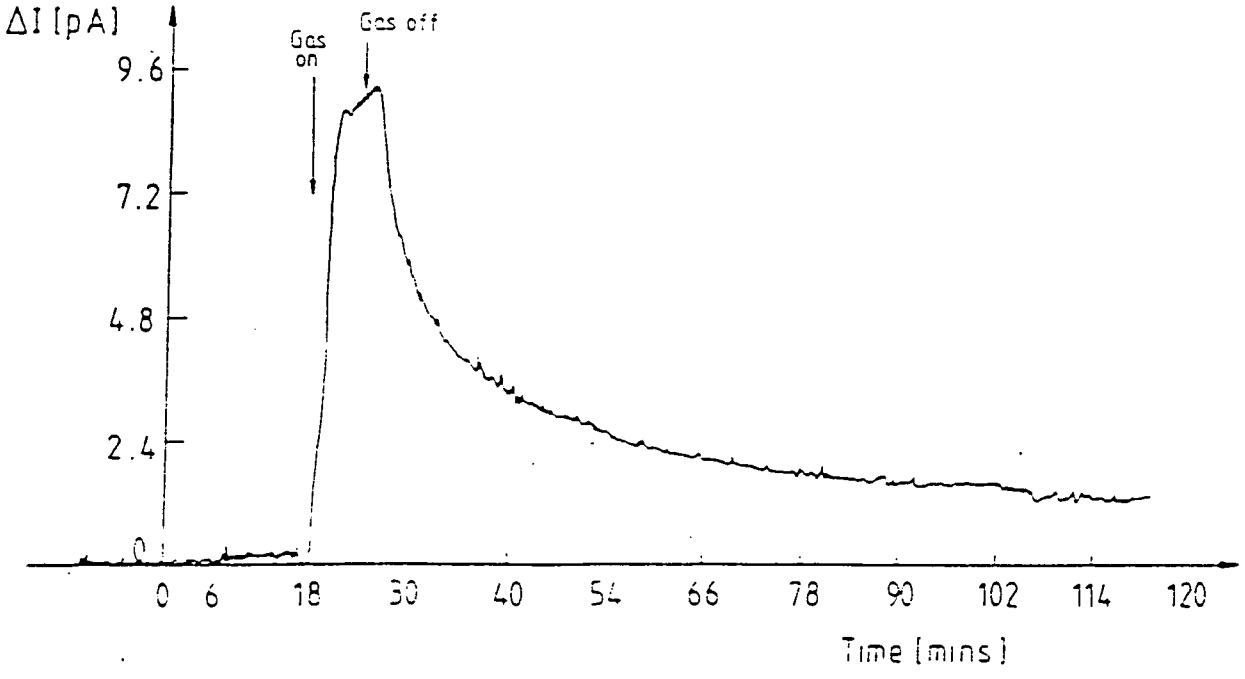

Figure 5.14b: The effect of 40ppm NO_x on an evaporated polyaniline chemiresistor at room temperature (film thickness 210nm, 2V supply).

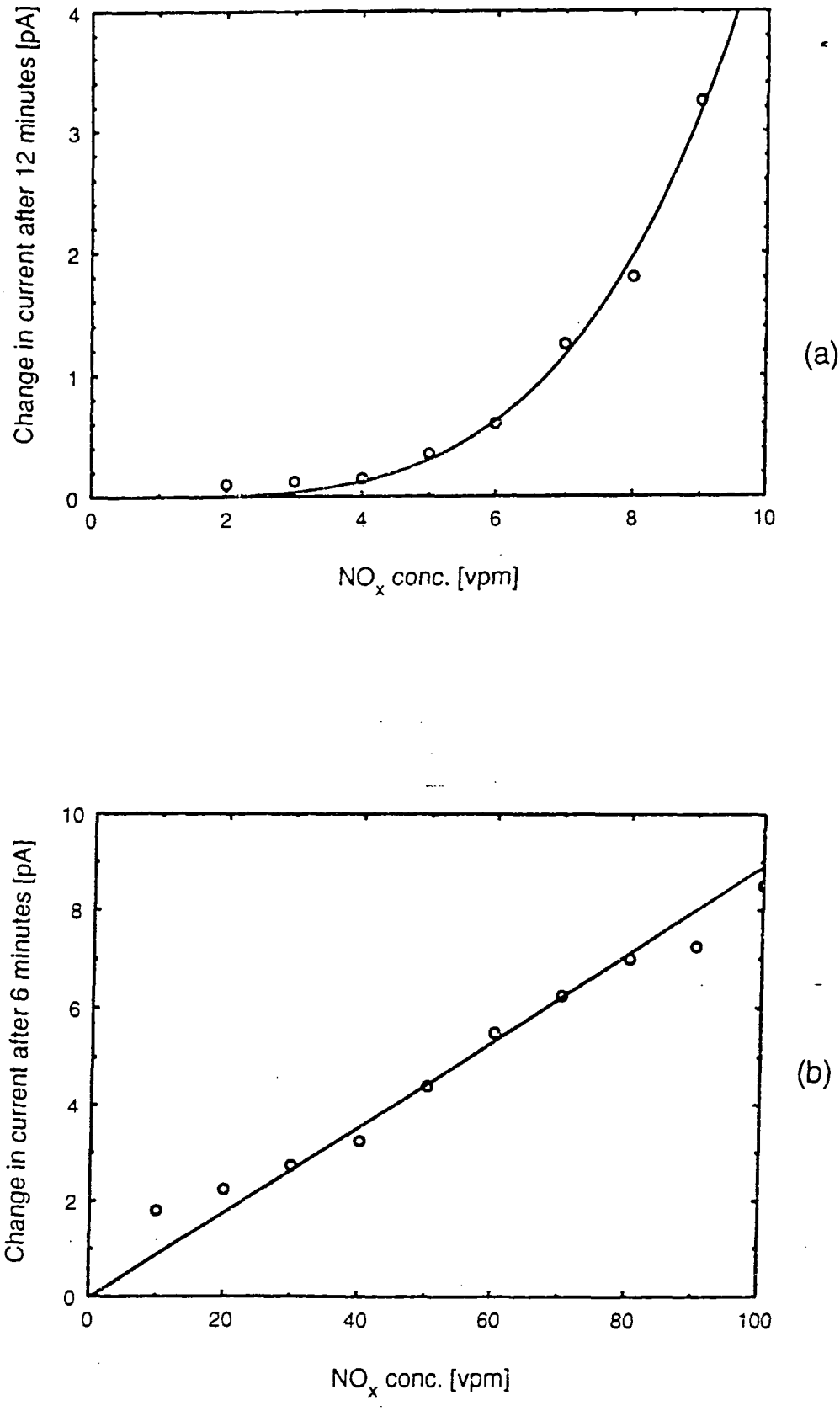

Figure 5.15: The response of an evaporated polyaniline chemiresistor to low (curve a) and high (curve b) concentrations of NO_X at room temperature.

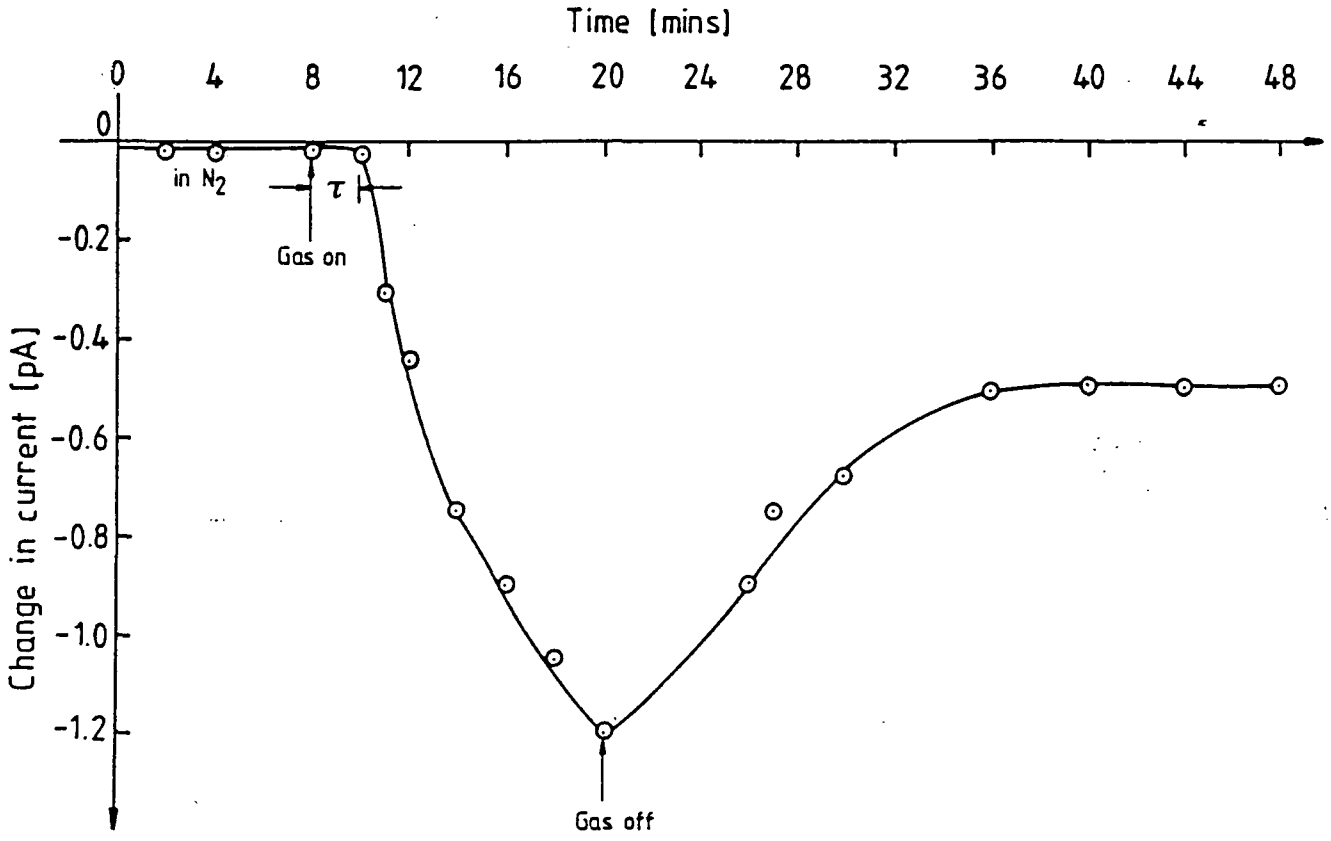

Figure 5.16a: The effect of 10ppm H_2S on an evaporated polyaniline chemiresistor at room temperature [film thickness 210nm, 2V supply].

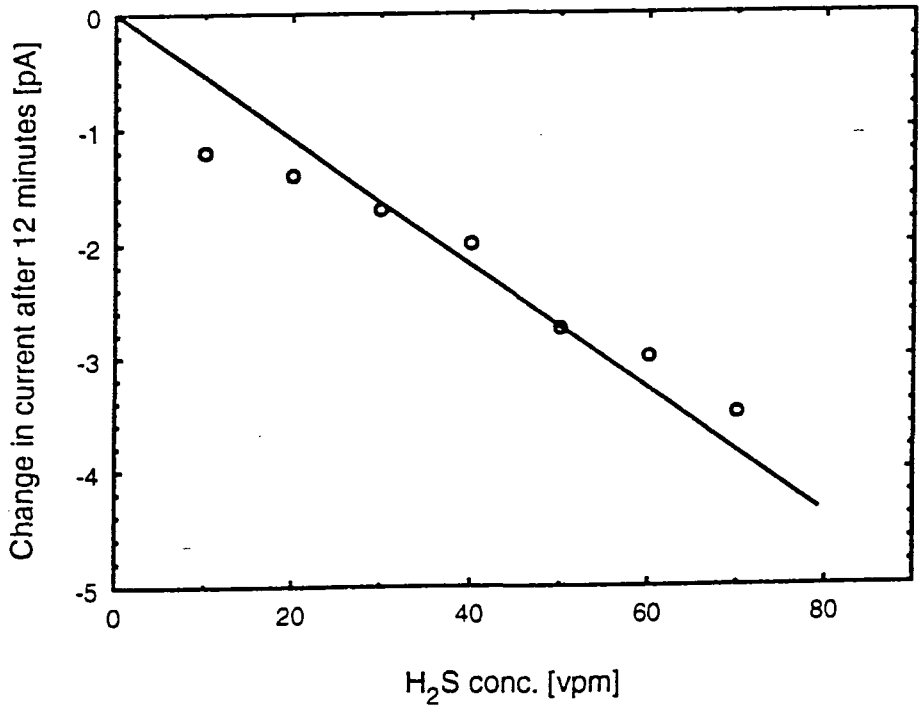

Figure 5.16b: The response of an evaporated polyaniline chemiresistor different concentrations of H_2S at room temperature.

The effect of different H_2S gas concentrations can be seen in figure 5.16b. Since H_2S is a reducing gas, we would expect it to donate electrons to the polymer, thereby reducing its conductivity. The minimum detection limit was 10ppm compared with 4ppm for the spin-coated polyaniline chemiresistor. This can be explained by the fact that the polymer is already in its most reduced state (leucoemeraldine), hence substantial further reductions in the oxidation state are unlikely at very low gas concentrations, say below 10ppm. Thus we may suggest that the observed changes in conductivity are due to oxidized portions of the material (quinoid rings, quinoid rings with covalently bonded oxygen) interacting with an electron donated by the gas molecule.

The effect of 10ppm SO_2 on the dc conductivity of the same evaporated polyaniline chemiresistor is shown in figure 5.17a. As can be seen, the conductivity increases after a delay time of about 30 seconds compared to 12 seconds for the spin-coated film (see figure 4.11a). Unfortunately, this interaction was not reversible. The increase in conductivity is probably associated with the oxidation of benzoid rings into quinoid rings. Irreversibility is probably due the formation of chemical bonds between the polymer with the gas molecules.

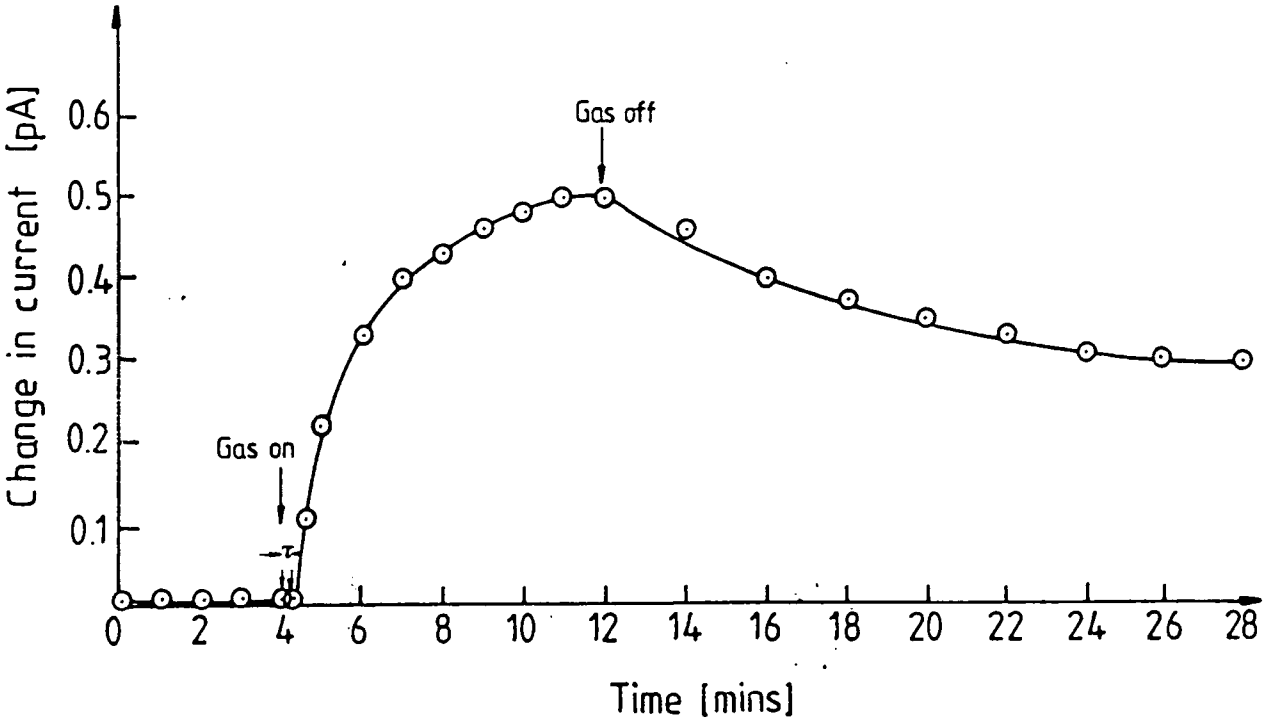

Figure 5.17a: The effect of 10ppm SO_2 on an evaporated polyaniline chemiresistor (2V supply and film thickness 210nm).

Figure 5.17b shows the device response to different concentrations of SO_2. Here, the detection threshold is about 10ppm, compared to 2ppm for NO_x. However, freshly evaporated polyaniline films showed a much higher sensitivity, down to 0.5ppm. This increased to 10ppm as the film was cycled continuously betwen air and nitrogen. This result suggests that the conversion of phenyl rings into the quinoid structures (as shown in section 5.3.2) on exposure to air (film oxidation) is equivalent to blocking the SO_2 reactive sites.

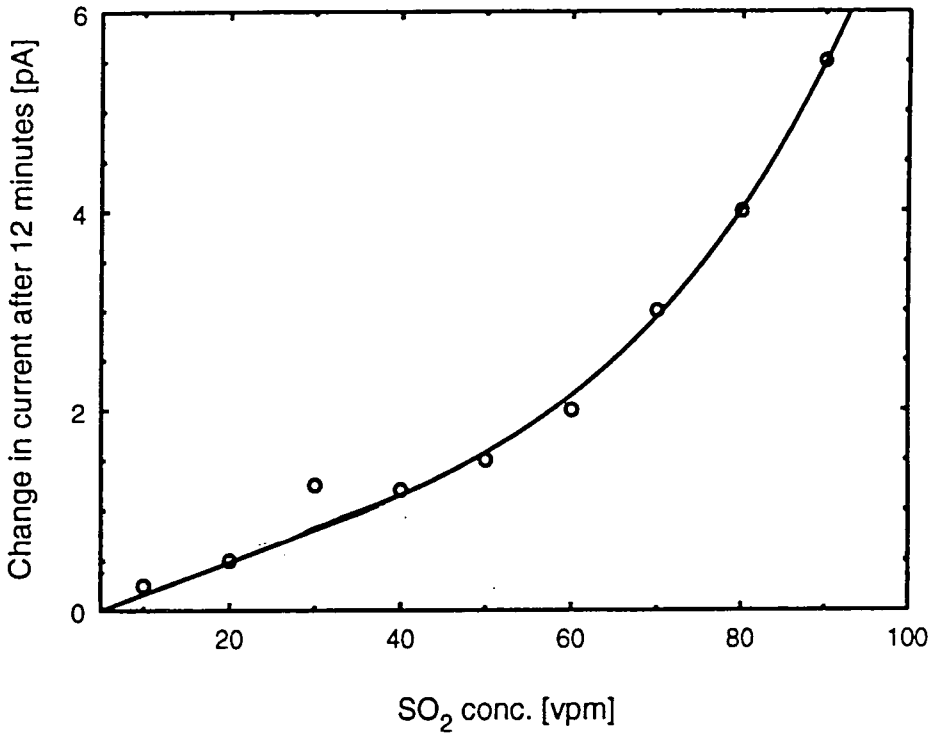

Figure 5.17b: The response of an evaporated polyaniline chemiresistor to different concentrations of SO_2 (2V supply and film thickness 210nm).

A summary of the effects of the various gases on evaporated polyaniline is shown in table 5.2, from which it is clear that NO_x is the most reactive and SO_2 is the least reactive of the gases investigated. It can also be seen that CO and CH_4 produced no change in the conductivity of the device. The effect of gas exposure on the chemical structure of the material will be discussed below in order to investigate the gas sensing mechanism in more detail and to elucidate the differences in response of the evaporated and spun polyaniline thin films.

Gas	Conc. in N_2 [ppm]	Delay Time τ_D [s]	Exposure Time [mins]	Recovery Time τ_R [mins]	Minimum Detection Level [ppm]	Normalised Change per ppm $\frac{\Delta R}{R} \div$ gas conc. in ppm
NO_x	10	<10	6	54	2	-0.1 (at 10ppm)
H_2S	10	144	12	partially reversible	10	0.06 (at 10ppm)
SO_2	50	30	12	partially reversible	10	-3.4×10^{-3} (at 50ppm)
CO	10000	No observed effect	50	N/A	N/A	N/A
CH_4	50000	No observed effect	50	N/A	N/A	N/A

Table 5.2: Summary of the effects of different gases on an evaporated polyaniline chemiresistor at room temperature (film thickness 210nm).

5.4.2 Insitu-Reflection Absorption Fourier Transform Infrared Spectroscopy

Thin films of evaporated polyaniline (EPANi) on 2mm square gold-on-glass substrates were used for their measurements and a new sample was used for each gas. Figure 5.18 shows the effect of exposure to 150ppm NO_x at room temperature. The changes in the spectrum can be seen mainly in the 3389-3000cm^{-1} region, the aromatic stretch region (1600-1400)cm^{-1}, 1293cm^{-1} and the CH bending region 1175cm^{-1}. When the gas is introduced, the intensity of the benzoid band at 1506cm^{-1} decreases while that at 1597cm^{-1}, due to quinoidal band stretch, increases. These changes can be explained as the result of the oxidation of phenyl ring to quinoid rings (see section 5.3.2). This oxidation reduces the number of phenyl rings in the polymer chain while increasing the number of quinoid rings. Also evident in figure 5.18 is the growth of the CH vibration at 1175cm^{-1} (in-plane CH bending mode of N=Q=N) and aromatic C-H stretch at 3045cm^{-1} which are both associated with the increase in conductivity of the film. However, we are unable to successfully interpret some of the changes in the IR spectrum: for example the decrease in the band at 1667cm^{-1} and the increase in the band at 1293cm^{-1}.

Figure 5.19 shows a difference spectrum, obtained insitu, by subtracting the spectrum before exposure (figure 5.18, curve a) from that after exposure to 150ppm NO_x (figure 5.18, curve b). The features in the difference spectrum show an increase in the absorption the quinoid ring stretch band at 1594cm^{-1}, in-plane CH bending at 1175cm^{-1} and aromatic CH stretch band at 3045cm^{-1}. Like changes in conductivity, the changes in the infrared spectrum were not reversible. Hence the observed increases in conductivity at such high NO_x concentrations are probably due to phenyl ring oxidation to give quinoids rings.

Figure 5.20 shows a similar difference spectrum of evaporated polyaniline after exposure to 150ppm SO_2. Compared with NO_x treatment, exposure of evaporated polyaniline to 150ppm SO_2 did not produced any significant changes in the infrared spectrum. This we believe is as a result of the less electrophilic character of SO_2 and to the absence of water vapour in the evaporated film (see section 4.3.2). The vibration at 1353cm^{-1} is ascribed to the SO_2 stretch while that at 2332cm^{-1} is due to CO_2 stretch [Banwell, 1972].

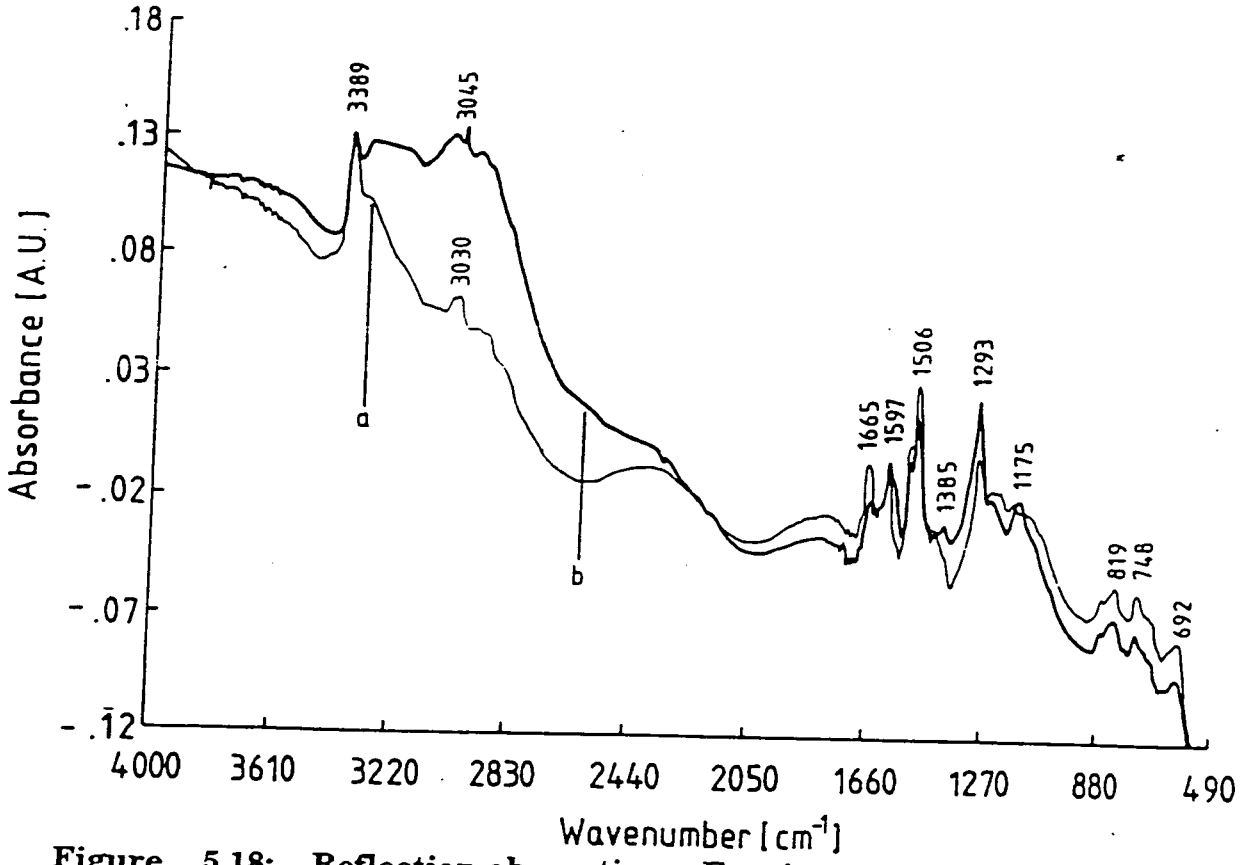

Figure 5.18: Reflection-absorption Fourier transform infrared spectra of an evaporated polyaniline film (a) before exposure (b) after 4 hours exposure to 150ppm NO_x.

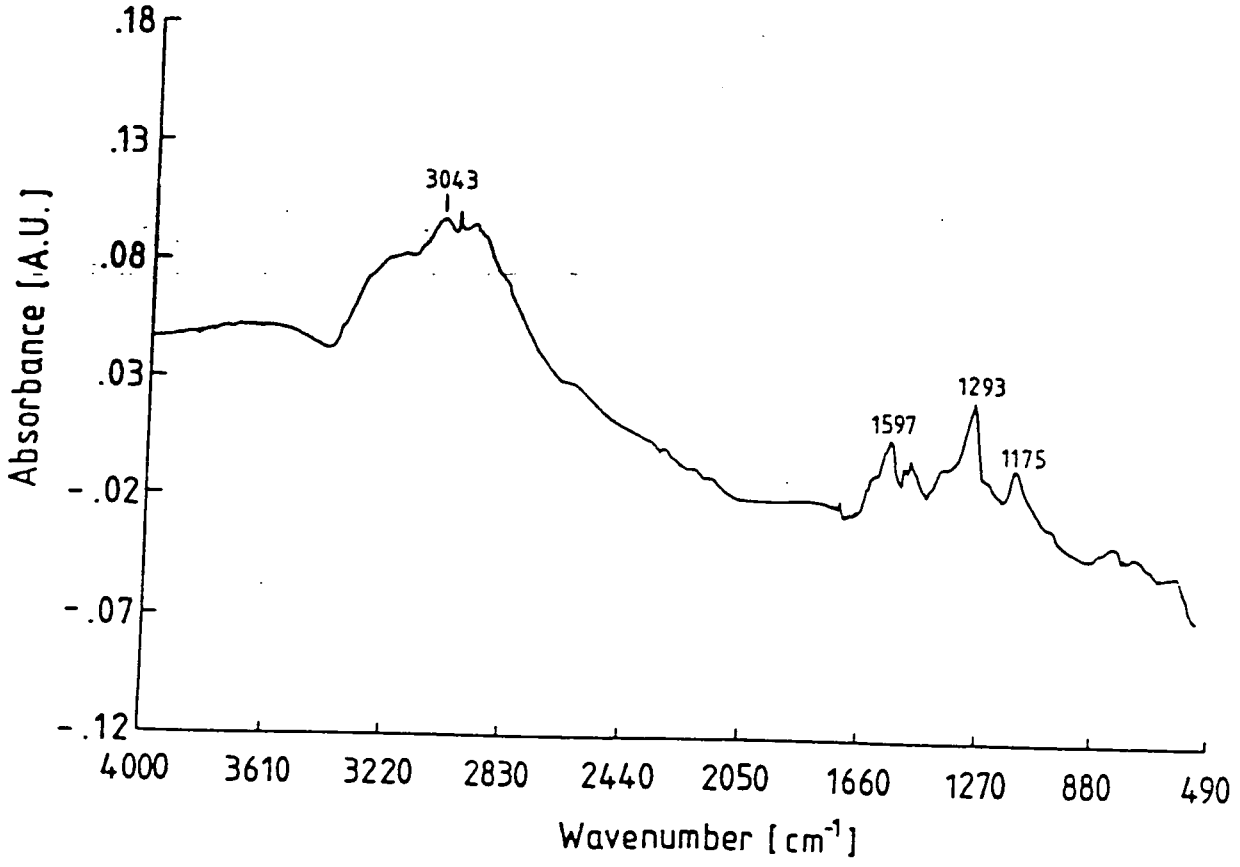

Figure 5.19: Difference spectrum of an evaporated polyaniline film after exposure to 150ppm NO_x for 4 hours.

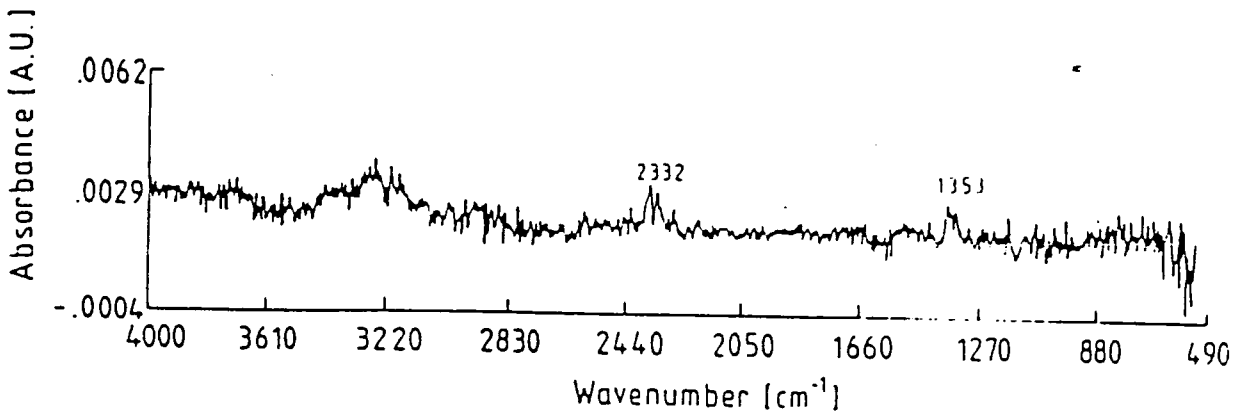

Figure 5.20: Difference spectrum of an evaporated polyaniline film after exposure to 150ppm SO_2 for 4 hours.

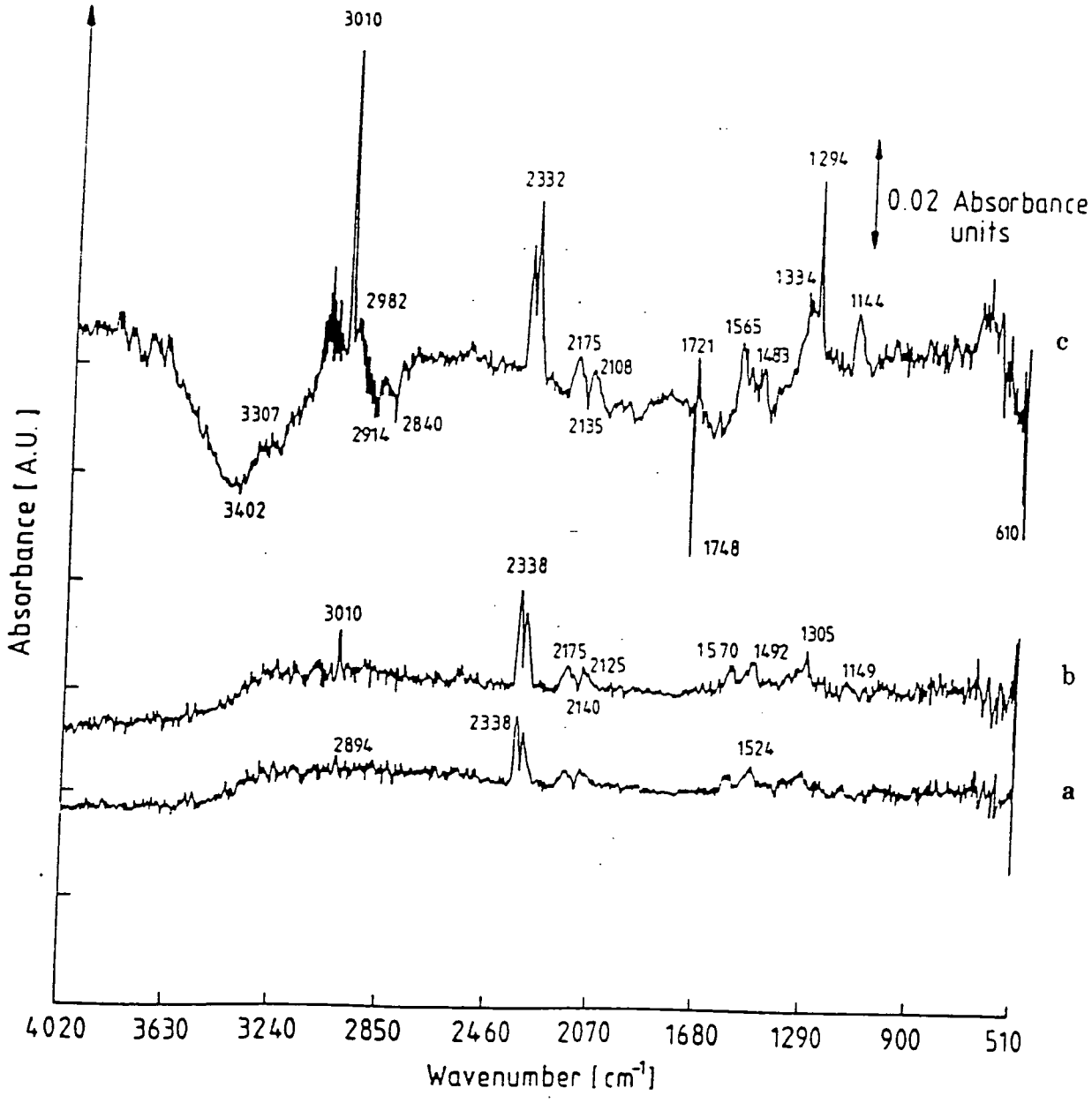

Figure 5.21: Difference spectra of an evaporated polyaniline film after exposure to 150ppm H_2S for (a) 1 hour (b) 2 hours and (c) 4 hours.

Unlike SO_2, 150ppm H_2S was found to have pronounced effects on the IR difference spectrum of EPANi. The difference spectra (obtained in the same manner as for SO_2) for various exposure times are shown in figure 5.21. Changes observed in the spectra include a CO stretch, extending from 2175-2108cm^{-1}. The definite cause of the CO band is not yet known especially as it can be seen to grow as shown in figure 5.21c. Its structure is similar to that of CO in the gas phase hence it may be due to leaks in the instrumentation. However, a similar CO peak has been reported for polypyrrole when exposed to NH_3 (a reducing gas like H_2S). In this case the cause was ascribed to pyrrole ring oxidation [Gustaffson, 1990].

Changes are also visible in the difference spectra at 1565cm^{-1} and 1483cm^{-1} (the aromatic ring stretch region). Figure 5.21 shows that, the intensity of the 1570cm^{-1} band increases with time compared to the 1492cm^{-1} band. These changes are likely due to the reduction of oxidised portions (quinoid rings with covalently bonded oxygen) of the evaporated film, resulting in an increase in the number of quinoid rings on the polymer chain. This is likely to be the case because these changes are also accompanied by increases in the CH bending vibration at 1144cm^{-1} and the aromatic CH stretch at 3010cm^{-1} that are both strongly associated with the number of quinoid rings in the polymer chain (see section 4.2.3).

Changes due to impurities in the material occur at 3402cm^{-1}, 2982cm^{-1} and 2914-2840cm^{-1}. Other changes occur at 1334cm^{-1} and 1294cm^{-1}. We could not determine their origin.

When the H_2S gas was turned off, the changes in the spectra discussed above remained completely irreversible as in the case of the electrical conductivity measurements.

5.5 SUMMARY

We have shown that thin films of polyaniline can be successfully deposited by thermal evaporation. The layers are initially colourless but change colour on prolonged exposure to air to the blue colour characteristic of the emeraldine base form of polyaniline.

From a series of optical and electrical characterization measurements, the structure of freshly evaporated polyaniline was determined to be that of leucoemeraldine, the reduced form of polyaniline. The as-deposited material has also been shown to form an ohmic contact with gold and the conductivity to be sensitive to a wide range of gases at room temperature. By comparing the results obtained to those from the spin-coated film, we may conclude that:

(i) Evaporated films can be made much thinner than spin-coated ones. From the measured conductivity changes with NO_x, it was observed that the delay time τ_D for the evaporated film was much reduced for the same gas concentration compared with the spun film. We also suggest that amine nitrogens are the main site of NO_x interaction. In both spun and evaporated films, the phenyl ring oxidation is the main cause of the increase in conductivity.

(ii) The interaction of H_2S with evaporated polyaniline is a reduction reaction in which oxidized portions of the film are reduced. In this interaction the gas donates an electron to the polymer.

(iii) SO_2 reacts with the evaporated film in the same manner as NO_x except that it is less electrophilic, thus producing a smaller change in conductivity for a similar gas concentration.

REFERENCES

Aktar, M., Weakliem, H.A., Paiste, R.M. and Gaughan, K. : Synthetic Metals, **26** (1988) 203-208

Banwell, C.N. : Fundamentals of Molecular Spectroscopy, 2nd edition, McGraw-Hill Ltd, London, 1972

Cao, Y., Li, S., Xue, Z. and Guo, D. : Synthetic Metals, **16** (1986) 305-315

Chevalier, J.W., Bergeron, J. and Dao, L.H. : Polymer Commun., **30** (1989) 308-310

Chiang, J. and Macdiarmid, A.G. : Synthetic Metals, **13** (1986) 193-205

Dannetun, P., Uvdal, K., Salaneck, W.R., Stafström, S., Bertilsson, L., Macdiarmid, A.G., Ray, A., Scherr, E.M., Löglund, M. and Epstein, A.J. : Synthetic Metals, **29** (1989) 451-462

Glaser, A.B. and Subak-Sharpe, G. : 'Integrated Circuit Engineering', Addison-Wesley, Reading, Massachusetts (1977)

Grate, J.W., Klusty, M., Barger, W.R. and Snow, A. : Analytical Chemistry, **62** (1990) 1928-1934

Gustafsson, G. : PhD thesis, Linköping University, Sweden, 1990

Hagiwara, T., Yamaura, M. and Iwata, K. : Synthetic Metals, **25** (1988) 243-252

Hanawa, T., Kuwabata, S., Hashimoto, H and Yoneyama, H. : Synthetic Metals, **30** (1989) 173-181

Monkman, A.P. and Adams, P. : Synthetic Metals, **40** (1991) 87-96

Nilsson, J.O. : PhD thesis, Linköping University, Sweden, 1989

Ohira, M., Sakai, K., Takeuchi, M., Kobayashi, Y. and Tsuji, M. : Synthetic Metals, **18** (1987) 347-352

Stafström, S. and Brédas, J.L : Synthetic Metals, **14** (1986) 297-308

Stafström, S. : Synthetic Metals, **18** (1987) 387-392

Stafström, S., Sjogren, B., Wennerstrom, O., Hjertberg, T. : Synthetic Metals, **16** (1986) 31-39

Tanaka, K., Shichiri, T., Kobashi, M. and Yamabe, T. : Synthetic Metals, **24** (1988) 167- 178

Vachon, D., Angus, R.O. Jnr., Lu, F.L., Nowak, M., Liu, Z.X., Schaffer, H., Wudl, F. and Heeger, A.J. : Synthetic Metals, **18** (1987) 297-302

Wessling, B., and Harald, V. : Synthetic Metals, **16** (1986) 127-131

CHAPTER SIX

POLYANILINE LANGMUIR-BLODGETT FILMS: RESULTS AND DISCUSSION

6.1 PREFACE

It has been shown in the last two chapters that thin films of polyaniline can readily be deposited by spinning or evaporation. However, in these two processes, control of film thickness, micro crystalline size and morphology are poor. In order to improve on the control of the above properties, thin films of polyaniline were deposited by LB technique. This method was first used by Cheung et al. to deposit ultra-thin films of deprotonated polyaniline [Cheung et al, 1991].

In section 6.2, the formation and deposition of polyaniline LB films are described. These films are studied using ultraviolet/visible spectroscopy, reflection-absorption Fourier transform infrared spectroscopy, surface plasmon resonance, in-plane dc conductivity and thickness measurements; the results are presented in section 6.3. This is followed by gas sensing measurements, in section 6.4.

6.2 LB FILM FORMATION

The prepartion of a solution of polyaniline for LB film formation has been described in section 3.2. The polymer solution that formed was blue in reflected light and spread uniformly on the water surface without any visible sign of aggregation. The surface pressure versus area isotherm at 20±2°C is shown in figure 6.1. After multiple (~4) compressions at a rate of about $0.01nm^2molecule^{-1}s^{-1}$ the material formed a reasonably condensed floating layer up to $40mNm^{-1}$ surface pressure. If we assume the area per molecule of the acetic acid is negligible, the area per emeraldine base repeat unit (shown as inset in figure 6.1) is approximately $0.20nm^2$ at $30mNm^{-1}$ surface pressure. This value is comparable to the dimensions of a space filling model of an aniline unit of $0.25nm^2$ given by Ando et al, 1987. We thus conclude that the

emeraldine base repeat unit does not form a true monomolecular layer on the water surface. Rather, it probably has a thickness of several monolayers. The floating film was stable for several hours at a surface pressure of $30mNm^{-1}$. The dipping speed for LB deposition was $0.03mms^{-1}$, allowing at least 20 minutes between the first and seconds dips. Z-type deposition was observed, as shown in figure 6.2 with a transfer ratio of 1.0±0.1 on all dip cycles. The films deposited were blue in reflected light and reasonably uniform, by visual inspection, for up to 50 layers.

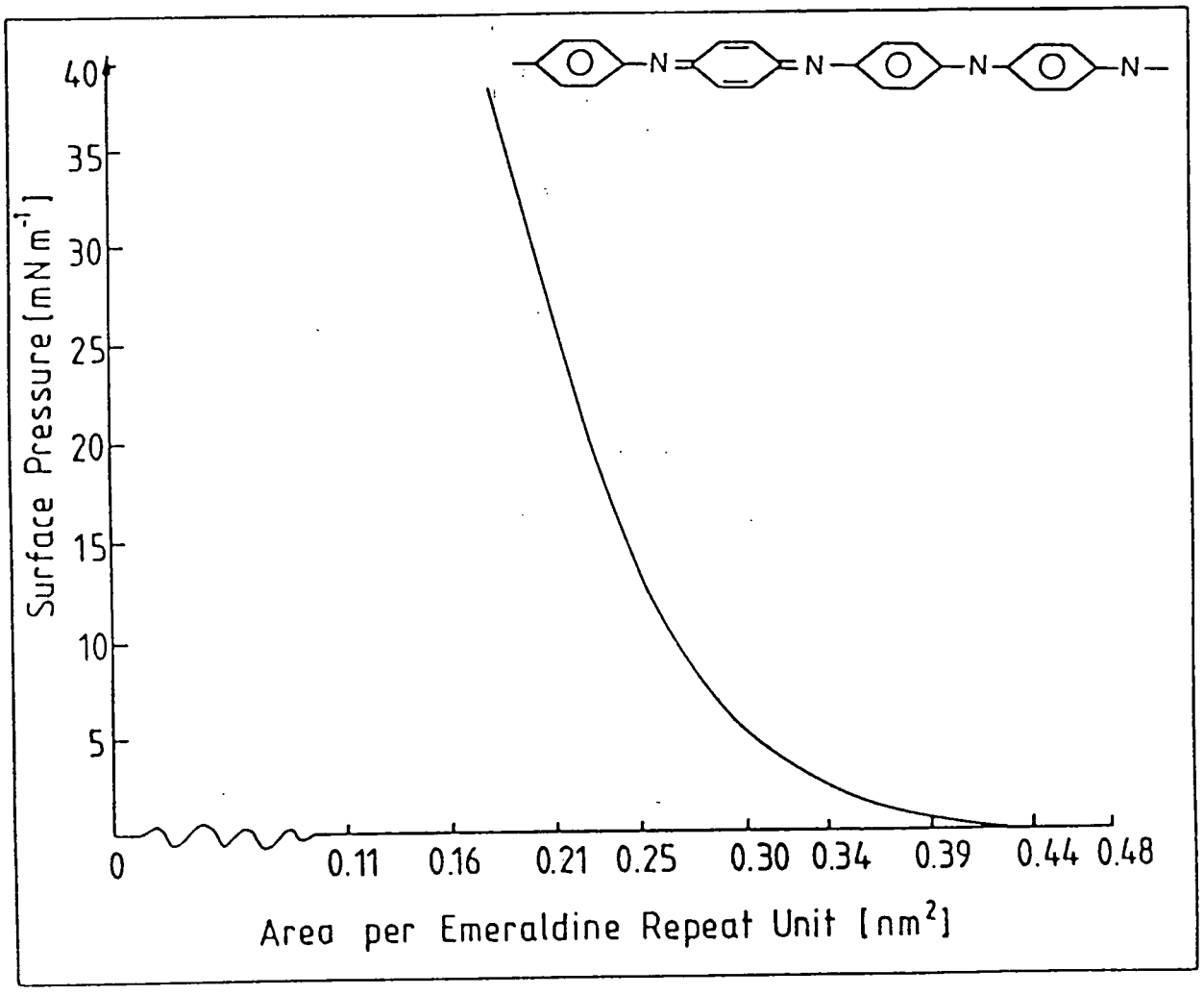

Figure 6.1: Surface pressure versus area for polyaniline on a pure water surface after 4 compressions. Inset shows the chemical structure of the emeraldine repeat unit. (Temperature 20±2°C).

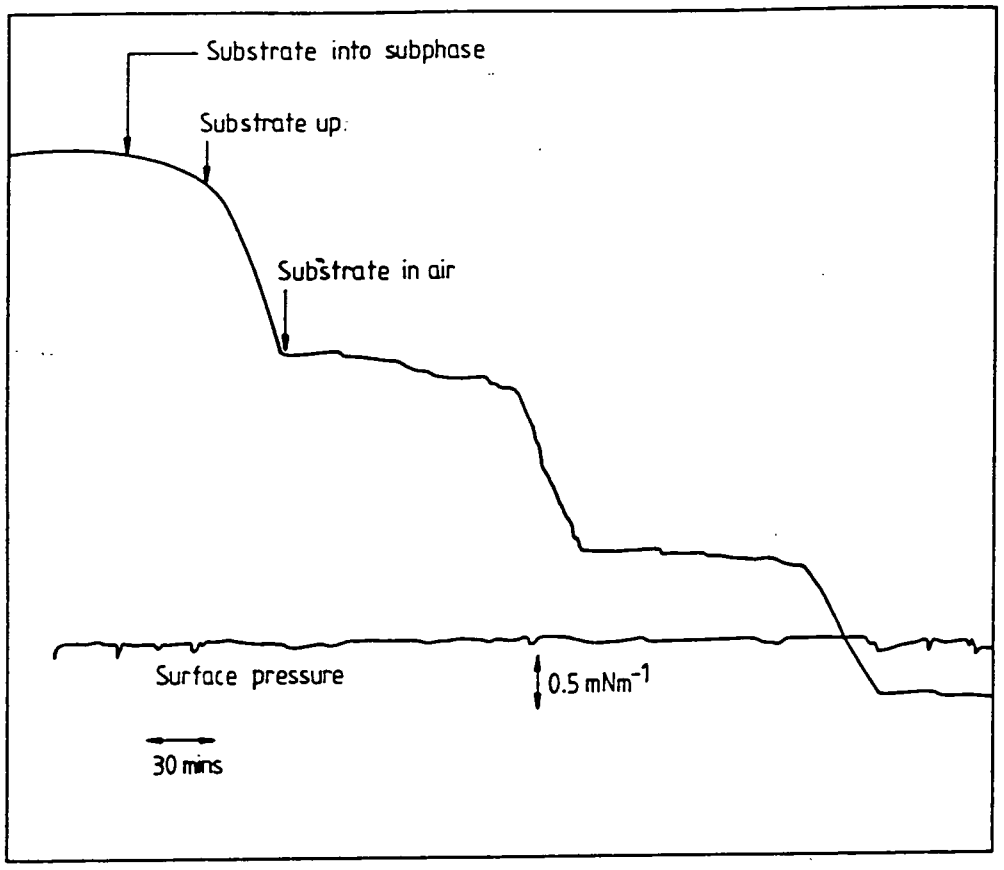

Figure 6.2: Z-type deposition record of polyaniline LB films on glass.

6.3 FILM CHARACTERIZATION METHODS

6.3.1 Ultraviolet/Visible Spectroscopy

The ultraviolet/visible spectrum for 20 layers of polymer deposited onto glass, shown in figure 6.3, (curve a), is similar to that of the emeraldine base form of the polymer [Monkman et al, 1990]. The maximum absorbance occurs around 320nm and may be attributed to π-π^* transition in the benzoid ring of the polymer backbone; the broad band evident around 620nm is due to self-trapped exciton formation on the quinoid ring [Duke et al, 1986 and Cao et al, 1989]. The variation of absorbance at 620nm with film thickness is shown in figure 6.4 and indicates good reproducibility of the LB film deposition for up to 60 layers. The thickness per layer measured by ellipsometry and the Talystep was

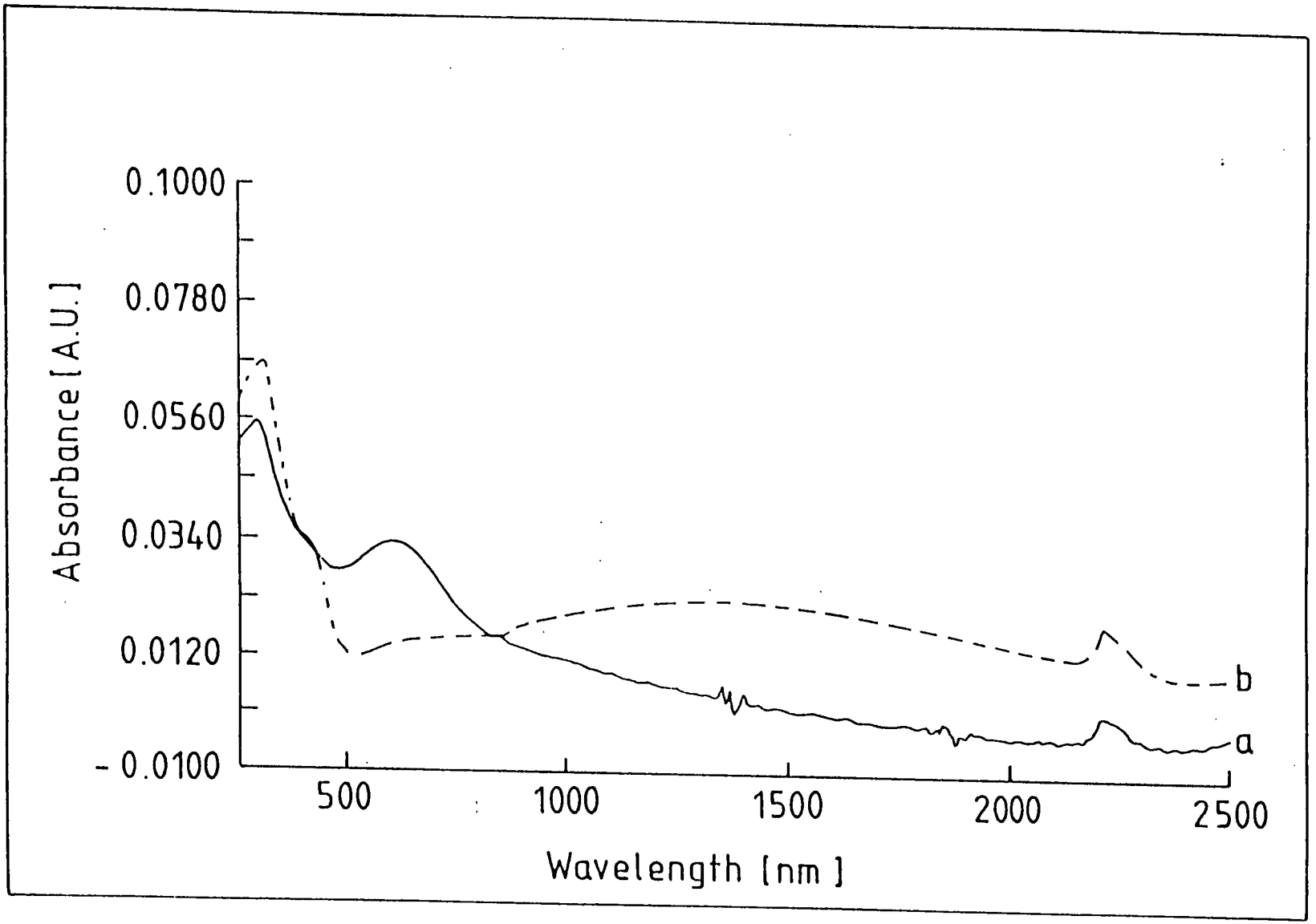

Figure 6.3: The ultraviolet/visible spectrum of 20 LB layers polyaniline for (a) as-deposited and (b) doped with HCl.

6.0±0.2nm and 5.5±0.6nm, respectively (average values for 20, 30 and 40 layers).

The LB films were protonated by exposure to 2M HCl vapour for 2 hours. The absorption band at 320nm decreased in intensity while that at 620nm disappeared almost completely as shown by curve b in figure 6.3. However, the absorbance remained relatively strong from 800nm into the near infrared region, consistent with the spectrum of a metal. Also observable in the visible is an emerging shoulder between 400-500nm, attributable to charged state formation. A similar effect for polyaniline free standing film has been reported [Monkman et al, 1990].

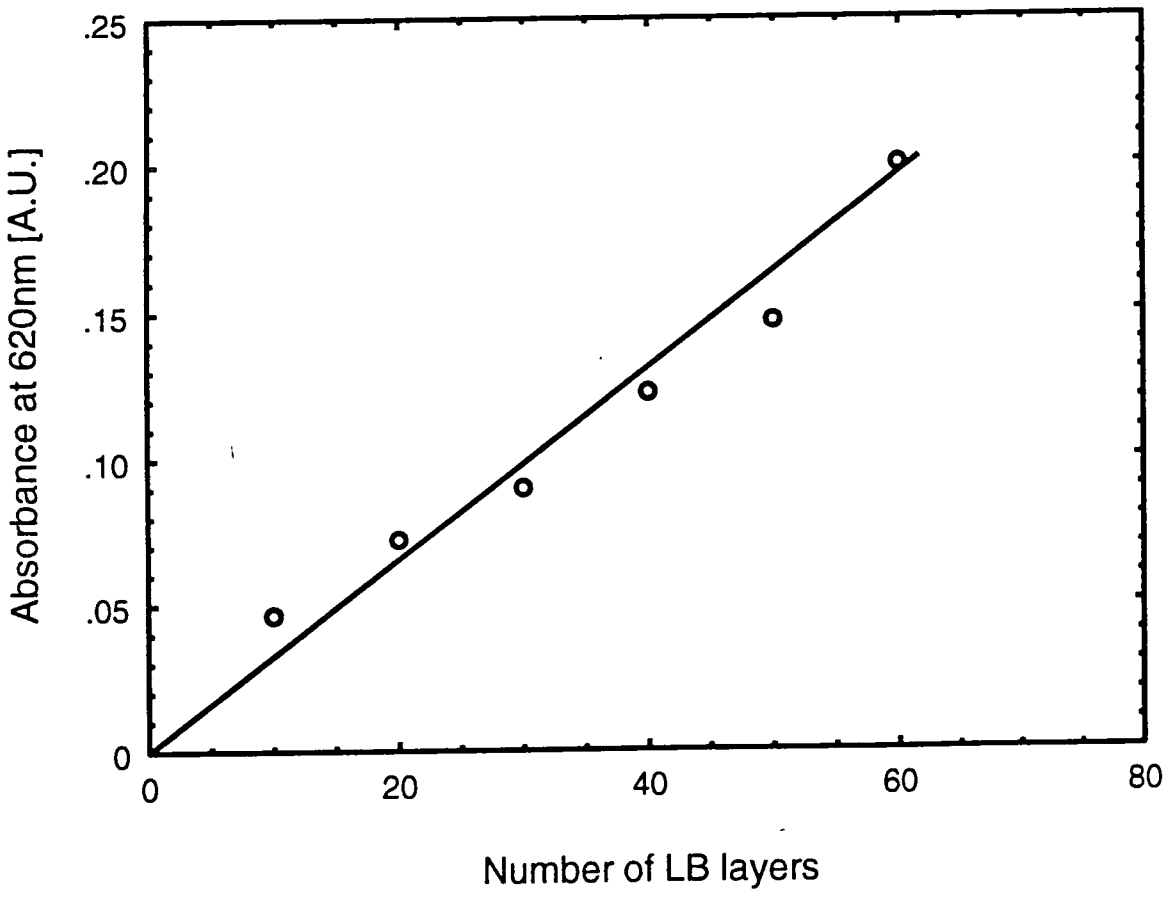

Figure 6.4: The variation of the absorbance at 620nm with number of polyaniline LB film layers deposited on one side of a glass slide.

6.3.2 Reflection-Absorption Fourier Transform Infrared Spectroscopy

The reflection-absorption FTIR (RAIRS) spectrum for 10 layers of the as-deposited material is shown in figure 6.5. This contains some features that can be related to both the spectrum of acetic acid [Pouchert, 1981] and that of the emeraldine base form of polyaniline [Monkman et al, 1991]. The RAIRS spectrum of polyaniline has been described in chapter four and by other authors [Kim et al, 1988] and will not be repeated here.

The addition of acetic acid to polyaniline can be likened to what is called protonic acid 'doping' [Macdiarmid et al, 1987] and leads to the protonation of the polymer. Changes caused by this doping effect in the RAIRS spectrum include a continuous increase in the optical absorbance from 2000-4000cm^{-1}, which is attributed to the formation of charge transfer band. A shoulder can be seen at 1466cm^{-1} and is associated with the protonation of quinoid rings into benzoid ones. This produces semiquinone radical structures that increases the degree of π-electron delocalisation along the molecule with a concomitant increase in conductivity [Furukawa et al, 1986]. The intensity of this vibration at 1466cm^{-1} can be directly related to the strength of the dopant or the degree of conversion of quinoid rings to semiquinoid rings. This quinoid-to-semiquinoid conversion results in an increase in conductivity of the polymer during protonation by about 15 orders of magnitude [Monkman et al, 1991].

Figure 6.6 shows the aromatic breathing region (1600-1400)cm^{-1} for LB and spin-coated film of polyaniline. The relative intensity of the quinoid (1593cm^{-1}) to benzoid (1501cm^{-1}) stretch bands is extremely sensitive to the polymer chain structure. In figure 6.6, curve a, the intensity of the quinoid vibration is greater than that of benzoid rings, in contrast to curve b for spin-coated films. Exposure of polyaniline to iodine vapour produces similar effects to mixing with acetic acid [Tang et al, 1988]. The net result is an increase in the effective chain conjugation length [Cao et al, 1986]. This is the result of increased π-electron conjugation between adjacent phenyl rings over the nitrogen heteroatom on the backbone.

From the above results, we suggest that the LB film is in a different state from emeraldine base polyaniline, probably pernigraniline or a close derivative.

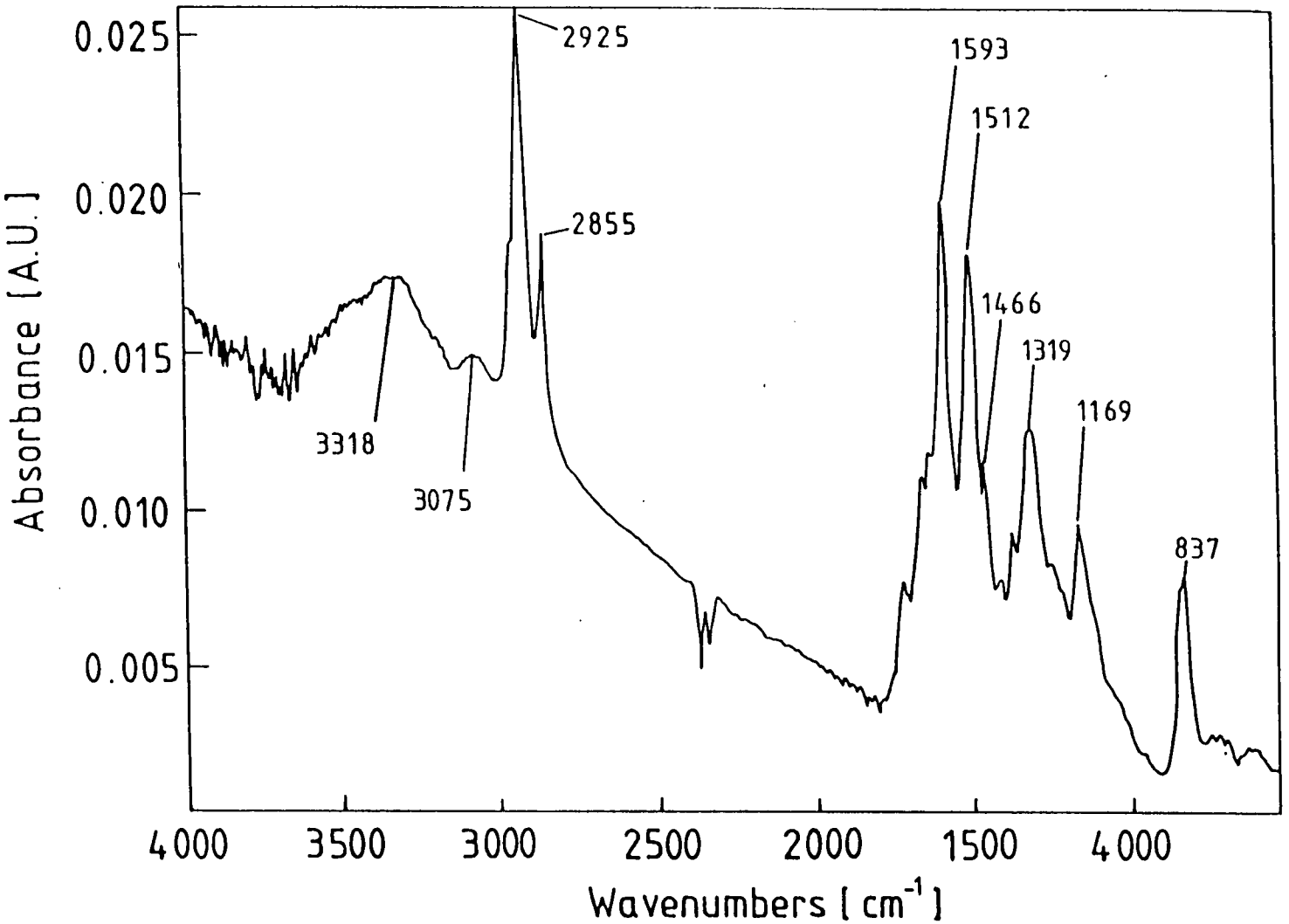

Figure 6.5: The reflection-absorption spectrum of 10 layers of an as-deposited polyaniline LB film on 500nm of gold.

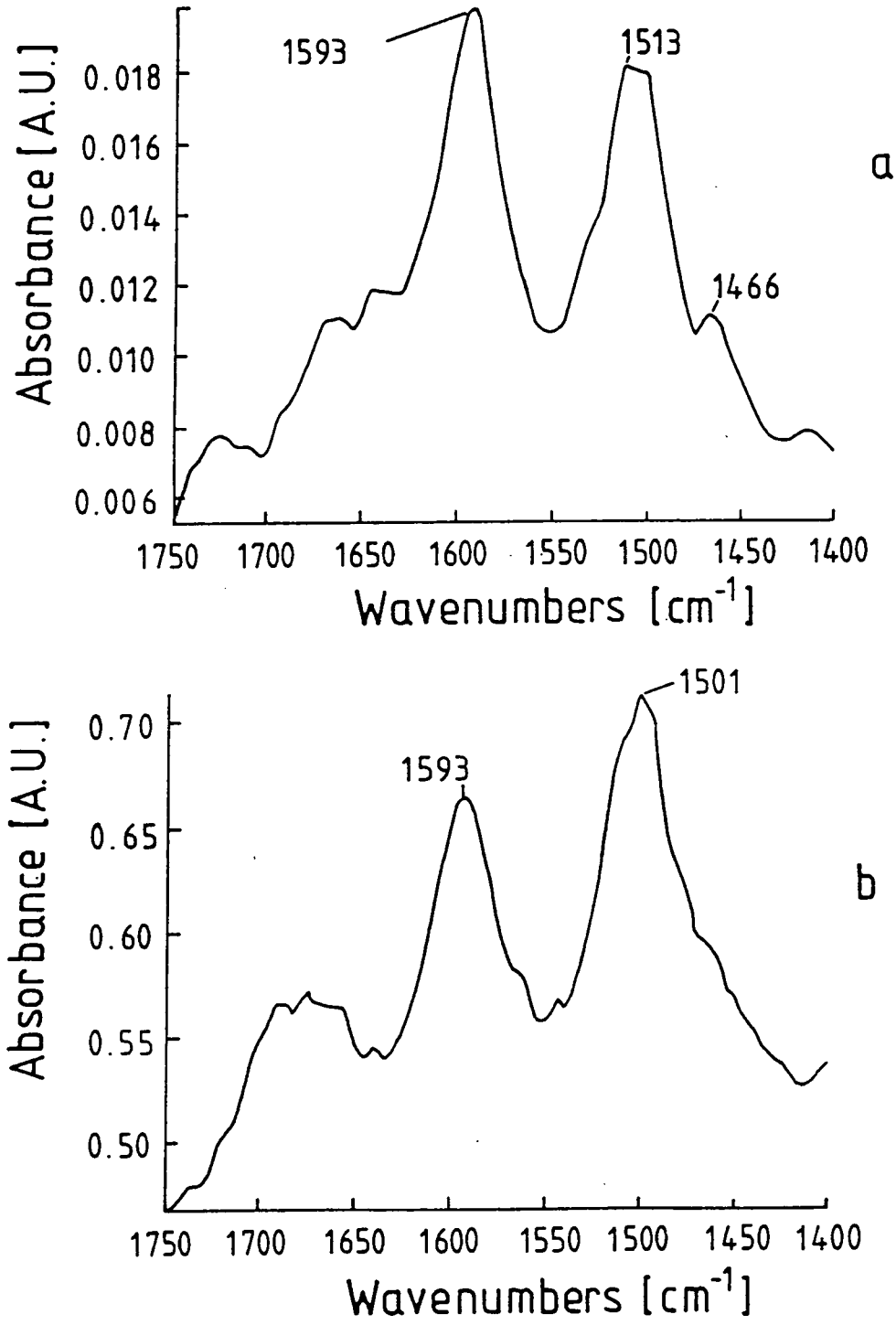

Figure 6.6: The aromatic breathing region of (a) as-deposited polyaniline LB film (b) spin-coated polyaniline.

6.3.3 Electrical Conductivity

The room temperature current versus voltage characteristics of 50 layers of an 'undoped' polyaniline LB film on glass is given in figure 6.7. This shows a linear increase in current with applied voltage. The slope of this curve changed as the distance between the electrodes was varied as well as with the number of LB film layers (data not shown). This confirms that the conduction was via the LB film and not dominated by contact or substrate effects. Furthermore, the results suggest that ohmic contacts were established between the polymer and the gold electrodes.

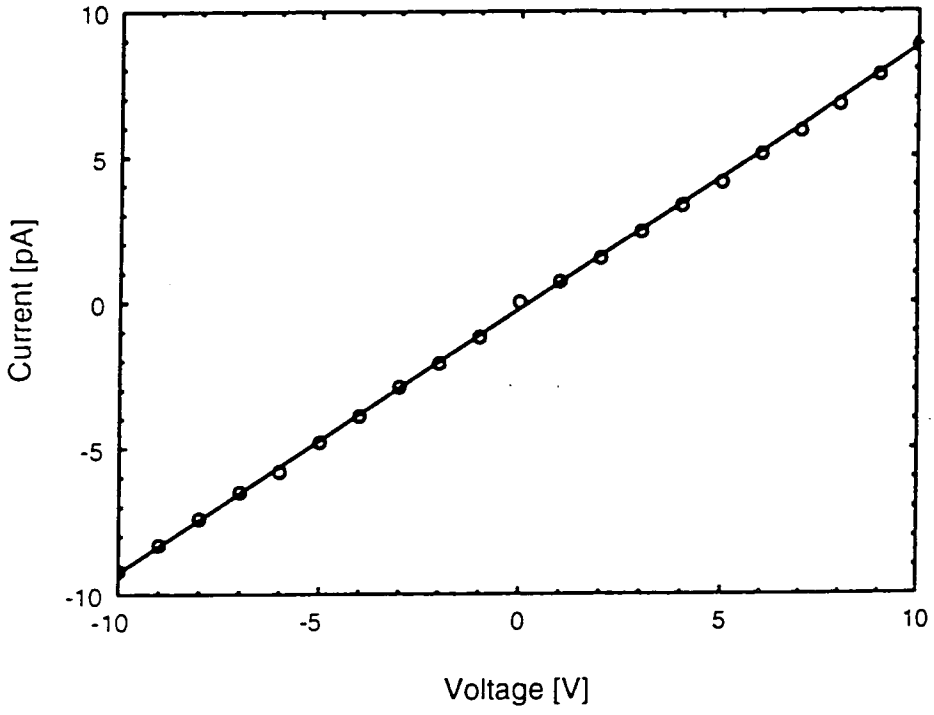

Figure 6.7: Current versus voltage characteristics for 50 layers of polyaniline LB film deposited on an interdigitated electrode structure. (film thickness ≈300nm and 10^{-3}mbar vacuum). Temperature 20±2°C.

DC conductivity measurements were undertaken for both the as-deposited and protonated materials. The room temperature in-plane dc conductivity of the LB film in vacuum was calculated to be approximately $1.0 \times 10^{-8} Scm^{-1}$, using the measured thickness per layer of 6.0nm. This value is significantly higher than that of deprotonated polyaniline spin-coated film ($10^{-11} Scm^{-1}$),

suggesting some degree of protonation (as shown in section 6.3). There is also the possibility of some oxidation or reduction of the polymer, as described below.

The dc conductivity of the 'doped' LB film was calculated to be $0.1Scm^{-1}$ at room temperature. This value, although small compared to that obtained for solution cast protonated polyaniline films ($350Scm^{-1}$) [Monkman et al, 1991], is comparable to that reported by the MIT group ($1Scm^{-1}$) [Cheung et al, 1991] for LB layers.

The value of the dc conductivity calculated above was for measurements perpendicular to the dipping direction. However, when measured parallel to the dipping direction, the conductivity was found to be smaller by a factor of approximately 7. It can therefore be suggested that the molecular chains in the polymer film are aligned perpendicular to the dipping direction as depicted in figure 6.8.

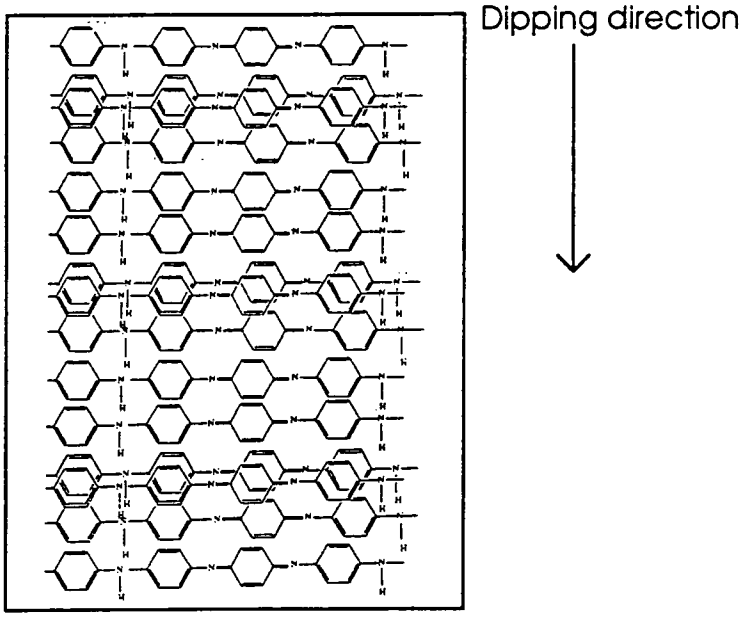

Figure 6.8: Proposed alignment of molecules of emeraldine base repeat unit on a glass substrate. The rectangular box representing the substrate plane with the dipping direction shown.

6.3.4 Surface Plasmon Resonance

LB films of polyaniline were deposited onto Ni/Ag substrates for SPR studies. The reflectance versus external angle of incidence is shown in figure 6.9 for 0, 1, 2 and 3 LB layers. The effects of the overlayers include a shift in the resonance position to higher angles with increasing film thickness, an increased broadening of the resonance curve and a decrease in the resonance depth. Similar effects were observed when thin films of polyaniline were thermally deposited on Ni/Ag substrate (see figure 5.12). The last two effects are almost certainly associated with the absorption of the laser light by the organic film, while the shift in resonance to higher angles is due to change in thickness of the overlayer.

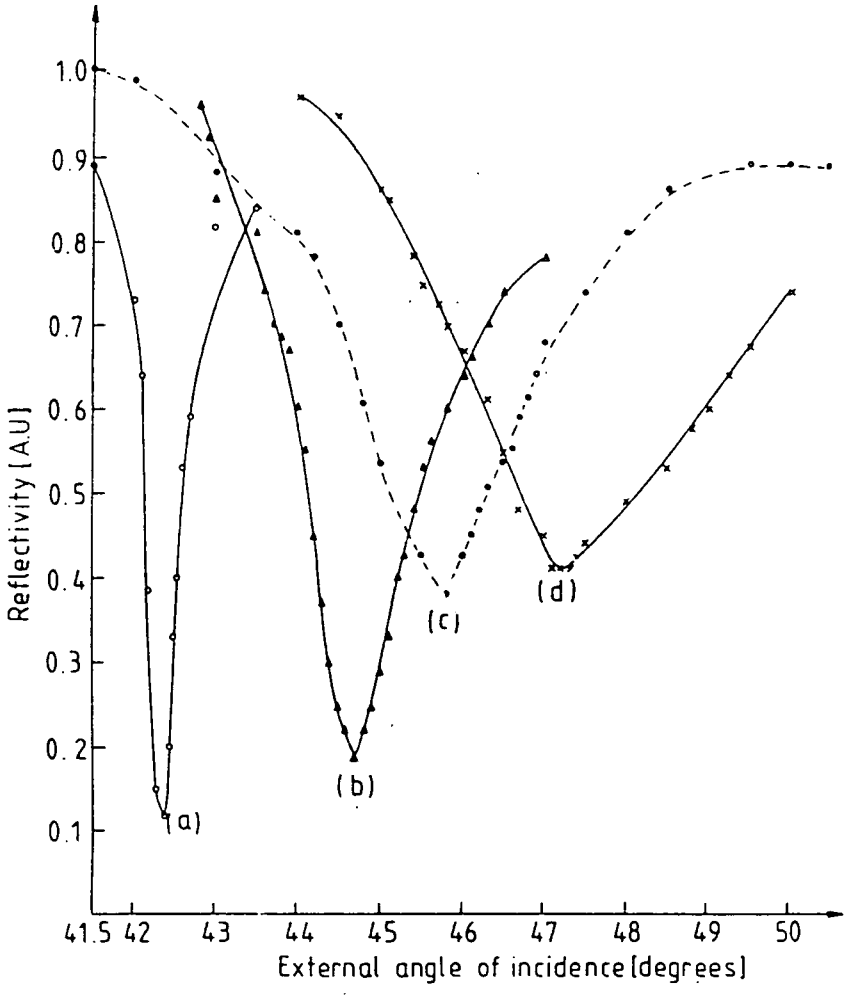

Figure 6.9: SPR curve of (a) Ni/Ag, (b) 1, (c) 2 and (d) 3 layers of polyaniline LB film on a Ni/Ag substrate.

6.4 GAS SENSING

Gas sensing studies have been undertaken using thin films of polyaniline deposited on Ni/Ag and gold. Measurements have included dc conductivity, surface plasmon resonance and reflection-absorption Fourier transform infrared spectroscopy. The experiments were all undertaken in a N_2 atmosphere and using the same gases as for the previous work, in chapters 4 and 5. N_2 produced the same effect on the device as was noted for the spin-coated film (see figure 4.10). This included a decrease in conductivity over a period of about 1 hour compared with only 12 minutes for the evaporated film. This time difference is probably due to the adsorption of water from the subphase. Before any sensing experiments, all secondary effects, such as those due to substrate and instrumentation, were minimised.

6.4.1 Insitu-Conductivity Gas Response

Figure 6.10a shows the effect of 100ppm NO_x on 18 LB layers of polyaniline (approximately 110nm) at room temperature. The response can be seen to be made up of two main parts: an initial rapidly increasing current followed by a more gradual increase with time. The rapidly increasing current phase occurs after a delay time of about 70 seconds. A similar profile can be seen when the gas was turned off where there is an initial rapid recovery and a non-reversible step. It is possible that the initial increase in current is due to physisorbed molecules on the surface while the more gradual change may be ascribed to bulk effects. The non-reversibility may also be explained by the difficulty of the deeply diffused chemisorbed molecules being recovered. Similar effects have been reported for polypyrrole on exposure to ammonia gas [Gustafsson, 1990].

The effect of different NO_x gas concentrations is shown in figure 6.10b. This graph exhibits a minimum detectable gas concentration of approximately 30ppm, compared to 4ppm for both the evaporated and spin-coated material. The reduced sensitivity could be due to the fact that acetic acid has occupied and chemically blocked some sites previously responsive to the gas.

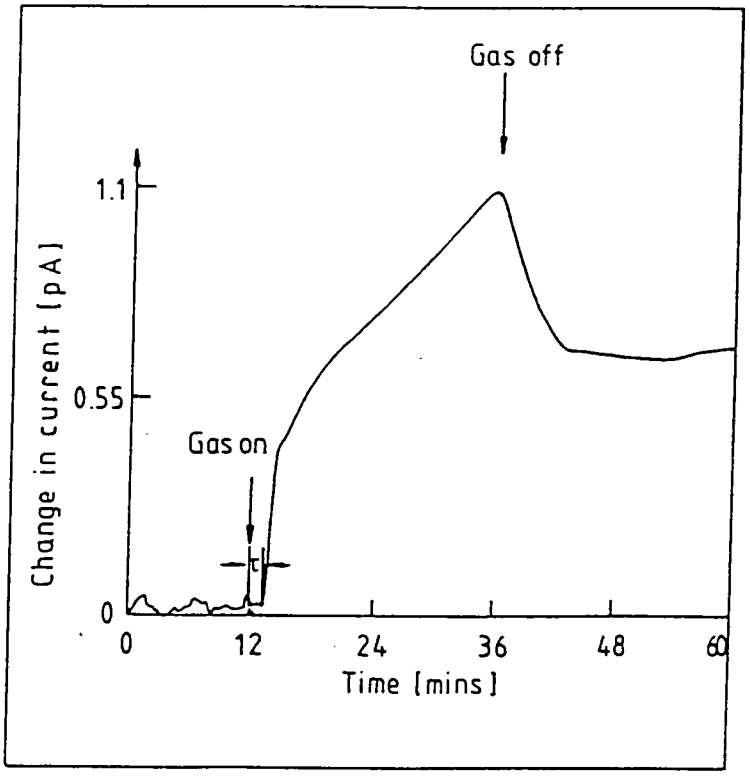

Figure 6.10a: The effect of 100ppm NO_x on 18 LB layers of a polyaniline chemiresistor at room temperature (applied voltage 2V).

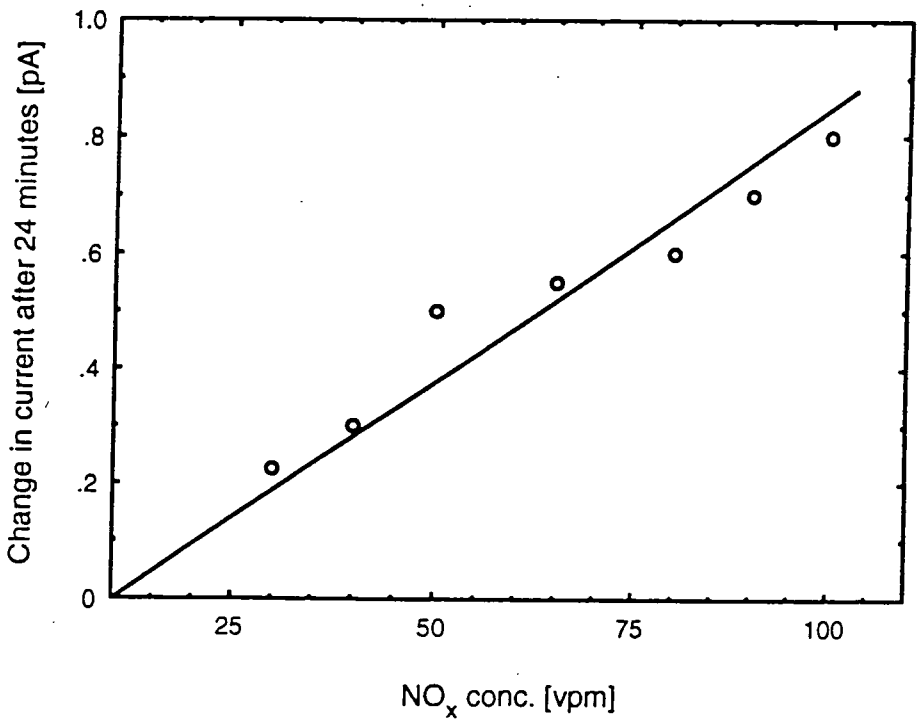

Figure 6.10b: The response of 18 LB layers of a polyaniline chemiresistor to different concentrations of NO_x at room temperature (2V supply).

NO_x is a highly oxidising gas. As a result, we anticipate its interaction with the LB film to involve the transfer of electrons to the gas during which semiquinones are formed. The formation of semiquinones increases the conductivity. However, from these results we cannot determine if these semiquinones originate from benzoid rings or quinoid rings or both.

Figure 6.11a shows the effect of 8ppm H_2S on 18 LB layers of polyaniline at room temperature. Significant change in the conductivity takes place after a delay time of about 100 seconds and, as observed, it is almost reversible after a period of about 80 minutes. Like NO_x it can be seen that the reaction results in an increase in conductivity similar to that observed with a spin-coated polyaniline film.

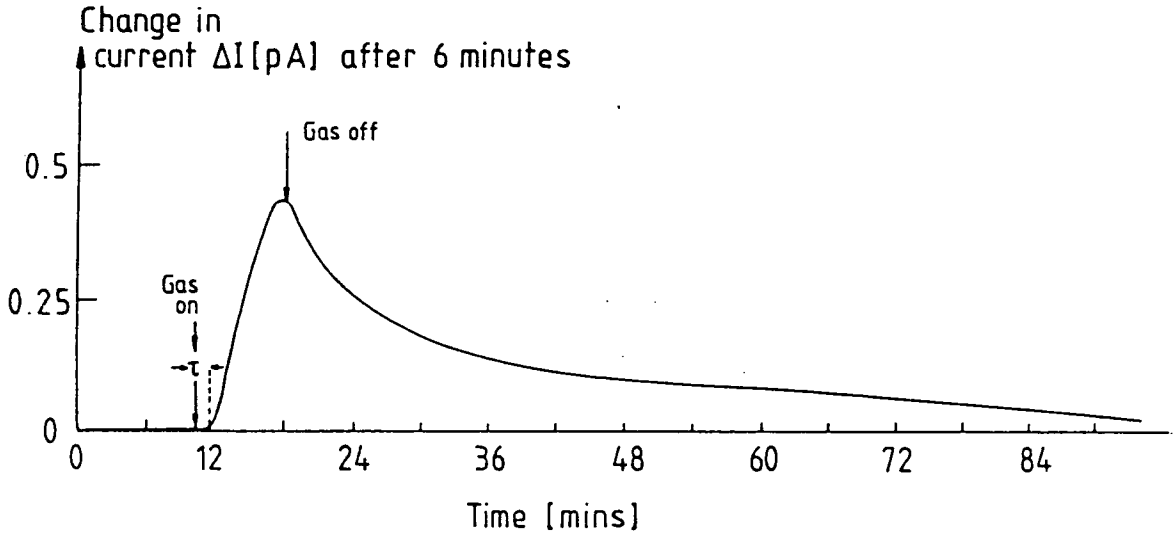

Figure 6.11a: The effect of 8ppm H_2S on 18 LB layers of a polyaniline chemiresistor at room temperature (applied voltage 2V).

Figure 6.11b shows the effect of different H_2S gas concentrations on the current flowing through the PANi LB film chemiresistor. The change in conductivity increases linearly with the gas concentration, with a minimum detection level of 5ppm.

The interaction between H_2S and LB polyaniline can follow the same reaction mechanisms as spun polyaniline, that also exhibits an increase in conductivity. H_2S/polyaniline LB film interaction is likely to be an equilibrium non-redox

process. Furthermore, in such a reaction no electrons are involved. Instead, as has been discussed in section 4.3, H_2S dissociates into H^+ and HS^-. This dissociation is subsequently followed by protonation of the remaining unprotonated sites in the polymer.

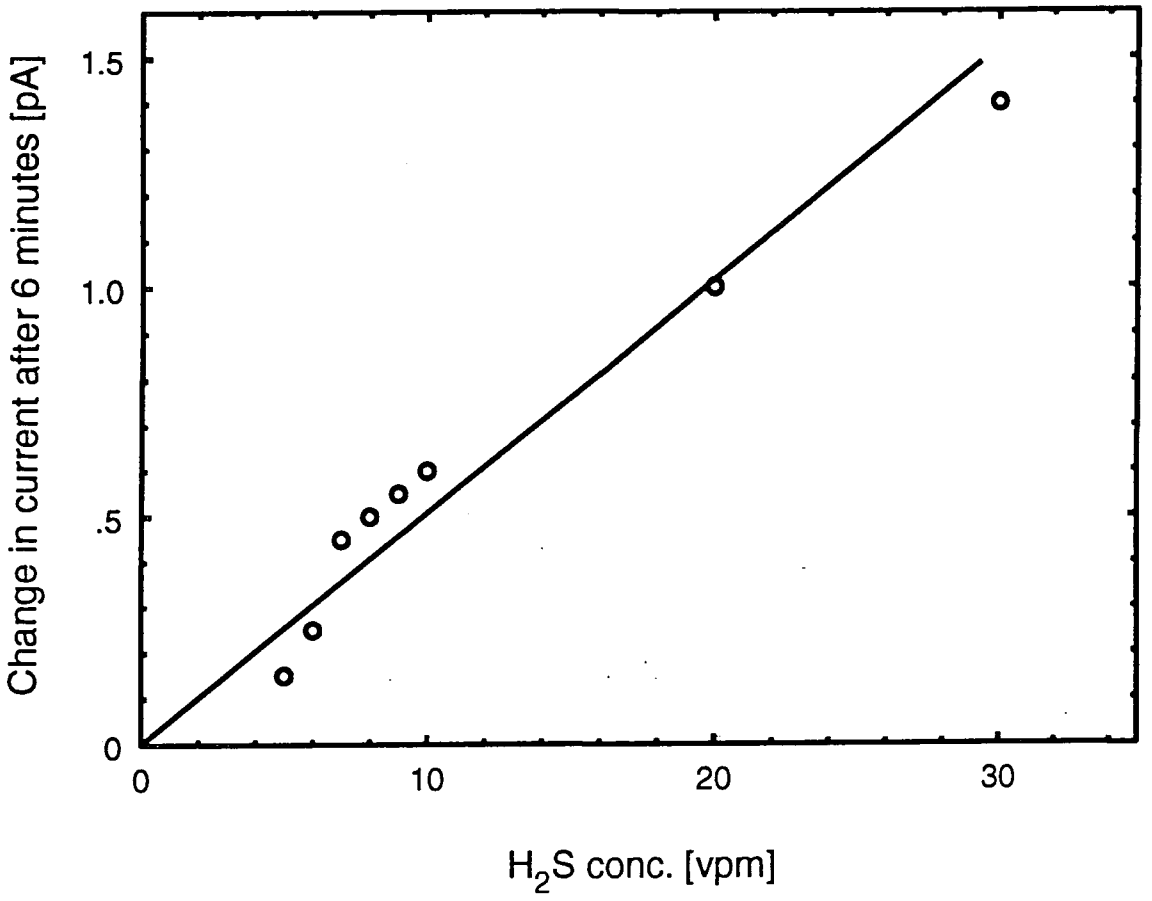

Figure 6.11b: The response of 18 LB layers of a polyaniline chemiresistor to different concentrations of H_2S at room temperature (2V supply).

No change in current was observed when the same chemiresistor was exposed to different concentrations of SO_2, CO or CH_4, in the latter case even up to concentrations of 10,000ppm. The negative results obtained for SO_2 substantiates our suggestion that acetic acid could be blocking sites in the LB film.

A summary of the effect of the various gases on 18 LB layers of polyaniline chemiresistor is presented in table 6.1.

Gas	Conc. in N_2 [ppm]	Delay Time τ_D [s]	Exposure Time [mins]	Recovery Time τ_R [mins]	Minimum Detection Level [ppm]	Normalised Change per ppm $\frac{\Delta R}{R} \div$ gas conc. in ppm
NO_x	100	70	24	partially reversible	20	-1.6×10^{-3} (at 100ppm)
H_2S	100	100	6	80	5	-0.011 (at 100ppm)
SO_2	1000	No observed effect	6	N/A	N/A	N/A
CO	10000	No observed effect	N/A	N/A	N/A	N/A
CH_4	50000	No observed effect	N/A	N/A	N/A	N/A

Table 6.1: Summary of the effects of different gases on an LB polyaniline chemiresistor at room temperature (film thickness ≈110nm).

6.4.2 Surface Plasmon Resonance

Figure 6.12 shows the effect of 600ppm NO_x on the SPR curve of 1 LB layer of polyaniline. A shift in the resonance curve by almost 0.2° is evident. The minimum reflectivity and the half width at half maximum (HWHM) do not appear to change. Referring to section 3.3b, we suggest that the effects are possibly associated with a simple change in the thickness of the LB layer. It has already been established that 1000ppm NO_x has no effect on Ni/Ag layer [Zhu et al, 1990]. Hence, the changes are due to the gas/material interaction resulting in a swelling of the film. The film thickness change is also likely to result in a change in the refractive index.

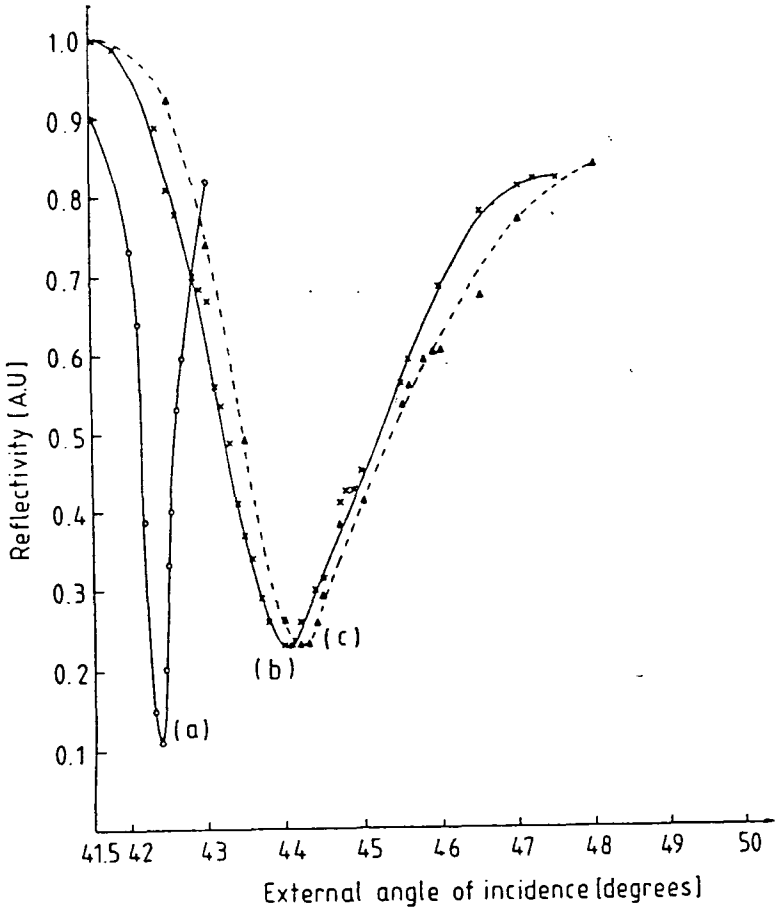

Figure 6.12: SPR curve of (a) Ni/Ag, (b) 1 LB layer of polyaniline on Ni/Ag and (c) after exposure to 600ppm of NO_x at room temperature for 36 minutes.

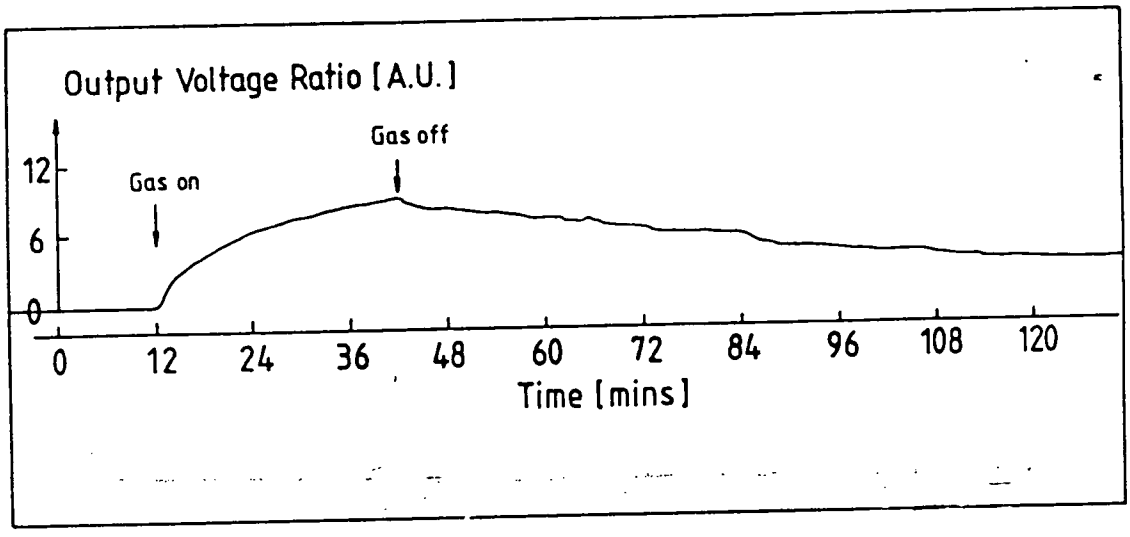

Figure 6.13: The effect of 400ppm NO_X on 1 LB layer of a polyaniline SPR sensor.

The time dependence of the reflectance change was investigated by fixing the incident beam close to resonance (at 43.5°) and monitoring the voltage ratio output from the photodiodes. Figure 6.13 shows the change in the reflectivity for 400ppm of NO_X at room temperature. We can see that an increase in reflectivity is produced on exposure to the gas. The increase takes up to 1 hour to saturate, then reverses partially when the gas is switched off.

The effect of different concentrations of NO_X are shown in figure 6.14. Here we can see that the detection threshold is 50ppm compared with 30ppm in conductivity measurements.

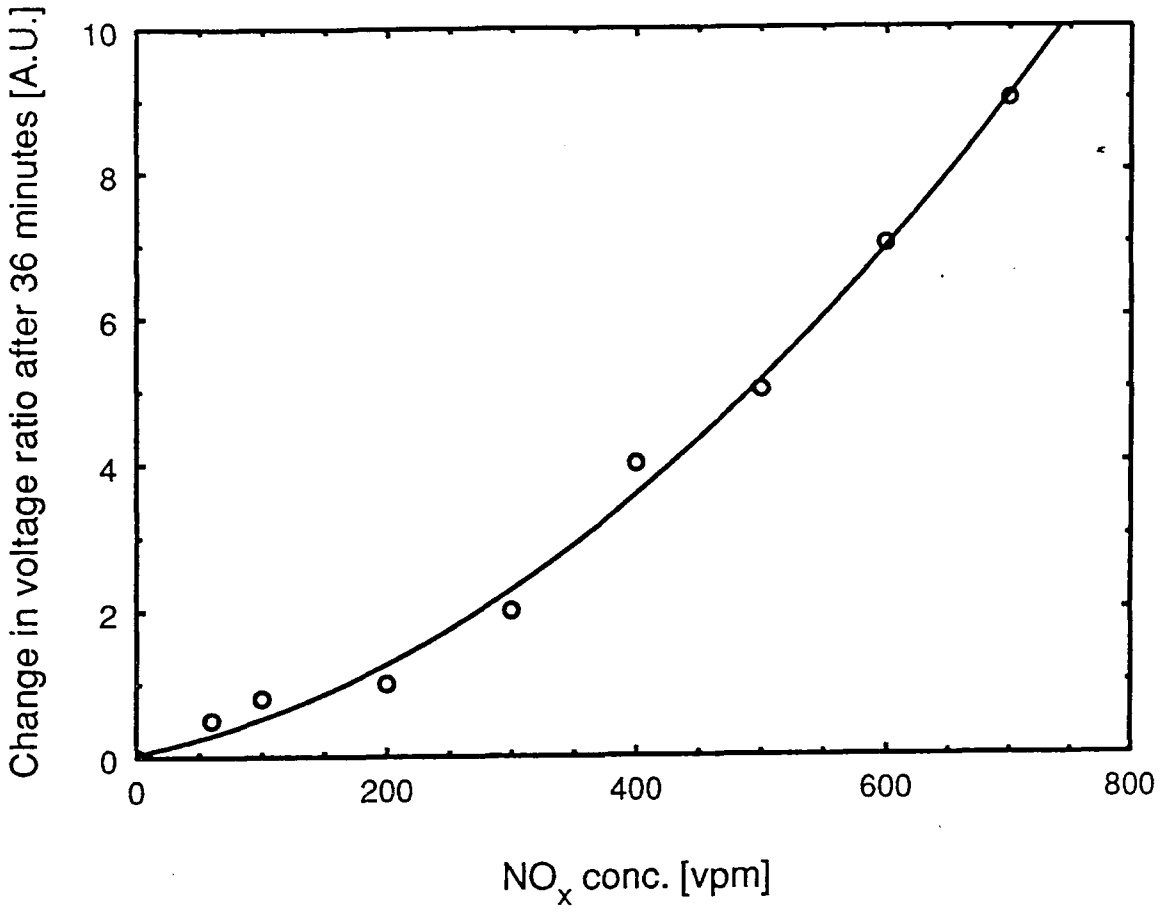

Figure 6.14: The effect of different concentrations of NO_x on 1 LB layer of a polyaniline SPR sensor.

Figure 6.15 shows the time dependence of the change in reflectance for 100ppm of H_2S. Like NO_x, it can be seen that the reaction is only partly reversible even after 2 hours in N_2. Figure 6.16 shows how the device responds to different H_2S gas concentrations.

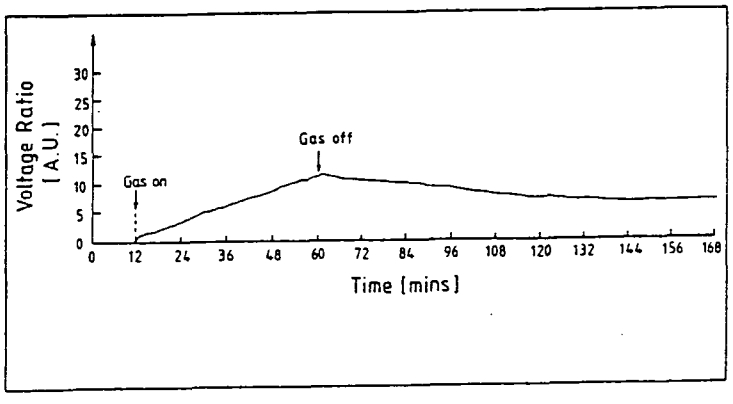

Figure 6.15: The effect of 100ppm H_2S on 1 LB layer of a polyaniline SPR sensor.

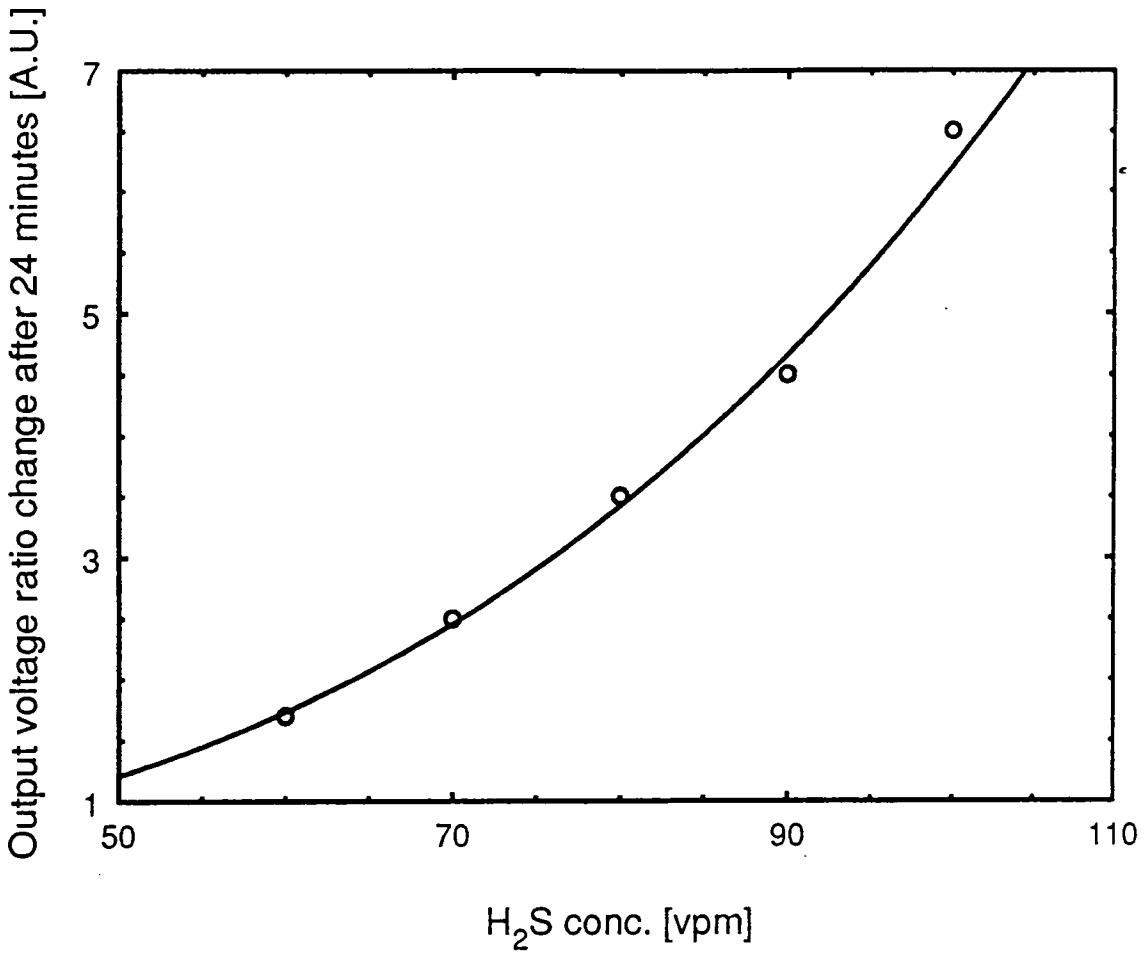

Figure 6.16: The effect of different concentrations of H_2S on 1 LB layer of a polyaniline SPR sensor.

As for previous measurements, SO_2, CO and CH_4 produced no measurable changes in the output of the SPR device.

The above experiments revealed that exposure of 1 LB layer of polyaniline to NO_x and H_2S produced an increase in reflectivity. These increases, may be attributed to increases in the film thickness and/or the refractive index of the film. Because of the high gas concentration used, the response curves show no delay time.

6.4.3 Insitu-Reflection Absorption Fourier Transform Infrared Spectroscopy

Infrared gas sensing studies on as-deposited polyaniline LB films were undertaken using NO_x and SO_2. Time did not allow for similar measurements using H_2S.

Figure 6.17 shows the difference spectra for 34 LB layers of polyaniline film after exposure to 150ppm NO_x for 1 hour (curve a) and 2 hours (curve b). These spectra were obtained using the same procedure, as has been described in previous chapters.

The difference spectra show an intense broad band centred at $3240cm^{-1}$. This was also observed in spun and evaporated polyaniline films for all gases. It was difficult to accurately determine its cause, hence it is referred to as a ghost band. Two possible causes are water vapour trapped in the film or leaks in the instrumentation.

Figure 6.17 also shows the quinoid band at $1594cm^{-1}$ decreases in intensity while the benzoid band at $1504cm^{-1}$, the CN stretch band at $1300cm^{-1}$ and the out-of-plane CH bending vibration bands at $750cm^{-1}$ increase. These latter vibrations are only expected to increase in intensity when the number of phenyl rings increases. Hence we may associate this increase with the conversion of some of the quinoid rings into semiquinone radicals which, as noted in section 4.2.2, possess a mixed benzoid/quinoid characteristic. When the exposure time increases, the number of semiquinoid radicals also increases, with a corresponding increase in conductivity.

When the gas was switched off, no further changes in the intensity of the $1504cm^{-1}$ band were observed in the difference spectra even after 2 hours. We relate this non-reversibility to that observed in dc conductivity measurements. Both observations are due to the formation of semiquinone radicals, formed from quinoid rings.

Figure 6.18 shows a difference spectrum when a 34 layer polyaniline LB film is exposed to SO_2. The vibration at $3240cm^{-1}$ is again evident, this time with a negative absorbance. We have already stated that, SO_2 gas has no effect on the

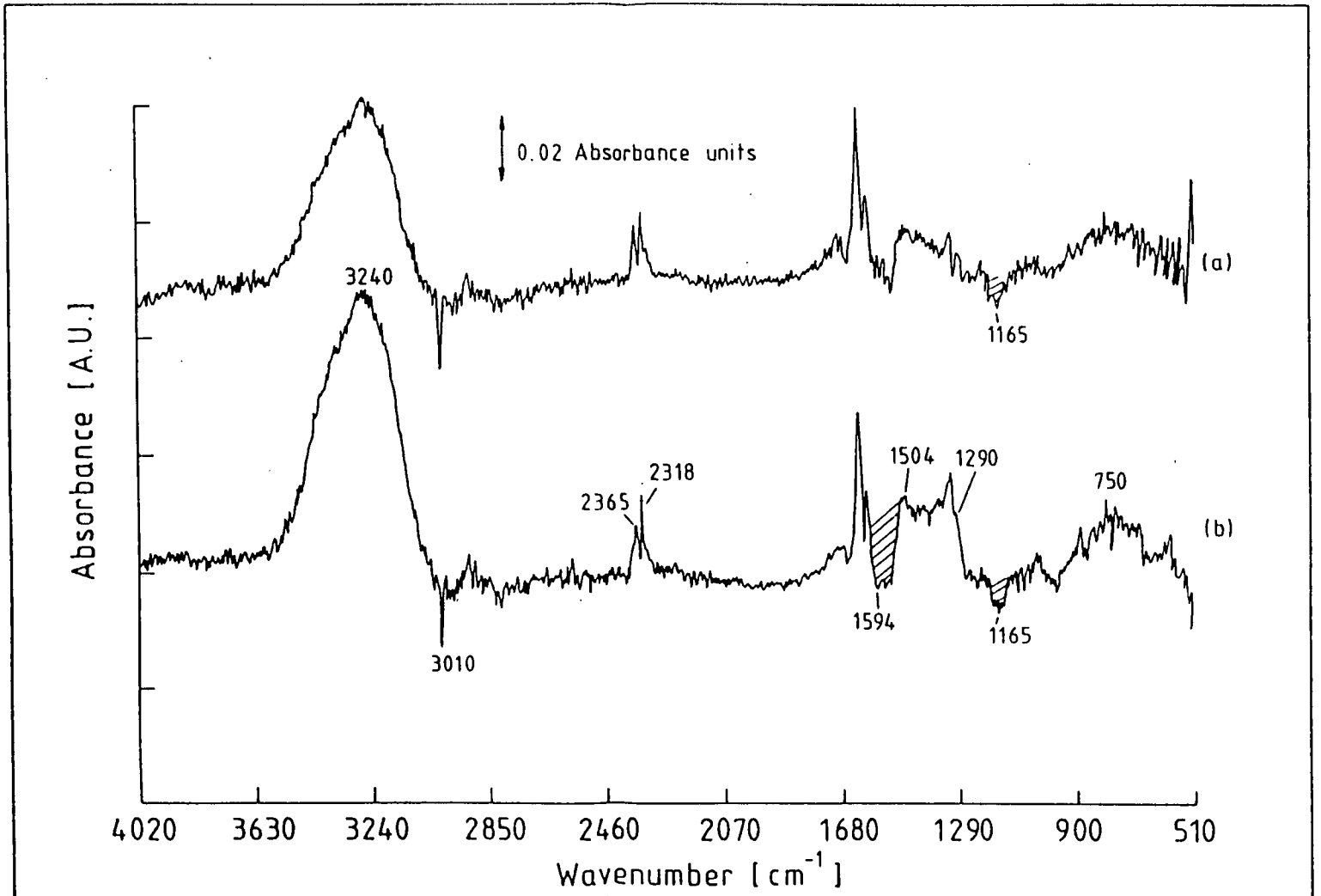

Figure 6.17: Difference spectrum of 34 LB layers of polyaniline before and after exposure to 150ppm of NO_x for 1 hour (curve a) and 2 hours (curve b).

film. This confirms that the band is a ghost band which can be either due water vapour from the instrumentation or leaks in the measurement chamber.

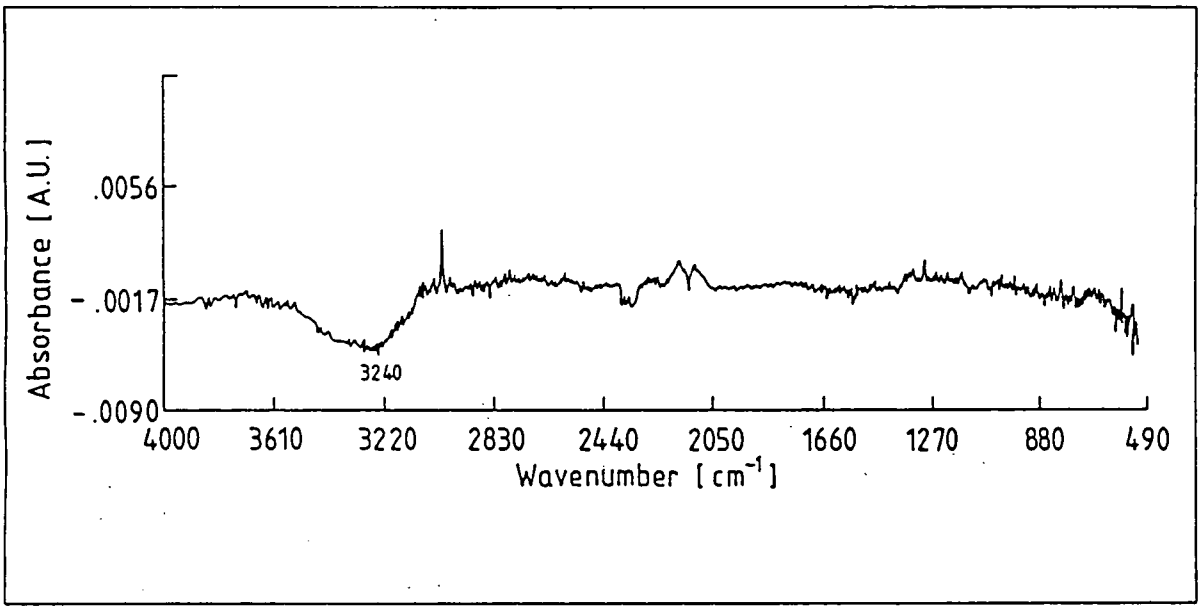

Figure 6.18: Difference spectrum of 34 LB layers of polyaniline before and after exposure to 150ppm of SO_2 for 2 hours.

6.5 SUMMARY

The reproducible deposition of polyaniline by the LB technique has been demonstrated. The ultraviolet/visible spectrum of the film is similar to that of the emeraldine base form of the polymer. Electrical measurements on as-deposited material reveal it to be slightly protonated, with an in-plane dc conductivity of $1\times10^{-8}Scm^{-1}$ at room temperature. However, after doping with

HCl, the in-plane dc conductivity increased to $0.1Scm^{-1}$, indicating a change in the oxidation state of the polymer, perhaps to the pernigraniline state. FTIR spectroscopy revealed vibrations associated with acetic acid as well as with polyaniline. Some modifications in the aromatic stretch region of the polymer suggested a degree of protonation. The effect of NO_x on the dc conductivity of 18 LB layers of a polyaniline chemiresistor has been shown to be non-reversible. Furthermore, this chemiresistor has been shown to be less sensitive compared with those based on evaporated or spun polyaniline films. Using FTIR spectroscopy, we associate this irreversibility with the formation of semiquinone radicals from quinoid rings. Surface plasmon resonance studies showed that the LB films were responsive to the gases H_2S and NO_x; however SO_2, CO or CH_4 produced no measurable effects.

REFERENCES

Ando, M., Watanabe, Y., Iyoda, T., Honda, K. and Shimidzu, T. : Thin Solid Films, **179** (1989) 225-231

Baughman, R.H., Wolf, J.F., Eckhardt, H. and Shacklette, L.W. : Synthetic Metals, **25** (1988) 121-137

Cao, Y., Li, S., Xue, Z. and Guo, D. : Synthetic Metals, **16** (1986) 305-315

Cheung, J.H., Punkka, E., Rikukawa, M., Rosner, R.B., Royappa, A.T. and Rubner, M.F. : Polymer Mater. Sci., Eng., **64** (1991) 263-264

Duke, C.B., Conwell, E.M. and Paton, A. : Chem. Phys. Letters, **131** (1986) 82-86

Furukawa, Y., Harat, T., Hyodo, Y., and Harada, I. : Synthetic Metals, **16** (1986) 189-198

Kim, Y.H., Foster, C., Chiang, J. and Heeger, A.J. : Synthetic Metals, **26** (1988) 49-59

Macdiarmid, A.G., Chiang, C.J., Richter, A.F. and Epstein, A.J. : Synthetic Metals, **18** (1987) 285-290

Monkman, A.P. and Adams, P. : Synthetic Metals, **40** (1990) 87-96

Monkman, A.P. and Adams, P. : Synthetic Metals, **41-43** (1991) 891-896

Pouchert, C.J. : 'The Aldrich Library of Infra-red Spectra' Edition **III** (1981) 281-282

Punka, E., Rubner, M.F., Hettinger, J.D., Brooks, J.S. and Hannahs, S.T. : Physical Review B, **43** (1991) 9076-9086

Tang, J., Jing, X., Wang, B. and Wang, F. : Synthetic Metals, **24** (1988) 231-238

CHAPTER SEVEN

LUTETIUM BISPHTHALOCYANINE THIN FILMS: RESULTS AND DISCUSSION

7.1 PREFACE

Thin films of lutetium bisphthalocyanine ($LuPc_2$) have been deposited, by the LB technique, onto glass and other substrates. The deposited films have been studied using optical and electrical techniques. The chapter is divided into four main sections. In section 7.2, film formation, which includes monolayer formation and LB deposition, are described. Section 7.3 discusses the optical and electrical properties of the LB films. This is followed in section 7.4 by a study of the gas effects on the LB layers.

There are many reports on the use of monophthalocyanine (Pc) films for gas sensing [Archer et al, 1989, Baker et al, 1985, Van Ewyk et al, 1980, Wohljen et al, 1989, Wright, 1987 and Zhu et al, 1990]. However, there is very little published work on bisphthalocyanine (Pc_2) derivatives [Souto et al, 1991]. The two groups of phthalocyanine molecules differ in many ways, for example: (a) in monophthalocyanines, changes in electronic properties are closely associated with the central metal ion, while in bisphthalocyanines it is due more to the macro-rings; (b) monophthalocyanines have a closed-shell structure in contrast to the bisphthalocyanines; and (c) bisphthalocyanines are reported to possess a much higher intrinsic conductivity and stability compared with monophthalocyanines [André et al, 1985]. Thus it would be instructive to investigate the bisphthalocyanines for gas sensing.

7.2 THIN FILM DEPOSITION

7.2.1 Monolayer Studies and LB Film Deposition

A solution of $LuPc_2$ was formed by dissolving 0.38mg in 10ml of chloroform. The solution was green in reflection and free from particulate matter, indicating complete solubility.

Figure 7.1 shows the surface pressure versus area for condensed floating layers of $LuPc_2$ on water subphase. The isotherms were recorded at a compression rate of $0.1nm^2molecule^{-1}s^{-1}$, a temperature of 20±2°C and a subphase pH of 5.6±0.1. The material formed a condensed isotherm and was capable of withstanding surface compression pressures up to $40mNm^{-1}$. There was also very little difference between the first and subsequent compressions (see figure 7.1). From the condensed isotherm plot, the area per molecule calculated was $0.78±0.04nm^2$ at a surface pressure of $30mNm^{-1}$. This value is comparable, within experimental error, to the figure of $0.74nm^2$ reported for the same material [Liu et al, 1989] but is slightly smaller than $0.85nm^2$ obtained for ytterbium bisphthalocyanines [Petty et al, 1989]. This limiting area per molecule is smaller than $1.7nm^2$ expected for a face-to-face orientation model of the molecule [Souto et al, 1991]. Hence, we suggest that the molecules are lying at an angle to the water surface and do not form a true monolayer on the water surface.

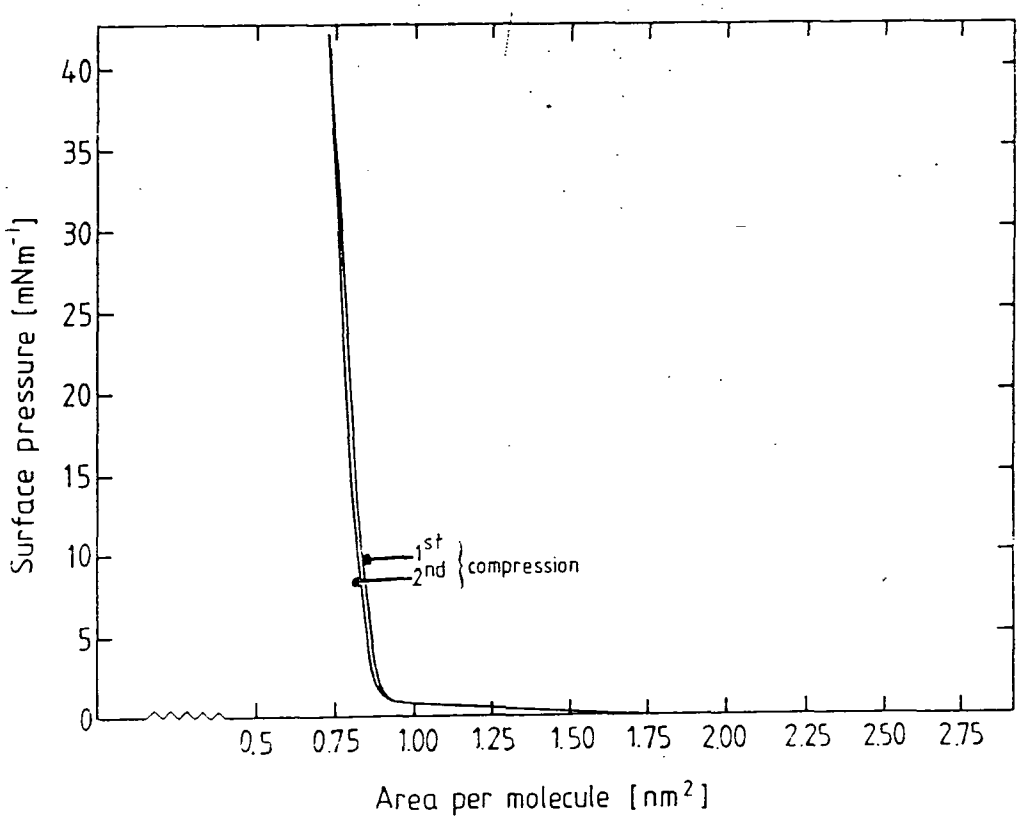

Figure 7.1: Surface pressure versus area isotherm for floating layer of $LuPc_2$ on water surface at a temperature of 20±2°C.

A suction test, carried out on the condensed film by removal of small amount of material, showed a rapid response. The expanded monolayer was compressed to a pressure of 30mNm^{-1} for deposition. Freshly prepared samples deposited Z-type on glass as observed by several authors [Liu et al, 1989 and Souto et al, 1991]. However, condensed monolayers made from older solutions formed Y-type films. This type of behaviour is shown in figure 7.2, starting with the substrate in air and has been reported for other bisphthalocyanines only when mixed with fatty acids [Petty et al, 1989]. The change from Z- to Y-type deposition, is possibly due to ageing of the sample solution. The films deposited with a transfer ratio of 0.9±0.1 for the upstrokes and 0.6±0.1 for down-strokes. A higher deposition ratio on up-stroke has also been observed [Liu et al, 1989]. This may be due to water in the subphase increasing the degree of ring-ring interactions through hydrogen bonding. The older solution was used for device fabrication.

The deposited films appeared green and uniform indicating the material was in a one-electron oxidised state [Cian et al, 1985]. Prolonged exposure to air produced no change in the colour of the film.

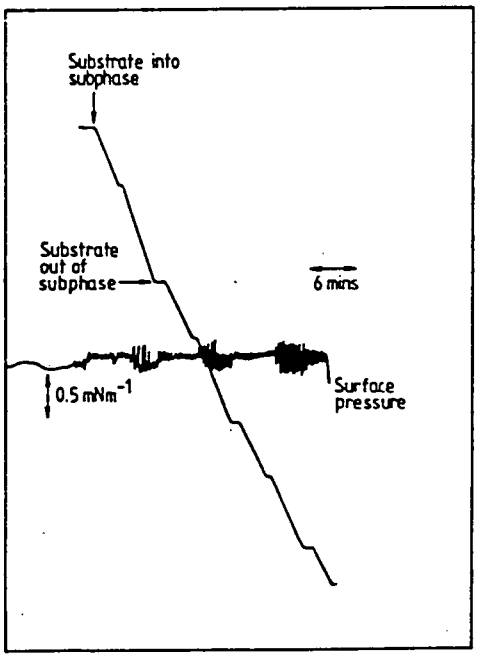

Figure 7.2: Y-type deposition record for $LuPc_2$ on glass.

7.3 THIN FILM CHARACTERIZATION

7.3.1 Ultraviolet/Visible Spectroscopy

Figure 7.3 shows the electronic absorption spectrum of 12 layers of $LuPc_2$ deposited (Y-type) on glass by the LB method. Similar electronic absorption bands with similar bandwidths have been recorded for other Pc_2 derivatives [Souto et al, 1991]. The spectrum consists of a sharp narrow red band at 665nm that is attributed to π-π^* transition within the phthalocyanine macrocycles [Souto et al, 1991]. Because the bandwidth of this transition is usually small compared with its height, it is referred to as a Q-band. On the high energy side of the Q-band is a weak band around 600nm. This is ascribed to an n-π^* transition and results from the lone pairs of electrons on the bridged N heteroatoms [Souto et al, 1991]. These two transitions indicate that the ground and excited states of the material have the same equilibrium geometry, hence giving the molecule great stability [Aroca et al, 1989]. This equilibrium geometry consists of a Lu^{3+} ion sandwiched between two cofacial phthalocyanine rings, with one ring being in the singularly reduced state and the other is doubly reduced (see figure 2.1). Also visible in figure 7.3 is a weak band at 480nm that increases with film thickness [Petty et al, 1989]. We may attribute it to transitions within each phthalocyanine ring. A Soret band occurs at 345nm. This is due to l-π^* transition and changes with the stereochemistry of the molecule.

Reproducibility in the deposition process was assessed by recording the variation of the intensity of the Q-band with the number of deposited layers. The result, shown in figure 7.4, shows that the LB film transfer was reasonably reproducible.

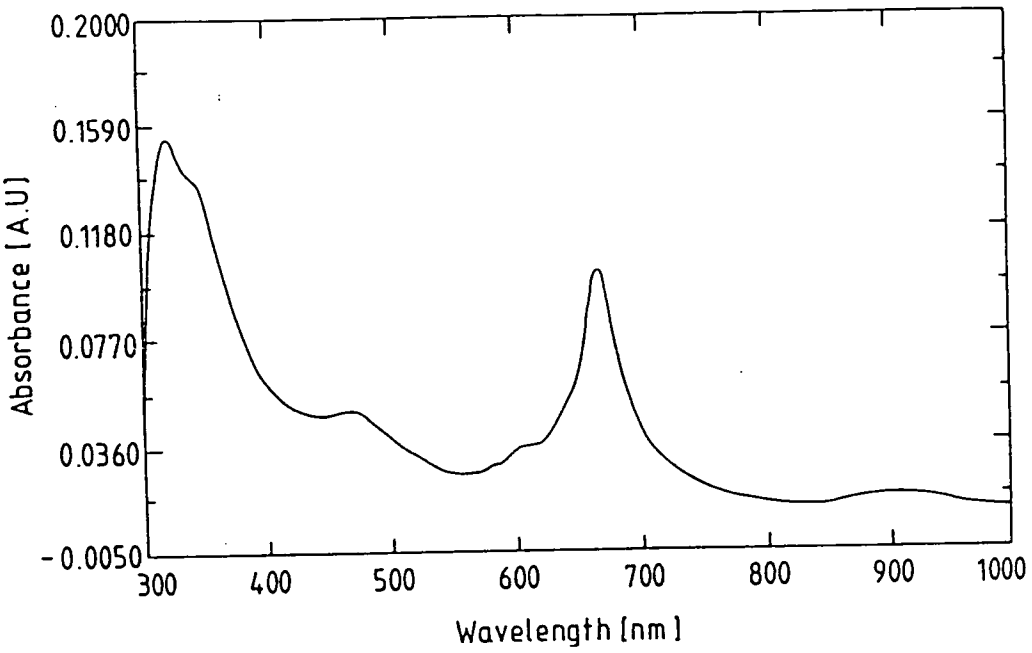

Figure 7.3: The ultraviolet/visible spectrum of 12 LB layers of $LuPc_2$ on a glass substrate.

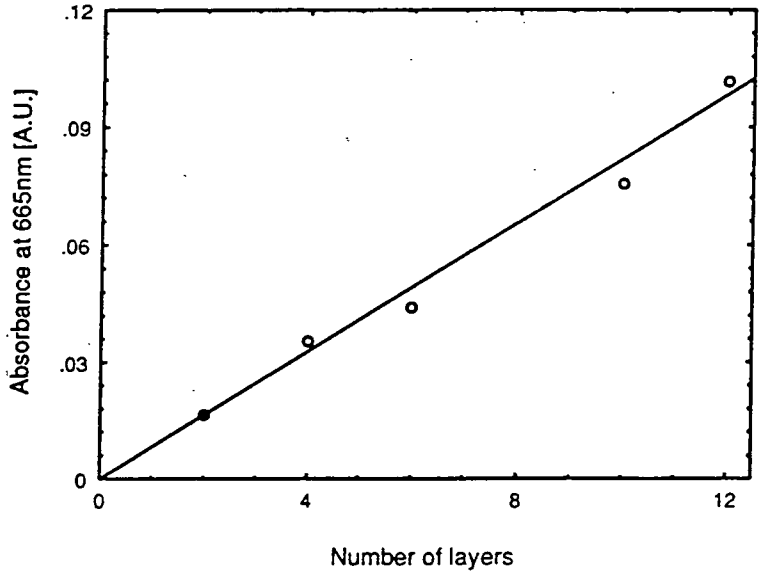

Figure 7.4: Absorbance at 665nm versus number of layers of $LuPc_2$ LB films deposited on one side of two glass slides dipped back-to-back.

7.3.2 Reflection-Absorption Fourier Transform Infrared Spectrum

Figure 7.5 shows the RAIRS spectrum of 20 LB layers of $LuPc_2$ on gold. The results obtained are comparable to published data for $LuPc_2$ LB films [Aroca et al, 1989]. A summary of the assignment of the various vibrations is shown in table 7.1. This is based on a comparison with published data on mono- and bis-phthalocyanine derivatives [Clavijo et al, 1989 and Jennings et al, 1985].

The spectrum can be seen to be dominated by a large peak at $2924cm^{-1}$ with a shoulder at $2855cm^{-1}$. Classically, these two vibrations have been assigned to asymmetric and symmetric CH_2 stretches [Traore et al, 1991]. However, $LuPc_2$ has no CH_2 groups (CH stretch vibrations in $LuPc_2$ occur at $3044cm^{-1}$ and $3079cm^{-1}$). Furthermore, these bands have not been observed in any spectrum of $LuPc_2$ or in another bisphthalocyanine derivative. Hence we attribute the vibrations to impurities. These are likely to originate from the synthetic process, possibly lutetium acetate and indicate that our material is very impure.

On the basis of resonance Raman studies, the vibration at $1601cm^{-1}$ has been assigned to benzene ring stretch [Souto et al, 1991]. Vibrations of the isoindole moieties are observed at $1464cm^{-1}$ and $1389cm^{-1}$. These are comparable to similar vibrations of some monophthalocyanines (such as PbPc) as the metal ion is out of the plane of the molecule [Jennings et al, 1985]. The vibration at $1366cm^{-1}$ may be due to pyrrole ring stretch, especially as this vibration is reportedly close to that of the isoindole stretch [Souto et al, 1991]. C-H bending deformation bands appear at $1231cm^{-1}$ and $1072cm^{-1}$, and wagging deformations at $756cm^{-1}$ and $700cm^{-1}$.

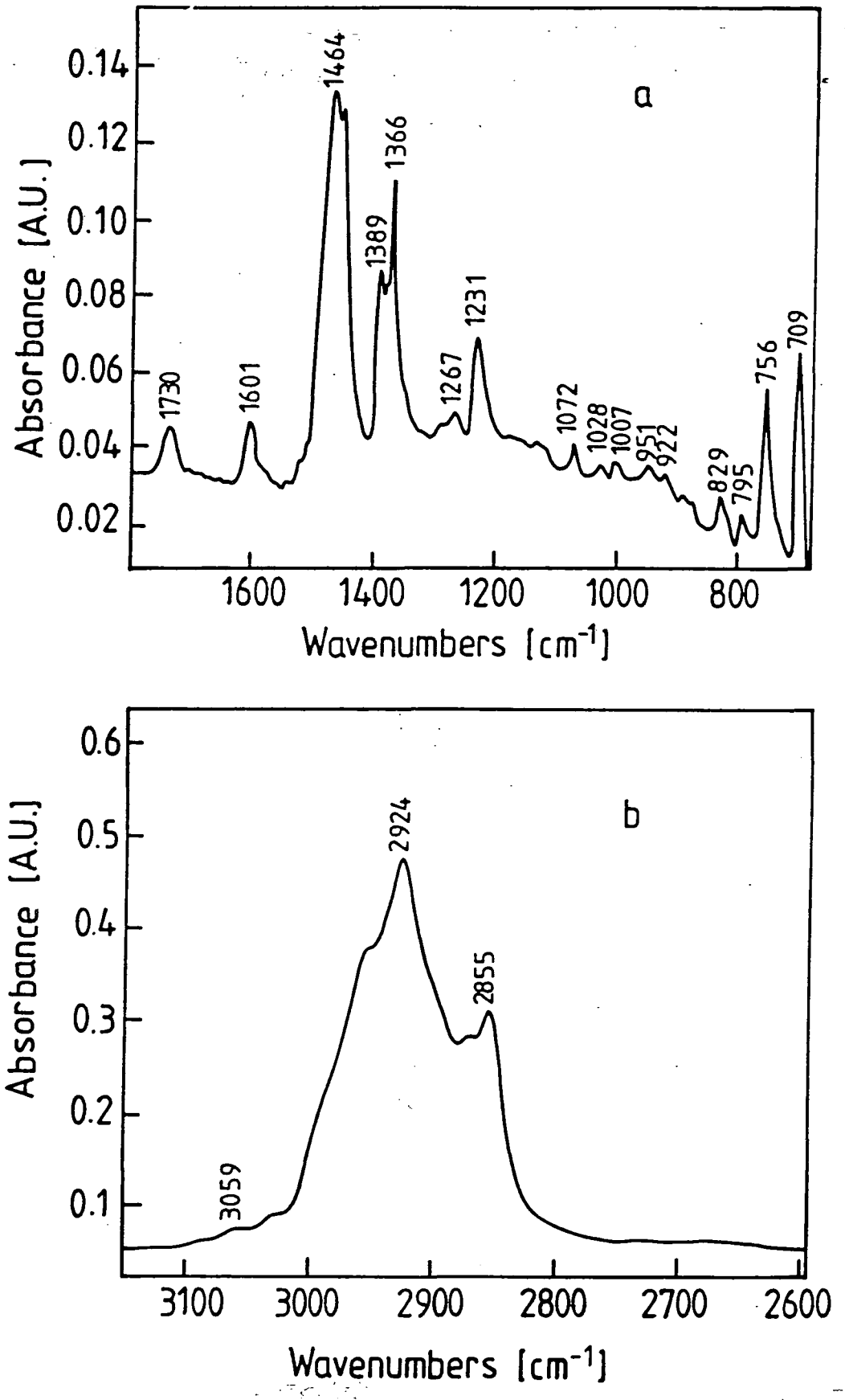

Figure 7.5: Reflection-absorption Fourier transform infrared spectrum of $LuPc_2$ on a gold substrate for 2000-600cm^{-1} (curve a) and 4000-2600cm^{-1} (curve b).

Band Position [cm^{-1}]	Assignment	References
2924	asymmetric CH_2 stretch	Traore et al, 1991
2854	symmetric CH_2 stretch	Traore et al, 1991
1730	carbonyl strech	
1601	benzene ring stretch	Souto et al, 1991
1454	isoindole stretch	Aroca et al, 1989
1384	isoindole stretch	Aroca et al, 1989
1365	pyrrole ring stretch	Souto et al, 1991
1263-461	CH bending	Aroca et al, 1989

Table 7.1: A summary of the assignments of infrared vibrations for 20 LB layers of $LuPc_2$ on gold.

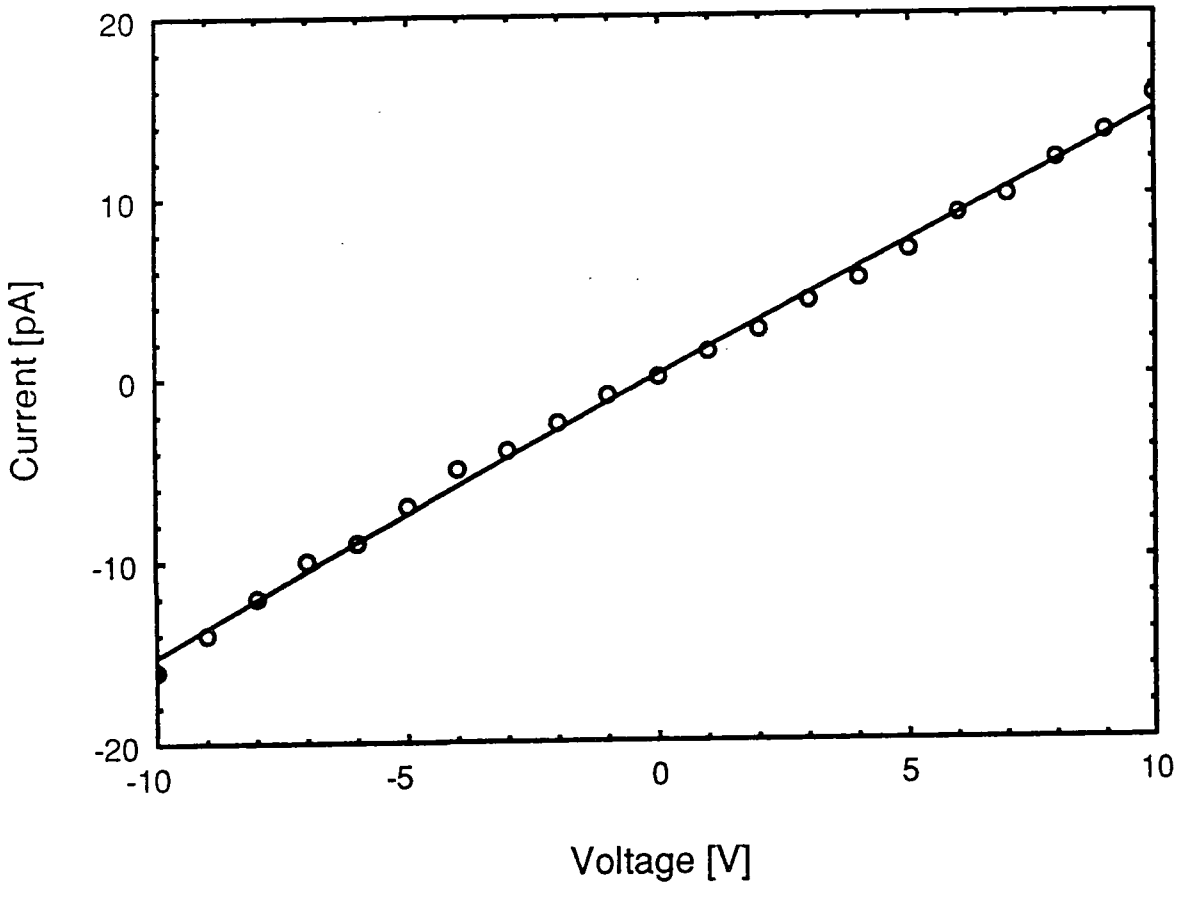

Figure 7.6: Current versus voltage characteristics of 7 LB layers of $LuPc_2$ on an interdigitated electrode structure. Measurements at room temperature and in 10^{-3}mbar vacuum.

7.3.3 Current versus Voltage Characteristics

Figure 7.6 shows the current versus voltage characteristics for 7 LB layers of $LuPc_2$ on an interdigitated electrode structure in vacuum. A linear increase in current is observed with increasing voltage and the resistance, calculated from the slope, varied with the number of layers deposited. Thus it was concluded that ohmic contacts had been established between the material and the gold electrodes. The average thickness per layer was measured by ellipsometry to be 9.0±0.1nm. This large value indicates that the material is more than one monolayer thick. The room temperature dc conductivity of the material was 2.3 $\times 10^{-6} Scm^{-1}$ in vacuum. This is comparable to that reported in the literature for the same material (deposited by sublimation) in vacuum ($2\times 10^{-6} Scm^{-1}$) [Andre et al, 1985].

7.3.4 Surface Plasmon Resonance

Figure 7.7 shows SPR curves for 1 and 3 LB layers of $LuPc_2$ deposited on a Ni/Ag substrate. One overlayer produced a shift of the resonance angle by 0.3^{o}, a small decrease in the resonance depth but no change in the curve width. This shift in the resonance angle is likely to be due to the finite thickness of the overlayer. One layer of CuPc deposited on a similar substrate produced larger changes in the resonance depth and resonance curve width (see figure 3.8) [Zhu et al, 1990]. This is because $LuPc_2$ absorbs at a significantly different wavelength (665nm) from the incident laser at 633nm.

As the film thickness increases to 3 layers, the resonance position shifts to even higher angles. This change is certainly caused by the increased overlayer thickness. Increase in overlayer thickness also increases the surface roughness [Raether, 1982] and beam scatterring [Pockrand et al, 1978], possibly contributing to the observed decrease in the resonance depth noted in figure 7.7.

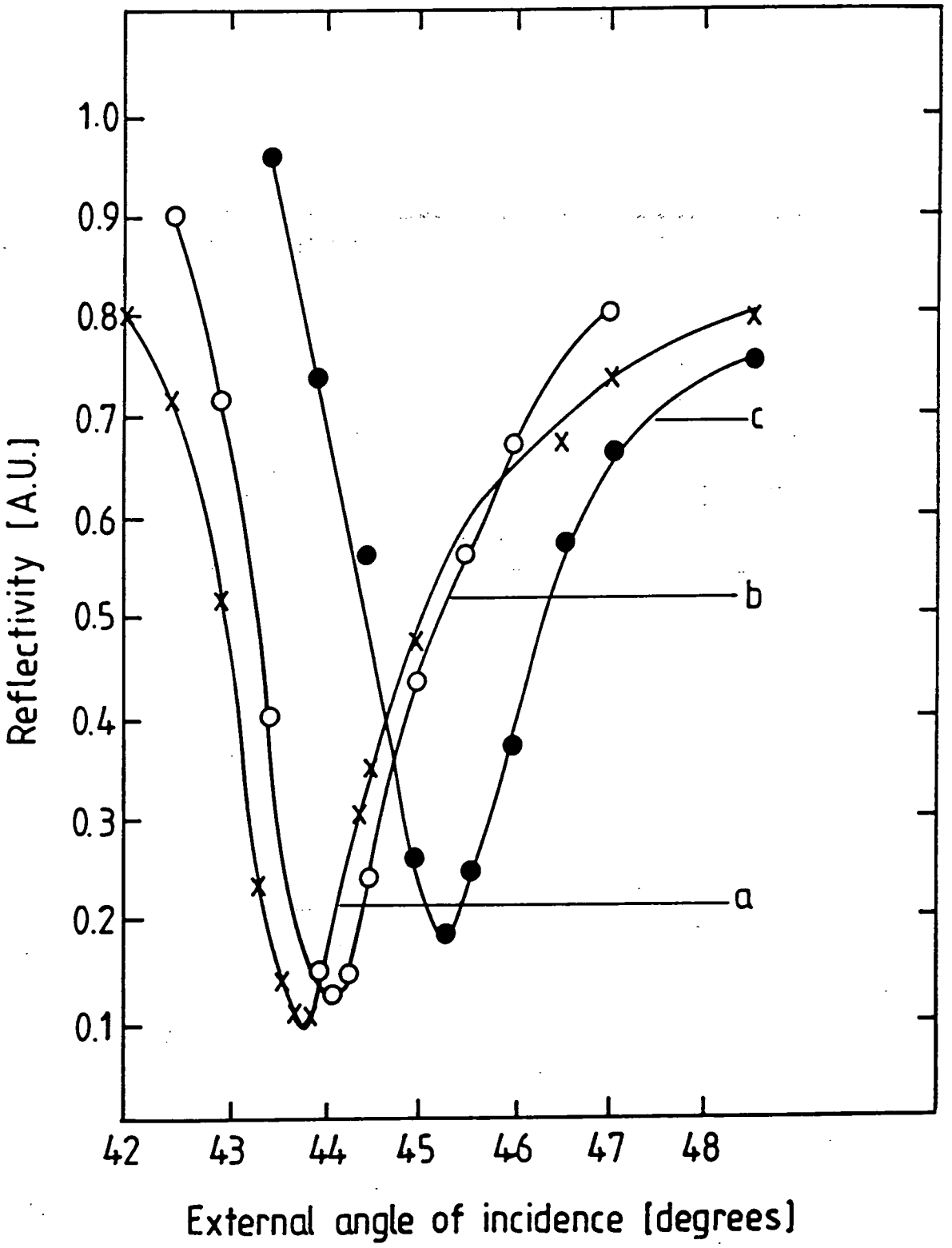

Figure 7.7: SPR curve for Ni/Ag (curve a); Ni/Ag covered with 1 LB layer $LuPc_2$ (curve b); Ni/Ag covered with 3 LB layers of $LuPc_2$ (curve c)

7.4 GAS SENSING

7.4.1 Insitu-Conductivity Gas Response

Gas sensing studies were carried out using 7 and 11 LB layers of $LuPc_2$.

N_2 produced a decrease in the conductivity of the LB films (lasting about 45 minutes), probably due to the elimination of trapped water vapour in material. A similar change was observed for spin-coated polyaniline (see figure 4.10) and will therefore not be further elaborated upon.

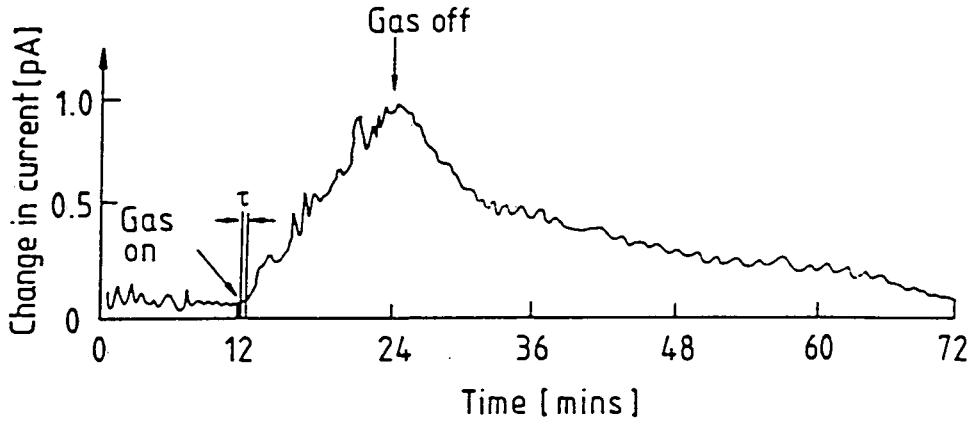

Figure 7.8a: The effect of 9ppm NO_x on 7 LB layers of a $LuPc_2$ chemiresistor (3V supply).

Figure 7.8a shows the effect of 9ppm NO_x on the dc conductivity of a 7 LB layer chemiresistor. The gas produced an increase in conductivity after a delay time of about 20 seconds. This increase continued for the duration of the experiment (6 minutes). When the gas turned off, the increase in conductivity reversed to within 10% of the original value. However, as shown in figure 7.8b, when the device was exposed to 90ppm NO_x, the conductivity was only partially reversible. The lack of complete reversibility could be due to some deeply diffused and/or covalently bonded gas molecules on the material. Figure 7.9 shows a study of the effect of different concentrations of NO_x on the $LuPc_2$ chemiresistor. The result shows a non-linear increase in conductivity with gas concentration, with a minimum detection level of 2ppm.

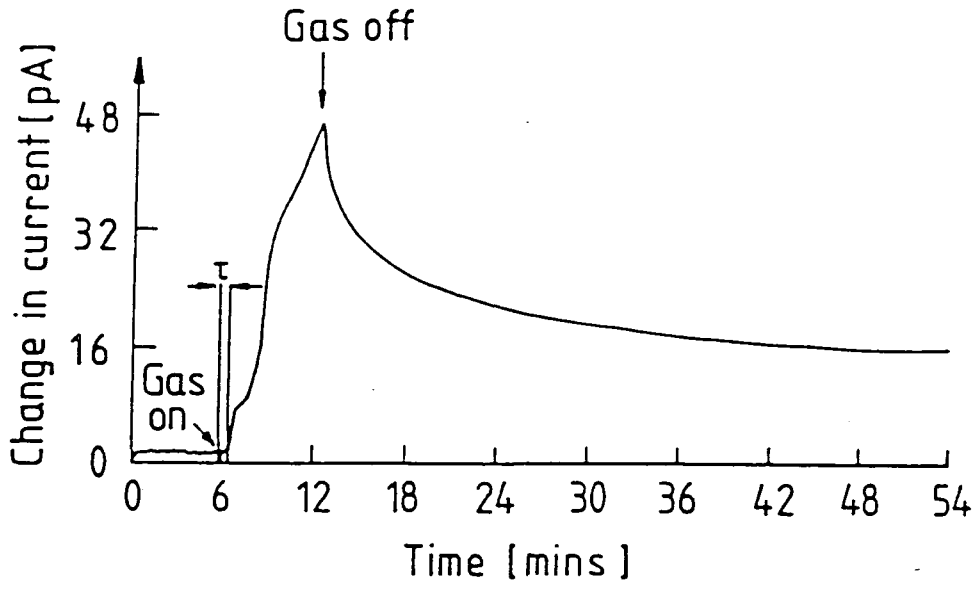

Figure 7.8b: The effect of 90ppm NO_x on 7 LB layers of a $LuPc_2$ chemiresistor (3V supply).

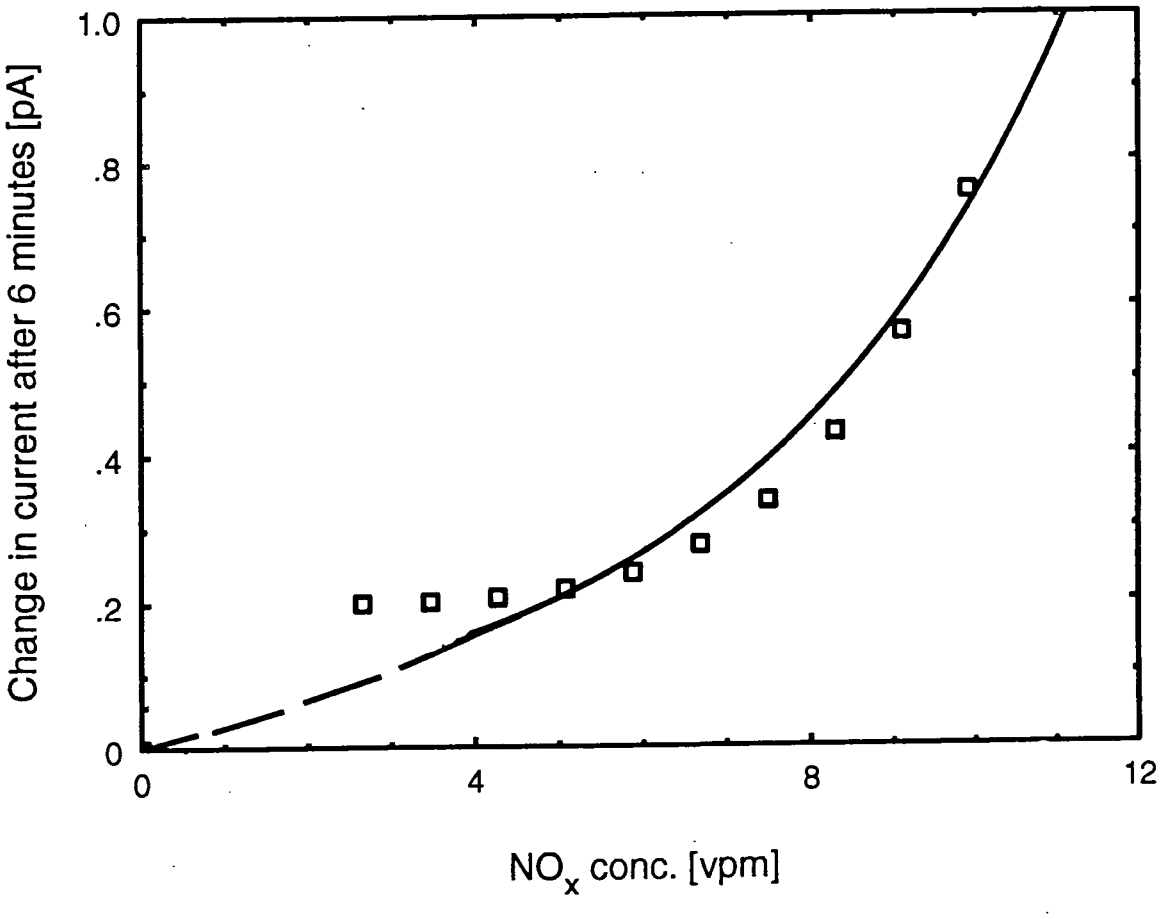

Figure 7.9: The effect of different concentrations of NO_x on a 7 LB layer $LuPc_2$ chemiresistor

Exposure of a 7 LB layer $LuPc_2$ chemiresistor to 40ppm H_2S, produced no change in device conductivity. However, when the number of layers was increased to 11, a decrease in film conductivity on exposure to H_2S was observed. The change occurred after a delay time of about 30 seconds and was irreversible at room temperature (see Figure 7.10).

At high concentrations (> 60ppm), H_2S produced an increase in conductivity (see figure 7.11). The increase occurred instantaneously, and recovered partially when the gas was turned off. However, when left under nitrogen overnight, the device completely recovered its original conductivity.

Figure 7.12 shows the effect of different concentrations of H_2S on 11 LB layers of a $LuPc_2$ chemiresistor. The minimum detection level can be seen to be about 10ppm.

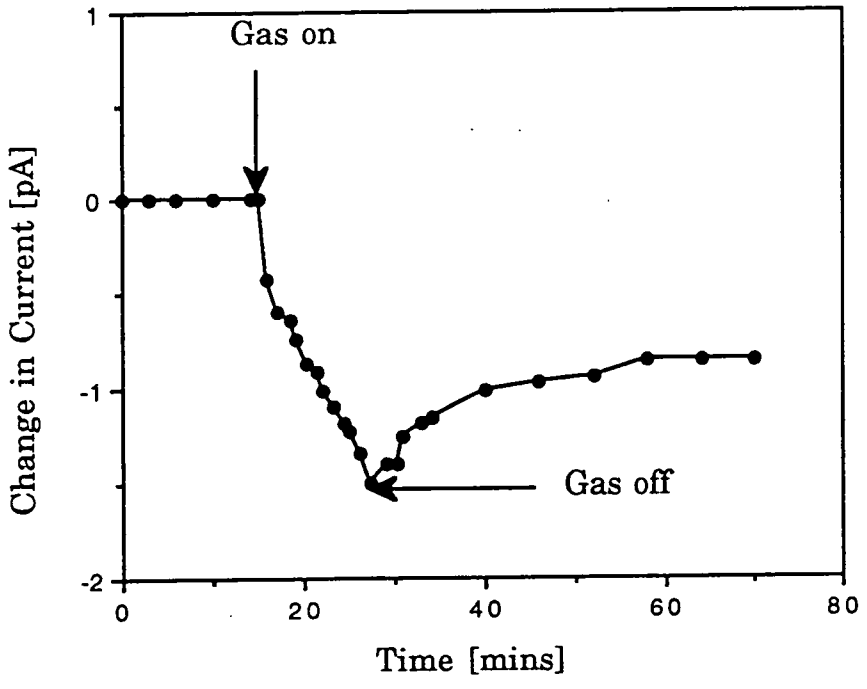

Figure 7.10: The effect of 40ppm H_2S on an 11 LB layer $LuPc_2$ chemiresistor at room temperature.

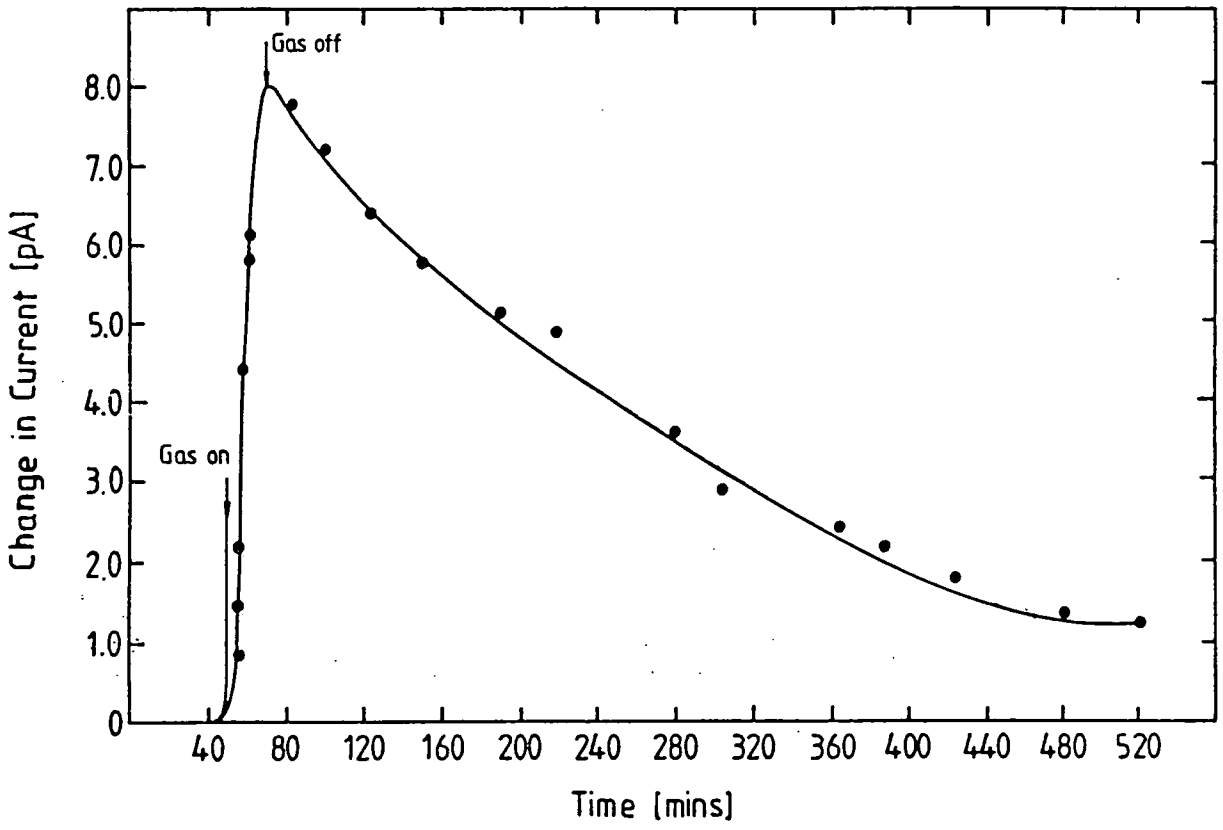

Figure 7.11: The effect of 80ppm H_2S on an 11 LB layer $LuPc_2$ chemiresistor.

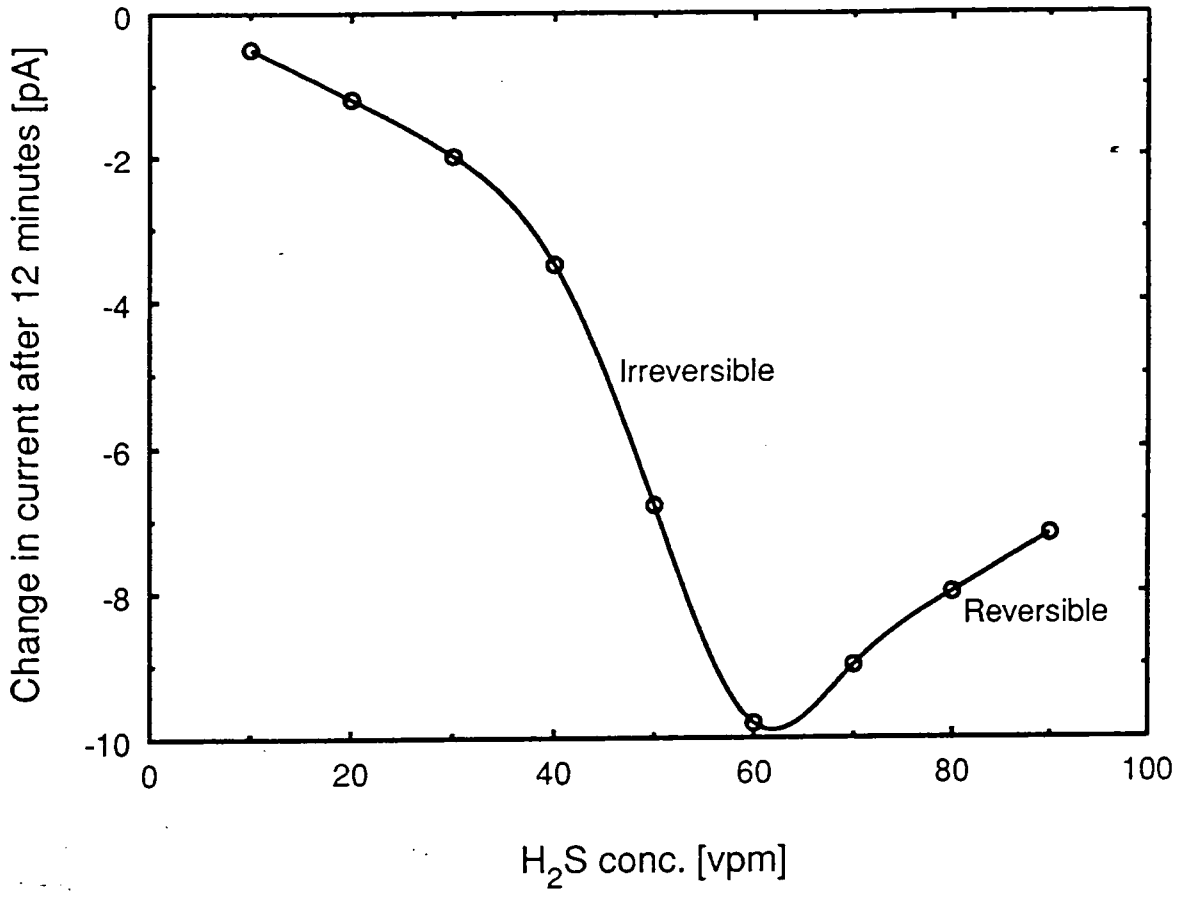

Figure 7.12: The effect of different concentrations of H_2S on 11 LB layers of $LuPc_2$ chemiresistor.

Before attempting to explain the observed increase and decrease in conductivity due to H_2S, it is worth noting (from the literature) that in the presence of water (from the subphase or in the atmosphere) and molecular oxygen (from air), parts of $LuPc_2$ are hydrogenated and then oxidized to $LuHPc_2^+O_2^-$ species [Nicholson et al, 1986]. In the LB film, both conditions are available and a number of $LuHPc_2^+O_2^-$ species will be formed depending on the quantity of material present. The very small number formed could possibly be the reason why H_2S had no effect on 7 LB layers of $LuPc_2$ chemiresistor.

The observed decrease in conductivity produced by H_2S at low concentrations, indicates that it donates an electron to the organic material. This electron possibly forms a pair (of opposite spin) with the mobile electron initially located in one or both rings of the molecule, thereby producing a diamagnetic or bipolaron structure of lower charge mobility [Chang et al, 1981 and Collins et

al, 1982]. For simplicity, we suggest that, at low concentrations of H_2S, the gas chemically reduces the hydrogenated/oxidized portions of the film in a compensating manner, so restoring its intrinsic conductivity.

In contrast, the observed increase in conductivity at high concentrations, is possibly due to gas-induced hydrogenation (see figure 7.13) which results in an increase in conductivity through the overlap of neighbouring π-electrons as illustrated in figure 7.13. Similar effects have been observed for bis(phthalocyanine)neodynium compressed disks under the same conditions [Yamana et al, 1982] and on the electrochemical 'doping' of $LuPc_2$ [Maitrot et al, 1987]. Infrared studies (section 7.3.2) showed that this material was very impure. Hence, it is not unreasonable to suggest these impurities may also be contributing to the observed response of the material to H_2S.

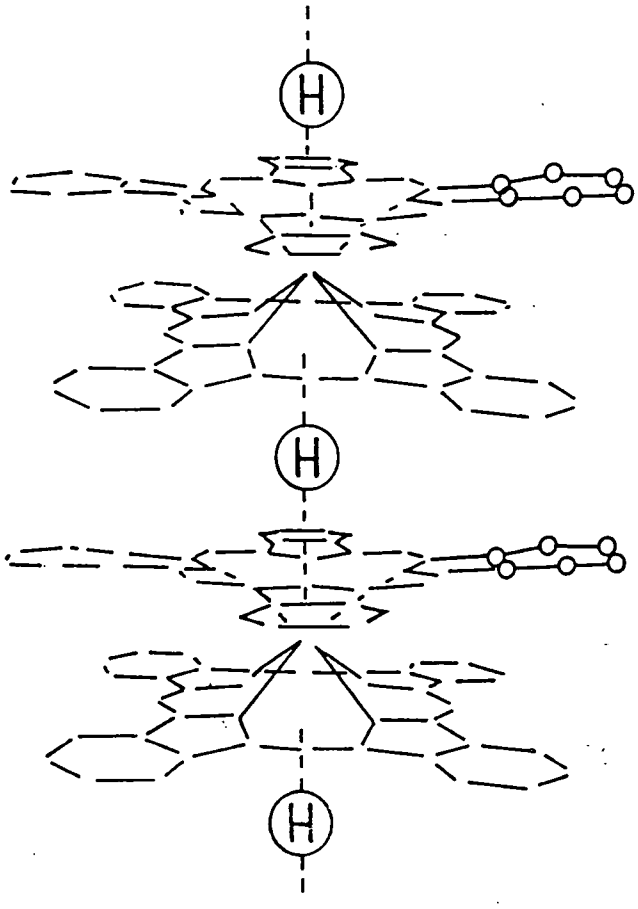

Figure 7.13: An illustration of the formation of hydrogen bonding between neighbouring phthalocyanine rings in $LuPc_2$ [Yamana et al, 1982].

Figure 7.14 shows the effect of 90ppm SO_2 on an 11 LB layer $LuPc_2$ chemiresistor at room temperature. This result shows that the gas produced an increase in conductivity after a delay time of about 60 seconds. However, this increase is significantly smaller than that for the same concentration of NO_x. This effect is probably due to the more electrophilic character of the latter. The increase in conductivity follows a two step process in which there is an initial rapid increase in current followed by a slower one. However, when the gas is turned off, the device recovers only slightly. This non-reversibility could result from chemically or deeply diffused gas molecules. The response of the $LuPc_2$ chemiresistor to different concentrations of SO_2 is shown in figure 7.15. Here we can see that the conductivity changes linearly with gas concentration, with a minimum detection level of about 10ppm. These results are contrary to those reported by Trometer et al, 1992. This author observed no response when evaporated $LuPc_2$ thin films were exposed to SO_2. The difference possibly results from the high impurity level in our material, as evidenced by the infrared spectrum (see figure 7.5).

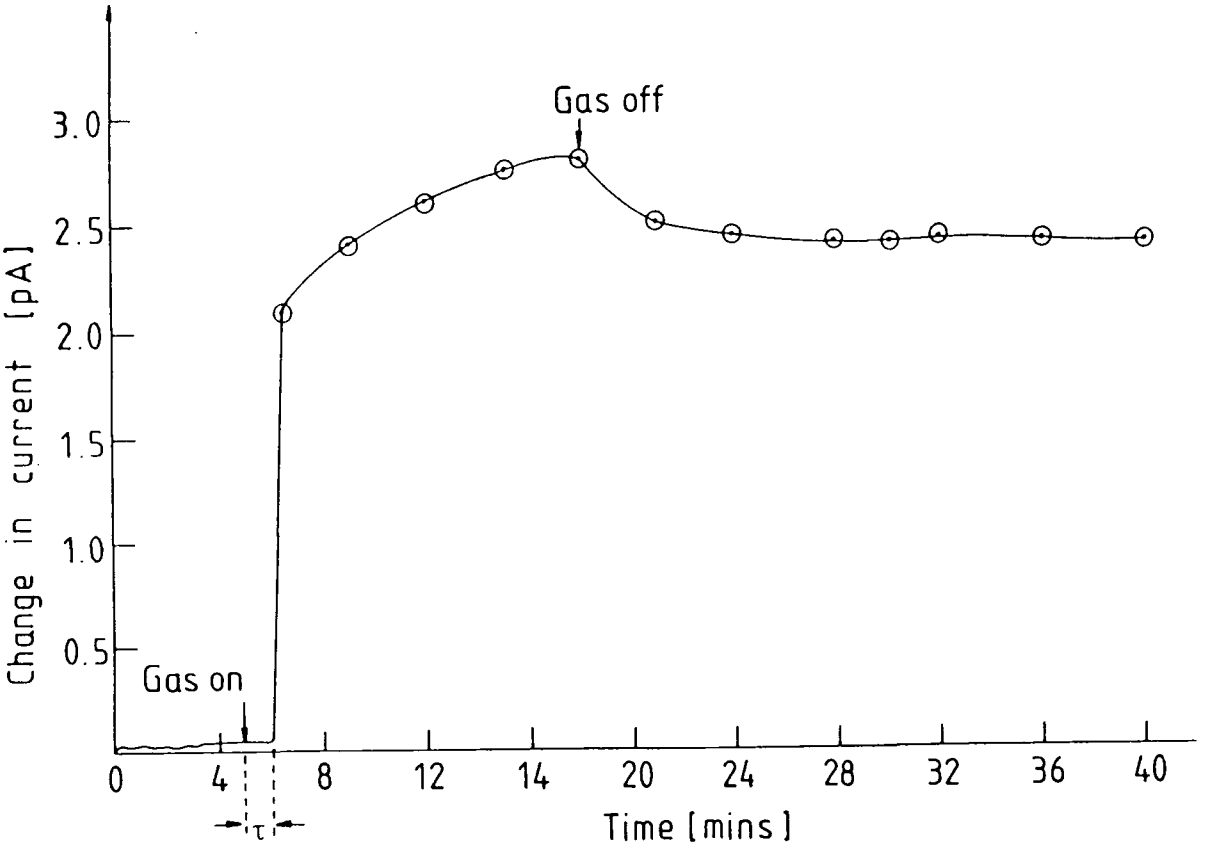

Figure 7.14: The effect of 90ppm SO_2 on an 11 LB layer $LuPc_2$ chemiresistor.

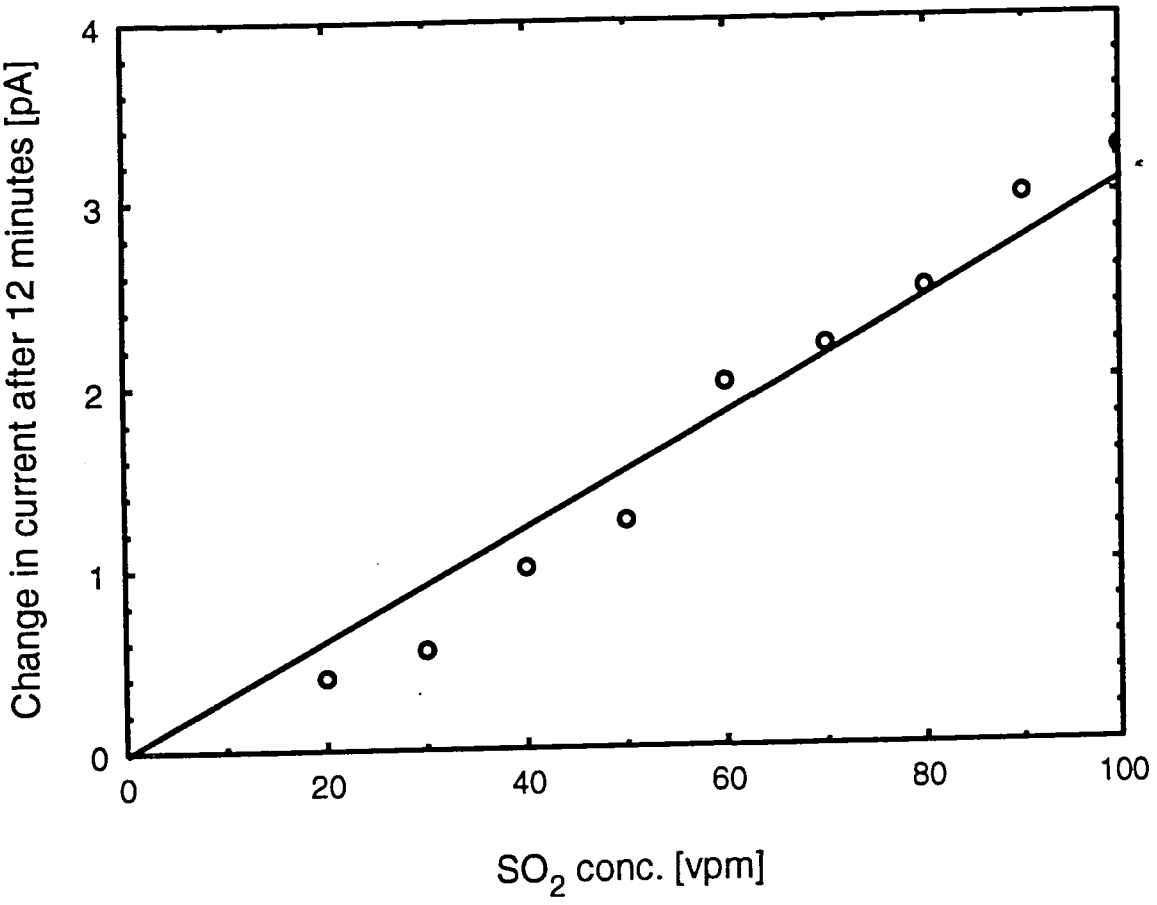

Figure 7.15: The effect of different concentrations of SO_2 on an 11 LB layer $LuPc_2$ chemiresistor at room temperature.

Gas sensing measurements using CO and CH_4 were unsuccessful. No conductivity changes were noted for gas concentrations up to 50,000ppm. A summary of the effect of the various gases on thin films of $LuPc_2$ is given in table 7.2.

7.4.2 SPR Sensor

An optical sensor based on SPR was fabricated using 1 LB layer of $LuPc_2$ deposited on a Ni/Ag substrate. The gas/material interaction was initially monitored by measuring the entire reflectivity curve for the uncoated substrate followed by that of the substrate covered with 1 layer of $LuPc_2$. Finally the curve was re-measured after exposure to the gas. Figure 7.16 shows these results for 1 LB layer of $LuPc_2$ exposed to 500ppm of NO_x. As can be seen, the

Gas	Conc. in N_2 [ppm]	Delay Time τ_D [s]	Exposure Time [mins]	Recovery Time τ_R [mins]	Minimum Detection Level [ppm]	Normalised Change per ppm $\frac{\Delta R}{R} + \text{gasconc in ppm}$
NO_x	2	20	12	48 (partially reversible)	2	-0.05 (at 10ppm)
H_2S	40	30	12	partially reversible	10	0.033 (50ppm)
SO_2	10	30	12	partially reversible	10	-0.03 (at 90ppm)
CO	10000	No observed effect	50	N/A	N/A	N/A
CH_4	50000	No observed effect	50	N/A	N/A	N/A

Table 7.2: Summary of the effect of different gases on 11LB layers of a lutetium bisphthalocyanine chemiresistor at room temperature.

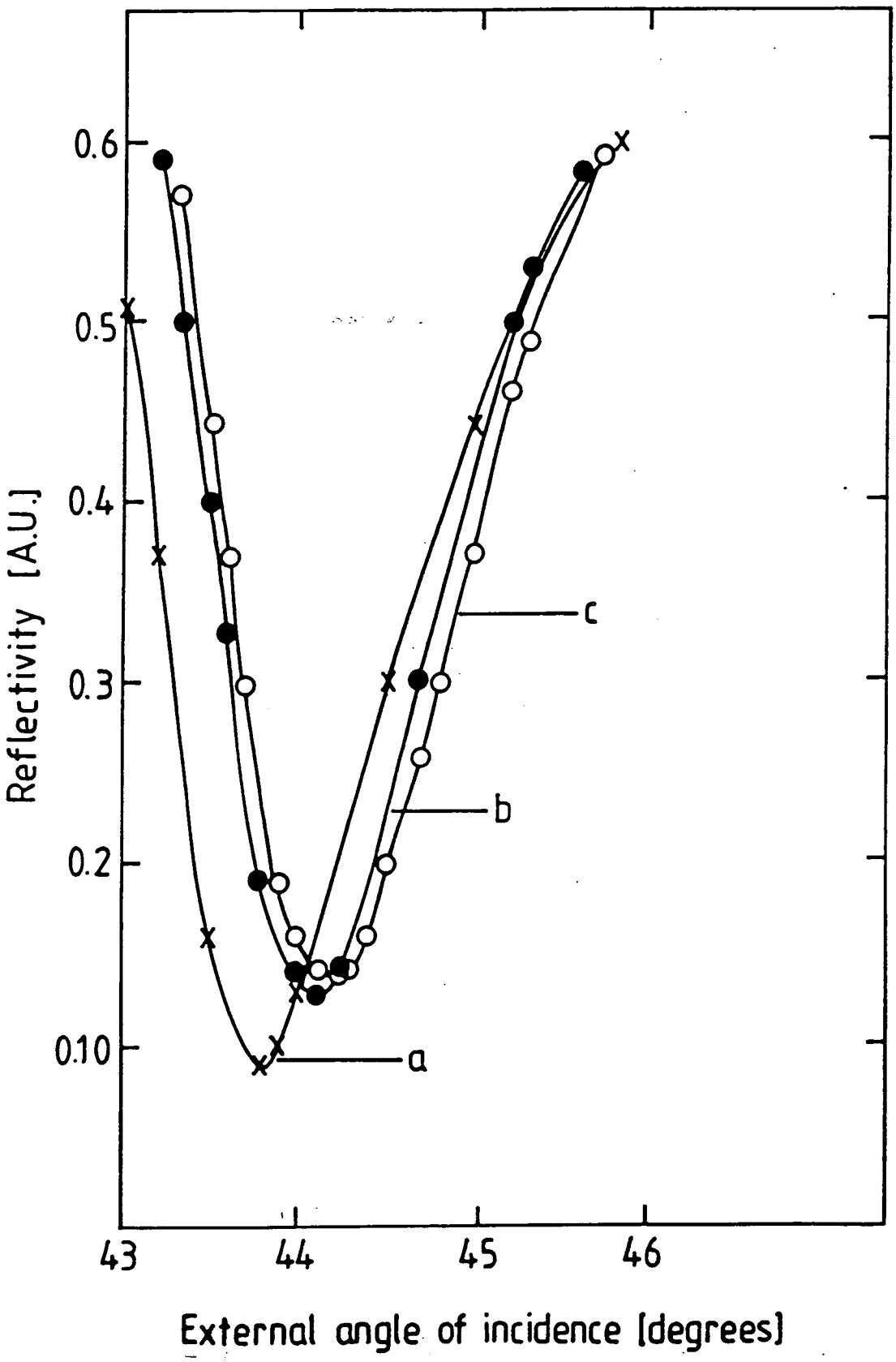

Figure 7.16: SPR curve for Ni/Ag (curve a); Ni/Ag covered with 1 LB layer of $LuPc_2$ (curve b); after exposure to 500ppm NO_x (curve c).

gas produced an increase in the resonance angle of 0.2°. This increase is due to an increase in the thickness and/or refractive index of the film. Such gas-induced increase in overlayer thickness can also affect the surface roughness (see section 3.3.2b), hence increasing the broadness of the SPR curve. However, in this case, increase in broadness is too small to be accurately measured. When the gas was turned off, these changes did not reverse, even after 4 hours.

The incident laser beam was next fixed at an external angle of 43.5° and changes in the reflectivity recorded. Figure 7.17 shows the time response of the change in reflectivity to 300ppm NO_x. We can see that, the device response is quiet fast, making it difficult to measure the delay time accurately. However, it was estimated to be less than 5 seconds. The output voltage ratio (i.e. reflectivity) increased for up to 12 minutes and then saturated. It can also be seen that the change is only partially reversible at room temperature. The device response to different concentrations of NO_x is shown in figure 7.18. This is almost linear with a minimum detection level of 50ppm.

Gas sensing measurements using H_2S and SO_2 below 100ppm were unsuccessful, as were as those using CO and CH_4 at concentrations of 10,000 and 50,000ppm respectively.

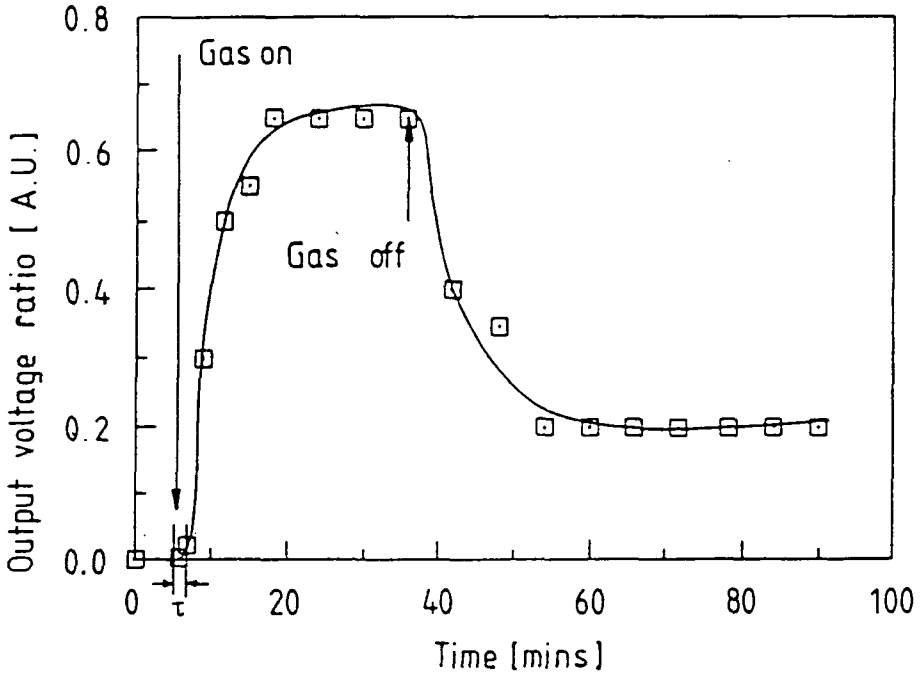

Figure 7.17: The effect of 300ppm NO_x on SPR sensor (1 LB layer film).

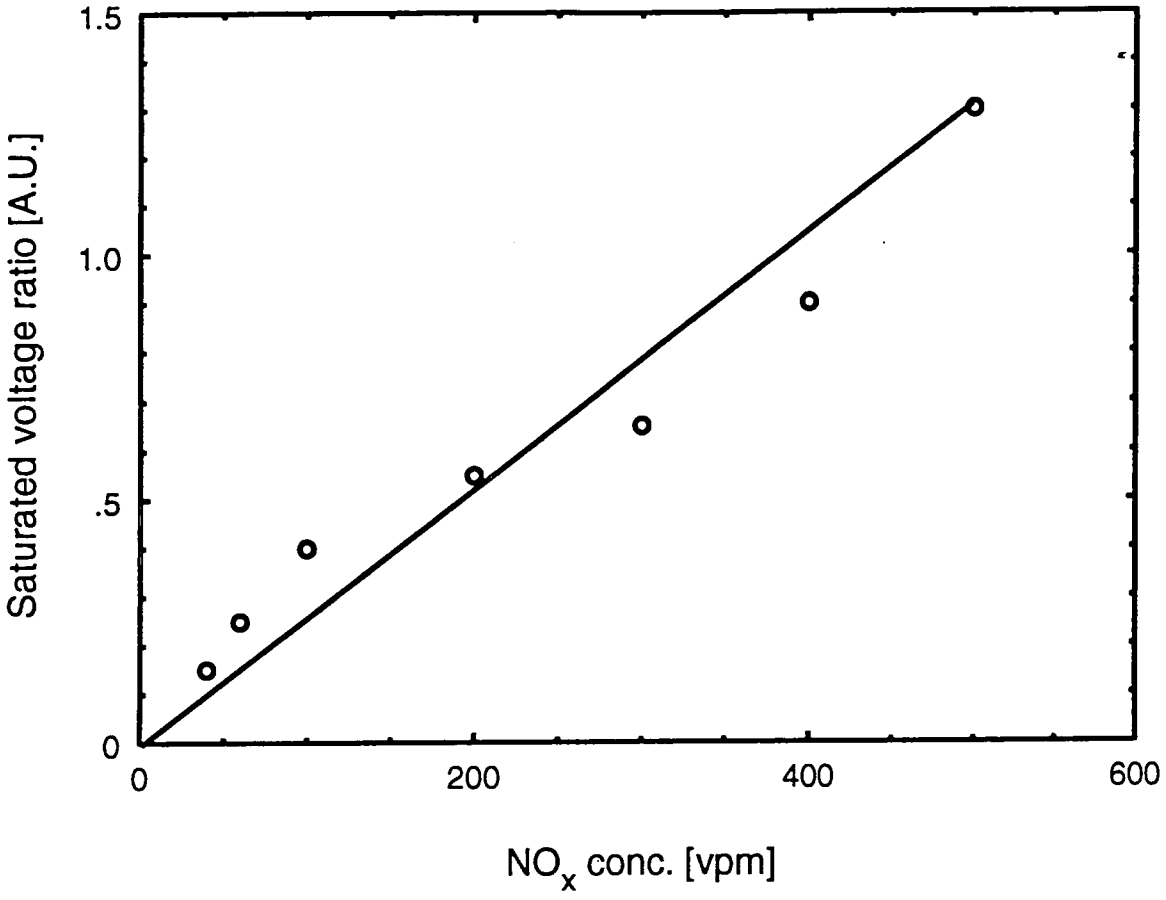

Figure 7.18: The effect of different concentrations of NO_x on 1 LB layer of a $LuPc_2$ SPR sensor.

7.4.3 Reflection Absorption Infrared Spectroscopy

Insitu-RAIRS gas sensing measurements using $LuPc_2$ were carried out using different samples from those used for the results in section 7.2.2. LB films produced interference fringes which obscured any vibrational features on the spectra. To assess the effect of the gas on the films, a difference spectrum was recorded by subtracting the spectrum before gas exposure from that after exposure. Like in previous samples, band positions in this discussion are specified within an error of $4cm^{-1}$.

Figure 7.19 shows the difference spectrum obtained when 20 LB layers of $LuPc_2$ were exposed to 150ppm NO_x for 90 minutes at room temperature. Prominent amongst the changes in the spectrum are the appearances of absorption bands at $3283cm^{-1}$, $1485cm^{-1}$, $1320cm^{-1}$ and $763cm^{-1}$. The vibration at $1485cm^{-1}$ is due to C-N stretch in the pyrrole ring that can be ascribed to pyrrole ring oxidation by the NO_x ambient. This ring oxidation produces a nitrated pyrrole ring possessing a positive charge. The vibration at $1320cm^{-1}$ is due to an oxidized isoindole group and grows in intensity with increased exposure. Also visible in the difference spectrum is a broad band centred at $763cm^{-1}$. This is due to changes in the C-H wagging vibration. Its growth is an indication that binding of the gas molecule occurs on the bisphthalocyanine ring rather than the metal. Exposure of other bisphthalocyanine derivatives has shown ring oxidation to take place resulting in an increase in conductivity [Souto et al, 1991].

A further experiment was undertaken by exposing the LB film to NO_x for successive lengths of time. The results are shown in figure 7.20, in which the isoindole stretch vibration increases with time in a fairly linear fashion. Other features include the ghost band at $3300cm^{-1}$ described earlier. In conclusion, we suggest the interaction of NO_x with $LuPc_2$ is primarily an oxidation process in which a mobile electron is donated to the gas molecule.

After these gas exposures, the NO_x was turned off and the reaction monitored for signs of reversibility. After 2 hours, no changes where observed in the spectrum indicating that the reaction is irreversible as was also observed when the chemiresistor was exposed to 90ppm NO_x.

Figure 7.21 shows the difference spectrum after exposing 20 LB layers of $LuPc_2$ to 150ppm of H_2S for 60 minutes. Unfortunately, no distinct spectral features are visible except the so-called broad ghost band centred around $3280cm^{-1}$. We ascribed this lack of spectral feature as due to the low gas concentration used, the low purity standard of the sample as well as the limited sensitivity of the instrumentation.

Figure 7.22 shows the difference spectrum for the 20 LB layers of $LuPc_2$ (new film) on exposure to 150ppm SO_2. The only change visible is the growth of the asymmetric CH_2 stretching vibration at $2915cm^{-1}$. These effects are possibly

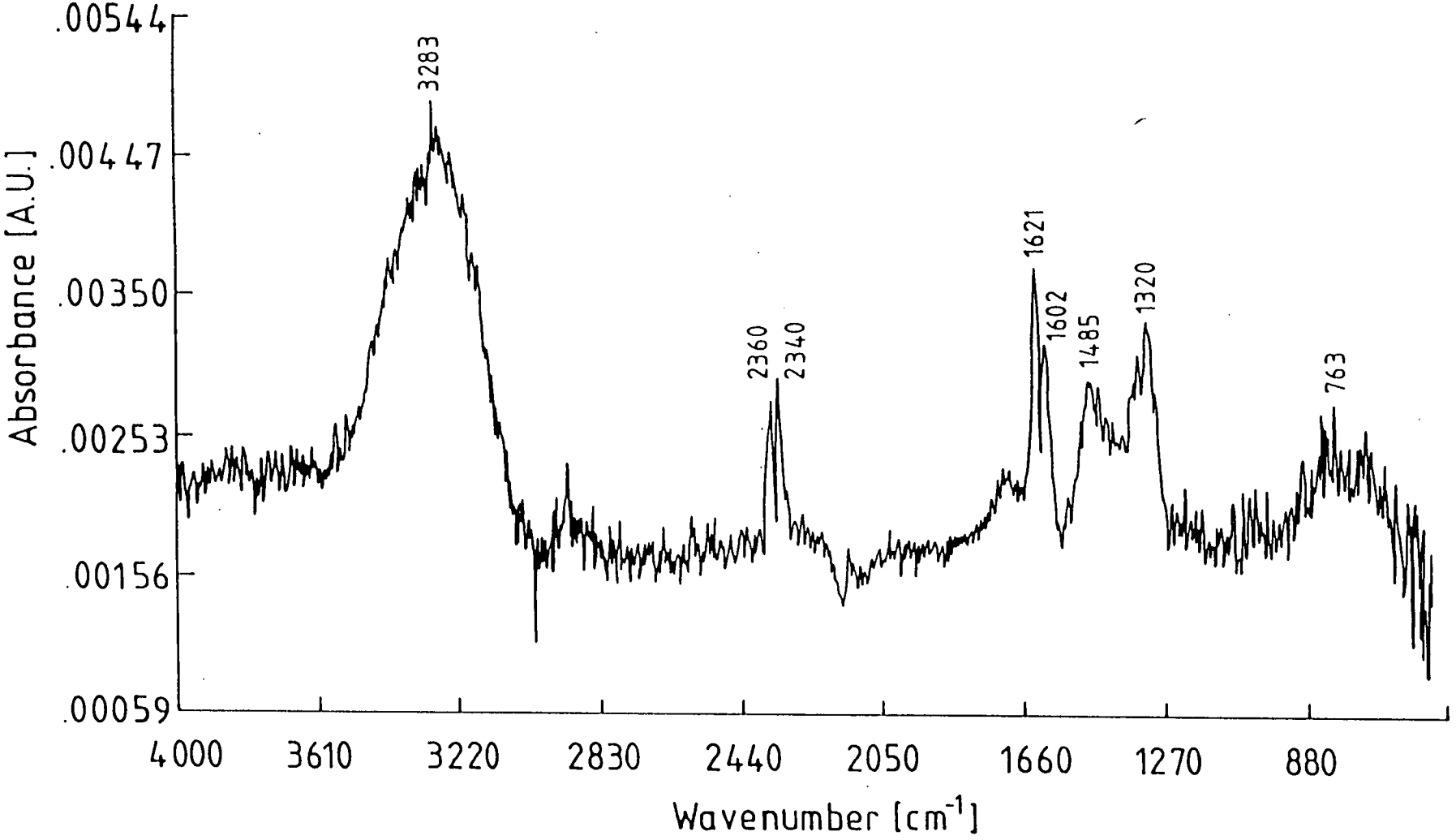

Figure 7.19: Difference spectrum for 20 LB layers of $LuPc_2$ after exposure to 150ppm NO_x for 90 minutes at room temperature.

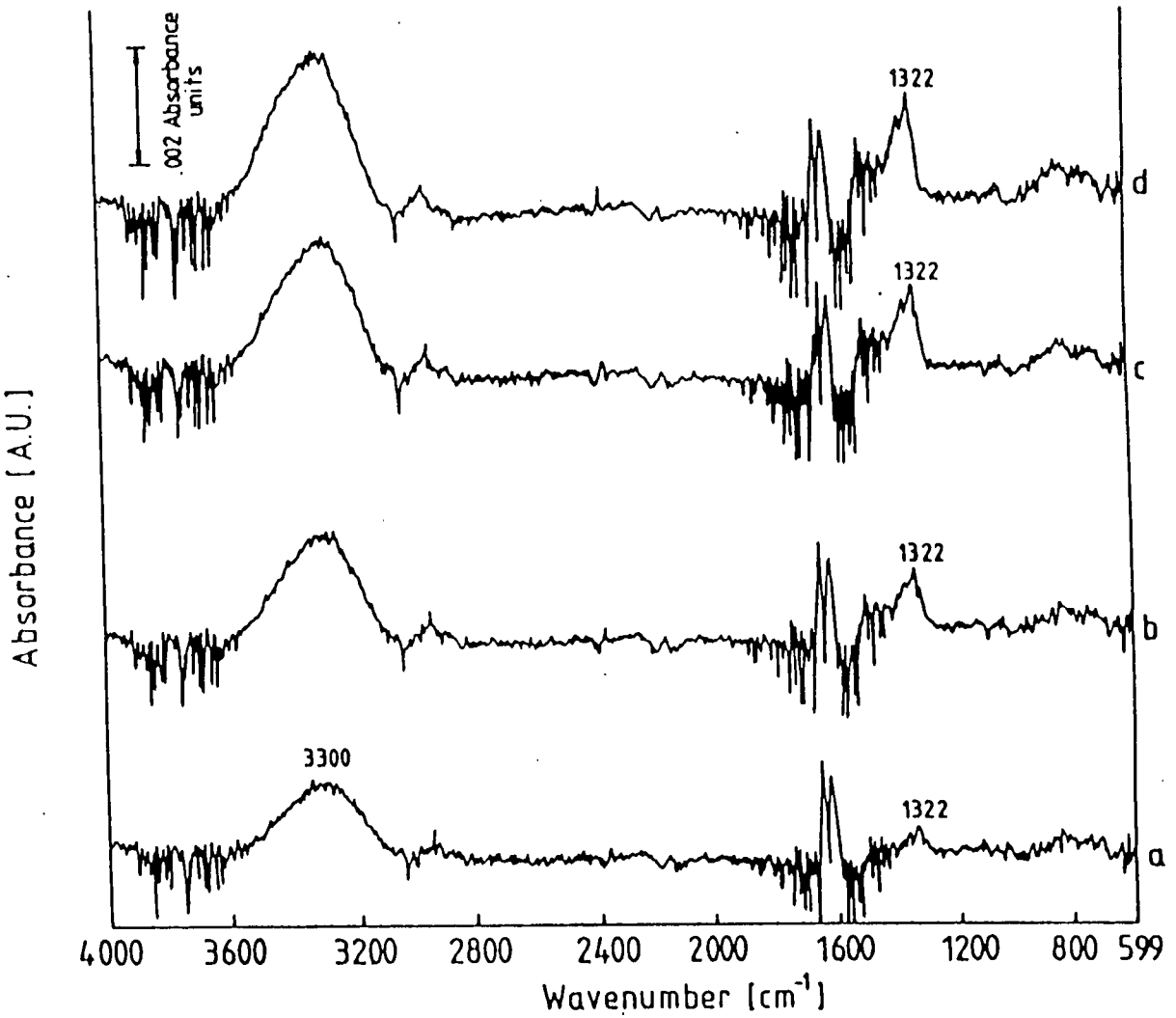

Figure 7.20: Difference spectra from exposure of 20 LB layers of $LuPc_2$ to 150ppm NO_x for 30 minutes (curve a); 60 minutes (curve b); 90 minutes (curve c) and 120 minutes (curve d).

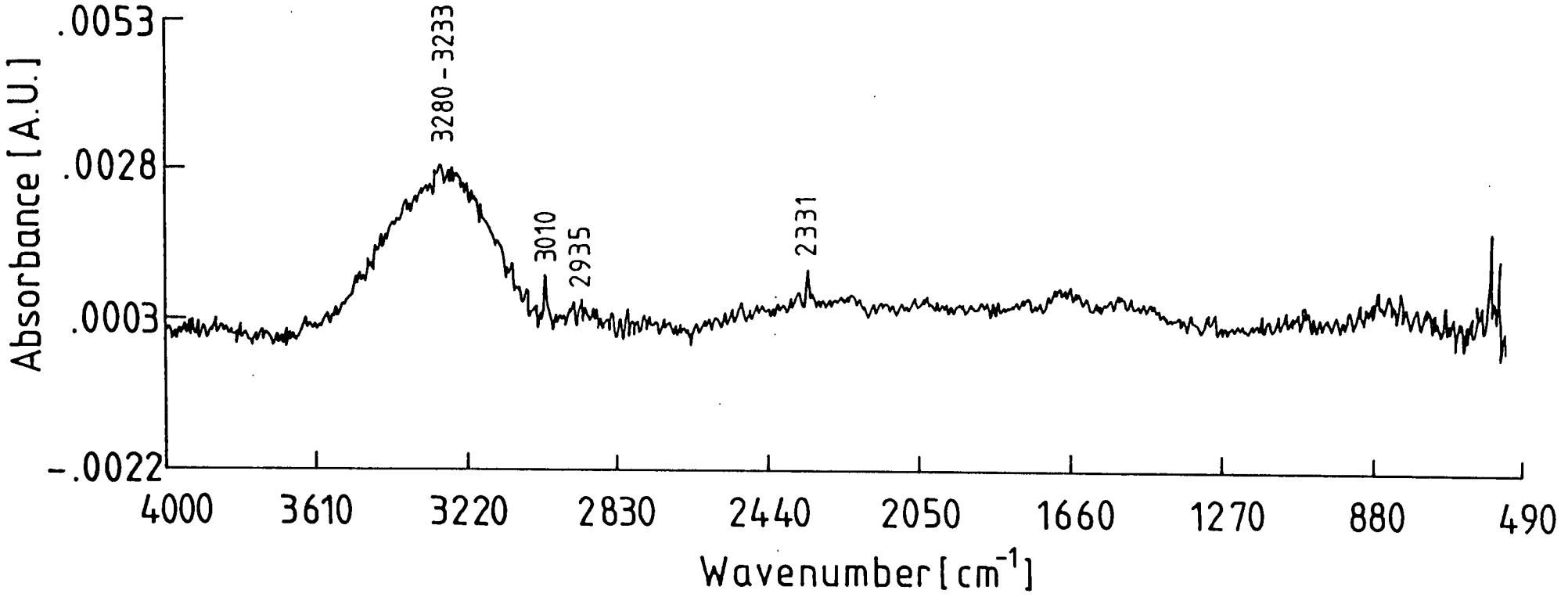

Figure 7.21: Difference spectrum of 20 LB layers of $LuPc_2$ after exposure 150ppm H_2S for 60 minutes at room temperature.

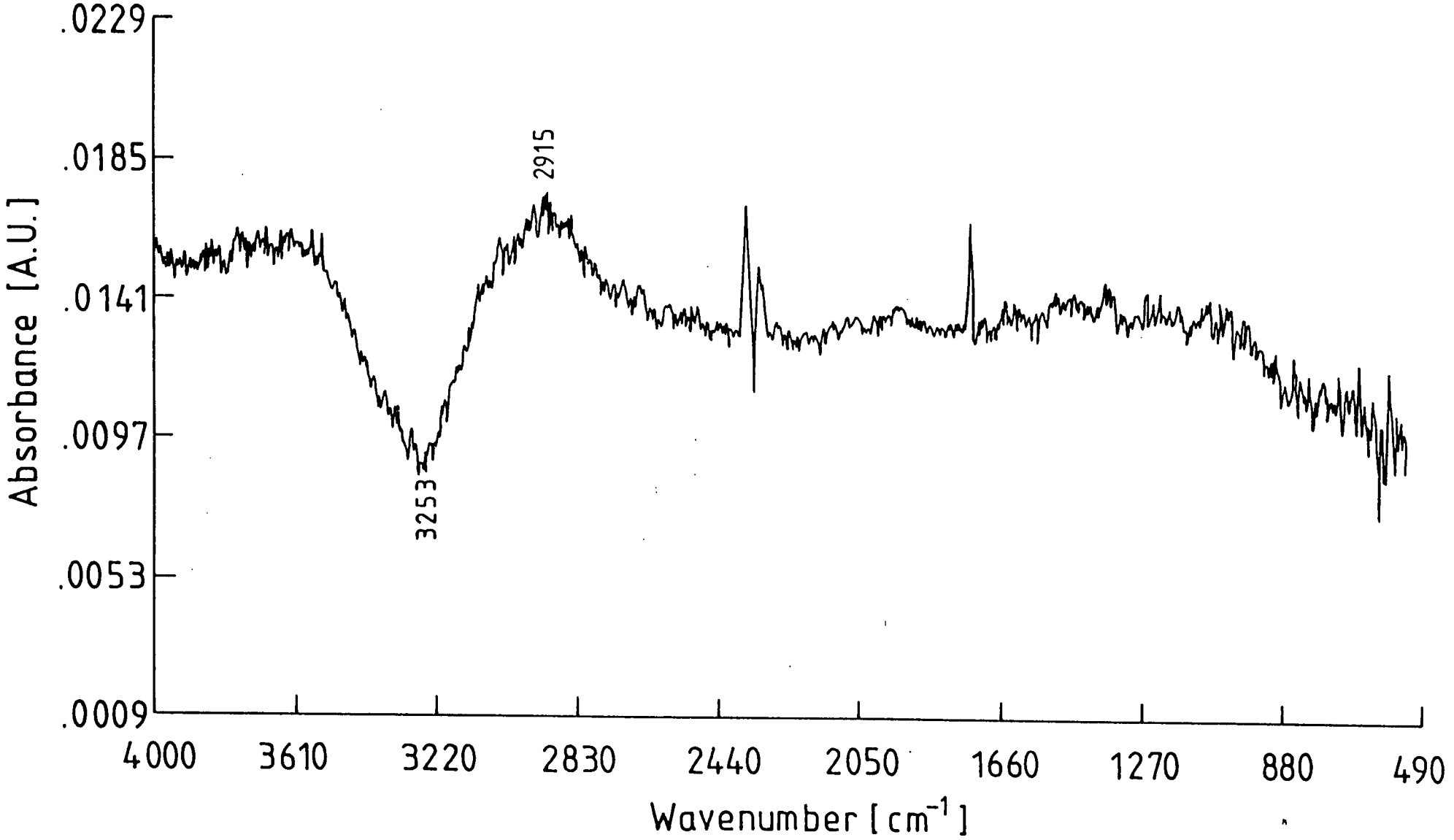

Figure 7.22: Difference spectrum of 20 LB layers of $LuPc_2$ after exposure 150ppm SO_2 for 180 minutes at room temperature.

due to acetate impurities resulting from the synthetic process (see section 7.3.2). Also visible is the ghost band, appearing this time at 3253cm^{-1}.

7.5 SUMMARY.

Thin films of lutetium bisphthalocyanine have been successfully deposited on glass, Ni/Ag, and gold using the LB technique. The films were green, smooth and produced no visible change in colour on exposure to air. Fresh solutions deposited as Z-type films but older solutions deposited Y-type, with a slightly higher up-stroke transfer ratio. The material possesses an electronic absorption band centred at 665nm which changes in proportion with film thickness. The calculated dc conductivity of the deposited films was 2.3×10^{-6}Scm^{-1}, comparable to values in the literature. A $LuPc_2$ chemiresistor has been shown to be responsive to the gases NO_x, H_2S and SO_2 at room temperature. The device is most responsive to NO_x and least to H_2S. Furthermore, the changes in conductivity observed were irreversible at high gas concentrations. No effect was recorded for CO and CH_4. Other gas effects on $LuPc_2$ LB layers were measured using changes in surface plasmon resonance and reflection-absorption Fourier transform infrared spectroscopy techniques. The interaction of NO_x with $LuPc_2$ has been ascribed to an electron exchange between the material and the gas. This interaction is thought to occur at the pyrrole and isoindole sites. This is demonstrated by an increase in the intensity of isoindole vibrations at 1322cm^{-1} with prolonged gas exposure. SO_2 being less electrophilic is likely to have the same effect as NO_x. Unfortunately this could not be confirmed due the reduced sensitivity of infrared spectroscopy to the gas. The changes observed in the difference spectrum were irreversible. Consequently, we can relate these changes to those in the electrical conductivity of a $LuPc_2$ chemiresistor at high gas concentration.

REFERENCES

Archer, P.B.M., Chadwick, A.V., Miasik, J.J., Tamizi, M. and Wright, J.D. : Sensor and Actuators, **16** (1989) 379-392

André, J.J., Holczer, K., Petit, P., Riou, M.T., Clarisse, C., Even, R., Fourmigue, M. and Simon, J. : Chemical Physics Letters, **115** (1985) 463-466

Aroca, R., Clavijo, R.E., Jennings, C.A., Kovacs, G.J., Duff, J.M. and Loutfy, R.O. : Spectrochimica Acta, **45A** (1989) 957-962

Baker S., PhD thesis, University of Durham, England, 1985

Chang, A.T. and Marchon, J.C. : Inorganica Chimica Acta, **53** (1981) L241-L243

Collins, G.C.S. and Schiffrin, D.J. : J. Electroanalytical. Chemistry, **39** (1982) 335-369

De Cian, A., Moussava, M., Fischer, J., Weiss, R. : Inorganic Chemistry, **24** (1985) 3162-3167

Jennings, C., Aroca, R., Hor, A.M. and Loutfy, R.O. : Spectrochimica Acta, **41A** (1985) 1095-1099

Liu, Y., Shigehara, K. and Yamada, A. : Thin Solid Films, **179** (1989) 303-308

Maitrot, M., Guillaud, G., Boudjema, B., André, J.J., Strzelecka, H., Simon, J. and Even, R. : Chemical Physics Letters, **133** (1987) 59-62

Markovitsi, D., Tran-thi, T.H., Even, R. and Simon, J. : Chemical Physics Letters, **137** (1987) 107-112

Nicholson, M.M. and Weismuller, T.P. : J. Electrochemical Society, **131** (1984) 2311-2313

Petty, M., Lovett, D.R., O'Connor, J.M. and Silver, J. : Thin Solid Films, **179** (1989) 387-395

Petit, P. : Synthetic Metals, **46** (1992) 147-163

Souto, J., Aroca, R. and DeSaja, J.A. : J. Raman Spectroscopy, **22** (1991) 787-790

Souto, J., Aroca, R. and DeSaja, J.A. : J. Raman Spectroscopy, **22** (1991) 349-353

Traore, M.K., Stevenson, T.K., McCormick, B.J., Dorey, R.C., Wen, S. and Meyers, D. : Synthetic Metals, **40** (1991) 137-153

Trometer, M., Even, R., Simon,J., Dubbon, A., Laval, J.Y., Germain, J.P., Maleysson, C., Pauly, A. and Robert, H. : Sensors and Actuators B, **8** (1992) 129-135

Van Ewyk, R.L.V., Chadwick, A.V. and Wright, J.D. : J. Chem., Society., Faraday Trans, **76** (1980) 2194-2205

Wohljen, H., Barger, W.R., Snow, A.W. and Jarvis, N.L. : IEEE Transaction on Electronic Devices, **ED-32** (1989) 173-181

Wright, J.D. : Material Science., **13** (1987) 295-298

Yamana., M., Tsutsui, M and Ham, J.S. : J. Chemical Physics, **76** (1982) 2761-2763

Zhu, D.G., Petty, M.C. and Harris, M. : Sensors and Actuators B, **2** (1990) 265-269

CHAPTER EIGHT

METALLOPORPHYRIN LANGMUIR-BLODGETT THIN FILMS: RESULTS AND DISCUSSION

8.1 PREFACE

In this chapter, the results of gas sensing devices made from metallotetraphenylporphyrin LB films are presented. Metalloporphyrins present in biological enzymes are known to influence the reactivity and selectivity of the biological molecules. For example, haemoglobin is known for selectively and reversibly carrying oxygen into, and carbon dioxide out of, the human body. On this basis, a close relative of haemoglobin, was chosen for further study: cobalt (II) 5,10,15,20 (4-methoxytetraphenyl)-21H, 23H-porphine (CMTPP). The deposition and gas sensing studies of this compound are discussed in the following section.

8.2 CMTPP

8.2.1 LB Films for NO_x Sensing

LB films were deposited from a solution of CMTPP in chloroform. Figure 8.1 shows the surface pressure versus area isotherm of the material on the water surface at a subphase temperature of 20±2°C. This was formed by compression at a rate of about $2.0\times10^{-2}nm^2molecule^{-1}s^{-1}$. The condensed isotherm is similar to that of a fatty acid with distinct transitions from the gas to the liquid and from the liquid to the solid phase. From the condensed isotherm plot, the area per molecule was calculated to be $0.27nm^2$ at $30mNm^{-1}$. Based on models in the literature, we would expect an area of $2.0nm^2$ if the porphyrin molecule is oriented parallel to the surface and about $0.5nm^2$ if the porphyrin was perpendicular to the subphase surface [Miller et al, 1985]. Thus, the measured area per molecule indicates that the material did not form a monomolecular layer on the subphase surface. The stable condensed layer exhibited a rapid

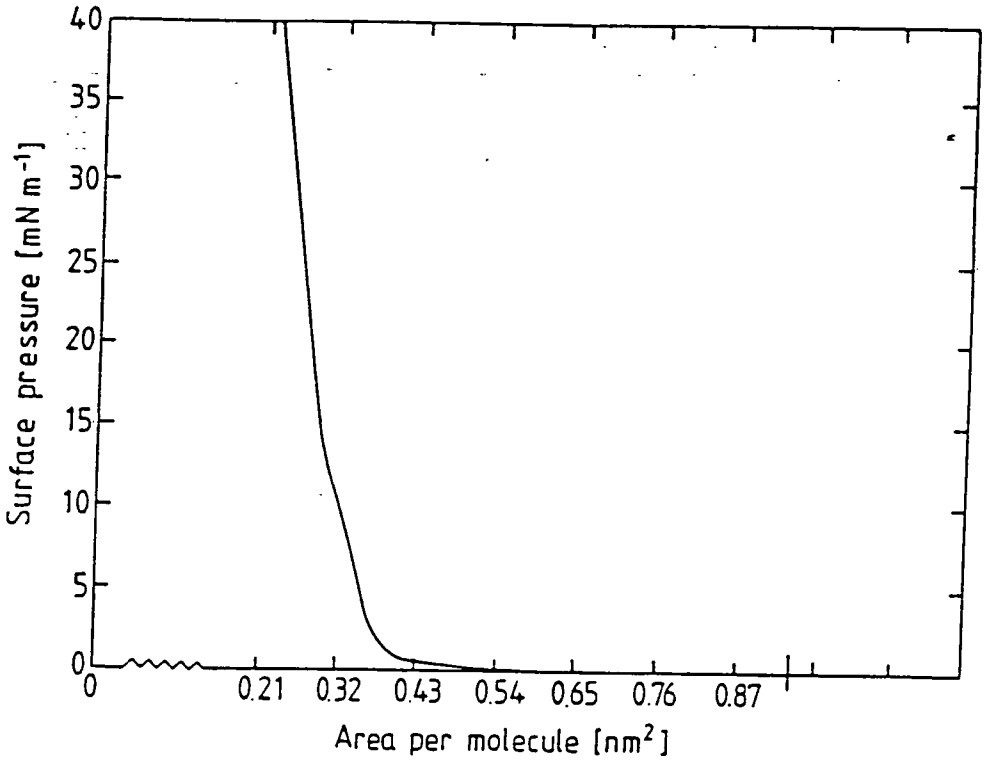

Figure 8.1: Surface pressure versus area isotherm of CMTPP on pure water surface.

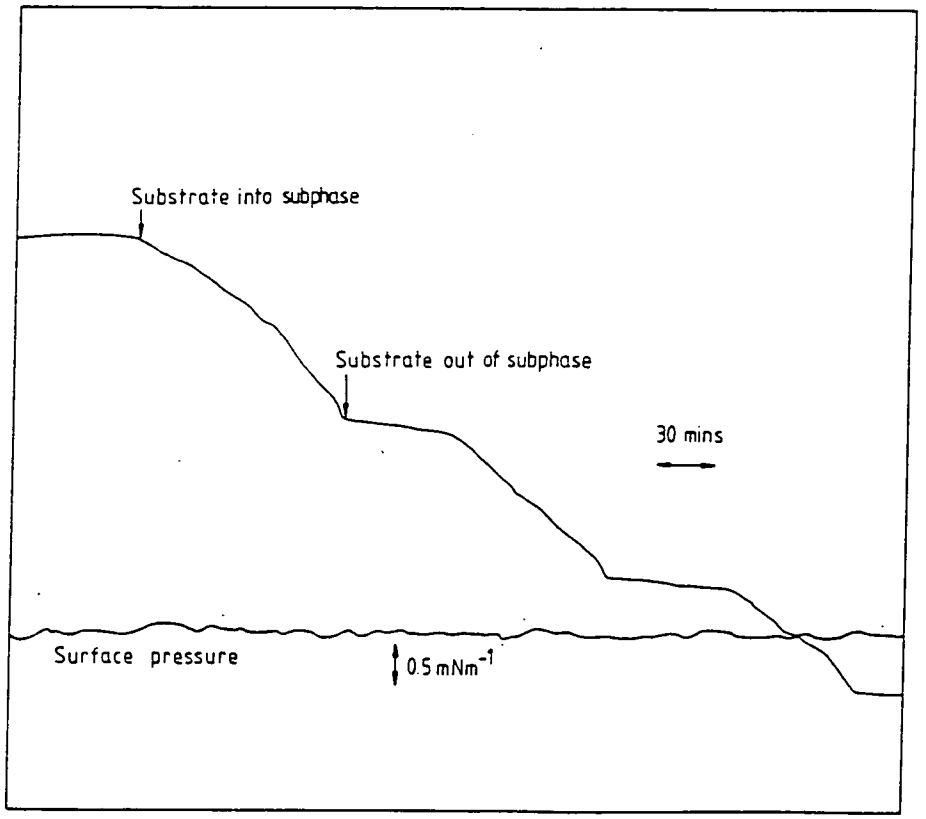

Figure 8.2: Y-type deposition record for material on printed circuit board substrate.

suction test when a small quantity of material was removed from the water surface.

The floating layer was subsequently compressed to a surface pressure of $30mNm^{-1}$ and became stable after 2 hours. Deposition was undertaken at a speed of $0.1mms^{-1}$.

The condensed film deposited Y-type at $30mNm^{-1}$ with a transfer ratio close to unity, as shown in figure 8.2, on PCB substrate. The deposited films had a brown colour when viewed under crossed-polarised microscope, similar to those cast directly from solution.

8.2.2 NO_x Gas Sensing Results

a. Gas-induced Conductivity Change

It was initially established that an ohmic contact existed between CMTPP and the gold interdigitated electrode using the current versus voltage measurements shown in figure 8.3; the overall resistance (the slope) clearly increases with film thickness.

Gas sensing began with the introduction of N_2, which decreased the conductivity of the material due to the removal of trapped water in the film. This process lasted only 20 minutes reflecting the much reduced amount of water present in the film compared to polyaniline (see figure 4.10).

Figure 8.4 shows the effect of 300ppm NO_x on a 10 LB layer CMTPP chemiresistor. The gas produced an increase in device conductivity after a delay time τ_D of about 30 seconds. The conductivity saturated after approximately 6 minutes and recovered, almost completely after the gas was turned off.

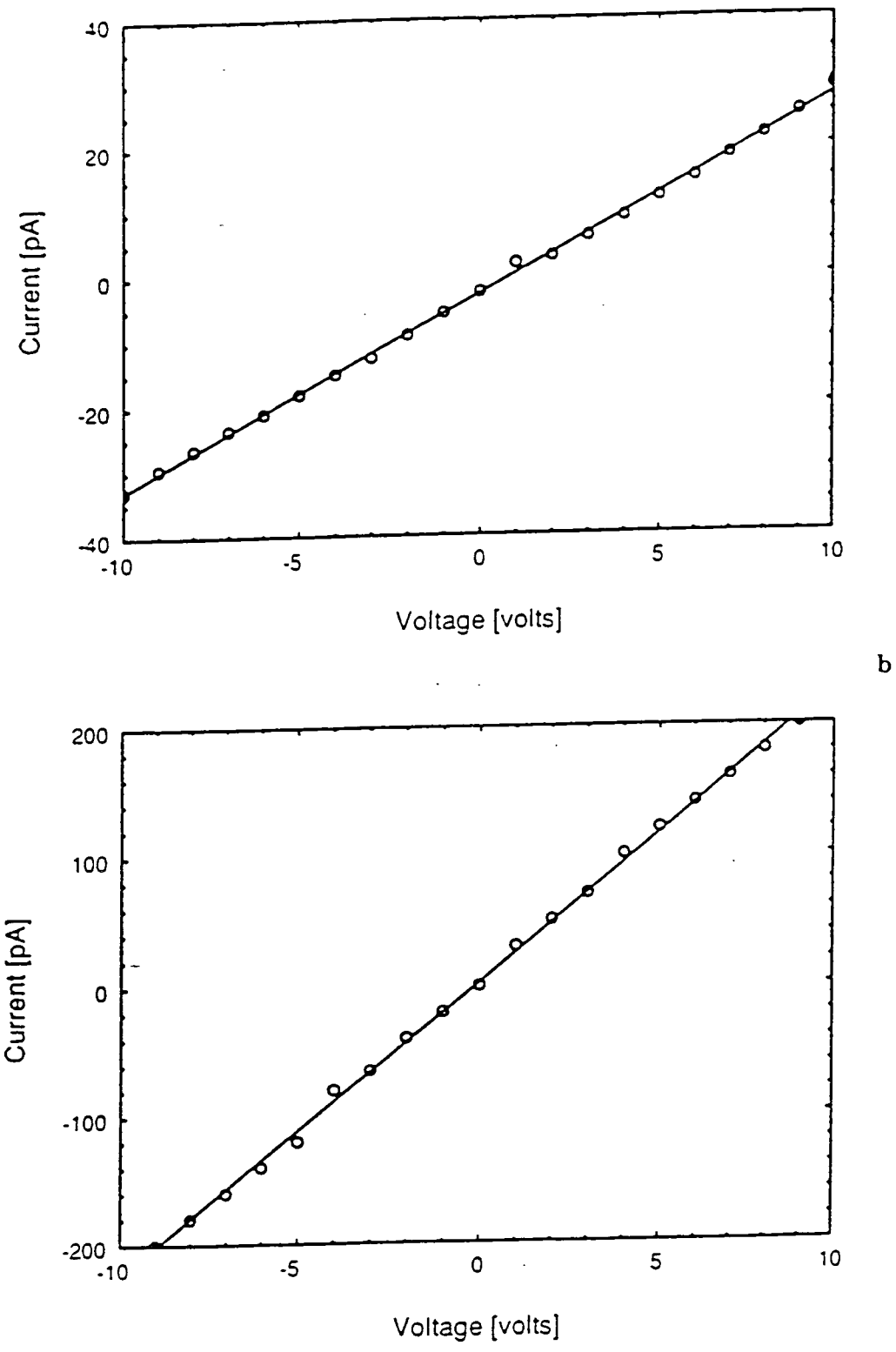

Figure 8.3: The current versus voltage characteristics for CMTPP LB layers deposited onto interdigitated electrodes for 4 layers (curve a) and 10 layers (curve b).

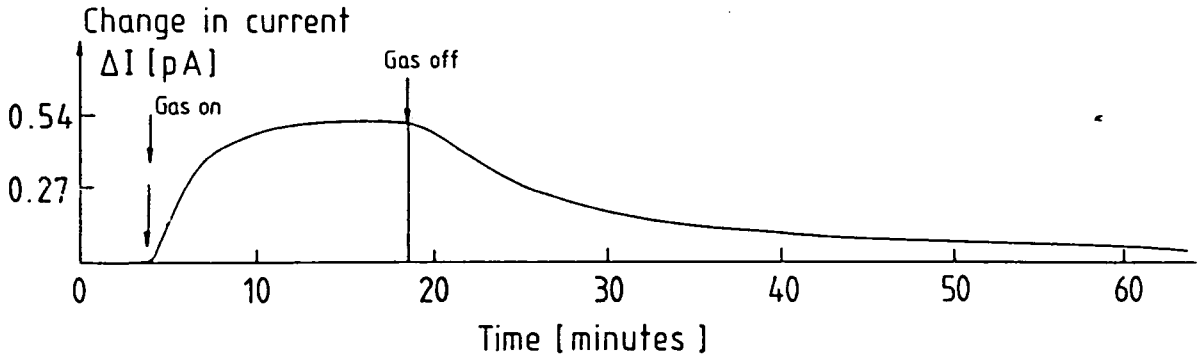

Figure 8.4: The effect of 300ppm NO_x on a 10 LB layer CMTPP chemiresistor at room temperature [10V supply].

Figure 8.5 shows the effect of exposing the device to different concentrations of NO_x. It is evident that the saturation current depends linearly on the gas concentration, perhaps indicating only one type of interaction site. At the moment we can only speculate this to be on the Co^{II} atom, located in the centre of the molecule. In this case, the interaction involves the removal of the unpaired electron located in the d^7-orbital of the Co^{2+} ion resulting in an increase in the conductivity.

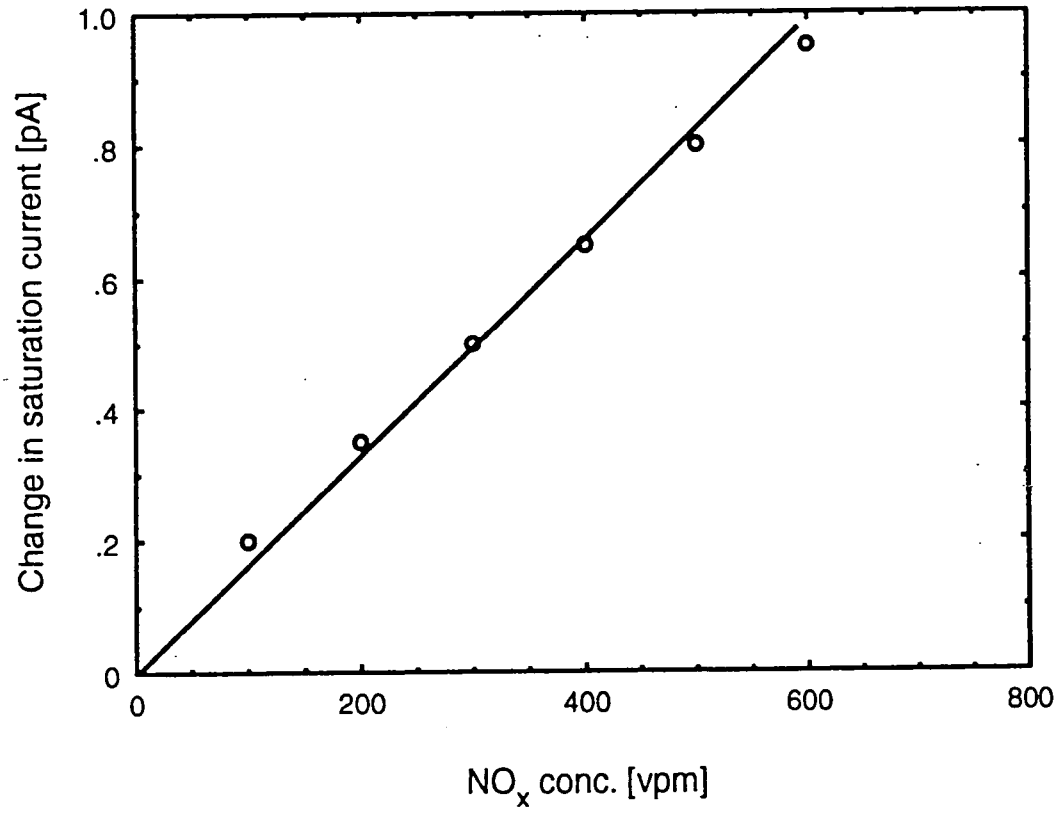

Figure 8.5: The effect of different concentrations of NO_x on a 10 LB layer CMTPP chemiresistor at room temperature.

Figure 8.5 also shows that the lower detection level is about 100ppm, significantly higher compared to polyaniline (4ppm for the spun film, 2ppm for the evaporated and 30ppm for the LB film) or lutetium bisphthalocyanine (2ppm). This may also be due to only one type of interaction site which easily becomes saturated with increasing gas exposure.

The selectivity of this device was investigated by exposing it to a wide range of other gases including H_2S, SO_2, CO and CH_4. None of these produced a change in the device conductivity at room temperature, even at gas concentrations of 50,000ppm.

b. SPR Sensor

Figure 8.6 shows the SPR curve for Ni/Ag (curve a), Ni/Ag with 2 layers of CMTPP (curve b) and Ni/Ag with 4 layers of CMTPP (curve c). The effect of the LB layers include a shift in the resonance angle and a reduction of the depth of resonance. These changes are due to the same factors already explained for polyaniline and $LuPc_2$ LB films.

Gas sensing was undertaken using the 4 layer structure. Initially, the incident laser beam was the fixed at 43.5°, equivalent to 50% reflectivity, and the reflectance monitored in air. Dry N_2 was introduced and, as shown for previous measurements, this produced a decrease in output voltage ratio (i.e. a decrease in reflectivity) which became stable after a period of about 60 minutes. Once again, we associate this decrease in reflectivity to the removal of water from the film.

Figure 8.7 shows the time response of 4 layers of CMTPP exposed to 500ppm NO_x. The output voltage ratio (equivalent to an increase in reflectivity) increases after a delay time of about 60 seconds and saturates after about 40 minutes. After the gas was turned off, the reflectivity recovered to its original level after a period of about 50 minutes.

Previous SPR measurements undertaken by other workers have shown some sensitivity to NO_x but **not** reversibility under the same conditions [Zhu et al,

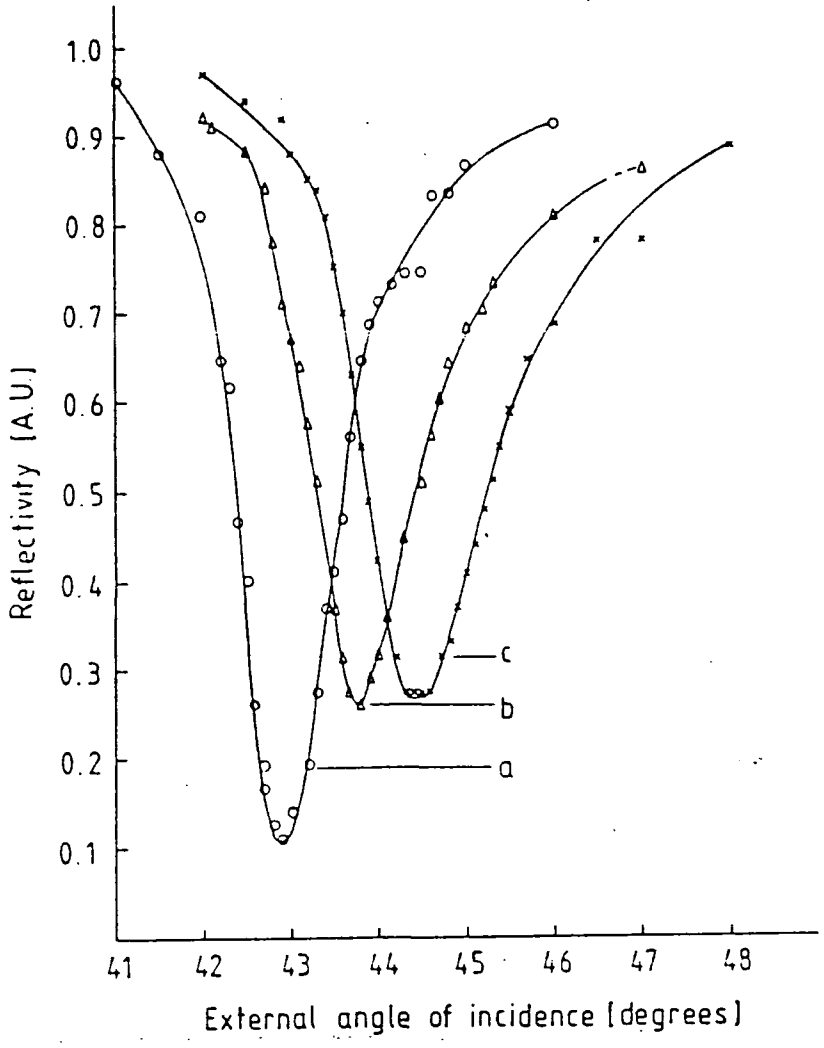

Figure 8.6: SPR curve for Ni/Ag (curve a); Ni/Ag covered with 2 LB layers of CMTPP (curve b); Ni/Ag covered with 4 LB layers of CMTPP (curve c).

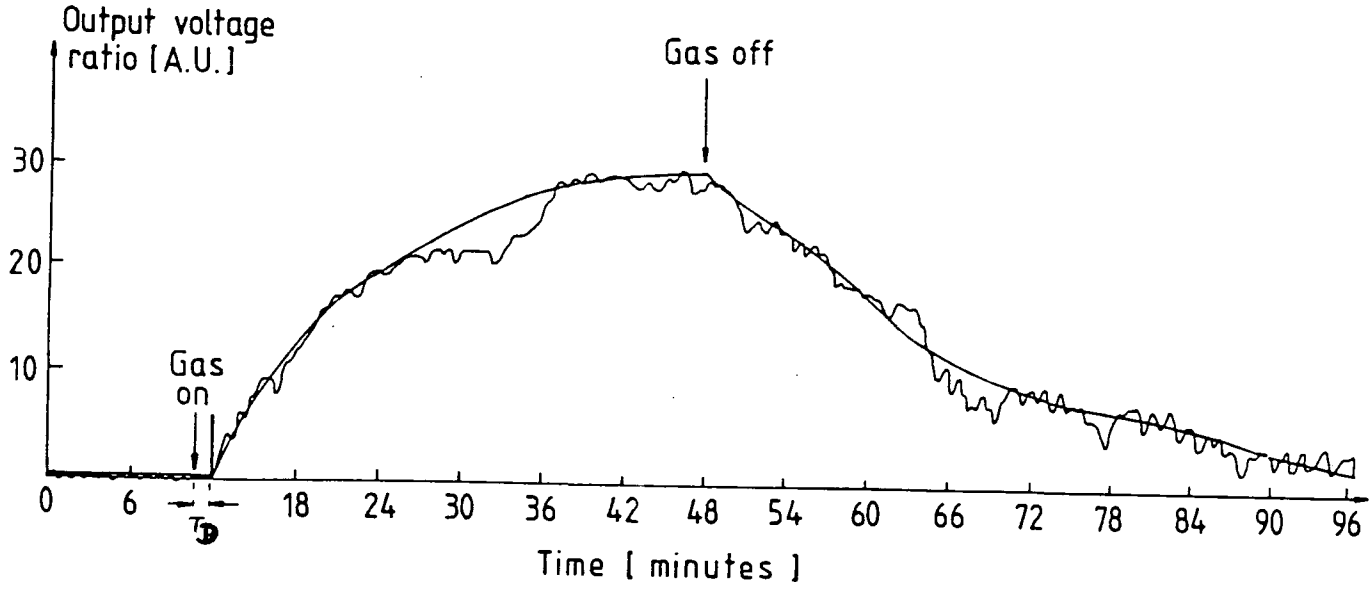

Figure 8.7: The effect of 500ppm NO_x on an SPR sensor with 4 LB layers of CMTPP on a Ni/Ag substrate.

1990]. Thus, this result represents a significant improvement on previously reported SPR based optical sensors.

The effect of different NO_x concentrations is shown in figure 8.8 in which the change in reflectivity (measured here as output voltage ratio) is observed to increase with increasing gas concentration. We can also see that the optical sensor is sensitive to the same concentration range as the conductivity based sensor (>100ppm). Hence this material could be used in both devices without any loss of sensitivity. This contrasts with our results for $LuPc_2$ for which the conductivity was significantly more sensitive (2ppm threshold level) than the reflectivity (50ppm threshold level).

Selectivity in the SPR system was investigated using the same gases as for the conductivity based sensors. No measurable change in the reflectivity of the device was found for H_2S, SO_2, CO or CH_4, even at concentrations of 10,000ppm.

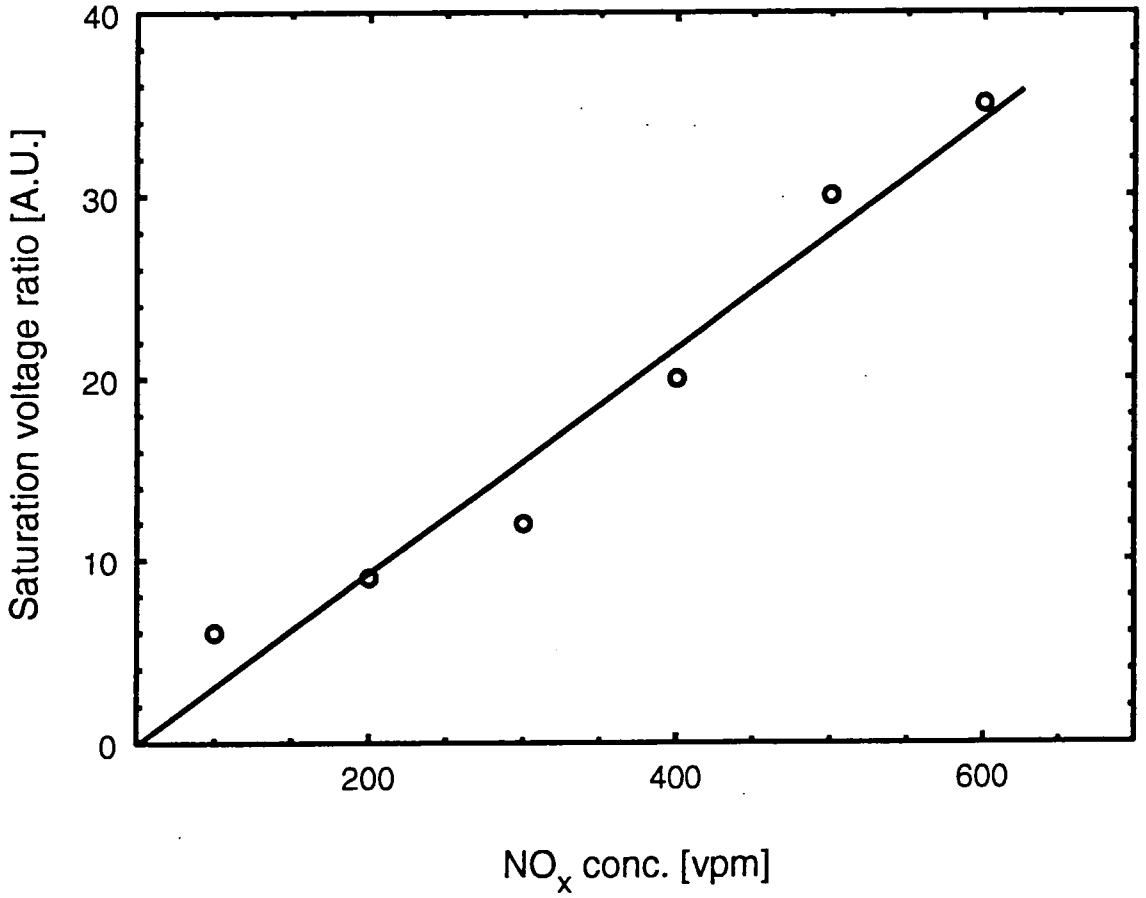

Figure 8.8: The effect of different concentrations of NO_x on a 4 LB layer CMTPP SPR sensor.

c. Insitu-reflection Absorption Fourier Transform Infrared Spectroscopy.

Figure 8.9 shows the RAIRS spectrum of 10 LB layers of CMTPP. This is comparable to that reported by others for CTPP sublimed on a KBr pellet [Alben et al, 1973 and Oshio et al, 1984]. A summary of the vibrations present in the film is given in table 8.1.

Band Position [cm^{-1}]	Assignment	Reference
2961-2852	CH_2 stretch	Alben et al, 1973
1721		
1598-1571	aromatic C-C stretch	Alben et al, 1973 and Oshio et al, 1984
1503		
1456		
1375-1347		
1266		
1164		
1075		
1063	$C_\beta H$ bending	Gladkov et al, 1986
1029		
927		
792-697	out-of-plane $C_\beta H$ bending	Oshio et al, 1984

Table 8.1: A summary of the assignments of infrared bands of CMTPP.

The RAIRS spectrum of CMTPP is characterized by three structure sensitive absorption band regions: (1) 1347-1375cm^{-1}; (2) 792-800cm^{-1}; and (3) 466-450cm^{-1} [Oshio et al, 1984]. These three regions are very sensitive to oxidation and/or spin state of the molecule. Furthermore, they vary with the central metal in the MTPP series [Kincaid et al, 1975].

Absorption bands between 466-450cm^{-1} were too weak to be measured in this work. Bands in the region 1347-1375cm^{-1} are ascribed to the C-C stretching

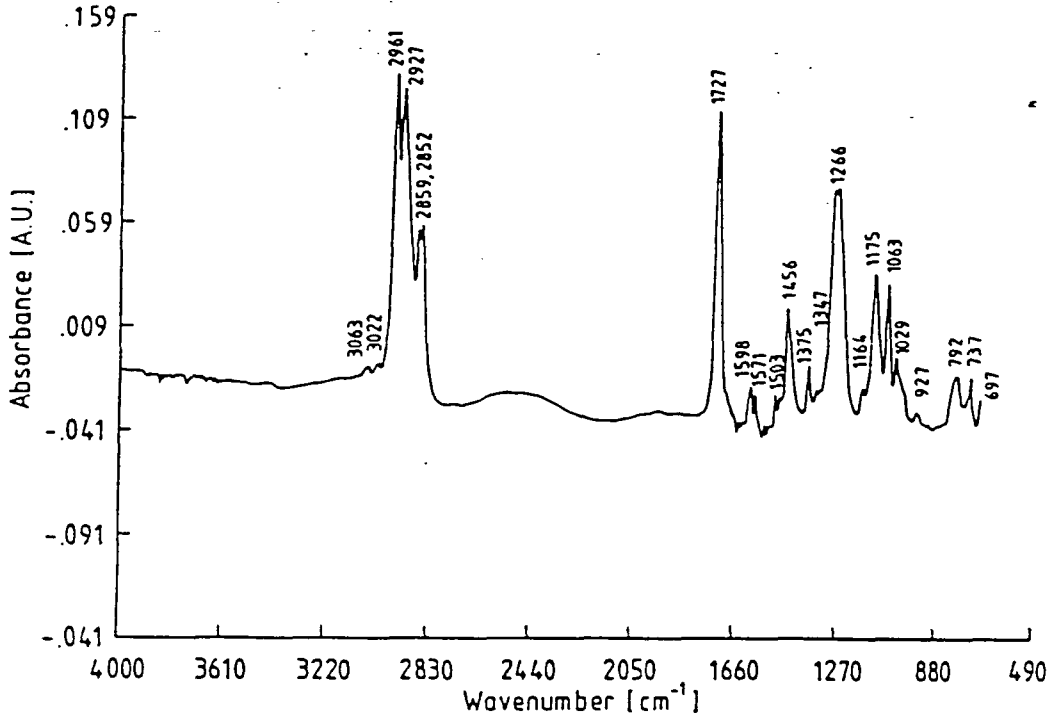

Figure 8.9: Reflection-absorption Fourier transform infrared spectrum of 10 LB layers of CMTPP on gold.

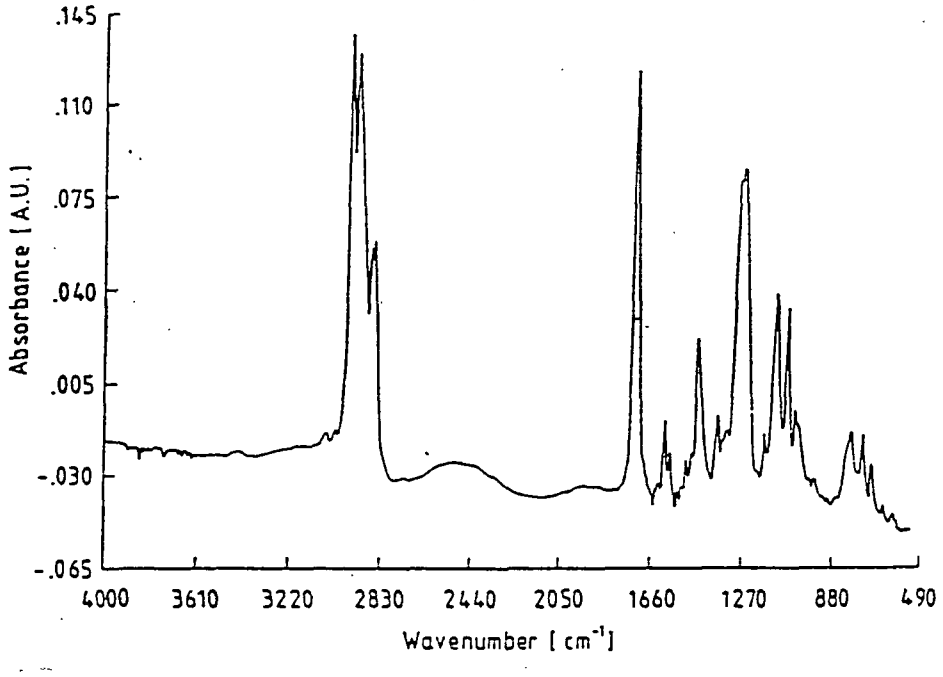

Figure 8.10: Reflection-absorption Fourier transform infrared spectrum of 10 LB layers of CMTPP after exposure to 150 ppm NO_x for 2 hours.

mode of the porphyrin core while those in the region 792-800cm^{-1} are assigned to the out-of-plane C-H bending vibrations.

The aromatic ring stretches are between 1571-1598cm^{-1}. The metal-nitrogen vibration is located between 330-180cm^{-1} which is outside the range of measurement of this system. The remaining bands in the spectrum can be attributed to porphyrin core vibrations, described by many authors [Kincaid et al, 1983 and Gladkov et al, 1986].

Figures 8.10 shows the RAIRS spectrum of 10 LB layers of CMTPP after 2 hours exposure to 150ppm NO_x. Except for changes in the baseline absorbance, no differences can be seen in terms of new absorption bands or changes to the existing bands when compared to figure 8.9.

Oxidation of the CMTPP and other MTPPs results in three possible products: a metal of higher oxidation state; a porphyrin π-cation radical; or a π-dication radical with an isoporphyrin [Carnieri et al, 1982]. Interactions involving the production of a porphyrin π-cation or dication radical are characterized by a 1550cm^{-1} absorption band, visibly absent in figure 8.10 [Li et al, 1990 and Salehi et al, 1986]. A possible reason for the absence of this band is the fact Co^{2+} is not sufficiently electronegative to locate the electron spin density on the β-pyrrolic position of the porphyrin molecule [Catalano et al, 1984]. Hence we suggest that the site of the oxidation interaction may be the low spin Co^{2+}, which possesses an unpaired electron in its d^7 orbital.

The selectivity of this device was further investigated using H_2S and SO_2. Both produced no observable changes in the infrared spectrum of CMTPP.

8.3. OTHER METALLOTETRAPHENYL PORPHYRIN MATERIALS

Figure 2.2 shows the chemical structure of a range of other porphyrin materials studied in this work. These were also prepared into thin films by the LB technique. A summary of their mono and multilayer film forming characteristics is shown in table 8.2. Generally, the gas sensing results

Material	Molecular Weight	Dipping Pressure [mN^{-1}]	Collapse Pressure [mNm^{-1}]	Average Area per Molecule [nm^2]	pH	Deposition Type	Transfer Ratio	Film Quality on Substrate	Overall Assessment	Comments
(1) NiTPP+TA 1:1 volume ratio (0.15 +0.94)g/l	678	30	45	1.06	6.9	Y (on Ag)	1±0.1	Visibly uniform	Good	Isotherm plot shows a plateau region which possibly corresponds to a re-organisation of the molecules on the subphase surface
(2) CuTPP+TA 1:1volume ratio (0.3+0.94)g/l	676	30	46	0.80	6.9	Y (on Ag)	1±0.1	Striations noted	Fair	Insoluble in $CHCl_3$ but sparingly soluble in 1:4 CH_3OH:$CHCl_3$. TA essential for spreading (as for NiTPP).
(3) ZnTPP+TA 2:1volume ratio (0.63+1.0)g/l	678	30	40	0.94	6.9	Y (on Ag)	1±0.1	Patchy Film	Good	Similar to CuTPP.
(4) VTPP+TA	680	30	41	0.44	6.9	Y (on Ag)	1±0.1	Smooth layers	Good	Film quality critically dependent on dipping conditions.

(5) CMTPP	759	30	41	0.27	6.9	Y (on Ag)	1±0.1	Striations noted	Good	Using old (2 weeks) solution, isotherm shows three distinct region (as for fatty acid: see figure 2.4)
(6) FeMTPP	792	15	25	0.84	6.9	Y (on Ag)	1±0.1	Smooth layers	Fair	Deposition possible without fatty acid.
(7) FeTFPP+TA 1:1volume ratio (1.3+1.0)g/l	1064	30	41	0.86	6.9	Y (on Ag)	1±0.1	Patchy with striations	Good	Films deposited at slower dipping speed are of better quality.
(8) MEDE 1.2g/l	599	30	40	0.74	6.9	Y (on Ag)	1±0.1	Smooth layers	Good	Dissolves easily in $CHCl_3$ and spreads uniformly on water surface
(9) Hemin 0.62g/l	660	15	20	0.80	6.9	Y (on Ag)	1±0.1	Smooth and uniform layers	Good	Dissolves sparingly in 4:1 $CHCl_3$:CH_3OH using ultrasonic agitation.
(10) Hematin 3.9g/l	648	15	25	0.80	6.9	Y (on Ag)	1±0.1	Slightly patchy	Good	Similar solution to Hemin. Isotherm reveals the floating layer to be very expanded

Table 8.2: Langmuir-Blodgett film characteristics of metallotetraphenylporphyrins used in this project.

obtained for these materials were poorer than found for the other compounds reported in this thesis

8.4 SUMMARY

Floating layers of cobalt (II) methoxyltetraphenyl porphyrin exhibit a condensed isotherm, capable of withstanding surface compression pressures of up to 40mNm^{-1}. The condensed films deposited mainly as Y-type layers on PCB and Ni/Ag substrates. The LB films have been shown to form the basis of a selective gas sensing device for NO_x at room temperature. NO_x was detected using electrical and optical measurement techniques. NO_x was detected mainly at high concentrations and, in most cases, the response was reversible within the limits of experimental error. DC conductivity changes and changes in SPR gave similar results in terms of sensitivity and selectivity.

REFERENCES

Alben, J.O., Choi, S.S., Adler, A.D. and Caughey, W.S. : Ann. N.Y. Acad. Science, **206** (1973) 278-295

Baker, S. : PhD thesis, University of Durham, 1985

Carnieri, N and Harriman, A. : Inorganica Chimica Acta, **62** (1982) 103-107

Catalano, M.M., Crossley, M.J., Harding, M.M. and King, L.G. : J. Chem. Society., Chem. Commun. (1984) 1535-1536

Gladkov, L.L. and Solovyov, K.N. : Spectrochimica Acta, **42A** (1986) 1-10

Kincaid, J.R. and Nakamoto, K. : J. Inorganic Nuclear Chemistry, **37** (1975) 85-

Kincaid, J.R., Urban, M.W., Watanabe, T. and Nakamoto, K. : J. Phys. Chemistry, **87** (1983) 3096-3101

Lecomte, C., Baudin, C., Berleur, F., Ruaudel-Teixier, A., Barraud, A., Momenteau, M. : Thin Solid Films, **133** (1985) 103-112

Miller, A., Knoll, W., Mohwald, H., and Ruaudel-Teixier, A. : Thin Solid Films, **133** (1985) 83-91

Oshio, H., Ama, T., Watanabe, T., Kincaid, J. and Nakamoto, K. : Spectrochimica Acta, **40A** (1984) 863-870

Salehi, A., Oertling, W.A., Babcock, G.T and Chang, C.K. : J. Am. Chem. Society, **108** (1986) 5630-5631

Zhu, D.G., Petty, M.C. and Harris, M. : Sensors and Actuators B, **2** (1990) 265-269

CHAPTER NINE

CONCLUSIONS AND SUGGESTIONS FOR FUTURE WORK.

9.1 CONCLUSIONS

This section is subdivided according to the various materials used for gas sensing studies. A comparison between chemiresistor and surface plasmon resonance sensors is also included.

9.1.1 Spin-coated Polyaniline

'Undoped' polyaniline powder has been dissolved in N-methylpyrrolidinone and deposited as thin films by spinning on glass, gold and gold-plated interdigitated electrode structures. After being heated in a vacuum oven at 120°C for 10 minutes, the as-deposited film was blue to the naked eye and without pinholes under microscopic examination. Using ultraviolet/visible spectroscopy, its chemical nature was determined to be that of the emeraldine base form of polyaniline. Using scanning electron microscopy, the physical structure of the film was shown to be fibrous with the numerous fibres randomly intertwining with each other. Simple resistive devices were found to be highly stable at room temperature and sufficiently conducting for gas sensing. The room temperature dc conductivity was calculated to be $1.5\times10^{-11}Scm^{-1}$, increasing with increasing temperature. The infrared spectrum of the material has been shown to be made up of several peaks in the mid-infrared region. This spectrum as a whole is dominated by two vibrations: at $1504cm^{-1}$, associated with the benzoid ring stretch, and at $1597cm^{-1}$, associated with the quinoid ring stretch. Both vibrations are sensitive to the chemical and physical structure of the polymer.

The spun film was 'doped' by protonation and changed colour from blue to green. Using the ultraviolet/visible spectroscopy, we established that the 'doped' material was in the emeraldine salt form of polyaniline. Using scanning

have changed substantially. In this case, the randomly intertwining fibres acquired some orientation, as in stretched polyaniline films. Resistive devices made with the 'doped' films were conducting at room temperature. Furthermore, in air the conductivity was seen to decrease with increasing temperature, as an ideal metal. The reasons for this behaviour were ascertained mainly to the loss of the Cl^- counter ion and the loss of the solvating water trapped in the film. Unfortunately, the conductivity of the 'doped' material was too unstable for reliable gas sensing measurements.

Conductivity based gas sensing measurements using the 'undoped' spin-coated polyaniline films have shown these to be sensitive to toxic gases such as NO_x, H_2S and SO_2 at very low concentrations and at room temperature. The response to all three separate gases was characterized by an increase in conductivity that was observed, at low concentrations, to be reasonably reversible, under nitrogen. The device conductivity was observed to increase with increasing gas concentration for all three gases, for concentrations above 4ppm. This increase in conductivity occurred after a delay time of less than 1 minute. Reversibility was achieved only for low gas concentrations after a period of about 2 hours. Comparing all three gases, NO_x produced the smallest increase in conductivity despite being more electrophilic.

In order to establish the origin of the gas-induced increases in conductivity (at high concentrations) in the 'undoped' film, gas sensing measurements were undertaken insitu using reflection absorption Fourier transform infrared spectroscopy. The results demonstrated that, using NO_x, oxidation of benzoid rings into quinoid rings was responsible for the increase in conductivity. For SO_2/spun polyaniline interaction, two types of reaction were identified to account for the increase in conductivity. These were the oxidation of phenyl rings into quinoid rings followed by protonation of existing quinoid rings into semiquinone radicals (rendering the polymer π-conjugated). These two processes combined, are responsible for the higher increase in conductivity of the polymer due to SO_2 compared with NO_x despite being less electrophilic. The H_2S/spun polyaniline interaction has been shown to be a protonation reaction aided by the ever presence of water trapped in the polymer matrix. This screens the effect of the HS^- counter ion on the molecular chain. The changes observed in the infrared spectrum were not reversible, similar to the changes in conductivity under the same (gas concentration) conditions.

9.1.2 Evaporated Polyaniline

Polyaniline was next deposited by thermal evaporation. Freshly evaporated films were colourless but, on prolonged exposure to air, changed to purple and finally to blue. Reproducibility of the deposition process was assessed by film thickness and optical absorbance measurements. The deposition process has been shown to be reproducible for a fixed starting mass and a fixed evaporation temperature of 400°C, for times ranging up to 60 minutes.

Using ultraviolet/visible spectroscopy, the film was determined to be in the leucoemeraldine base form of polyaniline, in which (theoretically) there are no quinoid rings.

The change in colour observed when the evaporated films were exposed to air has also been shown to be the result of benzoid ring oxidation and possibly some oxygenated portions in the polymeric backbone. This suggestion was investigated by exposing the film to I_2+HCl and NH_3. Using ultraviolet/visible spectroscopy, a small shoulder was revealed around 550nm, characteristic of quinoid ring formation. This was confirmed using infrared spectroscopy, in which the quinoid ring stretch at 1597cm^{-1} increased with respect to the benzoid ring vibration at 1507cm^{-1}.

Physically, the evaporated film possessed a globular morphology with some featureless regions. These globules were about 0.1μm in cross-section.

Gas induced changes in dc conductivity of a chemiresistor, using the evaporated film as the sensing layer, have been observed for NO_x, SO_2 and H_2S at room temperature. Exposure of the device produced a non-reversible increase in conductivity for both NO_x and SO_2. The increase in both cases was ascribed to benzoid ring oxidation. This contrasts to the spin-coated films, for which changes upon exposure to SO_2 were ascribed mainly to protonation. Furthermore, unlike the spin-coated film chemiresistor, the evaporated layer was more sensitive to NO_x than SO_2. The NO_x detection threshold level for the evaporated (2ppm) films was comparable to the spin-coated film (4ppm).

The interaction of H_2S with the evaporated film resulted in a non-reversible decrease in conductivity, in contrast to the effect observed with spin-coated

polyaniline films. We ascribe this decrease to an interaction involving the transfer of electrons from the gas to the material.

Using insitu-infrared spectroscopy, we have shown that exposure of evaporated polyaniline to NO_x results in benzoid ring oxidation into quinoid rings. The oxidation process was observed by an increase in the intensity of the quinoid stretch band at 1597cm^{-1} with respect to the benzoid stretch band at 1507cm^{-1}. Results from similar measurements with SO_2 was limited.

9.1.3 Polyaniline LB Films

Polyaniline has also been deposited as thin films by the LB method. The floating film deposited as Z-type layers on glass, with a transfer ratio of 1±0.1 for all dip cycles. Physically, the multilayers were found to be similar in colour to the spin-coated films. When protonated, the LB films also changed colour to green. However, using infrared spectroscopy, the as-deposited films have been shown to be chemically different to the spin-coated films. This was shown by a more intense quinoid stretch vibration band at 1593cm^{-1} with respect to the benzoid band at 1512cm^{-1}. Possible causes for this change include oxidation of benzoid rings into quinoid rings and a reduction in the degree of hydrogen-bonding between molecular chains by the added acetic acid. As a result, the new structure was likened to pernigraniline, in which, for every benzoid ring, there is one quinoid ring in the polymer chain.

At room temperature, NO_x and H_2S, have been shown to increase the dc conductivity of LB layers of a polyaniline chemiresistor. Unlike H_2S, the changes induced by NO_x were irreversible. SO_2, CO and CH_4 have been shown to have no effect on the LB layers of a polyaniline chemiresistor.

LB films of polyaniline have also been deposited on Ni/Ag substrates for surface plasmon resonance measurements. The effect of each gas on the substrate was minimized by coating the Ag with a thin layer of Ni. SPR gas sensing could detect NO_x and H_2S at room temperature. Changes induced by the gases on the sensor increase linearly with the gas concentrations.

The results of the IR experiments were found to be different to those using the evaporated and spin-coated films. For example, exposure of the LB film to NO_x produced a decrease in the intensity of the quinoid stretch band at 1593cm^{-1} with respect to the benzoid stretch band at 1512cm^{-1}. This effect has been related to the formation of semiquinoid radicals from the increased number of quinoid rings formed by the addition of acetic acid to the emeraldine base polyaniline. Furthermore, these changes were also irreversible. Similar measurements using SO_2 confirmed that there is no interaction between SO_2 and the polyaniline LB film.

9.1.4 Lutetium Bisphthalocyanine LB Films

Thin films of lutetium bisphthalocyanine have been deposited on glass and other substrates by the LB method. The as-deposited films were green in colour and retained the same colour when exposed to air. The ultraviolet/visible spectrum was dominated by a peak at 665nm which has been attributed to π-π^* transitions of the macromolecule.

LB films were deposited onto a substrate of Ni/Ag for SPR measurements. The effects of the overlayer, which include a change in the resonance depth and position as well as the half width at half maximum, are small compared to LB or evaporated polyaniline films. This effect is possibly due to the fact that the bisphthalocyanine overlayer absorbs at a wavelength significantly different from that for surface plasmon. Consequently, there will be very little interaction between the single electron located on the molecular ring with the surface plasmon. SPR gas sensing measurements could only detect NO_x at concentrations < 100ppm.

Gas sensing using a lutetium bisphthalocyanine chemiresistor showed responses to NO_x, H_2S and SO_2. The response to H_2S and SO_2 were completely irreversible while that to NO_x was reasonably reversible for low gas concentrations. No response was obtained using CO and CH_4.

Gas/lutetium bisphthalocyanine interactions were also investigated insitu using infrared spectroscopy. Results obtained with SO_2 and H_2S were not very

conclusive because of the limited sensitivity of the measuring system. However for NO_X, a ring oxidation process was evident.

9.1.5 Cobalt (II) methoxyltetraphenyl porphyrin LB Films

Cobalt (II) methoxyltetraphenyl porphyrin in chloroform solution has been shown to form a condensed floating layer on the water subphase surface. This layer deposited onto a solid substrate as a Y-type film, with a transfer ratio close to unity. The LB films have been shown, using a chemiresistor and an SPR sensor, to be sensitive to NO_X at room temperature. The response was observed after a delay time of about 30 seconds and recovered completely when the gas was turned off. Insitu infrared spectroscopy showed that NO_X was <u>not</u> bound on the porphyrin ring.

9.1.6 Comparison of the Chemiresistor and SPR Sensor

Gas sensing studies have been undertaken using conductivity, surface plasmon resonance and infrared experiments. In practice, however, only the first two systems can be used for domestic or small scale applications. By comparing the results obtained from these two techniques, we conclude that devices based on changes in conductivity are generally more sensitive than those based on surface plasmon resonance. In addition, the processing of devices for surface plasmon resonance applications requires a more stringent control of substrate and overlayer film thickness which will consequently increase the sensor cost. However these disadvantages are offset to some extent by the fact that SPR devices were less susceptible to fluctuations in temperature than those based on conductivity changes. Furthermore, in hazardous environments the optical technique might be more appropriate.

9.2 SUGGESTIONS FOR FUTURE WORK

We have shown that the gas response of most of the materials used in this work possesses a degree of cross interference from other gases (i.e., poor selectivity). In a practical sensor, this would be undesirable and may lead to false alarms.

In order to discriminate between the various gases, efforts must be directed at chemically changing the structure of the material.

One such methods has already been shown in this work. This involves mixing the original molecule with other chemical reagents of known redox characteristics. This has been used with polyaniline LB films by mixing acetic acid with 'undoped' polyaniline. Consequently, the SO_2 response was suppressed. The technique of chemical modification to effect a change in the material could be extended to obtain selectivity to other gases, such as H_2S. It is a better and cheaper way than attempting a modifications based on attachment of side groups to the original molecule.

Another problem encountered in this work has been fluctuations in room temperature which affected the stability of the devices. In order to improve on this, two chemiresistors can be arranged in the form of a voltage gain amplifier in which one chemiresistor is screened from the effects of gas exposure (see figure 9.1). The screened device will act as a reference while the other remains active. Such a circuit must possess a low bias input current operational amplifier, since these materials are very resistive. In this configuration, the device monitors only changes to the output voltage which can be related to the gas effect. Temperature compensation originates from the equality of the temperature coefficient of resistivity of the sensing and the reference chemiresistors. This requires an absolute control of the film thicknesses as well as homogeneity. Such a device is actively being researched.

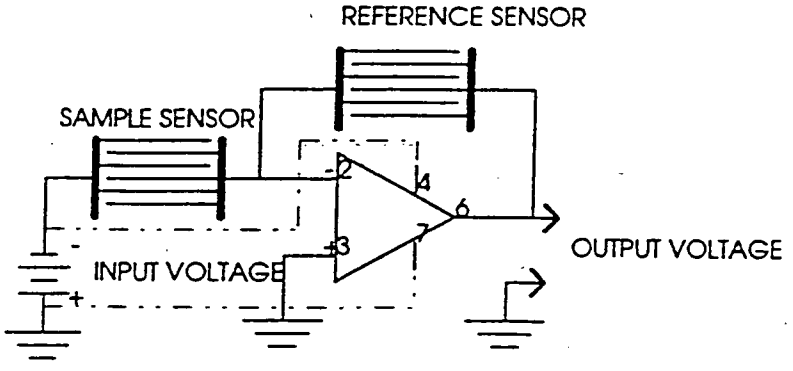

Figure 9.1: A temperature compensated gas sensor.

The materials used in this work are too resistive to be used in a practical gas sensing device based on chemiresistor or as the gate metal of a field effect transistor. At the same time, these materials are less insulating than SiO_2 and unlikely to be used as the insulator in a metal-insulator-semiconductor field effect transistor. This problem may be circumvented using a device known as a charge flow transistor (see figure 9.2). This device would generally operate as an MOS transistor except that the polymer (or any other similar organic material) will form part of the gate. Metallization and bonding represent the very final stages in its processing. The electrical characterisation of this device is now underway and initial results are favourable.

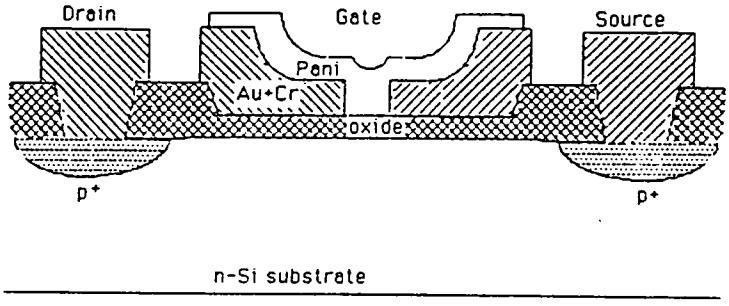

Figure 9.2: The cross-section of a charge-flow transistor.

Cross sensitivity still represents a fundamental weakness in present gas sensors. Suitable techniques for reducing this effect include using software systems based on pattern recognition or neural networks. We have successfully applied the latter method to discriminate between various organic vapours and water on various organic materials [Barker et al, 1993]. It also represents a new focus for research on gas sensors materials.

REFERENCES

Barker, P., Chen, J.R., Agbor, N.E., Monkman, A.P., Mars, P. and Petty, M.C. : submitted to Sensors and Actuators B.

APPENDIX A

PATENT APPLICATION NUMBER UK\9300560.1\1993

UK PATENT ACT 1977

APPLICATION UNDER SECTION 14 -16

INVENTORS:

AGBOR N.E.,
Petty, M.C.,
Scully, M.,
Monkman, A.P.

AGENTS : British Gas Plc, Watson House Research Centre, London. REF WH3429.

TITLE: GAS SENSORS

GAS SENSORS

The present invention relates to gas sensors and to methods of making them.

Applicants are particularly, though not exclusively, interested in gas sensors for use in monitoring gases, such as acid gases, e.g. H_2S, NO_2 and SO_2, in connection for example with industrial process control or environmental protection.

It is well known that organic polymers may form the gas sensing material in gas sensors. Such organic materials include conducting polymers which are normally p-type semiconductors whose conductivities are changed when exposed to oxidising gases such as NO_x or reducing gases such as NH_3. Sensors using such materials have been based on both electrical techniques and optical techniques (e.g. surface plasmon resonance).

Various organic polymers, such as polyaniline, which appear to be suitable as gas sensing materials are commonly deliberately 'doped' to improve the specificivity and/or sensitivity of the materials towards particular gases. Such 'doping' also increases the electrical conductivity and facilitates the detection of change in conductivity of the polymer on exposure to and interaction with the gases being sensed; the change in conductivity being used as a measure of the concentration of the sensed gases.

With some organic polymers, such as polyaniline, in order for doping to be achieved the cationic part of the dopant can only be a hydrogen ion. In such a case the doped form of the polymer can be regarded as the protonated form.

Applicants investigations have revealed that there is a disadvantage with gas sensors comprising such protonated polymers as the sensing material. Applicants have found that the protonated polymers are unstable as gas sensing materials in the sense that they have a tendency to produce inconsistent conductivity readings; thus unreliable results may be obtained. It is believed that this disadvantage is a consequence of the mechanism of the interaction between the gases being sensed and the polymer which involves a direct de-doping or de-protonating process resulting in undesired degradation of the material.

An object of the invention is to overcome or alleviate the disadvantages associated with protonated polymeric materials as mentioned above.

Accordingly, the present invention provides a gas sensor comprising a film or layer of non-protonated polyaniline as the gas sensing material.

In this specification the term "non-protonated" means that less than 1% of the protenatable imine nitrogen in the polyaniline is protonated.

The non-protonated polyaniline may be in the base (neutral) emeraldine form as depicted by the formula :-

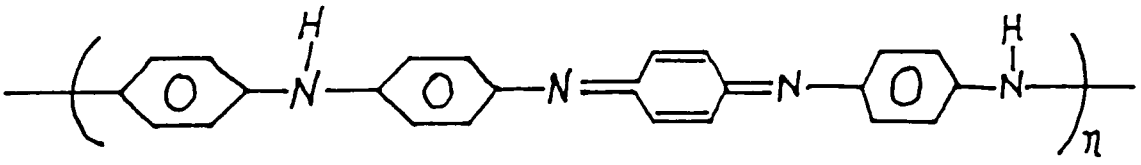

or may be in the base (neutral) leuco-emeraldine form (that is the fully reduced form), as depicted by the formula :-

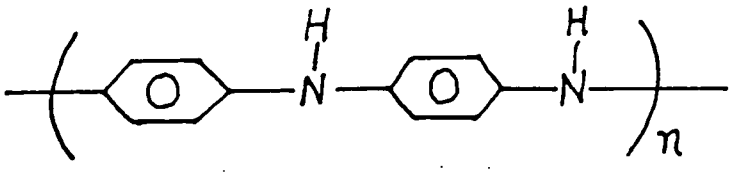

Alternatively, the non-protonated polyaniline may be formed of a mixture of base emeraldine and base leuco-emeraldine forms.

The base emeraldine form appears to be stable up to about 200°C in air while the base leuco-emeraldine form appears to be stable up to about 200°C in an inert atmosphere such as argon or nitrogen.

According to another aspect of the invention a method of making non-protonated polyaniline comprises treating protonated polyaniline with an alkaline solution to de-protonate the material.

The non-protonated polyaniline may be in the base (neutral) emeraldine form as depicted by the formula :-

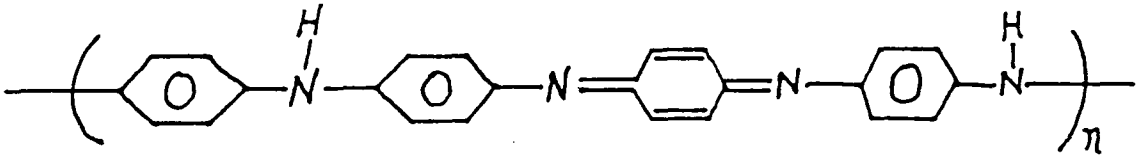

or may be in the base (neutral) leuco-emeraldine form (that is the fully reduced form), as depicted by the formula :-

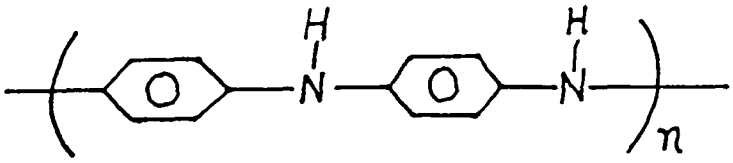

Alternatively, the non-protonated polyaniline may be formed of a mixture of base emeraldine and base leuco-emeraldine forms.

The base emeraldine form appears to be stable up to about 200°C in air while the base leuco-emeraldine form appears to be stable up to about 200°C in an inert atmosphere such as argon or nitrogen.

According to another aspect of the invention a method of making non-protonated polyaniline comprises treating protonated polyaniline with an alkaline solution to de-protonate the material.

The alkaline solution may be an ammonium hydroxide solution.

It will be appreciated that the non-protonated material should not be contacted with a proton-donating species, such as an inorganic acid before being incorporated into a gas sensor.

Dry, solid non-protonated material may be obtained by separating the material from the alkaline solution, for example by filtering, washing the filter cake with water, and optionally in addition with an organic solvent such as isopropanol, after which the filter cake may be suitably dried, for example under vacuum at room temperature.

The dried non-protonated material may be stored in a dry inert atmosphere, for example in a vacuum desiccator.

Where the gas sensor is based on an electrical technique, the film or layer of non-protonated polyaniline may conveniently be deposited on a substrate already supporting spaced electrodes, so that the deposited film or layer bridges the spaced electrodes. For example, the substrate may have thereon a pair of interdigitated electrodes.

The thickness of the film or layer may be from about 5 nanometers to about 5 micrometers.

The substrate may be any suitable insulating, inert material such as the material forming a printed circuit board or glass

or quartz.

The electrodes may be made of any suitable inert conductor, such as gold, platinum, or gold-plated copper.

Various methods or techniques may be used to deposit the film or layer on the substrate. For example, in one method the polyaniline may be dissolved in a suitable solvent, such as N-methyl-2-pyrrolidinone (NMP), to produce a solution, for example of 0.01 to 10% Wt/wt concentration, from which the film or layer may be cast or spun onto the substrate. In one such a method it is preferred to subject the solution to centrifuging which, in effect, serves as a spin filtration step which filters out undissolved particles of polyaniline, before 'spreading' a film on a horizontally disposed substrate employing a spinning operation. In the spinning operation a predetermined amount of the solution is deposited on the substrate which is supported on a horizontal spinning surface arranged to spin about a vertical axis. Initially the spinning surface is slowly accelerated to a relatively slow speed which is maintained for a period to distribute the polyaniline over the substrate, after which the speed is increased to a maximum in order to produce a substantially uniform thin film.

In another method the polyaniline may be deposited by vacuum evaporation or sublimation onto the substrate in accordance with procedures generally known per se. In a further method

the polyaniline film or layer may be formed by using Langmuir-Blodgett techniques generally known per se.

In order that the invention may be more readily understood reference will now be made, by way of example, to the accompanying drawings, in which :-

Figure 1 illustrates in schematic and block diagram form, apparatus for measuring the resistance/conductivity of a film of non-protonated polyaniline deposited on an interdigitated electrode structure to form a gas sensor,

Figure 2 is an ultra-violet/visible absorption spectrum of non-protonated emeraldine base form of polyaniline which the inventors made and heat treated at 120°C for ten minutes in vacuum,

Figure 3 shows a current against voltage characteristic of the non-protonated emeraldine base form of polyaniline in air at room temperature when using gold-plated copper interdigitated electrodes,

Figure 4 illustrates the effect that the presence of N_2 on non-protonated emeraldine base form of polyaniline has on the conductance of the film,

Figure 5 shows the conductivity response curve of the sensor when the non-protonated polyaniline film is exposed to 8ppm of

H_2S at room temperature,

Figures 6, 7 and 8 illustrate how the conductivity changes in a film of non-protonated polyaniline in the base emeraldine form (obtained by spin-coating) on exposure at room temperature to different concentrations of NO_x (i.e. NO_2O_4 etc.), SO_2 and H_2S, respectively,

Figures 9, 10 and 11 illustrate how the conductivity changes in a film of non-protonated polyaniline in the leuco-emeraldine form (obtained by vacuum evaporation) on exposure at room temperature to different concentrations of NO_2, SO_2 and H_2S, respectively,

Figures 12 and 13 illustrate how the conductivity changes in a film of non-protonated polyaniline in the base emeraldine form (obtained by Langmuir-Blodgett deposition technique) on exposure at room temperature to different concentrations of NO_x and H_2S, respectively,

Figure 14 is an infra-red absorption spectrum of a sample of non-protonated emeraldine base form of polyaniline made by the inventors,

Figure 15 is an infra-red absorption spectrum of a sample of slightly protonated form of polyaniline, and

Figures 16 and 17 show on an enlarged scale portions of

spectra similar to those shown in Figures 14 and 15, respectively.

A method of preparing non-protonated polyaniline in powder form

The "emeraldine base" form of polyaniline was prepared as follows. Aniline (0.1 moles) was added to hydrochloric acid solution (100ml, 3.5%, ca. 0.1 moles HCl) in a 250ml beaker, and mixed using a magnetic stirrer to give a solution with a final pH between 1 and 2, as measured by indicator paper. Ammonium persulphate (0.1 moles) to act as the oxidising agent to effect polymerisation of the aniline was dissolved in distilled water (60ml), and this was added to the stirred reaction mixture. The mixture turned a dark blue/green colour and the reaction was observed to be slightly exothermic over a period of about 10 minutes. The mixture was left to stir for a total of about 6 days, after which it was filtered and washed with water, then methanol (to remove any low molecular weight species), and finally with more water. The filter cake was added to an ammonia solution (100ml, 35%) and stirred for 7 hours before filtering and repeatedly washing with water, occasionally interspersed with washing with isopropanol. At this point the filtrate was colourless, indicating that the filtrate had been washed sufficiently. The filter cake was then dried under vacuum at 20°C for 24 hours to give a brown/purple product which was crushed using a mortar and pestle.

Elemental analysis showed that the material contained small residual amounts of chlorine (0.50 wt%) and sulphur (0.38 wt%). 4.69 wt% was not accounted for and, inventors believe, is ascribed to oxygen, possibly associated with the chlorine or sulphur, or with trapped solvent species (water, methanol, or isopropanol). Isopropanol was subsequently positively identified in ^{13}C spectra. Chlorine and sulphur residues are normally found in the products of such preparations and they remain largely unchanged by attempts to wash them out suggesting that they may be present as ring substituents.

Preparation of the Gas Sensor

Example 1 - using spin-coating to form a thin film of non-protonated polyaniline.

Polyaniline powder obtained from the above described method of preparation was dissolved in N-methyl-2-pyrrolidinone (NMP) at 20°C in an amount to produce a 5% (by wt.) solution (blue in colour) of polyaniline.

The solubility of the polyaniline in the solvent was found to improve with time and after 48 hours the solution was further prepared (prior to forming a thin layer on the electrode structure) in either of the two following ways :-

1. By centrifuging the solution and then decanting, Applicants obtained satisfactory results by repeating these operations several times, for example three times,

with the centrifuge operating each time at a speed of about 4000 rpm for a period of about 30 minutes.

2. By homogenising the solution, for example at a speed of about 20500 rpm for about 10 minutes.

The centrifuging process is used, in effect, as a filtration like step to remove relatively larger particles/aggregates from the solution whilst the homogenising process is used to break up and disperse the relatively larger particles/aggregates in the solution.

Samples from the resulting centrifuged or homogenised solution are then used in a spin-coating operation which deposits or forms a thin film of the polyaniline on the surface of the cleaned electrode structure.

Spin-coating techniques are known per se and in the present operation the parameters were controlled so that the resulting thin film on the electrode structure had a substantially constant thickness of, for example, about 1 micrometer (μm) (± 0.01 μm).

In the spin-coating operations conducted by the inventors it was possible to program specific spinning conditions into the spinner control apparatus in relation to the initial acceleration phase, the constant speed spinning periods and the deceleration phase so that duration times, spinning speeds

and ramp were controlled.

As an example, the inventors found that the following spinning conditions involving essentially four steps produced satisfactory films :-

(i) The spinner surface supporting the cleaned electrode substrate structure was accelerated from zero in a few seconds to 520 rpm which was maintained for 60 secs to distribute the polyaniline over the electrode structure.

(ii) At the end of the 60 secs at 520 rpm, the speed was accelerated to 1500 rpm (within a few tenths of a second) which was maintained for 60 secs in order to produce the thin film of substantially uniform thickness.

(iii) At the end of the 60 secs at 1500 rpm, the spinner was decelerated to 300 rpm (within a few tenths of a second) which was maintained for 20 secs to aid solvent removal so that the film does not shrink before it is 'dry'.

(iv) At the end of the 20 secs at 300 rpm, the spinner was decelerated to zero speed (within a few tenths of a second).

Thus the spinning operation only a little over 2 minutes 20 seconds.

The inventors found that high quality films could be reproducibly formed using the above described procedure. The quality of the films was judged using optical microscopy, with high quality films being considered to be ones which were not only of substantially uniform thickness but were relatively free from 'pin-holes'.

The interdigitated electrode structure comprised a pair of gold-plated copper electrodes which had been photolithographically developed onto a substrate of printed circuit board or glass. Each electrode had 32 digits or fingers. The overlap distance of the electrode digits or fingers was about 14.3mm whilst the finger width and spacing was about 0.381mm.

The electrode structure now carrying the thin film was then heated in a vacuum oven at about 10^{-2} mbar to a temperature of 120°C for 10 minutes to remove NMP solvent from the film substantially completely.

Both uncoated and coated electrode structures were subjected to experiments involving the recording of current passed therethrough against applied voltage at room temperature (20°C) in the dark by using the apparatus as shown in Figure 1.

Gas sensing measurements were performed on the gas sensor structure by exposing the sensor to different gases (diluted

in N_2) in a chamber through which the gases were passed - as will be described below. (The gases were all obtained from British Oxygen Company - Special Gases Division with purities up to 99% and were introduced into the chamber via a Signal Instrument Series 850 gas blender).

With the object of producing thin films of the polyaniline for analysis purposes, the thin films were produced by spinning the polyaniline onto glass substrates at a speed of about 3000 rpm for 30 seconds using solutions of the polyaniline powder (as prepared above) dissolved in NMP as solvent, in solvent:solute weight ratios of 10:1, 100:1 and 1000:1. In each case the solutions obtained were dark blue indicating that the polyaniline is in a non-protonated form. Protonated polyaniline does not dissolve in the NMP solvent to any significant extent unless specific surfactant counter ion acids are used to protonate the material.

Again the thin films, this time supported by the glass substrates, were transferred to a vacuum oven and heated at 10^{-2} mbar to a temperature of 120°C for 10 minutes.

The thickness of the thin films of polyaniline formed by the spinning process on the glass substrates was found to be of the order of 0.1 μm as measured using a surface profiling Talystep.

Figure 2 is a representative example of the UV-VIS spectrum of the heat treated polyaniline film, obtained using a Perkin-Elmer Lambda 19 spectrophotometer. Two adsorption bands are clearly evident at about 320nm and 635nm and these are considered to be characteristic of the non-protonated emeraldine base form of polyaniline.

The inventors interpret the above findings as confirmation that no significant thermally induced chemical degradation took place during the vacuum heating process to remove solvent.

Example 2 - using an evaporation deposition method for forming a thin film of non-protonated polyaniline.

An evaporation method carried out in a vacuum chamber was used to produce a thin film of non-protonated polyaniline in the base leuco-emeraldine form on a substrate such as a glass substrate or on an electrode structure located in the chamber. Incorporated into the system was a temperature controller which maintained a substantially constant source temperature, an adjustable shutter to control the deposition/growth time and a mask to define the specific area of deposition. Initially a source boat or container, located within the chamber but separated from the substrate, was heated up to 300°C to drive off surface contamination. 40 mg of non-protonated polyaniline powder obtained from the earlier described method were then introduced into the source boat and

the system was evacuated to a background pressure of 10^{-3}mbar. With the shutter closed, the temperature was raised to and maintained at 400°C by means of a heater. When a stable pressure was reached, the shutter was opened and evaporated polyaniline was thereby allowed to pass into the region containing the substrate and to deposit through the mask onto the substrate. The deposition was allowed to proceed for a predetermined or fixed length of time for control purposes. After such deposition, the system was allowed to cool to room temperature and return to ambient pressure, and the substrate bearing the deposited film removed. A typical thickness of the deposited film obtained by the above described method was found to be about 120 nm for a shutter time of 30 min.

Example 3 - using a Langmuir-Blodgett method for forming a thin film of non-protonated polyaniline.

Preparation of a solution of the Polyaniline

Using non-protonated polyaniline obtained from the earlier described method, a solution of the polyaniline for use in LB film deposition was prepared by first making a mixture of 1:10 by weight of acetic acid:polyaniline (as an aid to spreading). The acid was completely absorbed by the polymer and no change in colour from the dark blue of the polyaniline was observed. 0.1mg of the mixture was then dissolved into 10ml of solvent and sonicated for 30 minutes. The solvent used was a mixture of chloroform:n-methyl-2 pyrrolidinone in a 1:5 weight ratio.

LB Film Formation

The non-protonated polyaniline solution was added to a tank of water and the solution was found to spread uniformly on the water surface without any visible sign of aggregation. The surface pressure versus area isotherm at 20±2°C after multiple (~4) compressions revealed the material to form a reasonably condensed layer up to 40mNm^{-1} surface pressure. On the assumption that the area per molecule of the acetic acid was negligible, the area per emeraldine base repeat was 0.20nm^2 at 30mNm^{-1} surface pressure. It was thus concluded that the polymer did not form a monomolecular film on the water surface. The floating film was stable for several hours at a surface pressure of 30mNm^{-1}. The substrate on which the film was to be formed was dipped into the floating film at speeds of 2mmmin^{-1}, allowing at least 20 minutes between the first and second dips. Z-type deposition with a transfer ratio of 1.0±0.1 on all dip cycles was observed. The films formed on the substrates were reasonably uniform, by visual inspection, for up to 50 layers.

By way of illustration, the 10:1 sample which produced, via the spin-coat method, good quality films was used to form the thin film on the electrode structure.

With reference to the apparatus in Figure 1, a sample of the electrode structure bearing the thin film of non-protonated polyaniline 1 is held in the dark and at constant temperature

(20°C) in a sample chamber 2. A voltage is applied to the electrode structure via a D.C. voltage calibrator 3 (in effect, a constant voltage source) while current through the film is monitored via the picoammeter 4. A voltage output is derived from the picoammeter 4. A voltage output is derived from the picoammeter and applied to the y-axis of a y-t chart recorder 5. Thus the chart recorder will reflect change in current through the film (and thus the resistance/conductance) as a function of time. An offset unit 6 allows a constant voltage to be added (in parallel with the output from the picoammeter) in order to 'back-off' the output of the picoammeter and allow small current changes to be monitored.

A test gas source 7 and a dilution gas source 8 (nitrogen in present experiments) are connected to a gas blender 9 via respective inlets 10 and 11. An outlet 12 from blender 9 is connected to the sample chamber for introducing the blended gases into the chamber 2.

Figure 3 shows good linearity of the current versus voltage characteristic in respect of the thin film of polyaniline on the interdigitated electrode structure as a result of experiments conducted in air at room temperature (20°C). Experiments conducted on the uncoated electrode structure produced results (not shown) that confirmed that in the case of the coated electrode structure substantially all of the current which was flowing across the structure was flowing through the polyaniline film rather than the substrate. The

good linearity of the current versus voltage characteristic and the increase in slope of the line observed by the inventors for thicker films (data not shown) indicate that ohmic contacts were established between the electrodes and the polymer film.

The conductivity of the sample was calculated to be 1.5×10^{-11} Scm^{-1} which was a good comparison with a literature value of 1×10^{-11} Scm^{-1}.

The conductivity was found to be relatively stable in air but on exposure to a flow of nitrogen gas in the sample chamber it decreased, rapidly at first, over a period of minutes to a lower stable value. Such a change is shown in Figure 4 in a case where 200 mV was applied across the electrode structure. The change in conductivity is attributed to the removal of water molecules trapped in the polymer matrix. The final stable conductivity in N_2 was considered to provide a good baseline for the gas sensing experiments.

Gas sensing measurements were carried out at room temperature (i.e. 20°C) using test gases diluted in nitrogen, as mentioned above. For each experiment the polyaniline coated electrode structure served as a chemiresistor and the effect of exposing the chemiresistor to the different gas was studied. In separate experiments, each test gas (diluted with N_2) was introduced into the sample chamber, so as to be in contact with the polyaniline film, for a specific length of time which

was chosen having regard to the sensitivity of the device to the particular test gas.

The test gases used were NO_x, H_2S, SO_2, CO and CH_4. On exposure of the polyaniline film to any of the gases NO_x, H_2S and SO_2 a substantial increase in current flow through the film, and thus an increase in conductivity, was observed. In contrast, on exposure of the film to CO or CH_4 no measurable change in the conductivity was observed.

Figure 5 shows a typical response of the sensor when exposed to 8ppm of H_2S. The response was found to be reversible with a short delay time. In Figure 5, τ represents the delay time, i.e. the time between turning 'on' the test gas and the first measurable change in current through the polyaniline film sensor. This delay time includes the time taken for the test gas to flow from its source through connecting pipework to the sample chamber and the time to interact with, and cause a resistance change in, the film. Thus, although in Figure 5 the delay time is shown as approximately 30 seconds, the actual response of the sensor will be much less.

Conductivity measurements which resulted by exposing non-protonated base emeraldine form (obtained using the spin-coating method), when used as the gas sensing material, to different concentrations of NO_x, SO_2 and H_2S are shown respectively in Figures 6, 7 and 8. It can be seen that H_2S has the largest effect on the conductivity across the sensor

while NO_x has the smallest effect. Substantially reversible responses were obtained using any of these three gases.

Conductivity results obtained by exposing the non-protonated base leuco-emeraldine form (produced via the vacuum evaporation method), when used as the gas sensing material, to different concentrations of NO_2, SO_2 and H_2S are shown respectively in Figures 9, 10 and 11. It will be noted that while this form of the polyaniline was again also sensitive to exposure to the gases, it led to different responses compared with those shown in Figures 6, 7 and 8. In particular, with respect to sensing H_2S an increase in concentration of the gas led to an increase in current in Figure 8 but a decrease in current in Figure 11.

Illustrative conductivity measurements which resulted by exposing non-protonated base emeraldine form (obtained using the Langmuir-Blodgett preparation method), when used as the gas sensing material, to different concentrations of NO_x and H_2S are shown respectively in Figures 12 and 13. It will be noted that the responses obtained here are different compared with the previously illustrated responses.

Applicants have noted that the three different methods described above for forming the films or layers of the organic polymeric material enable a very wide range of film thicknesses to be obtained and it is envisaged that appreciation of this may enable the sensitivity of the films

to particular gases to be optimised.

Illustrations of results obtained from the experiments are summarised in Tables 1, 2 and 3. In these Tables, "Normalised change" relates to the sensitivity of the film to the various gases; it is the fractional resistance change ($\Delta R/R$) divided by the gas concentration (ppm). The greater the figure obtained, the more sensitive is the film to the particular gas concerned.

It will be appreciated that by initially employing known concentrations of gases the results can be used to calibrate the gas sensor, such that subsequently when an unknown concentration of gas is used the conductivity measurement can be used as a measure of the gas concentration.

The results obtained from the above described experiments indicated that non-protonated polyaniline, as opposed to protonated forms of polyaniline is stable at room temperature and with respect to the flow of gas thereover, and can be used as a selective, reproducible and reversible sensing material in a gas sensor for sensing the presence of e.g. H_2S, NO_x and SO_2 in very low concentrations (down to a few parts per million) at room temperature. The selectivity to different gases can be determined by the different values or the slope of the response curve.

To assess whether a sample of polyaniline is "non-protonated"

use can be made of infra-red absorption spectographs. Figure 14 shows an infra-red spectrum of a sample of non-protonated emeraldine base form of polyaniline made in accordance with the method of the invention, while Figure 15 shows an infra-red spectrum of slightly protonated (i.e. greater than 1%) polyaniline. In Figure 15, towards the high energy end of the spectrum a large rising background is visable. This is due to a charge transfer band of emeraldine caused by the protonation. The extent of protonation can be determined by comparing the relative peak heights of the peaks in about the 1594 cm^{-1} and 1512 cm^{-1} band regions. In the case of the slightly protonated sample, see Figure 17 where the peak in the 1594 cm^{-1} band region is of higher intensity. In the case of the "non-protonated" sample, it is the peak in the 1512 cm^{-1} band region which is of higher intensity, albeit shifted slightly in energy - see Figure 16 and the shift from about 1512 cm^{-1} to about 1501 cm^{-1}. The present inventors used this kind of data to estimate that the degree of protonation of the samples of "non-protonated" polyaniline was less than 1%.

CLAIMS

1. A gas sensor comprising a film or layer of non-protonated polyaniline as the gas sensing material.

2. A gas sensor as claimed in claim 1, in which the non-protonated polyaniline is in the base emeraldine form having the formula :-

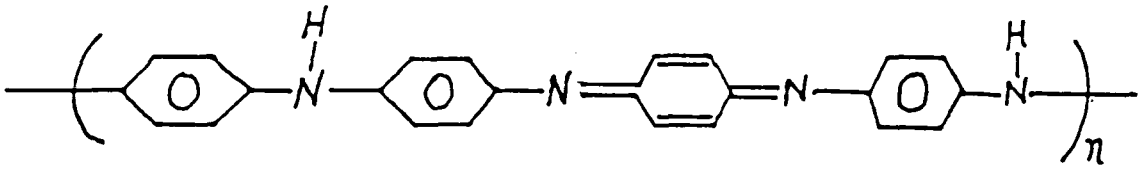

3. A gas sensor as claimed in claim 1, in which the non-protonated polyaniline is in the base leuco-emeraldine form having the formula :-

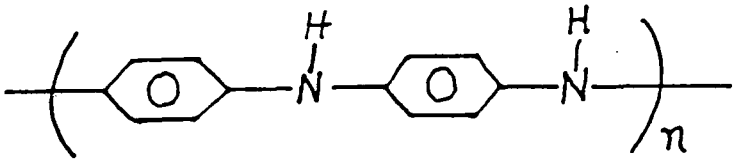

4. A gas sensor as claimed in any of the preceding claims, in which the film or layer of non-protonated organic material is deposited on a substrate which supports spaced electrodes, with the film or layer bridging the spaced electrodes.

5. A method of making non-protonated polyaniline comprises treating protonated polyaniline with an alkaline solution to de-protonate the material.

6. A method of sensing a gas, comprising contacting a film or layer of non-protonated polyaniline forming the gas sensing material with the gas, determining the conductivity of the film or layer so contacted, and using the determined conductivity as a measure of the concentration of the gas contacting the film or layer.

7. A method for the preparation of a gas sensor substantially as hereinbefore described with reference to the Examples.

ABSTRACT

GAS SENSORS

A gas sensor for use in monitoring gases such as H_2S, NO_2 or SO_2 comprises a film or layer of non-protonated polyaniline as the gas sensing material.

INFORMAL

1/19

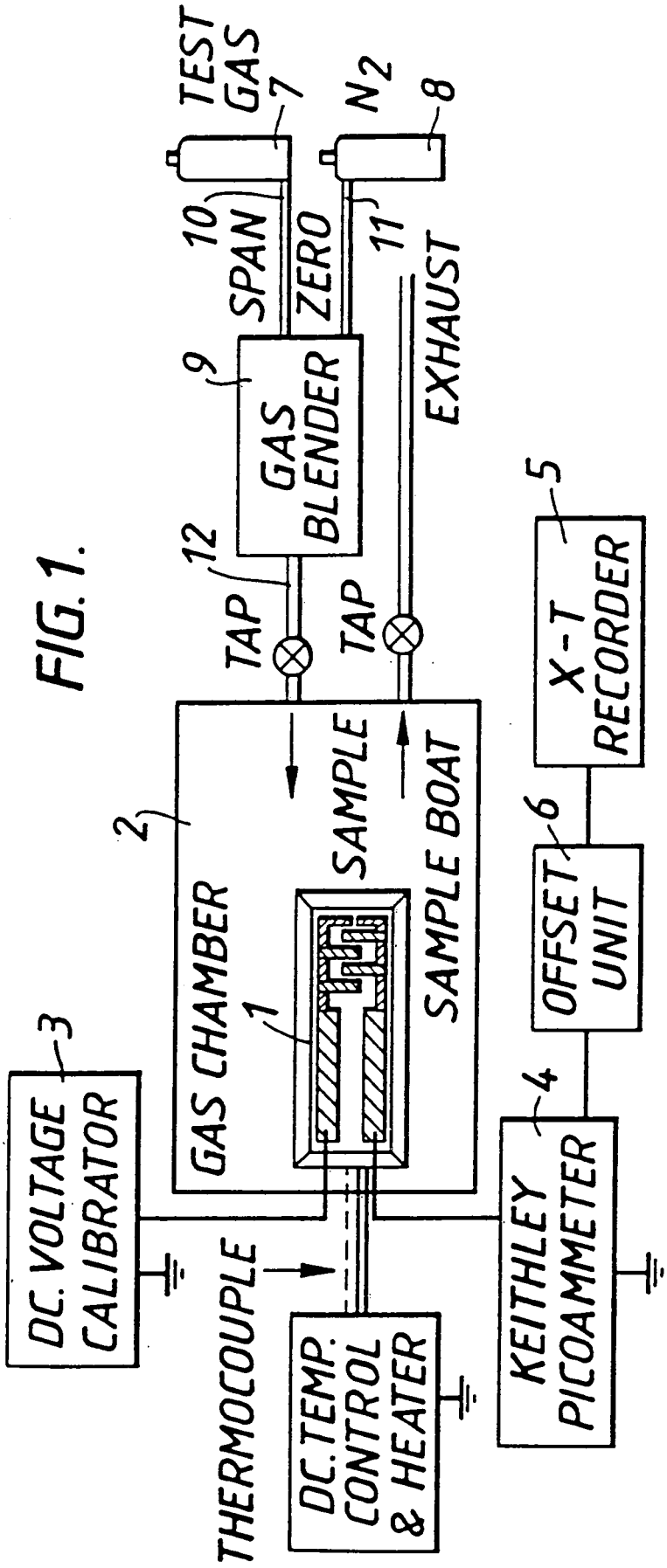

FIG. 1.

INFORMAL

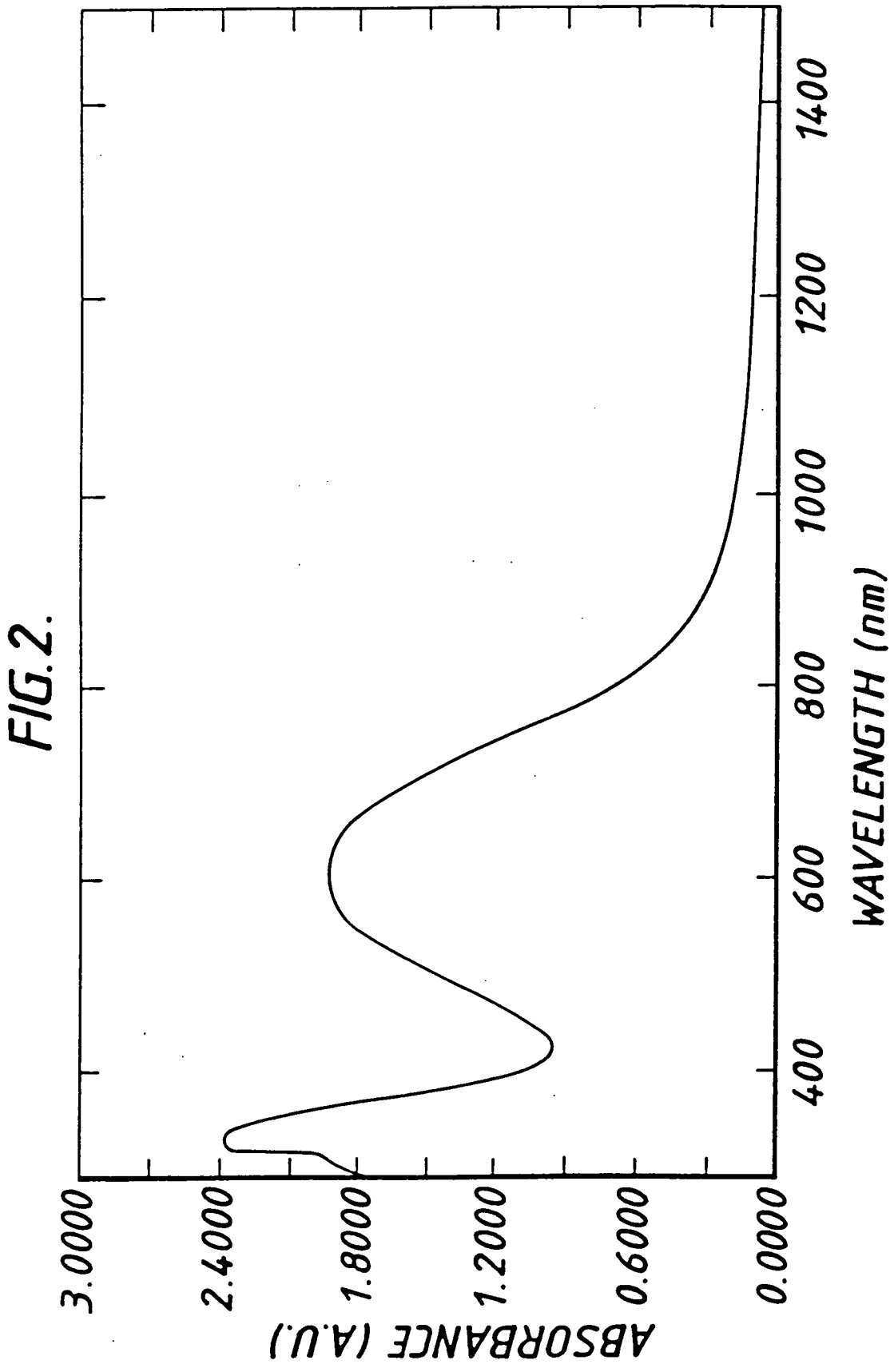

FIG.2.

INFORMAL

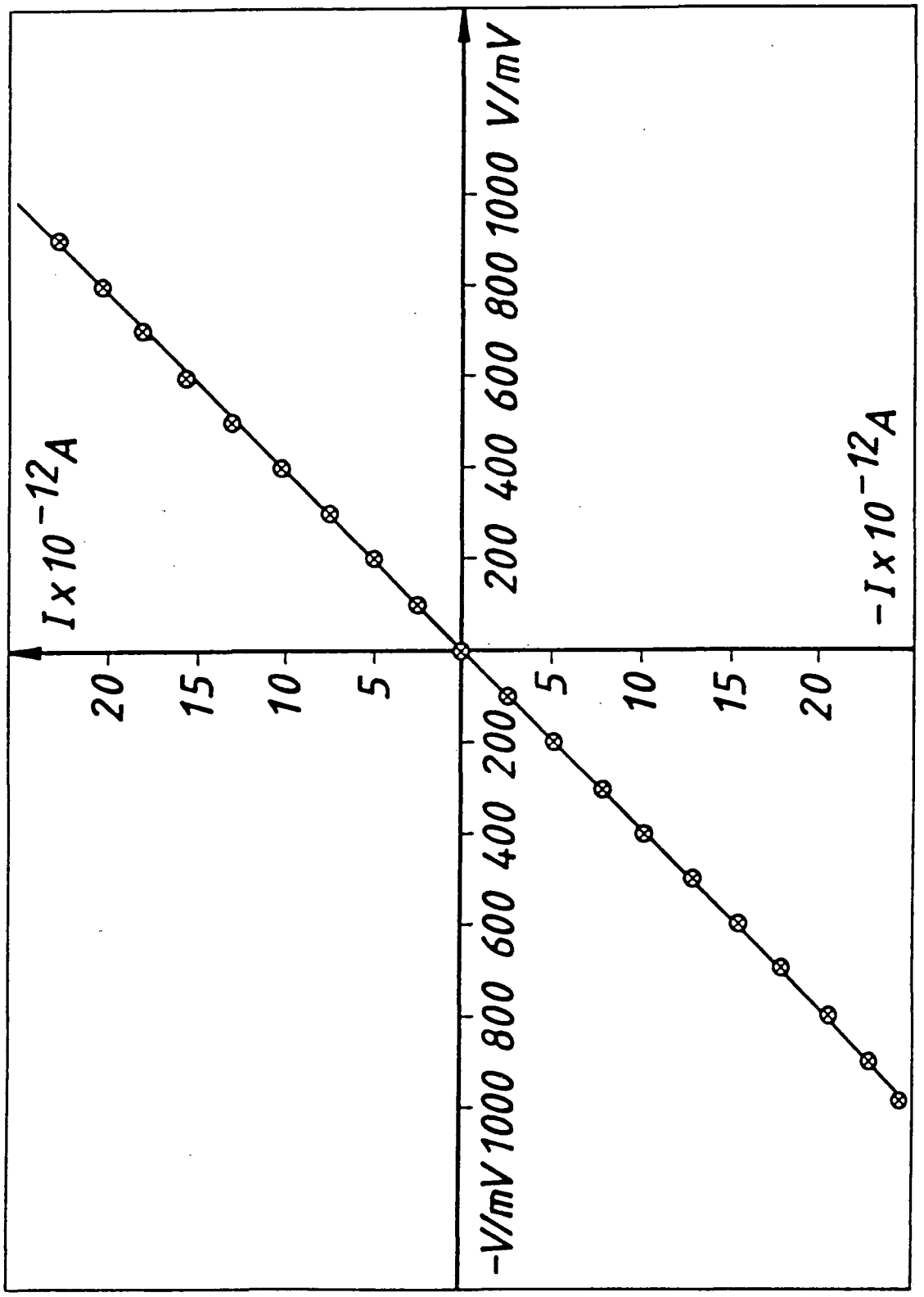

FIG.3.

INFORMAL

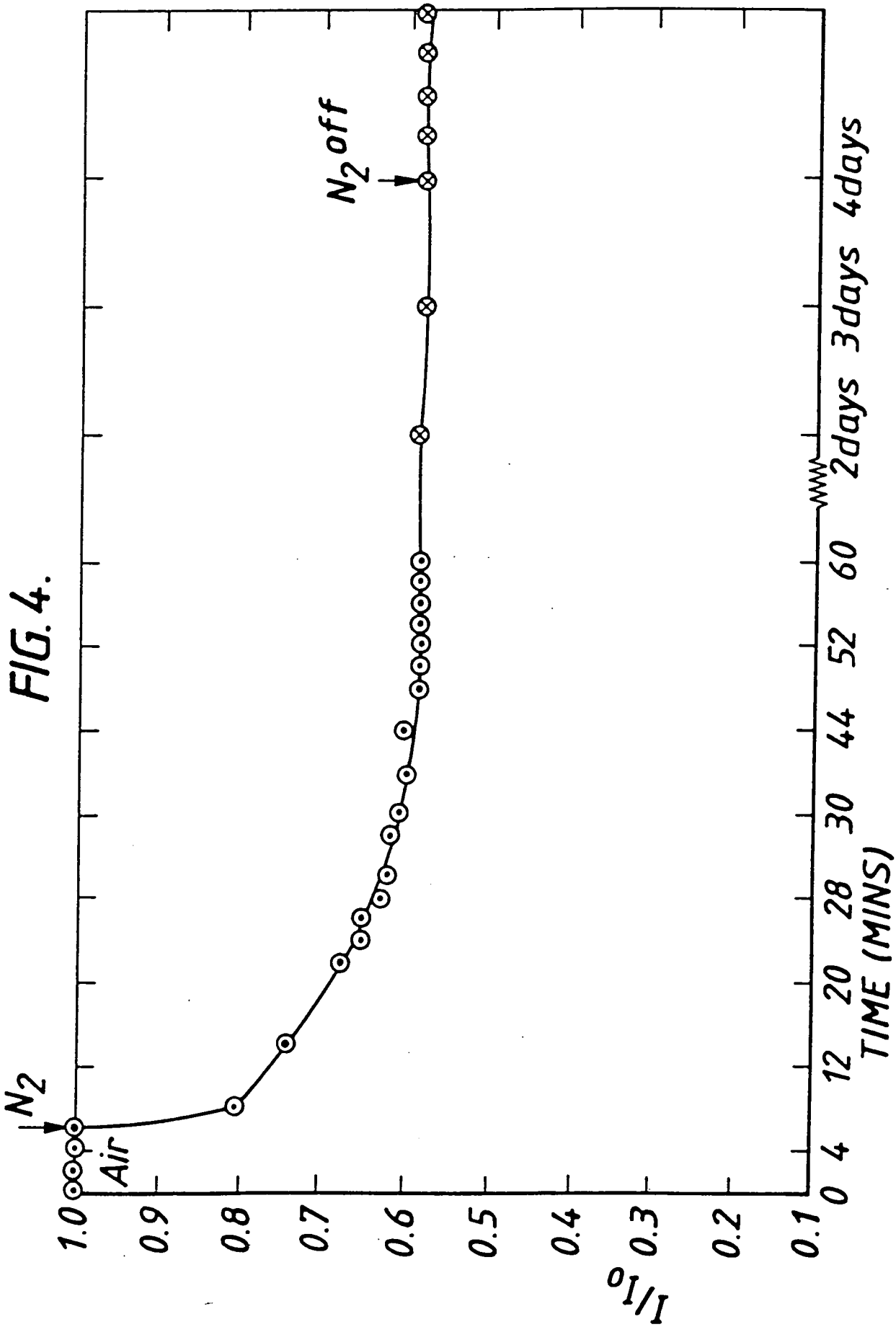

FIG. 4.

INFORMAL

5/19

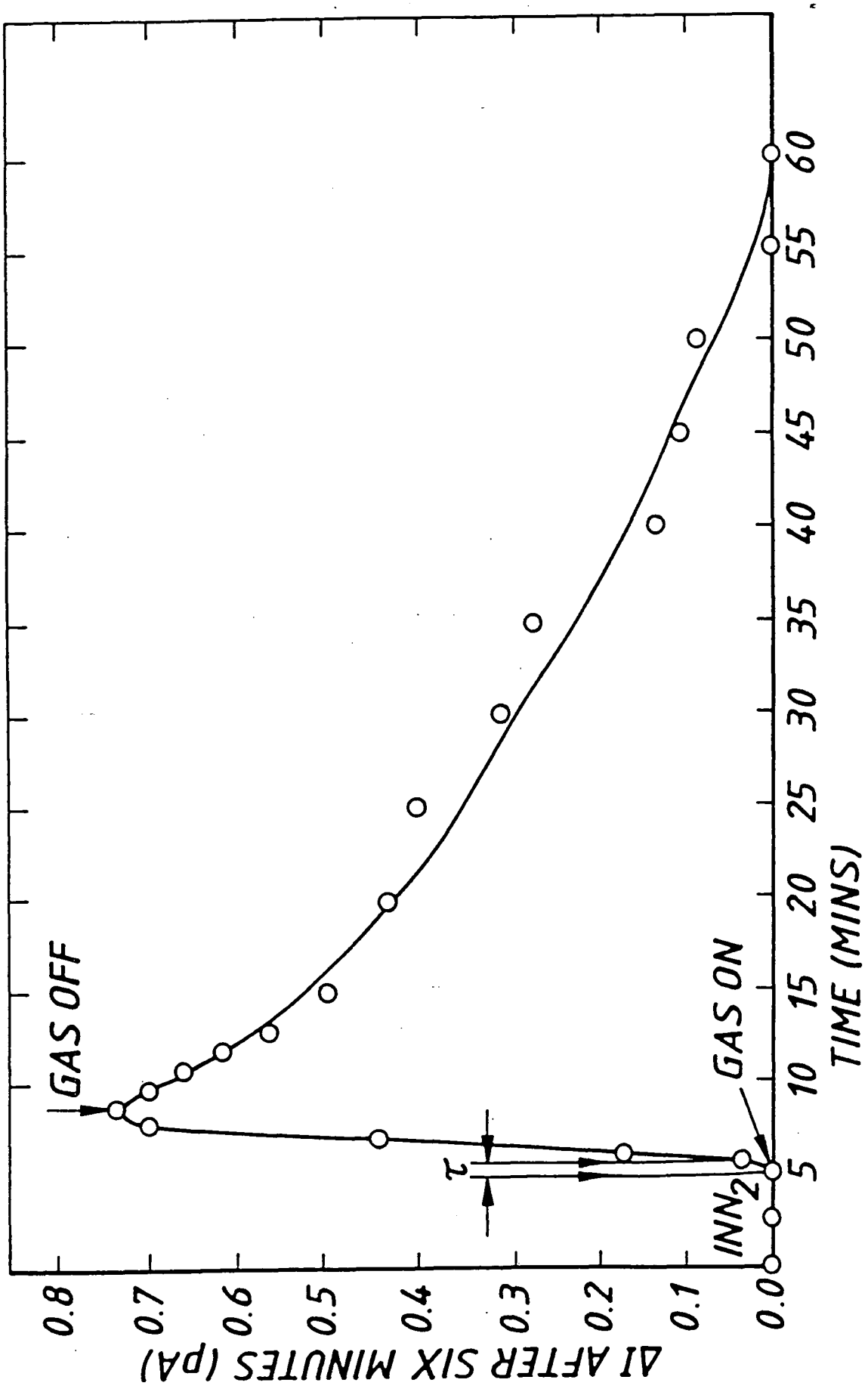

FIG.5.

INFORMAL

FIG. 6.

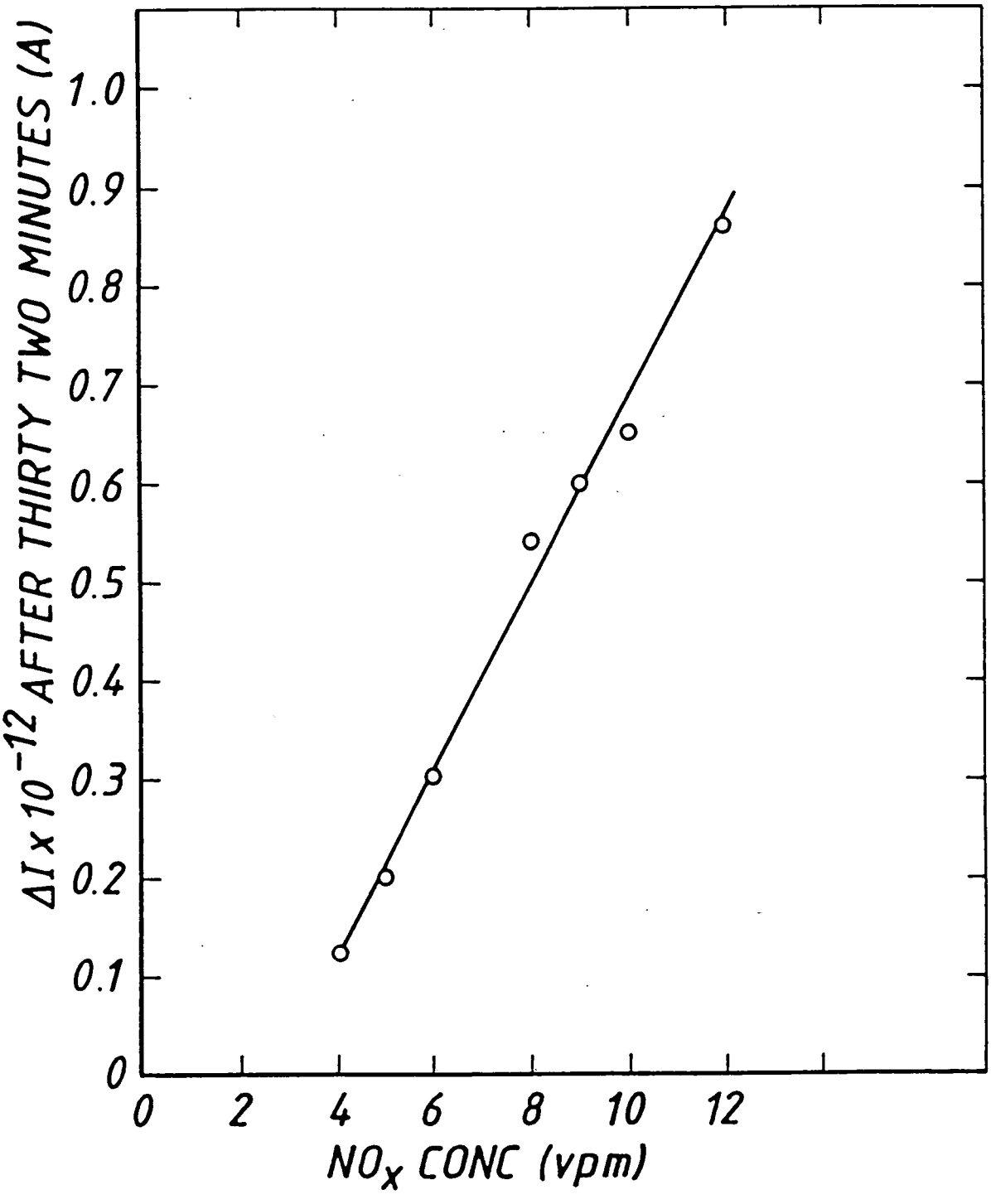

INFORMAL

FIG. 7.

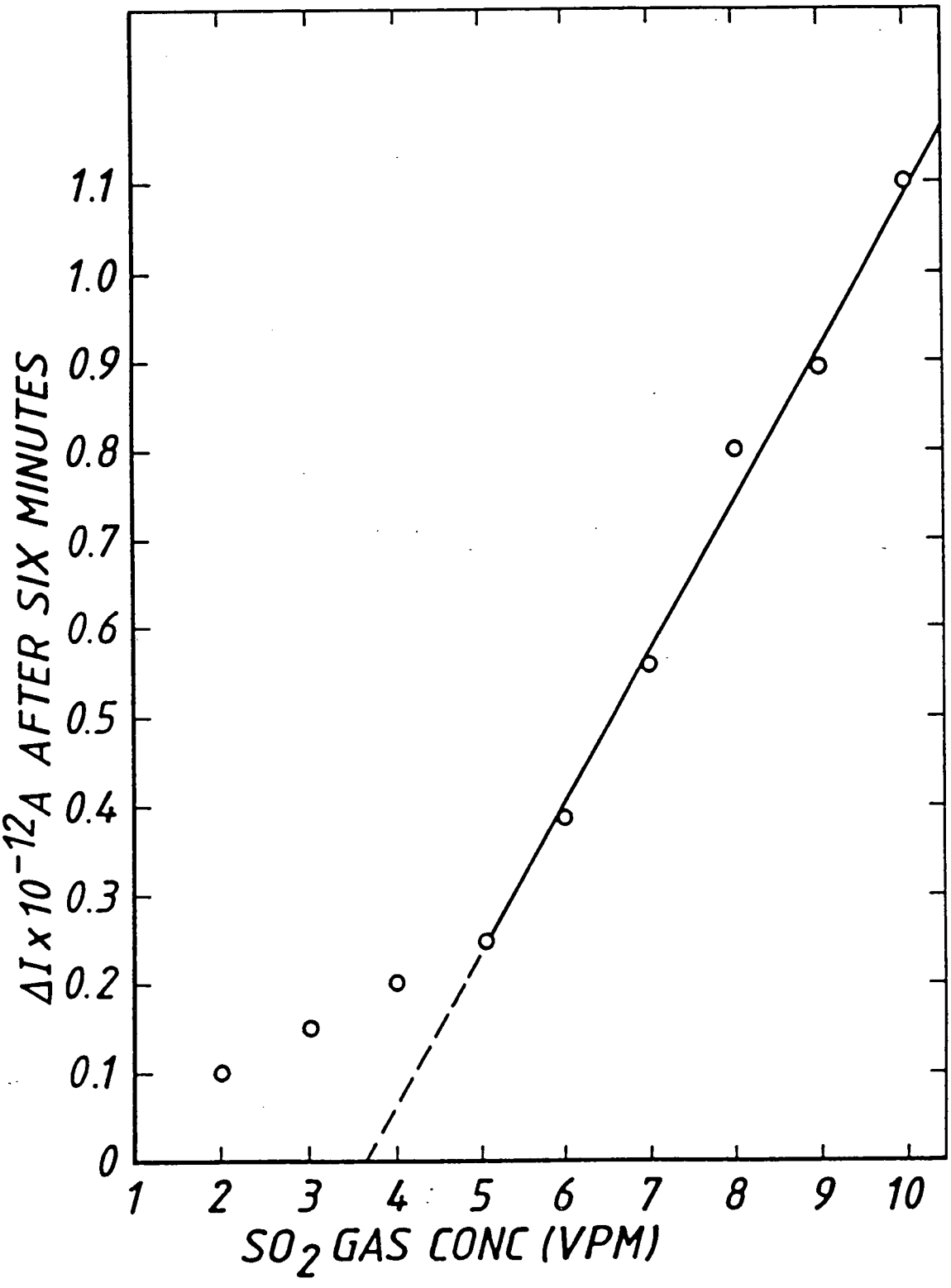

INFORMAL

8/19

FIG. 8.

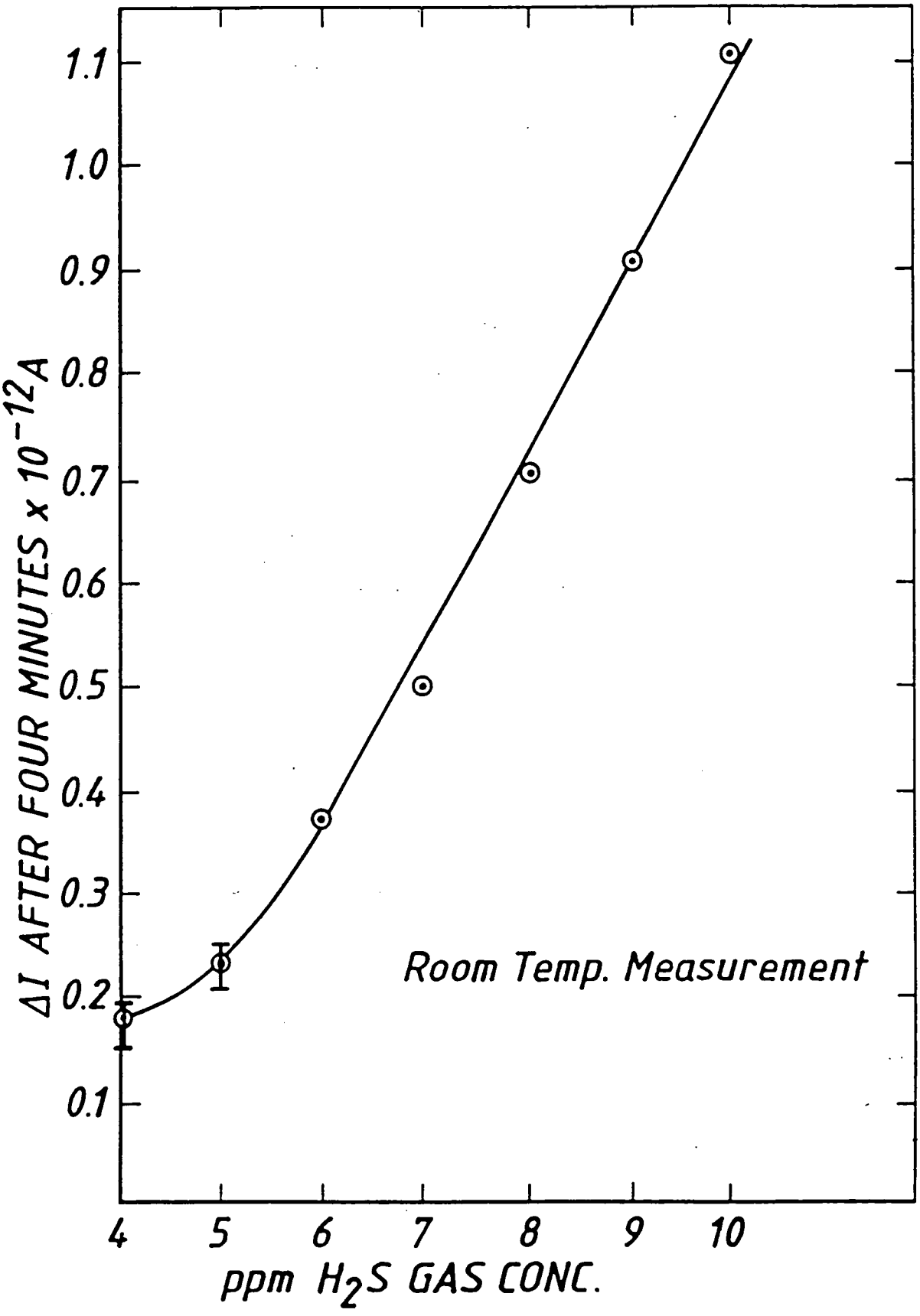

INFORMAL -

FIG. 9.

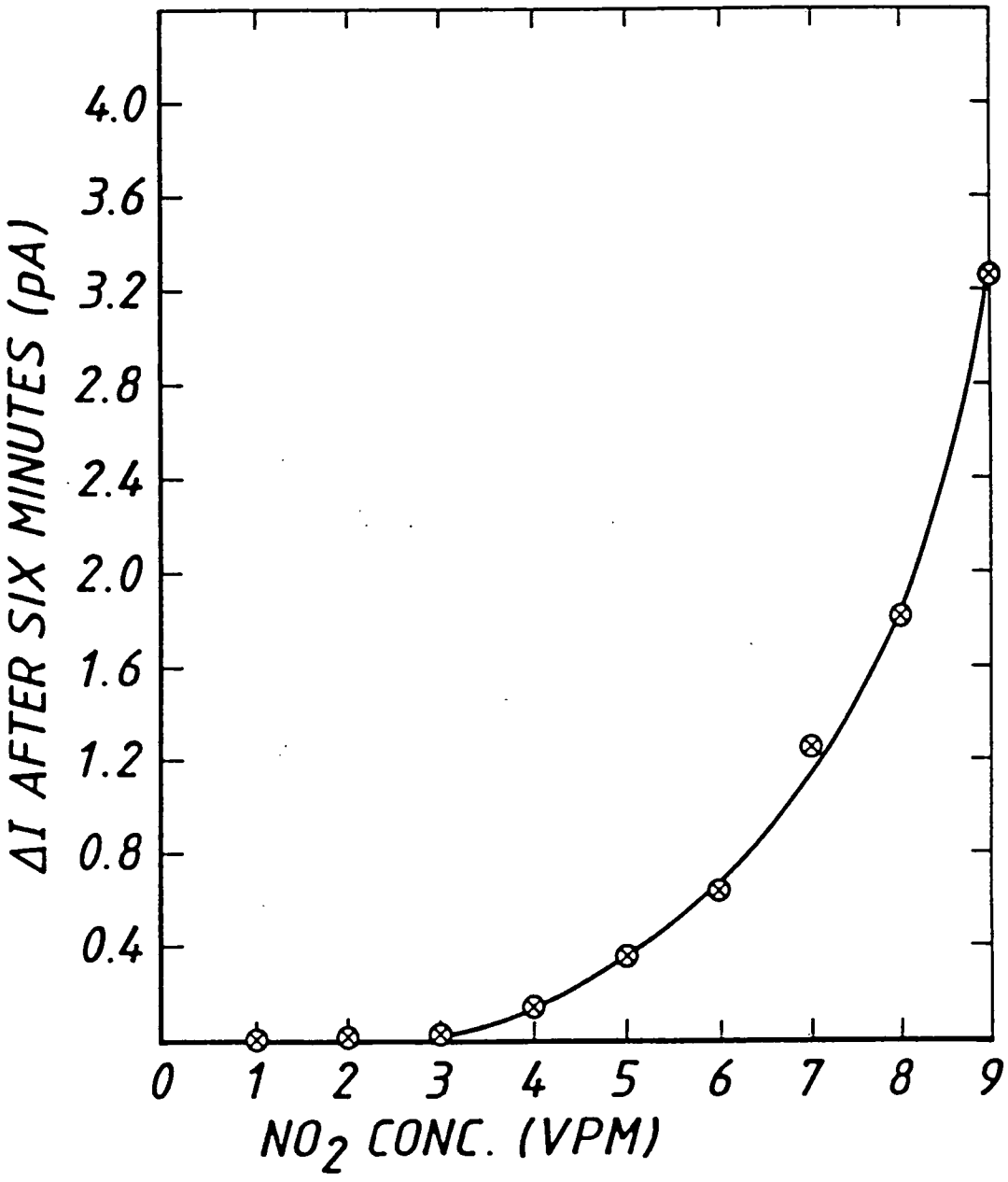

INFORMAL

FIG. 10.

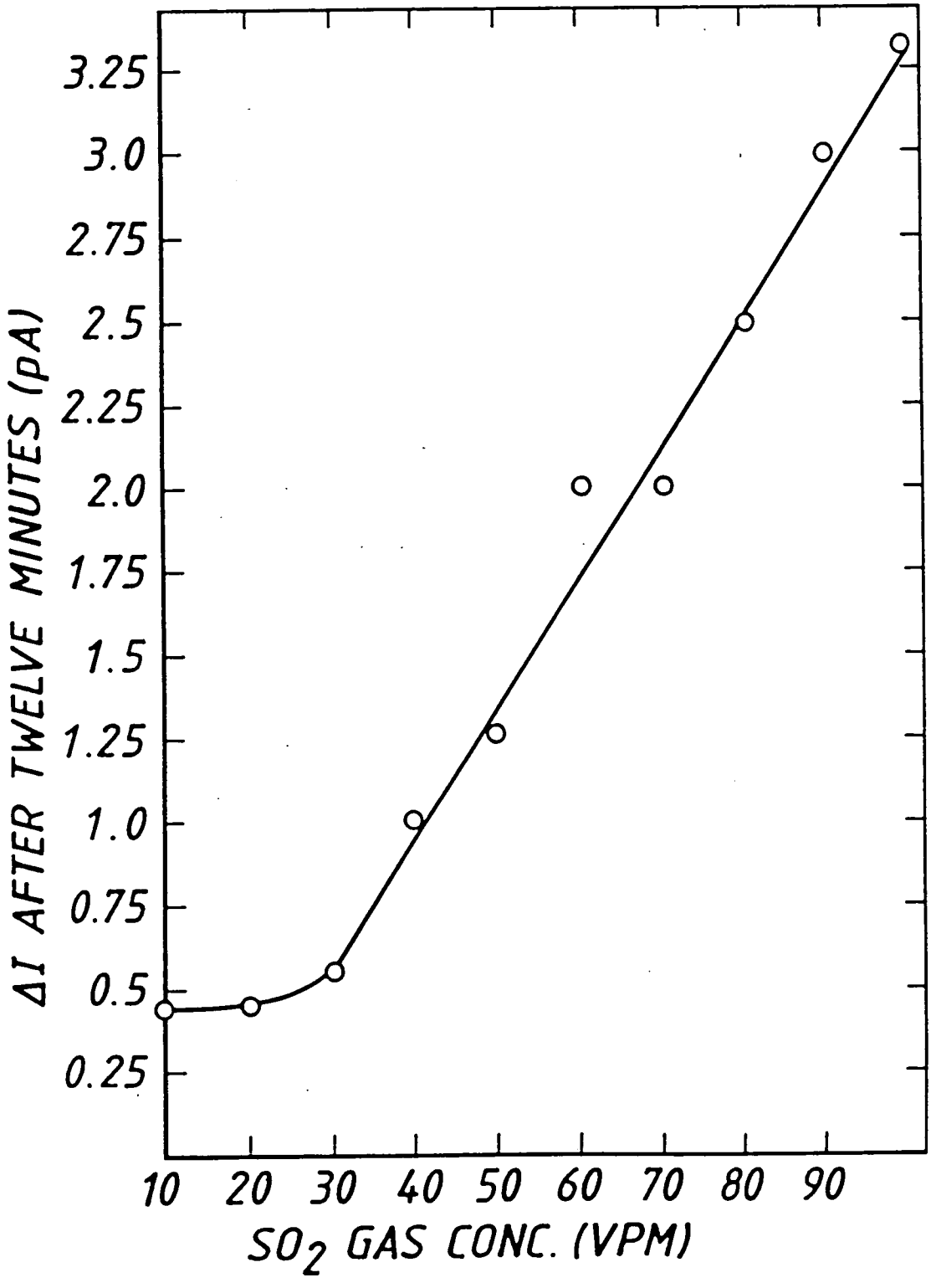

INFORMAL

FIG.11.

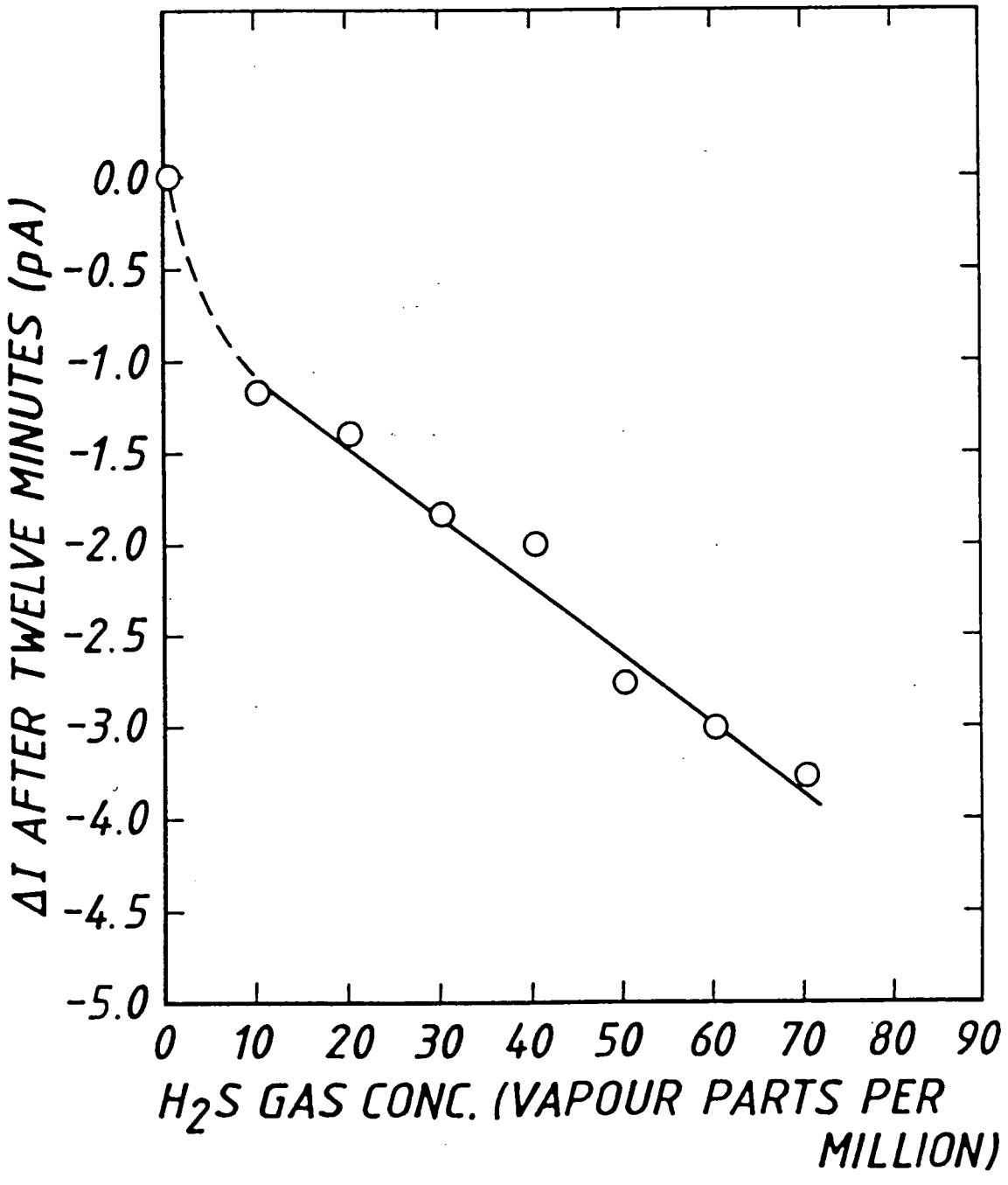

INFORMAL

FIG. 12.

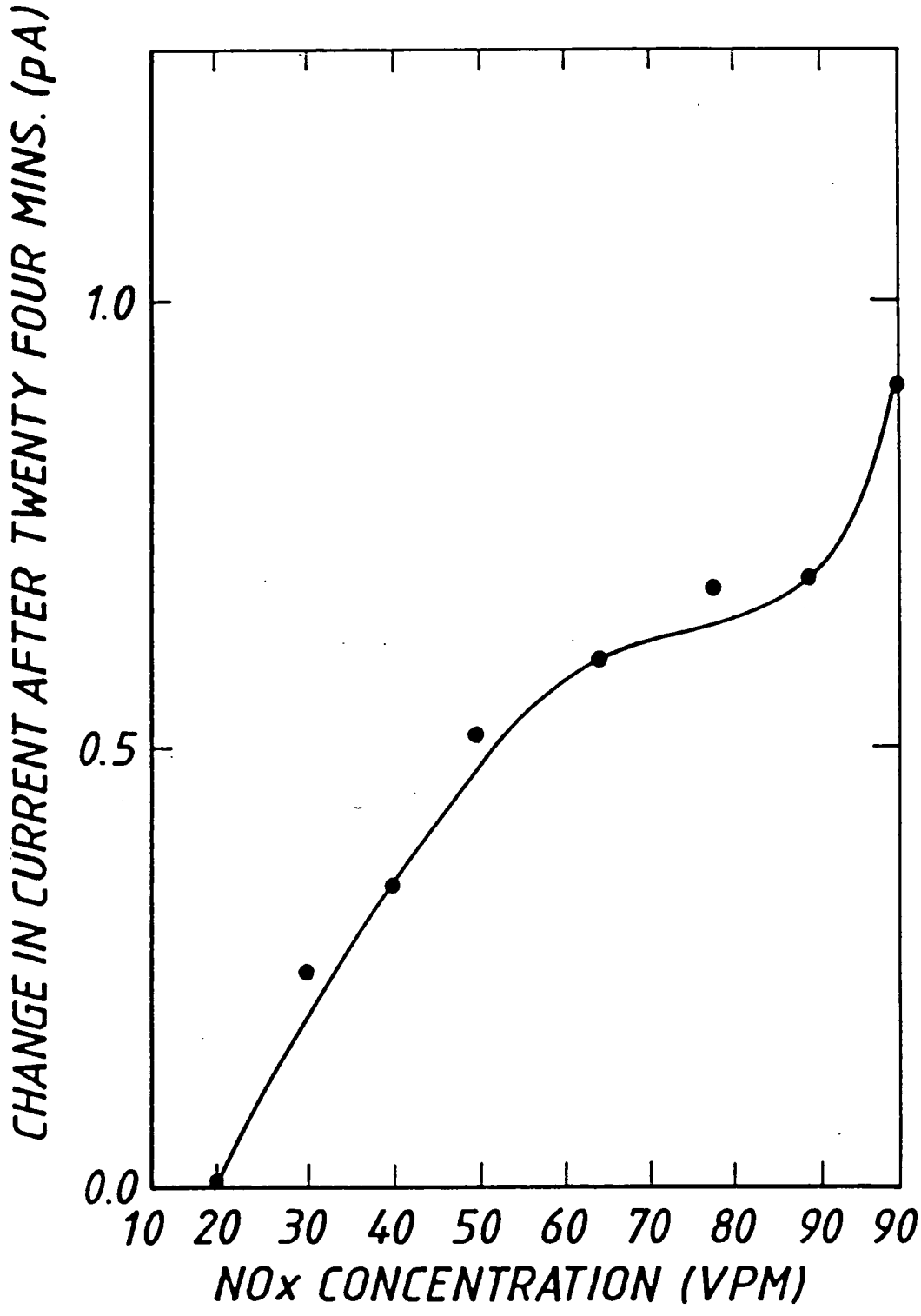

Effect of NOx on eighteen layers of LB-PANi at room temperature

INFORMAL

13/19

FIG.13.

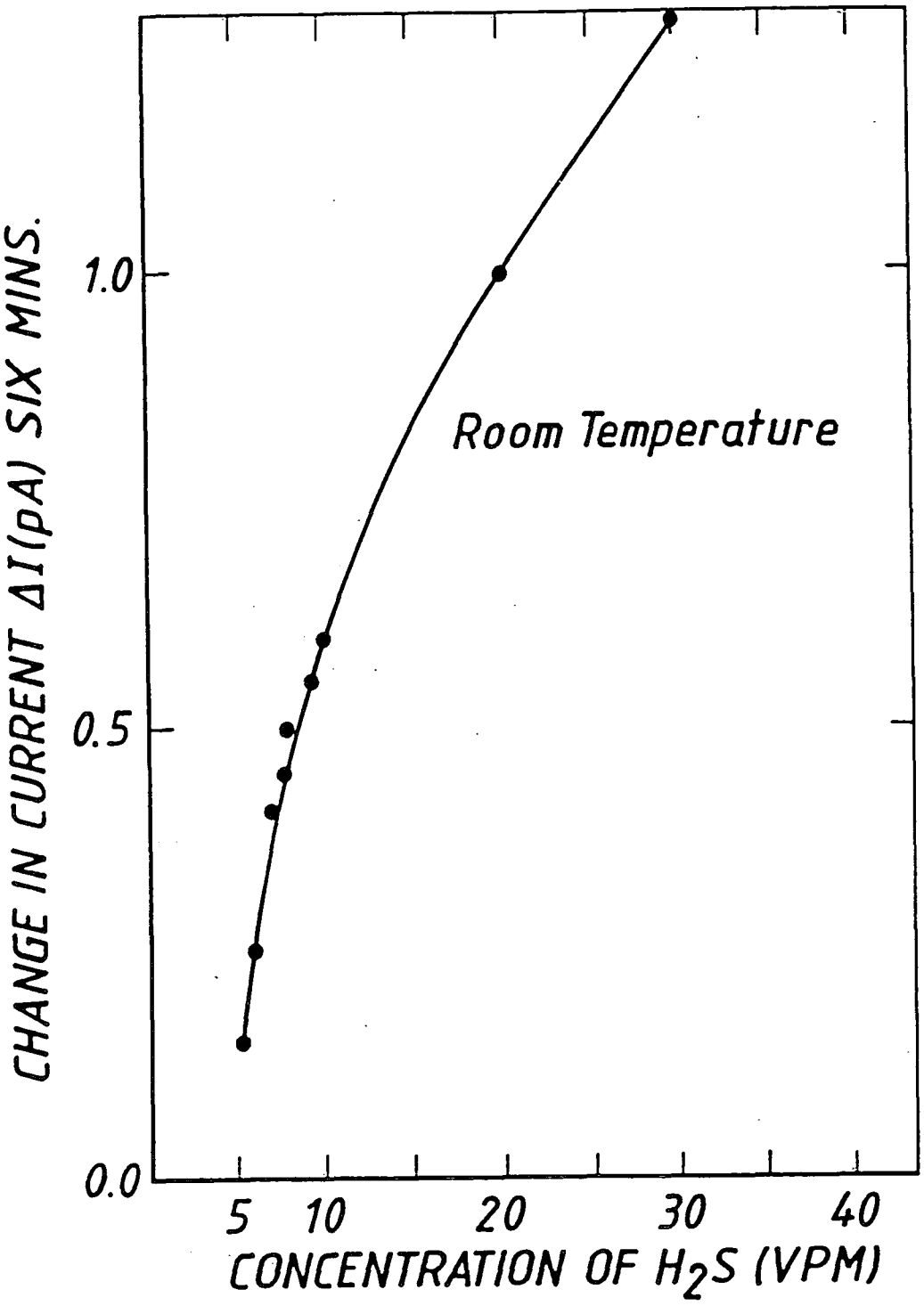

Variation of the effect of H_2S on eighteen layers LB PANi on interdigitated electrodes at room temperature

INFORMAL

14/19

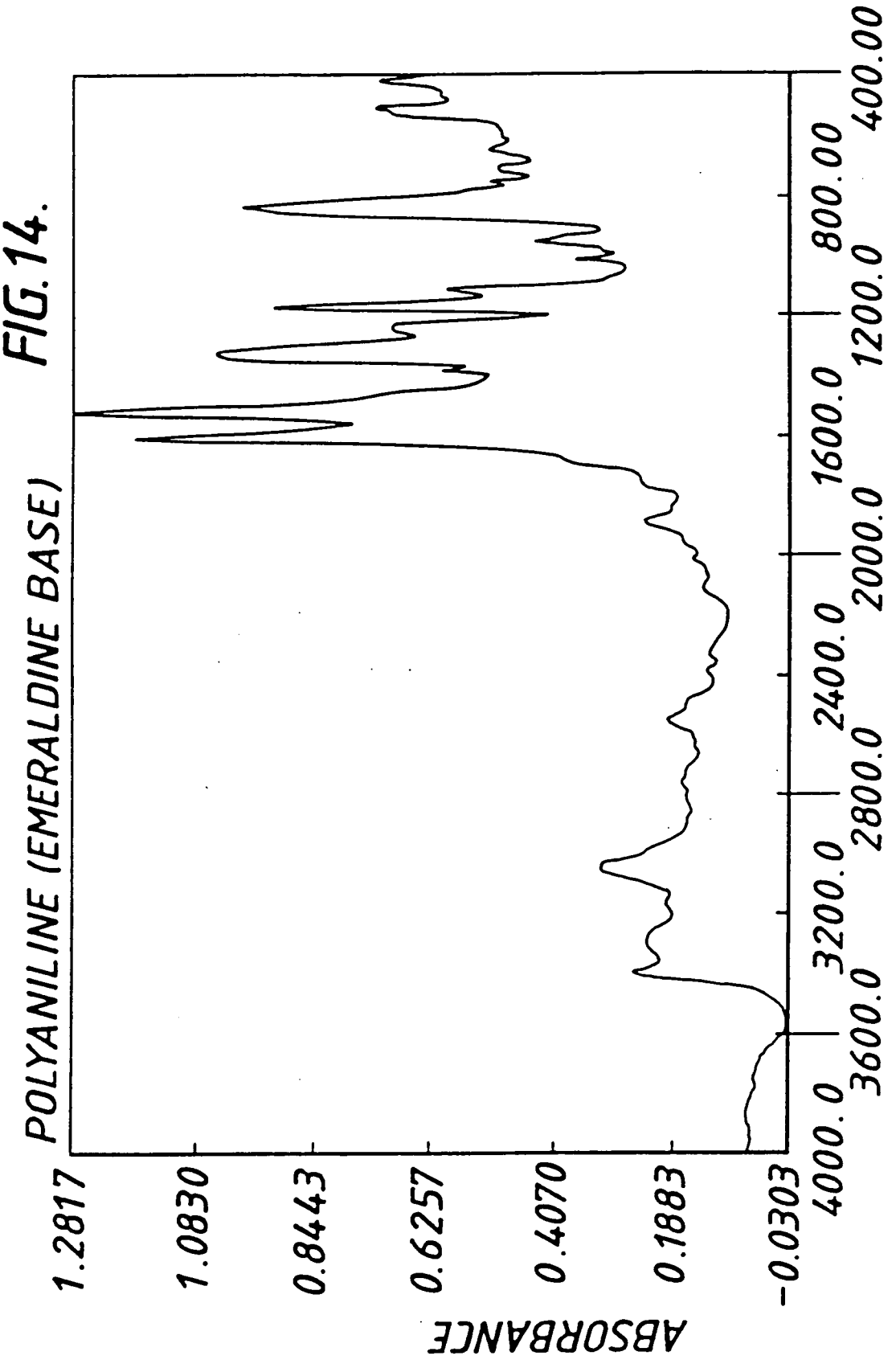

FIG. 14.

INFORMAL

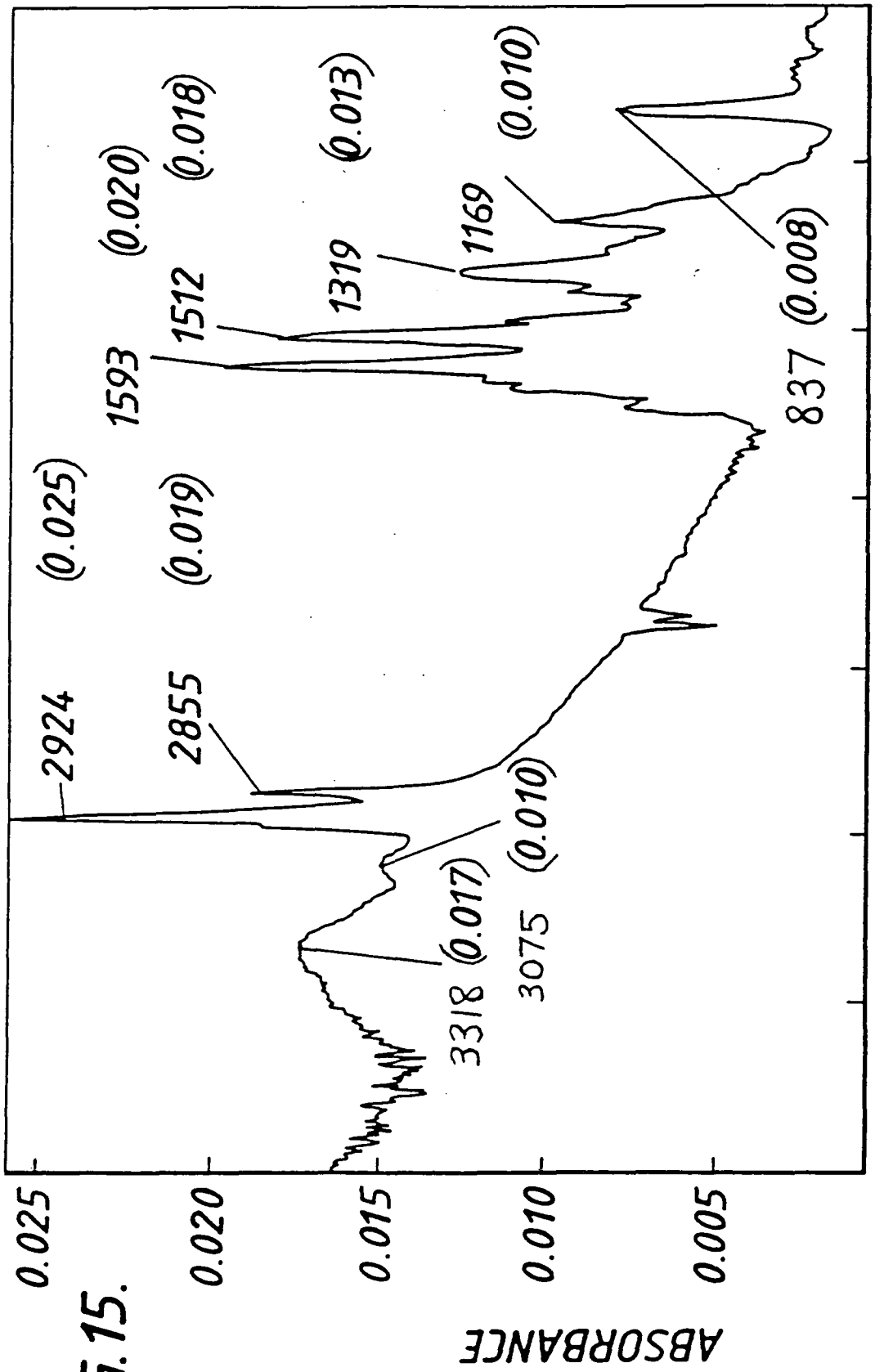

FIG. 15.

INFORMAL

FIG.16.

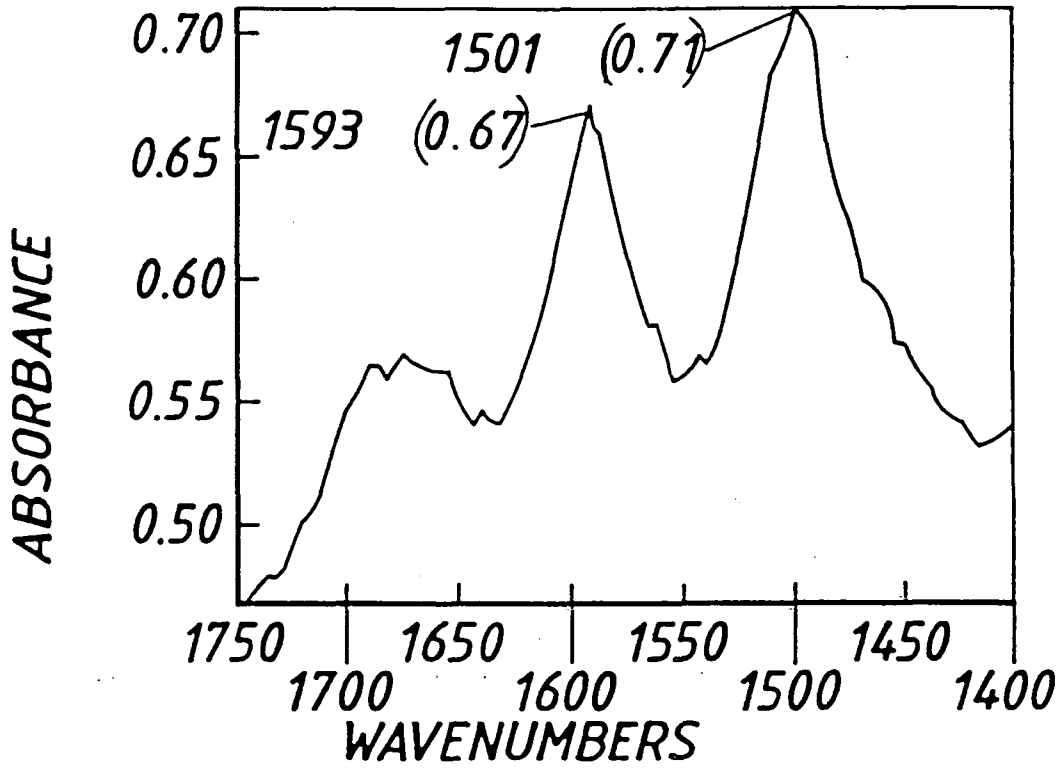

FIG.17.

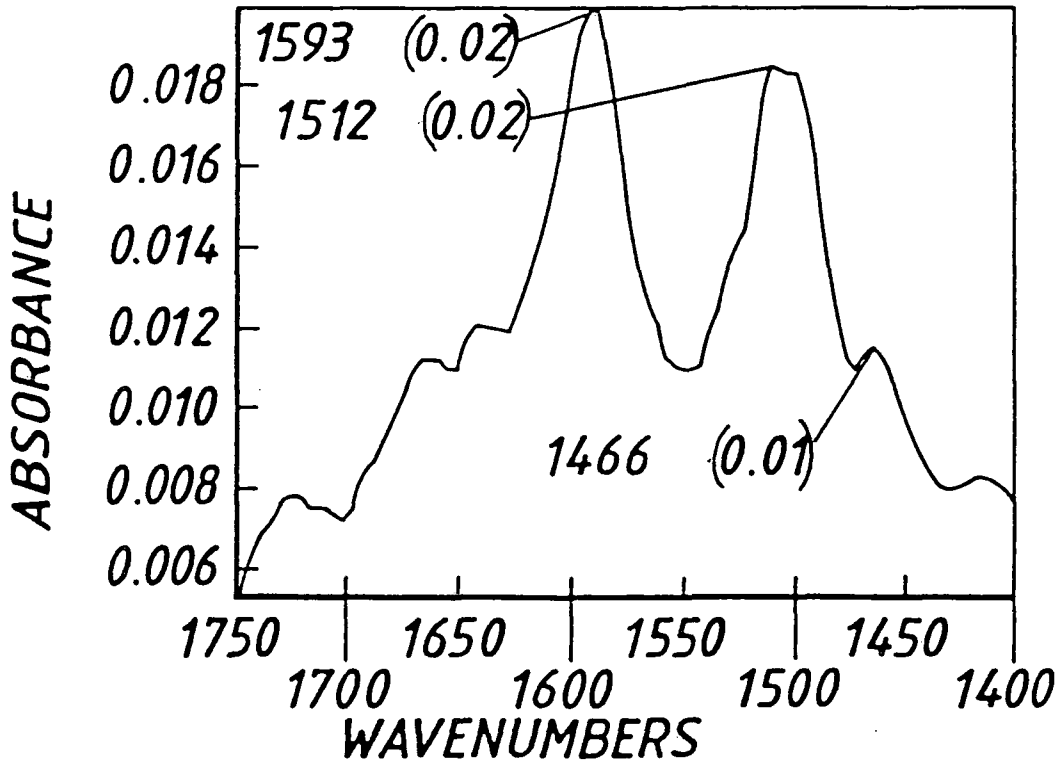

GAS	CONC. (ppm) in N_2	DELAY TIME τ (s)	RECOVERY TIME (mins)	EXPOSURE TIME (mins)	MINIMUM DETECTION (ppm)	NORMALISED CHANGE $\Delta R/R$/ppm
NO_x	10	48	28	6	4	-0.026
H_2S	10	36	56	4	3	-0.033
SO_2	10	12	110	6	2	-0.036
CO	10000	No measurable effect	N/A	25	N/A	N/A
CH_4	50000	No measurable effect	N/A	25	N/A	N/A

TABLE 1
Summary of the effect of different gases on spin-coated polyaniline at room temperature.

GAS	CONC. (ppm) in N_2	DELAY TIME τ (s)	RECOVERY TIME (mins)	EXPOSURE TIME (mins)	MINIMUM DETECTION (ppm)	NORMALISED CHANGE $\Delta R/R$/ppm
NO_x	10	<10	54	6	2	-0.02
H_2S	10	144	120	12	6	0.02
SO_2	50	30	<90	12	1	$-3.4 * 10^{-3}$
CO	10000	No measurable effect	N/A	50	N/A	N/A
CH_4	50000	No measurable effect	N/A	50	N/A	N/A

TABLE 2
Summary of the effect of different gases on evaporated thin film of polyaniline at room temperature.

GAS	CONC. (ppm) in N_2	DELAY TIME τ (s)	RECOVERY TIME (mins)	EXPOSURE TIME (mins)	MINIMUM DETECTION (ppm)	NORMALISED CHANGE $\Delta R/R$/ppm
NO_x	100	72	<120	24	20	$-1.6 * 10^{-3}$
H_2S	100	131	<90	6	5	-0.011
SO_2	1000	No measurable effect	N/A	6	N/A	N/A
CO	10000	No measurable effect	N/A	N/A	N/A	N/A
CH	50000	No measurable effect	N/A	N/A	N/A	N/A

TABLE 3
Summary of the effect of different gases on LB film of polyaniline at room temperature.

APPENDIX B

PUBLICATIONS

1. **Agbor**, N.E., Petty, M.C., Monkman, A.P. and Harris, M. : Synthetic Metals, **55-57** (1993) 3789-3794.

2. Barker, P., Chen, J.R., **Agbor**, N.E., Monkman, A.P. and Petty, M.C. : submitted to Sensors and Actuators **B**.